Oxidation of propane and methanol using metal oxide catalysts

Thesis submitted in accordance with the requirements of the

University of Cardiff for the degree of Doctor of Philosophy

by

Marie Naomi Gilmour

May 2010

ProQuest LLC
789 East Eisenhower Parkway
P.O. Box 1346
Ann Arbor, MI 48106-1346

DECLARATION

This work has not previously been accepted in substance for any degree and is not concurrently submitted in candidature for any degree.

Signed M. Gilmour ..... (candidate) Date 25/05/10 .....

STATEMENT 1

This thesis is the result of my own independent work/investigation, except where otherwise stated. Other sources are acknowledged by explicit references.

Signed M. Gilmour ..... (candidate) Date 25/05/10 .....

STATEMENT 2

I hereby give consent for my thesis, if accepted, to be available for photocopying and for inter-library loan, and for the title and summary to be made available to outside organisations.

Signed M. Gilmour ..... (candidate) Date 25/05/10 .....

Summary

The selective and nonselective oxidation of propane was investigated using a range of metal oxide catalysts. Total oxidation of propane was studied using Nb and W supported on Pd/TiO_2. The addition of Nb or W to Pd/TiO_2 promoted the activity of the catalyst to give 100% conversion by 450°C. The only reaction product observed was carbon dioxide. The addition of Nb and W significantly changed the nature of the palladium and oxygen mobility, from XPS studies. Niobium and tungsten exhibited the highest activity with a 6% loading with the best catalyst being $0.5\%Pd/6\%Nb_2O_5/TiO_2$. Oxidative dehydrogenation of propane was studied using vanadium on a ceria support and also with cobalt, iron and manganese oxides. Ceria on its own was very active for the total oxidation of propane, under the conditions used for oxidative dehydrogenation, but the sole reaction product was carbon dioxide. The addition of vanadium switched the activity of the ceria to give appreciable selectivity to propene of around 90%. The formation of a mixed cerium vanadium phase was of the most interest for future work where conditions could be optimised to give improved yields. Cobalt, iron and manganese oxides were prepared by grinding the corresponding nitrate with ammonium bicarbonate and their activity tested in propane oxidative dehydrogenation. The yields of propene were higher than the V/CeO_2 catalysts with the most active oxide being cobalt with a yield of 3.8%. The activity of cobalt was attributed to a small crystallite size, high reducibility and high ratio of O/Co. Methanol oxidation was also investigated using the cobalt, iron and manganese oxides. The main reaction product was formaldehyde and the highest yield, of 23%, was obtained for the manganese oxide. The activity was attributed to a high O/Mn ratio of 3.03 and an optimal particle size of 54nm.

Abstract

The total oxidation of propane was studied over Nb and W on a Pd/TiO_2 support. Catalysts with varying loadings of Pd, Nb and W on a titania support were prepared by a wet impregnation technique. The addition of Nb or W to Pd/TiO_2 promoted the activity of the catalyst for propane total oxidation. The catalytic activity was found to increase with higher loadings of Nb and W. The addition of Nb and W significantly changed the nature of the palladium from XPS studies. This promoted the presence of palladium species in a totally oxidised state and also produced easily reducible species. Niobium and tungsten exhibited the highest activities with a loading of 6%. The best catalyst amongst the range of catalysts investigated was $0.5\%Pd/6\%Nb_2O_5/TiO_2$. A propane conversion of 88% at 350°C was observed with carbon dioxide being the sole reaction product.

A nanocrystalline cobalt oxide was found to be active for the selective oxidation of propane which prompted the preparation of a nanocrystalline cerium oxide from a precipitation reaction. The ceria support was loaded with varying amounts of vanadium and tested for the oxidative dehydrogenation of propane. Ceria on its own was very active for the total oxidation of propane but it exhibited no selectivity towards propene with its sole reaction product being carbon dioxide. The addition of vanadium resulted in the selectivity switching to propene with appreciable selectivity. The lower loadings of vanadium gave highly dispersed vanadia species which were selective to propene. Higher loadings of vanadium resulted in the formation of a mixed cerium vanadium phase which was also

selective to propene. The highest selectivity of 100% was observed for the highest loading of vanadium, 15% w.t. It is the mixed phase which is of most interest for future work where yields can be optimised.

Further studies into cobalt oxides were carried out for the selective oxidation of propane. Iron and manganese oxides have been shown to have similar catalytic properties to cobalt oxide so were also investigated in propane oxidation. The preparation technique involved grinding the corresponding nitrate and ammonium bicarbonate together as it has been a successful method of preparing nanocrystalline metal oxides in the past. The yields of propene were higher than the V/CeO_2 catalysts with the most active oxide being cobalt with a yield of 3.8%. The activity of cobalt was attributed to a small crystallite size, high reducibility and high ratio of O/Co. The oxidation of methanol was investigated using cobalt, iron and manganese oxides to explore whether the activity observed differed from that in propane oxidation. The main reaction product was formaldehyde and the highest yield, of 23%, was obtained for the manganese oxide. The activity was attributed to a high O/Mn ratio of 3.03 and an optimal particle size of 54nm.

The catalysts prepared were characterised using a range of techniques which included BET, XRD, Raman, TPR, SEM, and XPS. The characterisation data and activity data are discussed throughout the thesis.

Abstract (Microfiche)

The total oxidation of propane was studied over Nb and W on a Pd/TiO_2 support. The addition of Nb and W significantly changed the nature of the palladium from XPS studies. Niobium and tungsten exhibited the highest activities with a loading of 6%. A nanocrystalline cerium oxide, prepared from a precipitation reaction, was loaded with varying amounts of vanadium and tested for the oxidative dehydrogenation of propane. The addition of vanadium resulted in the selectivity switching from CO_2 to propene. Cobalt, iron and manganese oxides gave yields of propene higher than the V/CeO_2 catalysts, with the most active oxide being cobalt with a yield of 3.8%. The activity of cobalt was attributed to a small crystallite size, high reducibility and high ratio of O/Co. The oxidation of methanol was investigated using cobalt, iron and manganese oxides where the main reaction product was formaldehyde. The highest yield, of 23%, was obtained for the manganese oxide. The activity was attributed to a high O/Mn ratio of 3.03 and an optimal particle size of 54nm. The catalysts prepared were characterised using a wide range of techniques.

Acknowledgments

I would like to thank Dr. Stuart Taylor for being a supportive supervisor and always being there for my questions. My time in the lab ran more smoothly with the help of Tom, Edwin, Matt, Albert, Sarwat and Charlotte. I would also like to thank everyone in lab 1.88 and the technicians that helped in the day to day running of my experiments. A huge thank you to David, mum and dad for being patient with me and giving me the support I needed. I'm not sure how you put up with me at times but I can't emphasise enough how much I love and appreciate you. The friends that managed to make me smile when times were stressful; Cassy, Lizzy, Alex and the rest of the motley crew.

Finally, I would like to dedicate this thesis to Grandma Nell who will always be dear to my heart.

Abbreviations/Nomenclature

VOCs = Volatile Organic Compounds

ODH = Oxidative Dehydrogenation

BET = Brunauer Emmet Teller surface area determination

XRD = X-ray Diffraction

SEM = Scanning Electron Microscopy

TPR = Temperature Programmed Reduction

XPS = X-ray Photoelectron Spectroscopy

GHSV = Gas Hourly Space Velocity

TCD = Thermal Conductivity Detector

FID = Flame Ionisation Detector

GC = Gas Chromatograph

HC = Hydrocarbon

Table of Contents

Chapter 1

CHAPTER 1

Introduction

1.1 Aims of project

The overall aim of this project is to investigate the selective and nonselective oxidation of propane using a range of metal oxide catalysts. The first part of the study will focus on the total oxidation of propane using a mixture of Pd, Nb and W on a titania support. Work has shown previously that vanadium is good at modifying Pd on a titania support and it was of interest to see if Nb and W would do the same [1].

A nanocrystalline cobalt oxide was found to be active for the selective oxidation of propane [2] which prompted the preparation of a nanocrystalline cerium oxide from a precipitation reaction. The support prepared was loaded with varying amounts of vanadium. Vanadium is a well known active component in oxidative dehydrogenation catalysts [3]. It has been reported to give high yields in oxidation studies and hopefully promising results will be obtained using a novel ceria support.

Further studies into cobalt oxides were carried out for the selective oxidation of propane. Iron and manganese oxides have been shown to have similar catalytic properties to cobalt oxide so were prepared following a similar method to previous studies [4] and tested for propane oxidation. Although

numerous work has involved mixed oxide catalysts, this research involved pure oxides. The preparation technique will involve grinding reactants together as this has been a successful method of preparing nanocrystalline metal oxides in the past [2].

The oxidation of methanol was investigated using cobalt, iron and manganese oxides to explore whether the activity observed differed from that observed in propane oxidation. Any differences could help probe the reaction taking place with the metal oxide catalysts.

1.2 Basic principles of catalysis

In 1835, the concept of catalysis was first termed by Berzelius [5]. A catalyst provides an alternative, energetically favourable mechanism to a non-catalytic reaction to enable processes to be carried out under industrially feasible conditions of pressure and temperature. Catalysts have the ability to accelerate a chemical reaction by forming bonds with the reacting molecules.

1.2.1 Homogeneous and heterogeneous catalysis

There are two categories which a catalyst can be divided into. One is 'homogeneous' and the other is 'heterogeneous'. Homogeneous catalysis involves a catalyst which is in the same phase as the reaction mixture. For example the hydrolysis of esters by an acid catalyst is as follows:

$$CH_3CO_2CH_{3\,(aq)} + H_2O_{\,(aq)} \leftrightarrow CH_3CO_2H_{\,(aq)} + CH_3OH_{\,(aq)}\ (H^+\ \text{catalyst})$$

A problem with homogeneous catalysis is it is often difficult to recover the reaction products from the solvent.

Heterogeneous catalysis involves a catalyst which is in a different phase to the reaction mixture, for example the synthesis of ammonia:

$$3H_{2\,(g)} + N_{2\,(g)} \leftrightarrow 2NH_{3\,(g)} \text{ over } Fe_{(s)}$$

In heterogeneous catalysis, a solid is catalysing molecules in the liquid or gas phase. The mechanism of the destruction of VOCs in gas flow has been stated by Golodets [6] as occurring "via a surface redox cycle". Molecular oxygen adsorbs on the catalyst surface, which then dissociates to oxygen atoms adsorbed onto the surface. The hydrocarbon also adsorbs onto the surface and reacts to form carbon dioxide and water.

Heterogeneous catalysts are used extensively in industrial applications and a summary of just a few of these reactions are highlighted in table 1.1. Products used on an everyday basis are produced by catalysis and this highlights how important these processes are.

Table 1.1 Common reactions involving heterogeneous catalysis.

Reaction	Common catalyst used	Reactants	Industrial purpose
Ammonia synthesis	Fe (magnetite)	H_2, N_2	Fertiliser and explosives
Methanol synthesis	$Cu/ZnO/Al_2O_3$	CO, CO_2, H_2	Bulk chemicals
Hydrocarbon synthesis (C_5-C_{11})	Co, Fe	Coal, Natural gas	Automotive fuel
Oxidation	Vanadium oxides	Xylenes	Polymers

1.2.2 Catalytic cycle for heterogeneous catalysts

In heterogeneous catalysis, the starting molecules react to form the product and then desorb from the catalyst surface leaving the catalyst unaltered and available for the next reaction, resulting in a catalytic cycle. The catalytic reaction is energetically favourable although the pathway is more complex, with a transition state present (as shown in figure 1.1). The activation energy (E) is reduced for the catalytic pathway. Catalysts do not change the position of equilibrium or the thermodynamics of the system but they do change the kinetics of a reaction, allowing lower temperatures and milder conditions to be used. This was shown by Lemoine in 1877 who stated "a catalyst which contributes no energy to a chemical system cannot change the position of equilibrium, it can only alter the rate at which it is reached" [7].

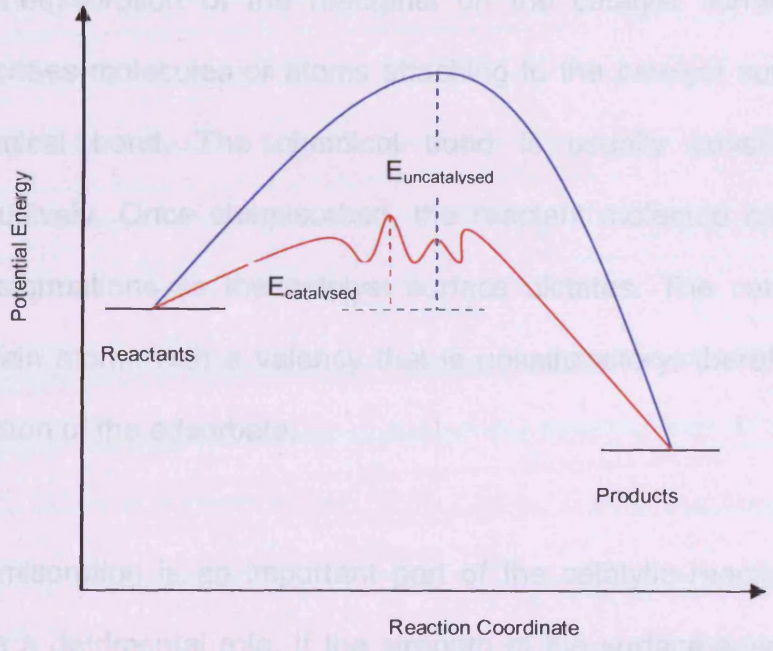

Figure 1.1 Catalytic Reaction Pathway.
Reaction pathway without catalyst shown in blue, reaction pathway with catalyst shown in red.
$E_{uncatalysed}$ = Activation energy of reaction without catalyst.
$E_{catalysed}$ = Activation energy of reaction with catalyst.

The Gibbs free energy is defined by G =H – TS. When the pressure and temperature are constant the expression can be stated as $\Delta G = \Delta H - T\Delta S$. When an adsorbate is chemisorbed to the catalyst surface the translational freedom is reduced resulting in ΔS being negative. For ΔG to be below zero, ΔH needs to be negative which is the case for exothermic reactions. As the reaction for oxidation is exothermic it is spontaneous. On rare occasions the translational freedom is not restricted (e.g. hydrogen on glass) and therefore the reaction may not proceed spontaneously.

1.2.3 The role of the catalyst

The activity of a catalyst is defined by how it converts the starting material into end products of the reaction and also the selectivity which the catalyst converts to the desired product. The catalytic activity depends on the strength of chemisorption of the reactants on the catalyst surface. Chemisorption describes molecules or atoms attaching to the catalyst surface by forming a chemical bond. The chemical bond is usually covalent, although not exclusively. Once chemisorbed, the reactant molecule can undergo further transformations as the catalyst surface dictates. The catalyst surface may contain atoms with a valency that is unsatisfactory, therefore catalysing the reaction of the adsorbate.

Chemisorption is an important part of the catalytic reaction but it can also have a detrimental role. If the strength of the surface-adsorbate bond is too strong the activity of the catalyst is lowered as the reactants are immobilised.

However, if the bond is too weak the components of the reaction cannot be brought together to react.

1.2.4 Catalyst support

The qualities of a 'good' catalyst include a high activity and high selectivity forming only the desired products. A metal oxide with a high surface area, such as TiO_2, can increase the dispersion of a noble metal deposited on the surface of the catalyst, allowing the quantity of the noble metal used to be decreased. This is extremely cost effective. The 'dispersion' is the fraction of atoms located at the surface of a particle of the catalyst support. The interaction between the noble metal and the support has a considerable effect upon the behaviour of the catalyst. For example, if there is a poor dispersion there is less interaction between the noble metal and the metal oxide support resulting in a less efficient catalyst.

Small metal particles are often unstable with sintering taking place but this is overcome by an inert support. The sintering process involves the migration of atoms from one crystallite to another via a surface or gas phase, resulting in a collapse of the pore structure, a reduction of surface area or the blocking of active sites. Active sites are areas on the catalyst that have surface defects, which result in surface atoms being unsaturated in their coordination allowing them to interact with the substrate molecule. Sabatier's principle states that "reactants should be adsorbed at the active site but after the reaction should be able to leave" [8].

Stable supports improve the performance of the catalyst. Alumina is commonly used but it is not stable at the high temperatures that are reached during combustion, as it undergoes a change of phase at 800°C and surface area is decreased [9]. Even though the reactor used may not be running at such a temperature, on the catalyst surface higher temperatures are reached due to exothermic processes taking place. The titania support was found to have a more pronounced effect upon the activity, in comparison to other supports, such as zirconia [10]. Gold and vanadia dispersed on the titania surface were shown to have a strong synergistic effect when molecular oxygen was used as an oxidising agent.

There are various other important factors that should be considered when choosing the support, which shall briefly be mentioned. The porosity of the support is important, as during the catalyst preparation the production of a 'skin' may occur, resulting in a surface less porous than the bulk. When different metals are added they may block pores and modify the pore distribution. The capacity of a unit area to adsorb the reactants, thermal resistance, chemical stability, selectivity, deactivation, acid-base character, valence state of metal cation, structural defects and the degree of crystallinity are all poignant in designing an effective catalyst [3].

1.3 Catalysis in oxidation

Catalytic oxidation is a process widely used across the industrial sector. There are different levels of oxidation from complete oxidation of the reactant molecule to partial oxidation to give a desired product. Complete oxidation

results in the formation of carbon dioxide and water, which is a wasteful process and can cause harm to the environment due to the greenhouse effect. In the case of volatile organic compounds (VOCs) the formation of carbon dioxide is required as it is less toxic to the environment. Partial oxidation can be tailored for the reaction product which needs to be obtained, such as selective oxidation of propane to give propene or methanol to give formaldehyde.

There is a generally accepted mechanism which appropriately describes the oxidation reaction, of a hydrocarbon, taking place on a d-metal (transition metal) oxide surface called the 'Mars-Van-Krevelen' mechanism [11]. For the reaction to proceed, the reactant molecule must adsorb on the catalyst surface. The adsorption involves the loss of a hydrogen atom to form a radical. An oxygen atom in the catalyst surface then transfers to the radical and the molecule formed can desorb. The hydrogen also desorbs from the surface with an oxygen atom forming a water molecule. This process is shown in the reaction scheme:

$$O_{2(g)} \rightarrow O_{2(ads)}$$

$$O_{2(ads)} \rightarrow 2O_{(ads)}$$

$$C_3H_{8(g)} + O_{(ads)} \rightarrow (C_3H_8)\text{-}O_{(ads)}$$

$$(C_3H_8)\text{-}O_{(ads)} + O_{(ads)} \rightarrow O_{(ads)} + CO_{2(g)} + H_2O_{(g)}$$

After desorption occurs, the catalyst surface is left with vacancies and the metal ions are left in lower oxidation states. The resulting vacancies on the

catalyst surface are rapidly filled with oxygen molecules in the gas feed. During this mechanism, some catalytic materials break up under the stress, known as catalyst sintering.

1.4 Volatile Organic Compounds

The contamination of air by the discharge of harmful substances has become a serious issue. There are environmental concerns over the major air pollutants in industrialised and high-income countries due to combustion, industrial (power systems, stationary gas turbines) [12] and agricultural processes.

Volatile organic compounds (VOCs) are considered atmospheric pollutants [13] and are present in low concentrations in industrial gas exhaust systems. By definition, a volatile organic compound is "any compound of carbon, excluding carbon monoxide, carbon dioxide, carbonic acid, metal carbides or carbonates and ammonium carbonates, which participates in atmospheric photochemical reactions" [14]. It can also be stated that the vapour pressure of a VOC exceeds 0.1mmHg under standard conditions with an ability to produce vapours easily at room temperature.

In Europe, the Gothenburg Protocol was put in place whereby a 40% reduction in the emissions of VOCs was required by 2010 [12]. This requirement by law to reduce emissions has instigated vast interest in the removal of these compounds. Although there is an infinite amount of organic compounds, many of the organic compounds that we use, either in industry or

in the home, do not occur in nature and have been synthesised in a laboratory. The most reactive compounds in urban air are those hydrocarbons that contain a double bond as they have the ability to add free radicals.

Some VOCs have direct toxicity, such as benzene and 1, 3-butadiene, as they are carcinogenic, whilst many other VOCs are considered precursors for photochemical oxidant pollution. Ozone naturally occurring in the upper atmosphere shields the earth from dangerous ultra-violet rays. VOCs can react with nitrogen oxides in the presence of sunlight, leading to photochemical smog, which results in depletion of the ozone layer and formation of ground level ozone [15]. This ground level ozone is a pollutant with highly toxic effects, such as:

-asthma;

-damage to lungs, liver, and central nervous system; and

-irritation of the eyes, nose and throat.

There are a wide variety of sources and over 300 compounds, which are considered to be VOCs. Major sources include industrial sites (for organic chemicals, polymers, synthetic fibres, paints, coating operations, food processing, printing), vehicles (cars), and the home [16]. In a typical ambient air sample the emission of different hydrocarbons has been recorded at around 200.

To remove VOCs, a system with high activity needs to be designed which is able to treat a variety of compounds, preferably with a long-term stable

activity, which resists deactivation. A common method to carry out this removal is oxidative destruction using catalysis. Catalysis results in less pollution due to careful control of emissions and less waste of raw materials, therefore reducing cost. Catalysis provides selective catalytic routes, which can replace stoichiometric processes that generate waste problems. The products of complete combustion include carbon dioxide. Although this is considered a harmful, major pollutant (greenhouse gas) [9] in itself it is actually preferential to the emission of VOCs.

There have been different suggested methods of removal of VOCs in emissions, from various sources, including thermal incineration and the use of catalysts. Catalysis is a more favourable method than thermal incineration as the latter requires higher temperatures, which can cause the formation of undesirable noxious by-products, such as NO_x and dioxins. The use of catalysts also allows the removal of VOCs when they are present in very low levels and the process operates at much lower temperatures [17]. The catalytic deep oxidation of VOCs gives carbon dioxide and water [18] and allows effective combustion of fuel-air mixtures in gas turbines [19].

There are different types of catalysts for the destruction of VOCs; the main types are supported noble metals, supported metal oxides and a supported mixture of a noble metal with a metal oxide catalyst. In this project we are investigating noble metals and supported metal oxide catalysts. Metal oxide based catalysts are cheaper but have previously been shown to exhibit lower catalytic activity. The nature of the top layer of atoms on the catalyst

determines how fast the catalytic reaction is taking place. Due to this, different additives on the surface of the catalyst can either reduce or enhance the rate of reaction. It is the available bonding sites on the catalyst, which provide lower energy pathways for the molecules to react.

Supported noble metal catalysts, involving Pd or Pt, have a high activity per atom of catalyst but they are prone to poisoning either by contact with compounds (often chlorinated), which in turn can block active sites, or sintering of the catalyst causing a loss of surface area. Fouling can also occur whereby carbonaceous residues are deposited after the destruction of the hydrocarbon, resulting in a loss of surface area and the number of active sites.

The noble metal supported is commonly platinum or palladium, due to them being established as highly reactive in their use in catalysis [12]. Platinum has been found to be less active than palladium on titania but is more active on alumina for the complete oxidation of methane [17]. In this project, palladium was investigated. Past work has suggested that as a minor component in the catalyst it has the ability to improve one or more of the properties of the material concerned with respect to the product formation [20]. It has also been shown to improve selectivity for the desired product, increase the lifetime of the catalyst and has the ability to neutralise acid sites. It has also been found that supported palladium catalysts are the most active for the deep oxidation of methane [21]. Methane is the hardest hydrocarbon to combust by catalytic

oxidative combustion so if a catalyst has been shown to exhibit a high activity for methane it is worth testing with higher alkanes.

At high temperatures (above 900°C) palladium became inactive for hydrocarbon oxidation [22]. An explanation for this could be the formation of metallic palladium. Metallic palladium is unable to adsorb oxygen from the gas phase, which is required for the oxidation process to occur. The reaction conditions are therefore very important for determining the most active form of the catalyst.

The use of alumina supported palladium based metal oxides has been found very useful in the control of automotive emissions [23]. The addition of ceria promotes carbon monoxide oxidation and nitrogen oxide reduction. In mixed oxide catalysts, the addition of another metal on a support has been found to enhance resistance to thermal deactivation and poisoning. Past work in the field of bimetallic catalysts has included palladium and vanadium on a titania support [24]. Vanadium was found to promote the rate of oxidation at lower temperatures even though vanadium decreased the palladium dispersion and surface palladium sites. Addition of MoO_3, WO_3 and V_2O_5 to platinum and palladium has been shown to increase catalytic activities [25].

The performance of a platinum catalyst was found to improve when it was dispersed onto a TiO_2 support doped with W^{6+} cations [13]. Doping and the metal particle size have an effect on catalytic activity. Platinum supported on titania with W^{6+} was more active than on gamma-alumina [26].

Niobium, as part of a mixed oxide catalyst is thought to have promoter properties due to its effects with palladium-alumina catalysts [23]. It is thought to allow a bifunctional mechanism, which is based upon the redox properties of the reducible support. However, the addition of niobium to rhodium-ceria catalysts decreased the dispersion of rhodium and diminished the reactivity rate [23]. Vanadium is in the same group as niobium and due to its activity towards VOCs, niobium was also chosen in this study as part of the bimetallic catalyst.

The performance of palladium on a support of TiO_2 will be tested as a catalyst for the total oxidative destruction of an organic compound. An area of interest is that of propane where much work has been carried out but a more efficient catalyst is still required. Different metals will also be introduced to the palladium-titania support to determine if some metals are more effective than others in this catalytic process. Metals suggested for the work carried out are tungsten and niobium.

Work previously has involved that of vanadium, which was proved to have the potential as a commercial environmental catalyst [24]. When testing the activity of the catalyst, the deep oxidation of propane was shown to increase, with a loading of 1.5% V and 0.5% Pd. From temperature programmed reduction studies it was possible to see there was ease in the catalyst reduction, which can account for the promotion of activity.

1.5 Oxidative dehydrogenation of propane

Traditional methods to produce alkenes include steam cracking, fluid catalytic cracking and direct dehydrogenation. Catalytic cracking results in several by-products of the reaction, therefore the yield of the alkene is not optimised [27]. Steam cracking and fluid catalytic cracking are currently used for propene production but the process has low selectivity and there are high separation costs [28]. In dehydrogenation, the yields of the alkene are greater as it is the main product formed. However, direct dehydrogenation is endothermic and is limited thermodynamically. A high temperature or low pressure is required for the reaction to occur. Due to the high energy consumption, side pyrolysis reactions and coke formation it is a technique with several disadvantages but has been used commercially since the late 1930s [29]. In World War II, the dehydrogenation of butane to butene was carried out over a chromia-alumina catalyst. The butene was then dimerised to octane, which was then hydrogenated to form octane to be used as high octane aviation fuel [30]. In the late 1980s, the chromium-alumina catalyst was used for the dehydrogenation of propane to propene.

Due to recent government regulations, environmentally friendly processes are required that are less wasteful and more economical [31]. The demand for alkenes, in particular propene, has increased over recent years and is expected to grow further. There is a 'need' for cleaner catalytic processes which remove the use of toxic chemicals and formation of unnecessary waste. A catalyst can reduce the number of steps in a process and allow milder conditions to be used. Oxidative dehydrogenation (ODH) has been

investigated by numerous researchers as an alternative method. Molecular oxygen is used as the oxidant with a recyclable catalyst. Dioxygen shifts the equilibrium of the reaction to the dehydrogenation products by converting the molecular hydrogen to water, resulting in an exothermic reaction. The presence of oxygen avoids any carbonaceous deposits, such as coke, as they are burnt away.

Alkanes are abundant and cheap raw materials which can allow ODH to become a low cost process; in particular propane is a component of natural gas. The current aims in the research of propane ODH is to develop an effective catalyst which can activate oxygen at ambient conditions and give high selectivity to the desired alkene. It is also necessary to find a catalyst capable of activating the C-H bond in the alkane.

The selectivity often depends on the metal oxide content loaded onto the catalyst support and the support itself. Although ODH is advantageous, deep oxidation is favoured thermodynamically to form significant amounts of CO_x. A catalyst needs to be developed with a high selectivity to the alkene but the alkene then needs to be isolated or desorbed from the catalyst surface before a consecutive reaction occurs to form the unwanted products. The importance of ODH was acknowledged by Brazidil where he stated that "the direct conversion of ethane and propane to give chemical intermediates has potential to radically transform the chemical industry. Activity and selectivity for desired products determines how attractive its use in industry is" [32].

Although ODH has many advantages over traditional methods of alkene production, its use in industrial applications will not be considered unless sufficient yields are obtained. Current techniques used provide 60% yields of the desired alkene, which is a high target to aspire to. However, due to environmental concerns and the involvement of the government passing new legal requirements it will be essential for research to continue in this field.

1.5.1 Vanadia and ceria based catalysts

The production of propene is essential as it is needed to manufacture acrolein, acrylic acid acrylonitrile and iso-propanol to name a few. Therefore it is a primary skeletal building block for many polymers in industry [33, 34]. ODH has been extensively studied over supported vanadium oxides [35, 36, 37] but the current yields of propene are not satisfactory. The V/MgO catalyst is one of the most active catalysts for propane ODH with yields of 52% at 500°C [38]. Although this is a good yield there is still scope for improvement. It has been found that the activity of a vanadium oxide catalyst increases with V_2O_5 loading [3]. Although the conversion may increase with loading, the selectivity to the alkene shows a maximum near a monolayer coverage of vanadium over the support. The catalyst performance of vanadium oxides depends on the surface structure of the species supported. Varying loadings of a metal oxide on a support can result in different oxygen species and redox properties. The dispersion of the metal oxide is also an important factor.

In the ODH of propane, high selectivities to propene are found at low conversions due to propene being more reactive than the starting material [39].

This inverse relationship between conversion and selectivity is another limiting factor when trying to optimise propene yields. The alkene can react with oxygen further to give a saturated aldehyde (acrolein) with the possibility of being oxidised further to undesirable CO_x products [37]. The C-H bond in propene is weaker than that in propane so the activation energy is lower. High temperatures must be avoided as the consecutive oxidation of propene can occur much easier than the activation of the starting molecule of propane.

A low selectivity to propene was found when VO_x species were highly dispersed and not fully covering the acidic sites of an alumina support [37]. Acidic sites promote propene adsorption which results in the non-selective oxidation to CO_x. When the loading of vanadium was increased, the VO_x species formed bulk V_2O_5 on the catalyst surface. The acidic sites were covered and the adsorption of propene was decreased. In contrast to low loadings of vanadium, a high selectivity to propene was observed as the propene was allowed to desorb before undergoing further reaction. A monolayer coverage of the vanadium oxide is required to fully cover the support to give high selectivity to propene. Below a monolayer coverage, vanadia forms isolated sites and although these sites are selective to propene, the exposed areas of the support cause further oxidation [40]. Wachs et al [41] found that a vanadium monolayer was the active phase responsible for hydrocarbon oxidation.

Bulk V_2O_5 formed above monolayer coverage on a support is selective to propene. Pure V_2O_5 with no support is predominantly a redox metal oxide with

a minor amount of acid sites and gives low selectivity to propene [42]. The interaction between the support and the vanadia determines the VO_x structure observed at different loadings. The common yields of propene using ODH are below 30% but one of the most promising catalysts is vanadia supported on MgO, with a conversion of 82% and selectivity of 64% at 500°C [43]. This catalyst gives comparable yields to those used in steam cracking with 69% conversion and 78% selectivity but at much higher temperatures of 833°C [28].

At temperatures higher than 700°C, propane cracking occurs; therefore a variety of products can be obtained rather than propene. Although the conversions of propane are high for ODH on vanadium oxides, selectivity needs to be improved. A selectivity of 81.5% for vanadium oxide on a silica-zirconia support was found but the conversion was only 8% at 550°C [44]. The high selectivity could be attributed to the zirconia support stabilising the dispersion of the vanadia. Most catalysts involving vanadium and the ODH of propane are active in the temperature region 500-800°C but at these high temperatures it is difficult to avoid the consecutive oxidation reactions. Research is ongoing into finding a catalyst which is active below 300°C.

Promising vanadium catalysts include V-Al_2O_3 with a selectivity of 51% and conversion of 8% at 550°C [45] and V-Mg-O with a selectivity of 78% and conversion of 4.3% at 510°C [46]. For the ODH of propane (and lower alkanes), the addition of an alkaline metal to V_2O_5/TiO_2 improves the propene selectivity due to the acid-base properties being modified [47]. The additive may also effect the strength of the M-O bond on the surface or in the bulk of

the catalyst. The oxygen between the metal and the support has been reported to be involved in ODH, as it is possible for a limited reaction to proceed without oxygen being present in the feed [27]. Propene is primarily formed from propane by the lattice oxygen of the VO_x species and not the adsorbed oxygen which is used for CO_x products [37]. At loadings above a monolayer of vanadium, a high density of neighbouring VO_x species provides sufficient oxygen for propene to undergo consecutive reactions [48].

As stated, the catalysts containing vanadium are the most promising for the ODH of propane. Vanadium has a high oxidation potential and can easily change between oxidation states of III and V allowing it to be employed as a redox catalyst [49]. It is suggested that the effect of the support on which the vanadia is loaded is more important than the vanadium loading itself. Therefore there is continuing research into different supports. V_2O_5 with no support has been studied [50] and was not effective for the ODH of propane. Even though there is a high surface density of VO_x groups, the reaction taking place was one of complete combustion. Vanadium appears to be essential in the ODH process but the yields currently obtained are not satisfactory. Some of the best reported catalysts include Mg vanadates [51], V-alumina [52], and V/TiO_2 [53]. A maximum yield of 30% was obtained for a K-Mo supported on SiO_2/TiO_2 but the conditions used were not realistic for an industrial application [54]. Transition metals that are very active for oxidation reactions, such as Mn and Fe oxides, have been found to have a high selectivity to propene but only low conversions at the low temperatures have been explored [55].

Titania is a well known and used support in the ODH of propane [56] with promising results. Common supports also include alumina and silica. The oxide support should be of a high surface area as with the addition of a transition metal it is likely to be reduced. The oxide should also be able to support the dispersed active metal species and should resist thermal degradation in the temperature range being explored.

Ceria has been used in the control of automotive pollution since 1980 with an ability to store oxygen during oxidation and release during reduction [57]. Ceria has received interest as a catalyst due to its redox behaviour. In the past, it has been found to be a good hydrocarbon oxidation catalyst and exhibit relative ease in cycling between reduced and oxidised states, Ce^{4+}-Ce^{3+} [58]. The principle product however was CO_2 [59]. Ceria has a high oxygen mobility with a fluorite crystal structure [60]. It has been found that when reduced, oxygen vacancies in the lattice are created allowing more oxygen to be adsorbed. This explains why it is such a good combustion catalyst as a poor alkene selectivity is often observed due to an excess of oxygen near the catalyst surface [48].

1.5.2 Cobalt, iron and manganese oxides as catalysts

One approach to the ODH of propane is to use metal oxides on a suitable support. Interestingly though, activity has been found from metal oxides alone with no additives. Cobalt oxide has been found to be one of the most active binary oxides for complete combustion of VOCs [61]. Nanocrystalline Co_3O_4 has been found to be extremely active for the total oxidation of propane and

butane at temperatures as low as 200°C [62]. In another study, at 523K 60% conversion of propane was observed forming only CO_x products. Hydrocarbons have been found to oxidise completely on Co_3O_4, in absence of gas phase oxygen, due to the excess oxygen species present and trivalent cobalt ions [63].

Even though cobalt oxide may not be viewed as a selective oxidation catalyst, studies have shown that the active oxygen species are the same for total and partial oxidation [60]. In particular, when cobalt oxide was supported on titania, a propane conversion of 28.8% and propene selectivity of 35.51% was found under 550°C [64]. In the case of unsupported cobalt oxide, a good selectivity to ethylene was observed of 43% but at conversions lower than 1% [65]. In the conversion of propane, the main product of the reaction was CO_2 but trace amounts of propene were detected [2] with unsupported cobalt oxide having a higher activity than the supported counterpart. A high surface area and smaller particle size are thought to contribute to greater activity due to active sites of reaction becoming more accessible. A small crystallite size suggests the presence of increased low coordination lattice oxygen sites.

Solid state studies on cobalt oxide in the spinel structure, Co_3O_4, have found that it adsorbs oxygen easily giving it p-type semi-conducting properties where Co^{3+} cations cover the catalyst surface. Bond stated that p-type semi-conductors should be more active than n-type conductors [66] although this contradicts the fact that the most active catalyst in selective oxidation involves vanadium which is an n-type conductor. When cobalt is in a trivalent state,

Co^{3+}, the d-orbital can act as an acceptor causing formation of holes in the O^{2-} valence band [62] which can act as charge carriers normally indicative of p-type semi-conductors.

The oxidising ability of Co_3O_4 is so strong it can attack the allylic C-H of propene even at room temperature. The high basicity of this oxide allows the oxidation of not only propane but also propene at the catalyst surface at ambient temperatures, resulting in the formation of CO_x products [62]. Cobalt oxide has been termed a total oxidation catalyst but at the surface of the oxide, two different oxygen species have been found which allow two possible pathways to occur [67]. Surface oxygen, as already known, was found to be responsible for total oxidation to CO_x products. The presence of lattice oxygen in the cobalt oxide was found to result in selective oxidation to give partial oxidation products. The affinity of cobalt to adsorb oxygen to the surface results in complete oxidation being the pathway taken.

Several studies have shown cobalt oxide to be a complete oxidation catalyst but another application of this catalyst was found for the oxidation of carbon monoxide to carbon dioxide [68]. This has been used since the 1920s [69]. The highly reactive catalyst was prepared by calcining in the presence of oxygen with reactions starting as low as 210K. Cobalt oxide on alumina has also been tested for the oxidation of CO but it was found to deactivate quickly due to the accumulation of carbonaceous products on the surface [70].

The oxidation state of cobalt oxide has an important effect on its activity. The activity of a CoO_x catalyst was found to decrease as the oxidation state of the cobalt increased [71]. Of all the different cobalt oxides studied it was found that Co_3O_4 was the most active, which would explain current research focussing on this stoichiometry. The Co_3O_4 spinel structure has been reported to change phase to the less active CoO at temperatures above 700°C due to sintering [63]. To avoid problems of sintering, the addition of niobium was investigated but although it increased stability it had a detrimental effect on the activity. A catalyst that is active at low temperatures would overcome this problem and allow the Co_3O_4 spinel phase to remain in tact.

Iron is also found in the first transition metal series and as an oxide has interesting catalytic properties. It is important in numerous applications which include well known processes such as the water-gas shift reaction and ammonia synthesis [72, 73]. The commonly used formation of iron oxide in catalysis is Fe_2O_3 as it is a thermodynamically stable oxide [74]. Catalytic applications of iron oxide have been explored in the oxidation of ethane where selective oxidation to ethene was observed with a selectivity of 60% and conversion of 9% [75]. The oxidation of butene to butadiene has been reported at 150°C on α-Fe_2O_3 but with short lived activity due to the formation of CO_2 and H_2O blocking active surface sites [76]. The by-products of the selective oxidation remain adsorbed to the surface at such low temperatures. In another study involving the same reaction, 62% selectivity and 9% conversion was observed at 350°C [77].

Iron oxide is similar to cobalt oxide in that it is effective in oxidising CO [78]. Also the activity of the iron oxide is dependant on the oxidation state and the chemical environment of the Fe^{3+} cations as these strongly influence the reduction mechanism [79]. The mechanism of oxidation on an iron oxide conforms to the Mars van Krevelen mechanism [80]. Therefore redox properties of hematite catalysts have a significant affect on their activity. In the ODH of propane, lattice oxygen is responsible for selective oxidation to propene with a selectivity of 84.1% and conversion of only 1.9% at 873K [76]. A major problem of this reaction is the formation of carbon products on the catalyst surface causing catalytic activity to diminish.

The active sites on different iron oxides have very different properties in oxidation reactions. On α-Fe_2O_3, butene is adsorbed and can undergo dehydrogenation easily [81] but on γ-Fe_2O_3 this reaction is not possible [82]. The formation of α-Fe_2O_3 seems essential for selective oxidation reactions although conversion needs to be greatly improved to be considered for industrial applications.

In the same area of the periodic table lies manganese whose oxides have been of catalytic interest. Manganese dioxide has been used in dry cell batteries, as an oxidising agent in organic synthesis and in several catalytic reactions associated with the formation of oxygen [83, 84]. Manganese oxides have become well known complete oxidation catalysts with activity in ozone decomposition [85]. Precious metals such as Pt, Pd and Au are commonly used for catalytic reactions (such as CO conversion) as they allow lower

operating temperatures than the transition metals [86]. Although higher activity is observed the cost of these noble metals and problems encountered with sintering has led to research focussing on transition metals in the hope to find cheaper alternatives.

The properties of manganese oxide are similar to the cobalt and iron oxides in that they are influenced by oxidation state, morphology, structure and preparation method [85]. In CO oxidation, it was found MnO_2 that was doped in Pd had a high activity and complete conversion was observed at temperatures lower than MnO_2 alone. The preparation method of MnO_2 was by co-precipitation therefore it would be interesting to see the effect of a different technique in its activity. Also reported for CO oxidation was a mixed copper and manganese oxide which was found to be active at ambient temperatures [87].

MnO_2 is able to catalyse the ozonation of oxalic acid at a moderately acidic pH and the mechanism was shown to involve the adsorption of the substrate on the solid [88]. Although the debate between using noble metals or transition metal continues, it was found that γ-MnO_2 was more active at removing VOCs into CO_2 and H_2O [89]. The catalyst was found to be stable after reaction but some improvements are needed before a commercial application.

The main studies have been on MnO_2 but like cobalt, manganese can form a spinel structure of Mn_3O_4. The spinel manganese oxide is an efficient and stable catalyst in the oxidative destruction of VOCs [90]. In the oxidation of

propane, 100% conversion to CO_2 was observed at 600K [91]. At lower temperatures, incomplete combustion occurred and small amounts of propene were produced. It was found that when the catalyst was in a less oxidised state more propene was detected, although frequently this was further oxidised to CO_2.

1.6 Partial oxidation of methanol

In the field of ODH many reactants are studied including methanol. Methanol can be synthesised from biomass, coal and natural gas [92]. The desirable selective oxidation product is formaldehyde as it is a versatile compound that has several applications in the formation of plywood, paper, paint, adhesives, cosmetics, explosives and fertilisers [93]. The ODH using methane is not a viable route as the formaldehyde is more easily oxidised than the methane, therefore trying to activate the alkane C-H bond would cause the formaldehyde to undergo consecutive reactions to CO_x products.

Past methods of methanol conversion have included steam reforming [91] but since the beginning of the 20th century the commercialised process has involved catalytic ODH over a silver catalyst [92]. Partial oxidation and dehydrogenation occurs with air, steam and excess methanol at temperatures of 680-720°C. Alternatively the formox process is used over a ferric molybdate catalyst where oxidation occurs in excess air at lower temperatures of 250-400°C but becomes inactive with excess methanol [94].

The silver catalyst is used by 55% of industrial production of formaldehyde due to its stable production but it is a highly exothermic reaction leading to parallel and consecutive reactions [93]. The undesirable by-products of the ODH methanol include CO_x products, formic acid, hydrogen and coke deposits. When used on a smaller scale in a microreactor conversions of 75% and selectivity of 85% were obtained at 783K [95]. The formox process is commonly used in industry due to lower operating temperatures and cheaper catalyst components. Both processes have been reported to have close to 99% conversion and 92% selectivity to formaldehyde [92].

The ODH of alcohols, such as methanol, has been a promising alternative to partial oxidation as it can occur in a single step with relative ease [96]. Mild conditions are required due to the reactive nature of methanol. Reactions with intermediates can take place if the temperature is too low and reactions with hydrocarbons can occur if the temperature is too high [97]. The ODH reaction of methanol involves the activation of the O-H bond to form methoxide species and H-atoms on the catalyst surface [98]. Once the formaldehyde is formed it is normally unstable at high temperatures therefore forming water and CO_2 in the presence of oxygen.

There are similarities of the ODH of methanol with the ODH of propane in that vanadium containing catalysts are found to give good yields of the desired product [99]. It was also found the activity increased directly with increased vanadium loading [100]. From studies on vanadium oxides for the ODH of methanol [101] it has been found that weaker acid sites are more selective for

the formation of formaldehyde [102]. With stronger acid sites, less selectivity to formaldehyde was observed with toxic by-products such as formic acid and dimethoxymethane being formed. Problems encountered with methanol ODH include the formation of volatile species during the reaction. Wachs et al discovered that vanadium containing catalysts did not form any volatile species during methanol oxidation [103]. The V-Mg-O catalyst which was one of the best catalysts for propane ODH was found to have a yield of 95% for methanol ODH [104].

The selective oxidation of methanol over metal oxides has been found to occur through the Mars van Krevelen mechanism [11]. Due to this, redox cycles are important when considering future catalysts. Rubidium oxide supported by various oxides, such as SnO_2, TiO_2 and Al_2O_3, was found to provide a low temperature path to formaldehyde due to a fast redox cycle [105]. Excluding vanadium, most studies have involved metal oxides on SiO_2. Pure SiO_2 has been found to be active in the ODH methanol giving selective products [106]. However the selectivity actually decreased with the addition of a metal oxide [107]. The reaction on SiO_2 proceeded at temperatures of 400-600°C but above 500°C the main product was carbon monoxide [108]. At ambient temperatures of only 60°C, palladium supported on fluoro tetrasilicic mica, exhibited a methanol conversion of 10.4% and selectivity of 65% [95]. Although the selectivity to CO_2 again increased with heightened temperature.

The ability for catalysts to enable reactions to occur at ambient temperatures is of great interest and an area that work will be carried out in the future.

Advantages of low temperature work include low cost of operation but also improved selectivity due to consecutive reactions being minimised. The aim of catalysis research is to obtain desired products at rates which are commercially viable. Due to increasing environmental concern it is essential to reduce air and water pollution which may be harmful to human health and the environment [109]. The majority of industrial catalysts involve a high surface area metal oxide with an active component dispersed over its surface.

1.7 References

[1] T. Garcia, B. Solsona, S. H. Taylor, *Catalysis Letters* **97 (1-2)** (2004) pp. 99-103.

[2] T. E. Davies, T. Garcia, B. Solsona, S. H. Taylor, *Chemical Communications* (2006) pp. 3417-3419.

[3] F. Cavani, N. Ballarini, A. Cericola, *Catalysis Today* **127** (2007) pp. 113-131.

[4] B. Solsona, T. E. Davies, T. Garcia, I. Vázquez, A. Dejoz, S. H. Taylor, *Applied Catalysis B: Environmental* **84 (1-2)** (2008) pp. 176-184.

[5] J.J. Berzelius, Årsberättelsen om framsteg I fysik och kemi, *Royal Swedish Academy of Sciences*, 1835.

[6] G. I. Golodets, *Heterogeneous Catalytic Reactions Involving Molecular Oxygen*, Studies in Surface Science and Catalysis, Elsevier, Amsterdam, **15** (1982).

[7] G. Lemoine, Annales des Chimie et des Physique, **12** (1877), pp. 145.

[8] G. Rothenburg, *Catalysis: Concepts and Green Applications* (2008) pp. 65.

[9] S. L. Escandon, S. Ordonez, A. Vega, F. V. Diez, *Chemosphere* **58 (1)** (2004) pp.9-17.

[10] D. Andreeva, T. Tabakova, L. Llieva, A. Naydenov, D. Mehanjiev, M. V. Abrashev, *Applied Catalysis A: General* **209** (2001) pp.291-300.

[11] P. Mars, D. W. van Krevelen, *Chemical Engineering Science* **3** (1954), pp. 41.

[12] M. Reinke, J. Mantzaras, R. Schaeren, R. Bombach, A. Inauen, S. Schenker, *Combustion and Flame,* **136** (2004) pp. 217-240.

[13] P. Papaefthimiou, T. Ioannides, X. E. Verykios, *Applied Catalysis B: Environmental* **15** (1998) pp. 75-92.

[14] C.S. Heneghan, G. J. Hutchings, S. H. Taylor, *Catalysis* **17** (2004) pp.105-151.

[15] A. C. Lewis, N. Carslaw, P. J. Marriot, R. M. Kinghorn, P. M. Lee, L. Andrew, K. D. Bartle, M. J. Pilling, *Nature* **405** (2000) pp. 778.

[16] A. Brayner, D. Cunha, F. Bozon-Verduraz, *Catalysis Today* **78 (1-4)** (2003) pp. 419-432.

[17] H. Widjaja, K. Sekizawa, K. Eguchi, H. Arai, *Catalysis Today* **47** (1999) pp. 95-101.

[18] A. Janbey. W. Clark, E. Noordally, S. Grimes, S. Tahir, *Chemosphere* **52 (6)** (2003) pp. 1041-1046.

[19] L. F. Liotta, G. Deganello, D. Sannino, M. C. Gaudino, P. Ciambelli, S. Gialanella, *Applied Catalysis A: General* **229** (2002) pp. 217-227.

[20] J. J. Spivey, *Industrial and Engineering Chemistry Research* **26** (1987) pp. 2165-2180.

[21] D. Ciuparu, L. Pfefferle, *Catalysis Today* **77** (2002) pp. 167-179.

[22] S. Colussi, A. Trovarelli, G. Groppi, J. Llorca, *Catalysis Communications* **8** (2007) pp. 1263-1266.

[23] F. B. Noronha, D. A. G. Aranda, A. P. Ordine, M. Schmal, *Catalysis Today* **57** (2000) pp. 275-282.

[24] T. Garcia, B. Solsona, D. M. Murphy, K. L. Antcliff, S. H. Taylor, *Journal of Catalysis* **229 (1)** (2005) pp. 1-11.

[25] C. Neyertz, M. A. Volpe, C. Gigola, *Catalysis Today* **57** (2000) pp. 255-260.

[26] P. Papaefthimiou, T. Ioannides, X. E. Verykios, *Applied Thermal Engineering* **18 (11)** (1998) pp. 1005-1012.

[27] E. A. Graaf, G. Zwanenburg, G. Rothenburg, A. Bliek, *Organic Process Research & Development* **9** (2005) pp. 397-403.

[28] A. A. Lemonidou, M. Machli, *Catalysis Today* **127 (1-4)** pp. 132-138.

[29] M. M. Bhasin, J. H. McCain, B. V. Vora, T. Imai, P. R. Pujadó, *Applied Catalysis A: General* **221 (1-2)** pp. 397-419.

[30] A. L. Waddams, *Chemicals from Petroleum*, 4th Edition, Gulf Publishing Company, Houston, (1978).

[31] R. A. Sheldon, R. S. Downing, *Applied Catalysis A: General* **189** (1999) pp. 163-183.

[32] J. F. Brazdil, *Topics in Catalysis* **38** (2006) pp. 289.

[33] R. K. Grasselli, J. D. Burrington, *Advances in Catalysis* **30** (1981) pp. 133.

[34] E. Serwicka, J. B. Black, J. Goodenough, *Journal of Catalysis* **106** (1987) pp. 23.

[35] E. Heracleous, M. Machli, A. A. Lemonidou, I. A. Vasalos, *Journal of Molecular Catalysis A: Chemical* **232 (1-2)** (2005) pp. 29-39.

[36] P. Viparelli, P. Ciambelli, L. Lisi, G. Ruoppolo, G. Russo, J. C. Volta, *Applied Catalysis A: General* **184 (2)** (1999) pp. 291-301.

[37] B. Mitra, I. E. Wachs, G. Deo, *Journal of Catalysis* **240 (2)** (2006) pp. 151-159.

[38] T. Punniyamurthy, S. Velusamy, J. Iqbal, *Chemistry Review* **105** (2005) pp. 2329-2363.

[39] E. V. Kondratenko, N. Steinfeldt, M. Baerns, *Physical Chemistry Chemical Physics* **8** (2006) pp. 1624-1633.

[40] E. V. Kondratenko, M. Baerns, *Applied Catalysis A* **260** (2004) pp. 101.

[41] I. E. Wachs, R. Y. Saleh, S. S. Chan, C. Chersich, *Applied Catalysis* **15** (1985) pp. 339.

[42] I. E. Wachs, L. E. Briand, J. Jehng, L. Burcham, X. Gao, *Catalysis Today* **57 (3-4)** (2000) pp. 323-330.

[43] C. Pak, A. T. Bell, T. D. Tilley, *Journal of Catalysis* **206** (2002) pp. 49.

[44] R. Rulkens, T. D. Tilley, *Journal of American Chemistry Society* **120** (1998) pp. 9959.

[45] M. J. Alfonso, A. Julbe, D. Farrusseng, M. Menéndez, J. Santamaría, *Chemical Engineering Science* **54 (9)** (1999) pp. 1265-1272.

[46] D. Creaser, B. Andersson, R. R. Hudgins, P. L. Silveston, *Applied Catalysis A: General* **187 (1)** (1999) pp. 147-160.

[47] A. Klisińska, K. Samson, I. Gressel, B. Grzybowska, *Applied Catalysis A: General* **309 (1)** (2006) pp. 10-16.

[48] J. Haber, *Catalysis Today* **142** (2009) pp. 100-113.

[49] K. Scheurell, E. Hoppe, K. Brzezinka, E. Kemnitz, *Journal of Material Chemistry* **14** (2004) pp. 2560-2568.

[50] R. Kozlowski, R. F. Pettifer, J. M. Thomas, *Journal of Physical Chemistry* **87** (1983) pp. 5176-5181.

[51] H. H. Kung, M. C. Kung, *Applied Catalysis A: General* **157** (1997) pp. 105.

[52] J. G. Eon, R. Olier, J. C. Volta, *Journal of Catalysis* **145** (1994) pp. 318.

[53] B. Grzybowska, *Applied Catalysis A: General* **157** (1997) pp. 263.

[54] J. B. Stelzer, J. Caro, M. Fait, *Catalysis Communications* **6** (2005) pp. 1-5.

[55] V. Ermini, E. Finocchio, S. Sechi, G. Busca, S. Rossini, *Applied Catalysis A: General* **198** (2000) pp. 67-79.

[56] M. Inomata, K. Mori, A. Mlyamoto, T. Ui, Y. Murakami, *Journal of Physical Chemistry* **87** (1983) pp. 754-761.

[57] C. Loong, M. Ozawa, *Journal of Alloy Compounds* **60** (2000) pp. 303-304.

[58] S. Zhao, R. J. Gorte, *Applied Catalysis A: General* **277** (2004) pp. 129-136.

[59] S. Sugiyama, Y. Iizuka, E. Nitta, H. Hayashi, J. B. Moffat, *Journal of Catalysis* **189** (2000) pp. 233-237.

[60] J. Y. Ying, A. Tschöpe, *The Chemical Engineering Journal* **64** (1996) pp. 225-237.

[61] E. Finocchio, R. J. Willey, G. Busca, V. Lorenzelli, *Journal of Chemistry Society: Faraday Transmissions* **93 (1)** (1997) pp. 175-180.

[62] B. Solsona, I. Vázquez, T. Garcia, T. E. Davies, S. H. Taylor, *Catalysis Letters* **116 (3-4)** (2007) pp. 116-121.

[63] E. Finocchio, G. Busca, V. Lorenzelli, V. S. Escribano, *Journal of Chemistry Society: Faraday Transmissions* **92 (9)** (1996) pp. 1587-1593.

[64] A. Xu, B. Zhaorigetu, Q. Lin, G. Dong, Y. Zhang, *Journal of Functional Materials* **39 (1)** (2008) pp. 130-132.

[65] Y. Schuurman, V. Ducarme, T. Chen, W. Li, C. Mirodatos, G. A. Martin, *Applied Catalysis A: General* **163** (1997) pp. 227-235.

[66] G. C. Bond, *Heterogeneous Catalysis, Principles and Applications*, Oxford University Press, Oxford, 2nd Edition, (1991).

[67] J. Haber, W. Turek, *Journal of Catalysis* **190** (2000) pp. 320-326.

[68] L. Simonet, F. Garin, G. Maire, *Applied Catalysis B: Environmental* **11** (1997) pp. 167-179.

[69] M. J. Pollard, B. A. Weinstock, T. E. Bitterwolf, P. R. Griffiths, A. P. Newbery, J. B. Paine, *Journal of Catalysis* **254 (2)** (2008) pp. 218-225.

[70] J. Jansson, A. E. C. Palmqvist, E. Fridell, M. Skoglundh, L. Österlund, P. Thormählen, V. Langer, *Journal of Catalysis* **211** (2002) pp. 387-397.

[71] H. Lin, H. Chui, H. Tsai, S. Chien, C. Wang, *Catalysis Letters* **88 (3-4)** (2004) pp. 169.

[72] R. M. Cornell, U. Schwertmann, *The Iron Oxides*, New York (1996).

[73] J. H. M. Kock, H. M. Fortuin, J. W. Geus, *Journal of Catalysis* **96** (1985) pp. 261.

[74] W. K. Jozwiak, E. Kaczmarek, T. P. Maniecki, W. Ignaczak, W. Maniukiewicz, *Applied Catalysis A: General* **326** (2007) pp. 17-27.

[75] Y. Schuurman, V. Ducarme, T. Chen, W. Li, C. Mirodatos, G. A. Martin, *Applied Catalysis A: General* **163** (1997) pp. 227-235.

[76] S. E. Golunski, A. P. Walker, *Journal of Catalysis* **204** (2001) pp. 209-218.

[77] B. L. Yang, S. B. Lee, D. D. Cheng, W. S. Chang, *Journal of Catalysis* **141** (1993) pp. 161-170.

[78] S. E. Golunski, A. P. Walker, *Chemical Communications* (2000) pp. 1593.

[79] P. Michorczyk, P. Kuśtrowski, L. Chmielarz, J. Ogonowski, *Reaction Kinetics Catalysis Letters* **82 (1)** (2004) pp. 121-130.

[80] H. H. Kung, M. C. Kung, *Advances in Catalysis* **33** (1985) pp. 159.

[81] B. L. Yang, H. H. Kung, *Journal of Catalysis* **77** (1982) pp. 410.

[82] B. L. Yang, M. C. Kung, H. H. Kung, Journal of Catalysis 89 (1984) pp. 172.

[83] M. Kang, E. D. Park, J. M. Kim, J. E. Yie, *Catalysis Today* **111** (2006) pp. 236-241.

[84] M. S. Islam, R. A. Davies, J. D. Gale, *Chemistry Materials* **15** (2003) pp. 4280-4286.

[85] B. Dhandapani, S. T. Oyama, *Chemistry Letters* (1995) pp. 413-414.

[86] A. V. Salker, R. K. Kunkalekar, *Catalysis Communications* **10** (2009) pp. 1776-1780.

[87] G. J. Hutchings, A. A. Mirzaei, R. W. Joyner, M. R. H. Siddiqui, S. H. Taylor, *Applied Catalysis A: General* **166** (1998) pp. 143-152.

[88] R. Andreozzi, A. Insola, V. Caprio, R. Marotta, V. Tufano, *Applied Catalysis A: General* **138** (1996) pp. 75-81.

[89] C. Lahousse, A. Bernier, P. Grange, B. Delmon, P. Papaefthimiou, T. Ioannides, X. Verykios, *Journal of Catalysis* **178** (1998) pp. 214-225.

[90] M. Baldi, E. Finocchio, F. Milella, G. Busca, *Applied Catalysis B: Environmental* **16** (1998) pp. 43-51.

[91] G. Busca, E. Finocchio, V. Lorenzelli, G. Ramis, M. Baldi, *Catalysis Today* **49** (1999) pp. 453-465.

[92] E. Manova, T. Tsoncheva, C. Estournès, D. Paneva, K. Tenchev, I. Mitov, L. Petrov, Applied Catalysis A: General 300(2) (2006) pp. 170-180.

[93] M. Cozzolino, R. Tesser, M. D. Serio, P. D'Onofrio, E. Santacesaria, *Catalysis Today* **128** (2007) pp. 191-200.

[94] M. Qian, M. A. Liauw, G. Emig, *Applied Catalysis A: General* **238** (2003) pp. 211-222.

[95] E. Cao, A. Gavriilidis, *Catalysis Today* **110** (2005) pp. 154-163.

[96] T. Ohtake, T. Mori, Y. Morikawa, *Journal of Natural Gas Chemistry* **16** (2007) pp. 1-5.

[97] I. Villegas, M. J. Weaver, *Journal of Chemical Physics* **103** (1995) pp. 2295.

[98] A. Khodakov, B. Olthof, A. T. Bell, E. Iglesia, *Journal of Catalysis* **181** (1999) pp. 205.

[99] T. Kim, I. E. Wachs, *Journal of Catalysis* **255** (2008) pp. 197-205.

[100] C. M. Sorensen, R. S. Weber, Journal of Catalysis **142** (1993) pp. 1.

[101] L. J. Burcham, G. T. Gao, X. T. Gao, I. E. Wachs, *Topics in Catalysis* **11** (2000) pp. 85.

[102] D. Zeng, H. Fang, A. Zheng, J. Xu, L. Chen, J. Yang, J. Wang, C. Ye, F. Deng, *Journal of Molecular Catalysis A: Chemical* **270** (2007) pp. 257-263.

[103] L. E. Briand, J. Jehng, L. Cornaglia, A. M. Hirt, I. E. Wachs, *Catalysis Today* **78** (2003) pp. 257.

[104] G. V. Isaguliants, I. P. Belomestnykh, *Catalysis Today* **100** (2005) pp. 441-445.

[105] H. Liu, E. Iglesia, *Journal of Physical Chemistry* **109 (6)** (2005) pp. 2155-2163.

[106] S. Kasztellan, J. B. Moffat, *Chemical Communications* **N21** (1987) pp. 1663.

[107] F. Arena, F. Frusteri, A. Parmaliana, N. Giordano, *Journal of Catalysis* **143** (1993) pp. 299.

[108] S. Yao, F. O. Yang, S. Shimumora, H. Sakurai, K. Tabata, E. Suzuki, *Applied Catalysis A: General* **198** (2000) pp. 43-50.

[109] A. T. Bell, *Science* **299** (2003) pp. 1688-1691.

Chapter 2

CHAPTER 2

Experimental

This chapter describes the experimental details, including how the different catalysts were prepared, the reactors used to test catalyst activity and the different characterisation techniques employed.

2.1 Catalyst preparation

2.1.1 Pd/Nb/TiO_2

$PdCl_2$, (Aldrich, 99.999%) was dissolved in a minimal amount of hot de-ionised water (~ 4.2ml/g). The solution was then heated to 80°C while continuously stirred, giving a brown solution. Ammonium Niobium (V) Oxalate, $C_{10}H_8N_2O_{33}Nb_2$, was added and dissolved, giving a dark/grey solution. TiO_2, (Degussa, P_{25}) was added to the heated solution and stirred at 80°C to evaporate all of the water to form a white paste. The paste was then placed in an oven and left to dry at 110°C for 24 hours. The solid was then crushed and calcined in static air at 550°C for 6 hours (ramp rate 10°C/min^{-1}), to give a white/grey powder. Masses of reactants used are shown in table 2.1.

2.1.2 Nb/TiO_2

Ammonium Niobium (V) Oxalate was dissolved in a minimal amount of hot de-ionised water (~ 4.2ml/g). The solution was then heated to 80°C while continuously stirred. TiO_2, (Degussa, P_{25}), was added to the heated solution

and stirred at 80°C to evaporate all of the water to form a white paste. The paste was placed in an oven and left to dry at 110°C for 24 hours. The solid was then crushed and calcined in static air at 550°C for 6 hours, to give a white/grey powder. Masses of reactants used are shown in table 2.2.

Table 2.1 The values used in the preparation of the $Pd/Nb/TiO_2$ catalysts.

Catalyst.	Mass of $PdCl_2$ (g)	Mass of $C_{10}H_8N_2O_{33}Nb_2$ (g)	Mass of TiO_2 (g)
0.5%Pd/1.0%Nb/TiO_2	0.0167	0.0936	1.8897
0.5%Pd/2.0%Nb/TiO_2	0.0167	0.1873	1.7960
0.5%Pd/3.0%Nb/TiO_2	0.0167	0.2809	1.7024
0.5%Pd/6.0%Nb/TiO_2	0.0167	0.5618	1.4215
1.0%Pd/3.0%Nb/TiO_2	0.0335	0.2809	1.6857
2.0%Pd/3.0%Nb/TiO_2	0.0669	0.2809	1.6522

Table 2.2 The values used in the preparation of the Nb/TiO_2 catalysts.

Catalyst.	Mass of $C_{10}H_8N_2O_{33}Nb_2$ (g)	Mass of TiO_2 (g)
3.0%Nb/TiO_2	0.2809	1.7191
6.0%Nb/TiO_2	0.5618	1.4382

2.1.3 $Pd/W/TiO_2$

$PdCl_2$, (Aldrich, 99.999%) was dissolved in a minimal amount of hot de-ionised water (~ 4.2ml/g). The solution was then heated to 80°C while continuously stirred, giving a brown solution. H_2WO_4, (Aldrich, 99%) was added and dissolved, giving a yellow solution. TiO_2, (Degussa, P_{25}), was added to the heated solution and stirred at 80°C to evaporate all of the water to form a white paste. The paste was placed in an oven and left to dry at 110°C for 24 hours. The solid was then crushed and calcined in static air at 550°C for 6 hours, to give a white/yellow powder. Masses of reactants used are shown in table 2.3.

Table 2.3 The values used in the preparation of the $Pd/W/TiO_2$ catalysts.

Catalyst.	Mass of $PdCl_2$ (g)	Mass of H_2WO_4 (g)	Mass of TiO_2 (g)
0.5%Pd/1.0%W/TiO_2	0.0167	0.0272	1.9561
0.5%Pd/2.0%W/TiO_2	0.0167	0.0544	1.9290
0.5%Pd/3.0%W/TiO_2	0.0167	0.0815	1.9017
0.5%Pd/6.0%W/TiO_2	0.0167	0.1631	1.8202
1.0%Pd/3.0%W/TiO_2	0.0335	0.0815	1.8850
2.0%Pd/3.0%W/TiO_2	0.0669	0.0815	1.8516

2.1.4 W/TiO_2

H_2WO_4, (Aldrich, 99%) was dissolved in a minimal amount of hot de-ionised water (~ 4.2ml/g). The solution was then heated to 80°C while continuously

stirred. TiO_2, (Degussa, P_{25}), was added to the heated solution and stirred at 80°C to evaporate all of the water to form a white paste. The paste was placed in an oven and left to dry at 110°C for 24 hours. The solid was then crushed and calcined in static air at 550°C for 6 hours, to give a white/yellow powder. Masses of reactants used are shown in table 2.4.

Table 2.4 The values used in the preparation of the W/TiO_2 catalysts.

Catalyst.	Mass of H_2WO_4 (g)	Mass of TiO_2 (g)
$3.0\%W/TiO_2$	0.0816	1.9184
$6.0\%W/TiO_2$	0.1631	1.8369

2.1.5 Nanocrystalline ceria, homogeneous precipitation method

Ceric ammonium nitrate (Aldrich, 99.99%), 10g, was dissolved in de-ionised water and mixed with urea (Aldrich, 98%), 30g, in a 1:3 molar ratio. The solution was stirred whilst heating, under reflux, to 100°C until a white gel formed. The gel was aged for 24 hours at 100°C and the final precipitate collected by filtration. The solid was dried at 120°C for 12 hours and calcined in static air at 400°C for 10 hours.

2.1.6 Vanadium loaded onto nanocrystalline ceria

Appropriate amounts of ammonium metavanadate (Aldrich, 99.99%) (shown in table 2.5) were dissolved in the minimal amount of hot water (~ 4.2ml/g) with oxalic acid (Aldrich, 98%, 1.58g). When completely dissolved the

appropriate amount of ceria was added to the solution and continuously stirred for 1 hour. The resulting mixture was dried at 80°C for 24 hours and calcined in static air at 550°C for 6 hours.

Table 2.5 The values used in the preparation of the VO_x/CeO_2 catalysts.

Catalyst.	Mass of NH_4VO_3 (g)	Mass of CeO_2 (g)
0.5%V/CeO_2	0.0338	1.9662
1.0%V/CeO_2	0.0676	1.9324
2.0%V/CeO_2	0.1352	1.8648
4.0%V/CeO_2	0.2703	1.7297
5.0%V/CeO_2	0.2310	1.7690
10.0%V/CeO_2	0.4619	1.5381
15.0%V/CeO_2	0.6929	1.3071

2.1.7 Vanadium loaded onto titania

Appropriate amounts of ammonium metavanadate (Aldrich, 99.99%) (shown in table 2.6) were dissolved in the minimal amount of hot water (~ 4.2ml/g) with oxalic acid (Aldrich, 98%, 1.58g). When completely dissolved the appropriate amount of titania (Degussa, P_{25}) was added to the solution and continuously stirred for 1 hour. The resulting mixture was dried at 80°C for 24 hours and calcined in static air at 550°C for 6 hours.

Table 2.6 The values used in the preparation of the VO_x/TiO_2 catalysts.

Catalyst.	Mass of NH_4VO_3 (g)	Mass of TiO_2 (g)
0.5%V/TiO_2	0.0574	4.9426
2.0%V/TiO_2	0.2298	4.7702
4.0%V/TiO_2	0.4596	4.5404
6.0%V/TiO_2	0.6894	4.3106
6.8%V/TiO_2	0.7814	4.2186
10%V/CeO_2	1.1491	3.8509

2.1.8 Nanocrystalline cobalt oxide, solid state method

Cobalt (II) nitrate hexahydrate, $Co(NO_3)_2.6H_2O$ (Aldrich, 99.999%) and ammonium hydrogen carbonate, NH_4 HCO_3 (Aldrich, 99.0%) were ground together in a pestle and mortar for 0.5h before being washed thoroughly with distilled water and filtered. Different ratios of the two materials were used (5:1, 5:2 and 5:3). Grinding the two materials gave an instant reaction with the formation of a purple substance and ammonia gas being released. The prepared catalysts were dried for 16 hours at 80°C and calcined at 300°C for 2 hours in static air. Masses of reactants used are shown in table 2.7.

Table 2.7 The values used in the preparation of the Co_3O_4 catalysts.

Catalyst ratio.	Mass $Co(NO_3)_2.6H_2O$ (g)	Mass NH_4HCO_3 (g)
5:1	10	0.5433
5:2	10	1.0866
5:3	10	1.6128

2.1.9 Nanocrystalline iron oxide, solid state method

Iron(III) nitrate nonahydrate, $Fe(NO_3)_3.9H_2O$ (Aldrich, 99.99%) and ammonium hydrogen carbonate, NH_4HCO_3 (Aldrich, ≥99.0%) were ground together in a pestle and mortar for 0.5 hours before being filtered. (The material was not washed in water as the iron was hygroscopic). Three different ratios of the two materials were used (5:1, 5:2 and 5:3). Grinding the two materials gave an instant reaction with the formation of a brown substance and ammonia gas being released. The prepared catalysts were dried for 16 hours at 80°C and calcined at 300°C for 2 hours in static air. Masses of reactants used are shown in table 2.8.

Table 2.8 The values used in the preparation of the Fe_2O_3 catalysts.

Catalyst ratio.	Mass $Fe(NO_3)_3.9H_2O$ (g)	Mass NH_4HCO_3 (g)
5:1	10	0.3908
5:2	10	0.7816
5:3	10	1.1724

2.1.10 Nanocrystalline manganese oxide, solid state method

Manganese (II) nitrate hexahydrate, $Mn(NO_3)_2.6H_2O$ (Aldrich, ≥98%) and ammonium hydrogen carbonate, $NH_4\ HCO_3$ (Aldrich, ≥99.0%) were ground together in a pestle and mortar for 0.5 hours before being filtered. (The material was not washed in water as the manganese was hygroscopic). Different ratios of the two materials were used (5:1, 5:2 and 5:3). Grinding the two materials gave an instant reaction with the formation of a white substance and ammonia gas being released. The prepared catalysts were dried for 16 hours at 80°C and calcined at 300°C for 2 hours in static air. Masses of reactants used are shown in table 2.9.

Table 2.9 The values used in the preparation of the MnO_2 catalysts.

Catalyst ratio.	Mass $Mn(NO_3)_2.6H_2O$ (g)	Mass $NH_4\ HCO_3$ (g)
5:1	10	0.8836
5:2	10	1.7672
5:3	10	2.6508

2.1.11 Cobalt, iron and manganese oxides

Cobalt, iron and manganese oxides were prepared by a calcination of their respective nitrate in static air, at 300°C for 2 hours (cobalt (II) nitrate hexahydrate, iron (III) nitrate nonahydrate and manganese (II) nitrate hexahydrate). These will be referred to as the 5:0 ratio as no ammonium bicarbonate was involved.

2.2 Characterisation

2.2.1 Brunauer Emmet Teller (BET) surface area determination

The BET theory is based on the analysis of the physical adsorption of gas molecules on a solid surface and was developed in 1938 by Stephen Brunauer, Paul Hugh Emmett and Edward Teller [1]. In the case of surface area measurements, nitrogen gas is used at 77K and non specific physisorption takes place. The nature and mass of the sample under analysis and the adsorbent pressure determines the amount of gas adsorbed. This equation is used if the analysis gas is below its critical temperature:

$$n/m = f\,(p/p^{o})_{T}$$

p^{o} = saturation pressure of adsorbent at T.

n = amount of gas adsorbed.

m = mass of solid.

p = pressure.

T = temperature.

The BET isotherm is an extension to the Langmuir adsorption isotherm. The Langmuir isotherm is based on only one monolayer of adsorption occurring and is based on the following assumptions: only one adsorbed molecule per site is allowed, the enthalpy of adsorption is the same for all sites and finally the adsorption at each site is independent of the surrounding sites.

The BET isotherm allows multilayer adsorption with the following assumptions: gas molecules can physically adsorb on a solid in layers

infinitely, there is no interaction between each adsorption layer and the Langmuir theory can be applied to each individual layer.

Different experimental points are plotted to represent each adsorption isotherm. To measure the amount of gas adsorbed there are different methods, including a differential flow technique and gas adsorption gravimetry. In this case differential gas adsorption manometry is used.

There are 6 different adsorption isotherms [2], which are shown in figure 2.1:

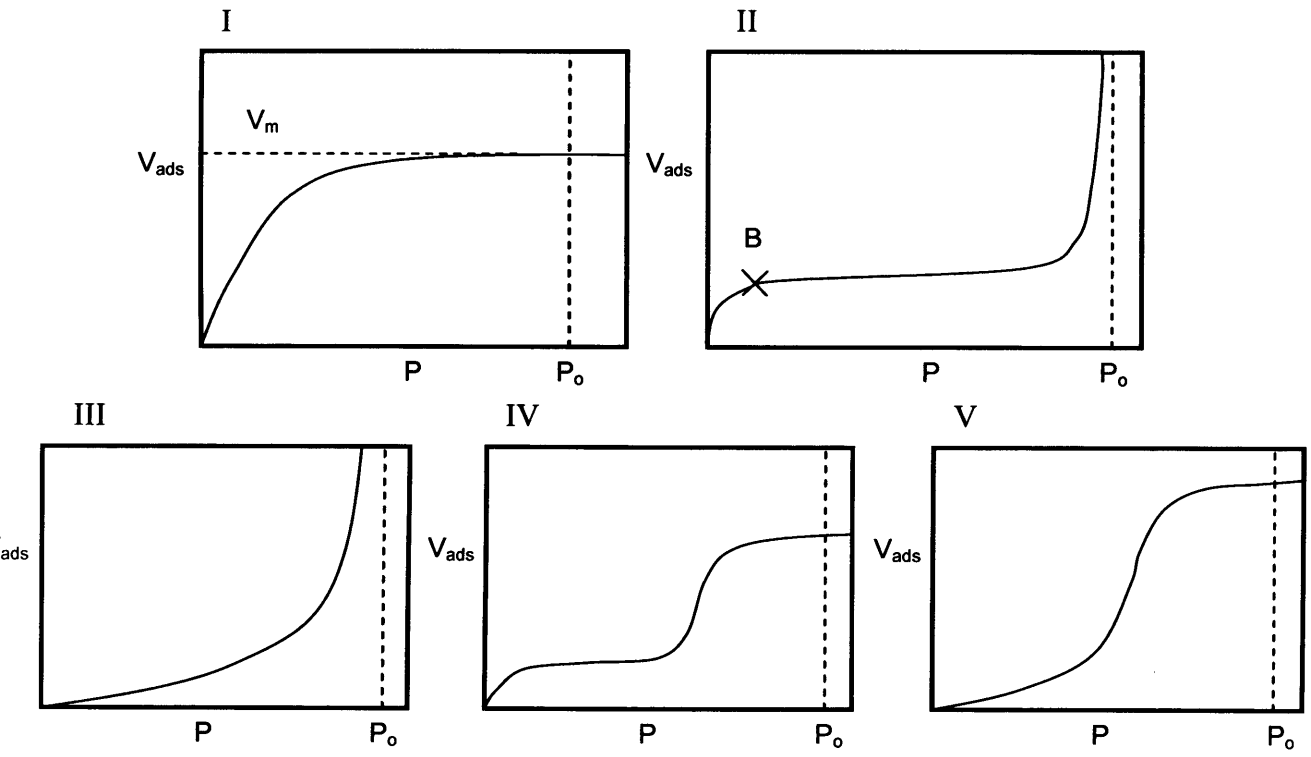

Figure 2.1 The adsorption isotherms.

An adsorption isotherm is a plot of the equilibrium amount of a substance adsorbed against the pressure of the adsorbing substance (gas phase) measured at a constant temperature.

The BET equation is applied only to type II (and IV) isotherms where point B can be determined (an estimation of the amount of adsorbate required to cover the unit mass of the solid surface with one complete monolayer). Once an isotherm is obtained, a BET plot needs to be made, allowing the determination of the monolayer capacity (n_m) and therefore $a_{(BET)}$ otherwise known as the specific surface area.

Linear form of BET equation:

$$\frac{p/p^o}{n\,(1-p/p^o)} = \frac{1}{n_m C} + \frac{C-1\ (p/p^o)}{n_m C}$$

C = BET constant.

Corrections are made due to 'n' being unable to be determined by the ideal gas law. This is due to N_2 not showing ideal behaviour at the temperatures and pressures used. A plot made from the BET equation should show a linear relationship. The plots are normally of the range (p/p^o)= 0.05 - 0.35 with 5 points from the isotherm (1 or 3 points can also be measured). If the plot is non-linear and there is no line of best fit then the data is invalid for analysis by the BET method.

The value of C obtained gives an indication of the data validity. For example:

- point B is well defined when C is high (> 350), and the pressure corresponding to the monolayer coverage is low ($(p/p^o) < 0.05$).
- point B is ill defined when C is low (< 20), and the pressure corresponding to the monolayer coverage is high ($(p/p^o) > 0.18$).

The monolayer capacity obtained from the BET plots allows the specific surface area of a solid to be determined using the equation below:

$$a_{(BET)} = n_m L \sigma$$

L = Avogadro's constant.

σ = average area occupied by adsorbent gas (for N_2 this is 0.162 nm^2).

The final value of surface area (m^2/g) is then given by dividing $a_{(BET)}$ by the sample weight.

2.2.1.1 Equipment

A Micrometrics Gemini 2360 Analyser was used to measure BET surface areas. The samples were de-gassed for 2 hours at 120°C, to remove water and any physisorbed or chemisorbed compounds, by heating under a Henot vacuum.

The system was evacuated and then the sample was dosed with a controlled volume of the adsorptive gas to a particular pressure and allowed to reach

equilibrium. The gas was adsorbed and the process repeated at different pressures to obtain the adsorption isotherm.

2.2.2 Powder X-ray Diffaction (XRD)

X-ray diffraction is a useful technique in identifying crystalline phases within the catalyst by structural parameters. This technique also allows an indication of particle size to be obtained [3].

The process itself involves the elastic scattering of X-ray photons by atoms in the periodic lattice. When monochromatic radiation illuminates a sample, reflections are only observed if the scattered monochromatic X-rays are in phase giving constructive interference. This is because the Bragg condition is satisfied. If the X-rays are out of phase there is destructive interference and the Bragg condition is not met. In other words, lattice planes at the Bragg angle will diffract the incident beam. The angle between the diffracted and undiffracted beams is 2θ.

The Bragg equation; $n\lambda = 2d\sin\theta$

n = an integer, (the order of reflection).

λ *= the wavelength of the x-rays.*

d = the interplanar distance.

θ *= angle between the incoming x-ray and the normal to the reflecting lattice plane.*

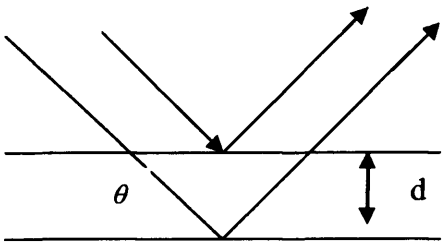

Figure 2.2 The basis of Bragg's Law.

It is important that the sample is finely ground so that crystals of every orientation are present, at every possible angle to the incident beam. This allows the Bragg condition to be met for every lattice plane and every possible allowed reflection. Factors that need to be considered before carrying out XRD are:

1) The sample must be crystalline – packing of sample must be random and have a uniform flat surface;
2) XRD is a bulk analysis technique;
3) The data is averaged over a relatively large sample area; and
4) The crystallite size is limiting, diffraction not detected for below 20-50 Å.

Lattice spacings are derived from the Bragg equation and these are unique for a particular compound. Diffraction patterns identify crystallographic phases present in the catalyst. X-ray diffraction does not detect particles that are too small or amorphous. This can result in phases not being detected, which can sometimes be the phase with catalytic activity.

X-rays were produced by high energy particles colliding with matter and energy transferred to form electromagnetic radiation. This resulted in white radiation that cannot be used in XRD as it is necessary for the radiation to be monochromatic. The solution to this was for the incident high energy electrons to strike a copper target. Ionisation of some 1s electrons, in the K shell, occurred and an electron in an outer orbital dropped down to occupy the vacant level. The excess energy was emitted as x-rays. There were two transitions possible, 2p to 1s, or 3p to 1s, resulting in k_α and k_β respectively. K_α was more frequent and more intense than k_β. It occurred as a doublet because there is a difference in energy between the spin states of 2p and 1s levels.

A heated tungsten element emitted the electrons, which were accelerated through a vacuum to strike the target. Within the tube X-rays were generated and the tube was shielded with lead. Beryllium windows were in place to direct the beams. To stop the target melting, due to conversion of energy to heat, a water cooling system was necessary. The operating conditions of the XRD were 30mA and 40kV.

A Ge (III) single crystal monochromator was used to select K_α radiation, so that removal of k_β and white x-ray contributions was possible. An X-ray scintillation counter was used and position sensitive detectors with an angle of 120° covered. A current was detected on a knife-edge placed on the circumference of the focusing circle. The time difference between the ends was used to calculate the position. This enabled fast data collection.

When the X-ray diffraction pattern has been collected, the full width half maximum values for peaks can be used to calculate the average crystallite size, in the material, using the Debye-Scherrer equation. The peak broadening was referenced to a silicon standard.

$$\text{Crystallite size} = (K\lambda) / (FWHM\cos\theta)$$

K= Scherrer constant

λ= Wavelength

FWHM= Full width half maximum of peak

θ = Diffraction angle

2.2.2.1 Equipment

XRD analysis was carried out on an Enraf Nonius FR590 sealed tube diffractometer with a rotating sample holder. The sample was placed in an aluminium holder, which was allowed to spin in the centre of the focusing circle. The diffracted x-rays were focused on the circumference of the circle, where the detector was mounted. Each sample was run for 30 minutes. Peak positions were determined and lists of d-spacings with relative intensities were obtained. XRD patterns were calibrated against a silicon standard and phases were identified by matching experimental patterns to JCPDS powder diffraction files.

2.2.3 Raman Spectroscopy

In Raman spectroscopy [3], an intense monochromatic light source (laser) is directed at the sample and it is the frequency of the reflected light that is analysed to determine the molecular structure of the material. The majority of light passes straight through or is elastically scattered from the sample, which is known as Rayleigh scattering. Photons losing energy, in the interaction of light with the sample, have a lower frequency than the incident light, known as Stokes scattering. Photons with a gain in energy from the interaction have a higher frequency than the incident light source, known as anti-Stokes scattering. It is worth noting that anti-Stokes scattering can only occur when the molecule is in an excited state and are therefore of a much lower intensity due to the proportion of excited molecules being much smaller than those in the ground state.

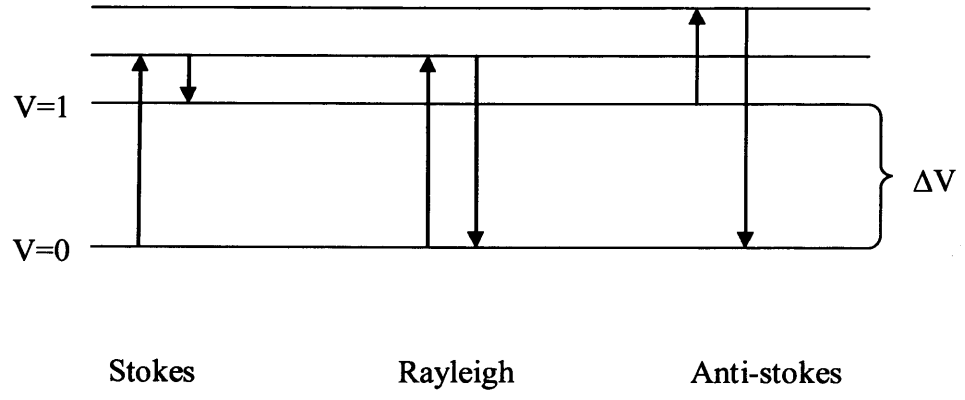

Figure 2.3 The basis of Raman spectroscopy.

In the Raman spectrum, there are lines due to rotational and vibrational transitions which occur in the IR region of electromagnetic radiation. However, it should be noted that there are definite differences between Raman and IR spectroscopy. The selection rule for Raman to take place is that a molecular vibration or rotation must result in a change in polarisability of the molecule.

2.2.3.1 Equipment

A Renishaw Ramanscope instrument was used to obtain Raman spectra, with a silicon standard for reference. Green argon ion lasers (514.5nm) were used as a source of monochromatic radiation, operated at 20mW, with a known frequency and wavelength. Only light scattered at 180° to the incident beam goes to the detector requiring it to be very sensitive, with 10 accumulations per 100 seconds. A computer manipulates charges from the detector to give an electronic image.

The sample was placed on a stage where the white light was focused. Beam splitters in the light path switched the white light to the laser light and the scattered light returned to the spectrometer where computer software enabled a spectrum to be obtained.

The heat from the laser may damage the sample and the sample may be Raman inactive. The main problem with Raman spectrometry is fluorescence. This occurs when the laser frequency promotes electrons to the lowest electronic energy levels, which are close to the highest vibrational levels. The electron energy decays from the excited state to the vibrational ground state

giving multiple transitions. To avoid this, a laser of a different frequency can be used or the addition of an inorganic salt will allow the alteration of the d-d transition levels.

2.2.4 Scanning Electron Microscope (SEM) and Energy Dispersive X-ray Analysis (EDX)

SEM uses electrons rather than light to form a 3-D image of the catalyst sample with the size of particles and morphology being examined [4]. An electron beam, generated from a tungsten filament, is generated in the electron gun under ultra-high vacuum (UHV). This beam is attracted through an anode, condensed and focused to a very fine point on the sample by an objective lens. A magnetic field is generated so the beam hits the sample in a controlled pattern. SEM is always carried out under ultra-high vacuum otherwise the electron beam would not be stable. There are many advantages to using this technique:

1) A large depth of field allows a large amount of sample to be focused at one time;
2) Images are of high resolution; closely spaced features can be examined at high magnification (nanometre scale); and
3) Preparation of sample is relatively easy.

EDX analysis is used in conjunction with SEM analysis. The process allows determination of the elemental composition and chemical characterisation of the catalytic material. When an atom is bombarded with a beam of electrons,

electrons are ejected from the atoms which make up the sample surface. The resulting electron vacancy is filled by an electron in a higher shell and an X-ray is emitted to balance the energy difference between the two electrons.

Each element gives different characteristic X-rays which determines the elemental composition of the sample. However, only a small sample is studied at one time so several areas of the sample need to be analysed to enable an accurate chemical composition to be deduced.

2.2.4.1 Equipment

For SEM, a Carl Zeiss EVO-40 instrument was used with BSD, SED and Oxford instruments EDAX detector. The catalyst sample was mounted on carbon lite adhesive pads which were attached to aluminium sample studs. An accelerating voltage of 20-25 keV was used.

2.2.5 Temperature Programmed Reduction (TPR)

TPR determines the reducibility of a material as a function of temperature. The process is an adaptation of a temperature programmed gas chromatograph. The modifications made have allowed reduction processes to be monitored while the temperature is increased linearly with time.

At the critical temperature, hydrogen reacts with the sample to form H_2O, which is removed by the cold trap (mixture of liquid nitrogen and isopropanol). The amount of hydrogen in the sample decreases therefore the proportion

between the carrier gas and the reactant alters and this affects the thermal conductivity. The detector signal gives a measure of the hydrogen content before and after the reaction.

2.2.5.1 Equipment

The TPR equipment required a gas handling system, thermal conductivity cell and associated electronics, linear temperature programmer, recorder, sample holder, furnace and cold traps. A Thermo 1100 TPD/R/O instrument was used with a TCD detector. The sample (0.05-0.1g) was placed in a quartz tube, with quartz wool plugs, in an electric furnace where a linear temperature programmer controlled the temperature. The temperature range of 30-900°C was explored with a ramp rate of $10^{o}Cmin^{-1}$. A gas stream of known composition (10%H_2 in Ar with a flow rate of 50 mL min^{-1}) passed through one arm of the thermal conductivity cell, then through the reactor and finally through a series of traps. The other arm of the thermal conductivity cell was monitored by a change in the hydrogen concentration of the gas stream which was brought about by any reduction process.

The gas flow remained constant therefore the change in hydrogen concentration was proportional to the rate of catalyst reduction. Distinct reducible species in the catalyst showed as peaks in the TPR spectrum on the recorder. The area under the TPR curve was equivalent to the hydrogen consumption (moles of hydrogen consumed per mole of metal atoms). The technique also allowed the temperature required for complete catalyst reduction to be obtained.

2.2.6 Pulsed CO chemisorption

The dispersion of a metal on a support is important and is determined by a pulse chemisorption measurement. With an increased dispersion of a metal, an increase in the catalysts activity is normally observed due to a larger number of active sites. The dispersion of a particular metal can be determined using hydrogen or carbon monoxide, but the latter is more commonly used.

Pre-treatment involves oxidation and reduction at high temperatures to clean the metal surface. After this step, the sample is cooled and pulsed with CO gas. The CO is pulsed until the pulse value remains constant. The initial pulse area obtained is subtracted from the final pulse area to give the value of chemisorption.

2.2.6.1 Equipment

A micrometrics Autochem 2910 instrument was used with a thermal conductivity detector. Only the palladium dispersion was determined by this technique. A temperature of 35°C, argon flow of 20ml min^{-1} and pulses of 0.35ml of 10% CO in argon were used. Before the CO uptake was determined, all samples were treated under flowing hydrogen (50 ml min^{-1}) at 500°C and then flushed with argon (20 ml min^{-1}) for 60 minutes. In order to calculate the metal dispersion, an adsorption stoichiometry of Pd/CO = 1 was assumed.

2.2.7 X-ray Photoelectron Spectroscopy (XPS)

XPS is a technique used to determine elemental composition, oxidation states of the elements and dispersion of different phases in the material.

XPS is based on the photoelectric effect where an atom absorbs a photon, of energy hv, and a core electron, with binding energy E_b, is ejected with a kinetic energy.

$$E_k = hv - E_b - \Phi$$

E_k = kinetic energy of photon

h = Planck's constant

v = Frequency of exciting radiation

E_b = Binding energy

Φ = Work function of spectra

XPS measures the intensity of the photoelectrons produced, N(E), as a function of the kinetic energy, which can be plotted as a graph but more frequently N(E) is plotted against the binding energy.

When observing the spectrum obtained there will be expected photoelectron peaks but also Auger electron peaks due to the de-excitation of photo ions by an Auger transition. Auger electrons have fixed kinetic energies independent of the X-ray energies therefore when plotted on the binding energy scale they have no significance. The spectrum is recorded at two different X-ray energies as the XPS peaks will have the same binding energy but the Auger peaks will

shift. Once the Auger peaks have been identified any overlaps between the XPS and Auger peaks can be avoided. The photoelectron peaks are labelled according to quantum number of the level from which the electron originated.

The binding energy increases with increased atomic number and increased oxidation state. Each set of binding energies is characteristic of one particular element. XPS is a surface sensitive technique where it is more sensitive to those atoms at the surface than in the bulk of the material. Electrons have to escape the material without loss of energy therefore inelastic electron scattering is not allowed.

2.2.7.1 Equipment

A Kratos Axis Ultra DLD Spectrometer using monochromatised Al K_{α} radiation and analyser pass energies of 160eV (survey scans) or 40eV (detailed scans) was used. Binding energies were referenced to the C (1 s) peak from adventitious carbonaceous contamination, assumed to have a binding energy of 284.7eV. Electrons are slowed or accelerated to a 'pass' energy which then pass through a filter. A lower pass energy results in a small number of electrons passing through to the detector but a more precise determination of their energy is obtained. Attached to the detector is an electron multiplier which can amplify the incoming photons to create a measurable current.

2.3 Catalyst testing

2.3.1 Propane BOC reactor

A fixed bed laboratory micro-reactor was used to test the catalytic activity. The powdered catalyst (0.05g) was placed in a stainless steel reactor tube ($^1/_4$" o.d.) and supported by silica wool plugs, packed to a constant volume. The reactor feed contained propane in air (BOC, 1.5%), and helium (BOC) with a total flow rate of 50mL min^{-1}. Heating tape was applied to all the lines running to and from the reactor to ensure that the samples remained gaseous for the chromatography to be efficient and accurate.

The samples were analysed every ten minutes, in the temperature range 100-400°C, using Varian Star software, to give a chromatograph with signal intensity plotted against time. The temperature was measured by a thermocouple placed in the catalyst bed. The computer software allowed analysis of the products during the run. The peaks were then integrated to give the percentage conversion of the VOC:

$$\text{Percentage Conversion, \%} = \frac{\text{integral of peak}}{\text{GHSV}} \times 100$$

Conversion data was calculated by the difference in inlet and outlet concentrations. The carbon balances were in the range of 100 +/-10%. The Gas Hourly Space Velocity (GHSV) for each run was the volume of gas per hour (ml) over the amount of catalyst (ml) at standard temperature and pressure. In this case it was 60000h^{-1}.

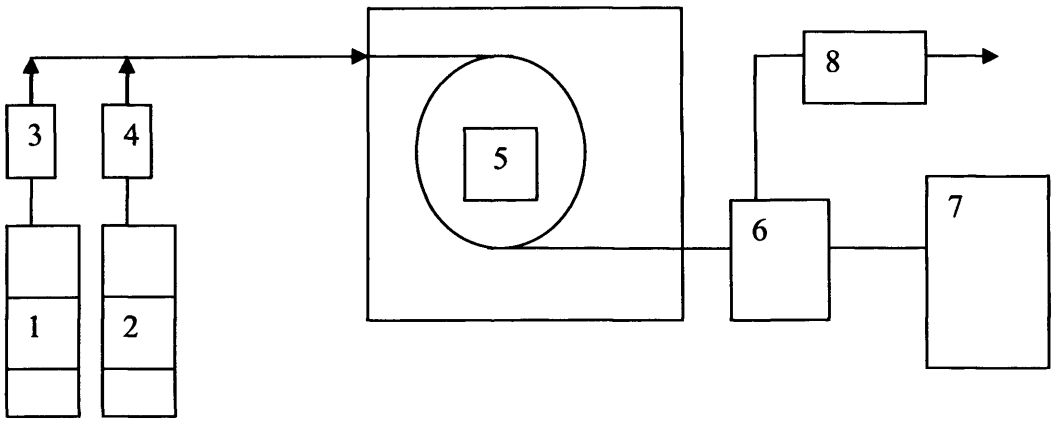

1= Helium supply, 2= Propane (1.5%)/air supply, 3= Helium MFC,

4= Propane/air MFC, 5= Gas Chromatograph, 6= TCD and FID detectors,

7= Computor. 8= Waste gases to fume hood.

Figure 2.4 The arrangement of the BOC propane reactor.

2.3.2 Selective propane oxidation

Catalytic performance was measured using a fixed bed laboratory micro-reactor at atmospheric pressure. For each experiment, powdered catalyst (0.25g) was placed in a $^1/_4$" o.d. quartz reactor tube. The reactor feed contained propane (BOC), oxygen (BOC) and helium (BOC). The propane/oxygen/helium ratio was 2/1/8.5 with a total flow rate of 40 mL min^{-1}. Catalysts were packed to a constant volume to give a constant gas hourly space velocity of 9600 h^{-1}.

The reactants and products were analysed by an online gas Varian 3800 chromatograph using Porapak Q and molsieve columns, with thermal

conductivity and flame ionisation detectors. The temperature range of 100-450°C was explored and the reaction temperature was measured by a thermocouple placed in the catalyst bed. The differences between the inlet and outlet concentrations were used to calculate conversion data, and all carbon balances were in the range 100±10 %. Analyses were made at each temperature until steady state activity was attained, and three analyses were taken and data averaged. Blank experiments were conducted in an empty reactor which showed negligible activity over the temperature range used in this study.

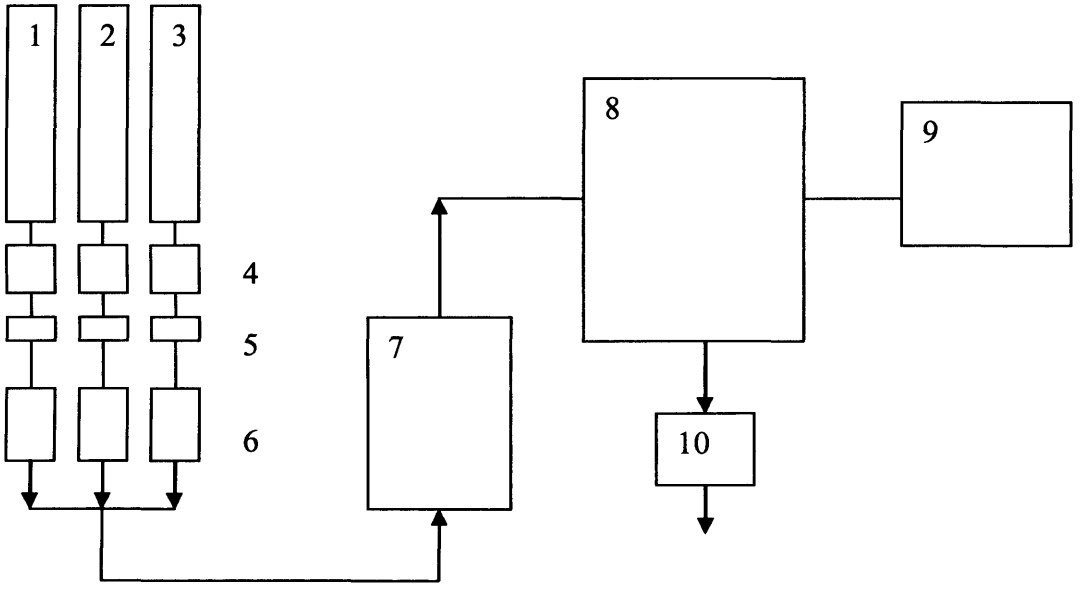

1= Helium cylinder, 2= Oxygen cylinder, 3= Propane cylinder, 4= 7 Micron filter, 5= Back pressure regulators, 6= Mass flow controllers, 7= Reactor (catalyst bed and carbolite tube furnace),

8= Gas chromatograph, 9= Computer, 10= Waste gases to fume hood.

Figure 2.5 The arrangement of the reactor for the selective oxidation of propane.

2.3.3 Methanol oxidation

Catalytic performance was measured using a fixed bed laboratory micro-reactor at atmospheric pressure. For each experiment, powdered catalyst (0.5g) was placed in a $^1/_4$" o.d. quartz reactor tube. The reactor feed contained 12% vapour pressure of liquid methanol (Fisher Scientific, HPLC grade), oxygen (BOC) and helium (BOC). The methanol/oxygen/helium ratio was 3.6/5.4/30 with a total flow rate of 39 mL min^{-1}. Catalysts were packed to a constant volume to give a constant gas hourly space velocity of 4680 h^{-1}.

The reactants and products were analysed by an online gas Varian 3800 chromatograph using Porapak Q and molsieve columns (95°C), with thermal conductivity and flame ionisation detectors (175°C). The temperature range 50-450 °C was explored and the reaction temperature was measured by a thermocouple placed in the catalyst bed. The differences between the inlet and outlet concentrations were used to calculate conversion data, and all carbon balances were in the range 100±10 %. Analyses were made at each temperature until steady state activity was attained, and three analyses were taken and data averaged. Blank experiments were conducted in an empty reactor which showed negligible activity over the temperature range used in this study.

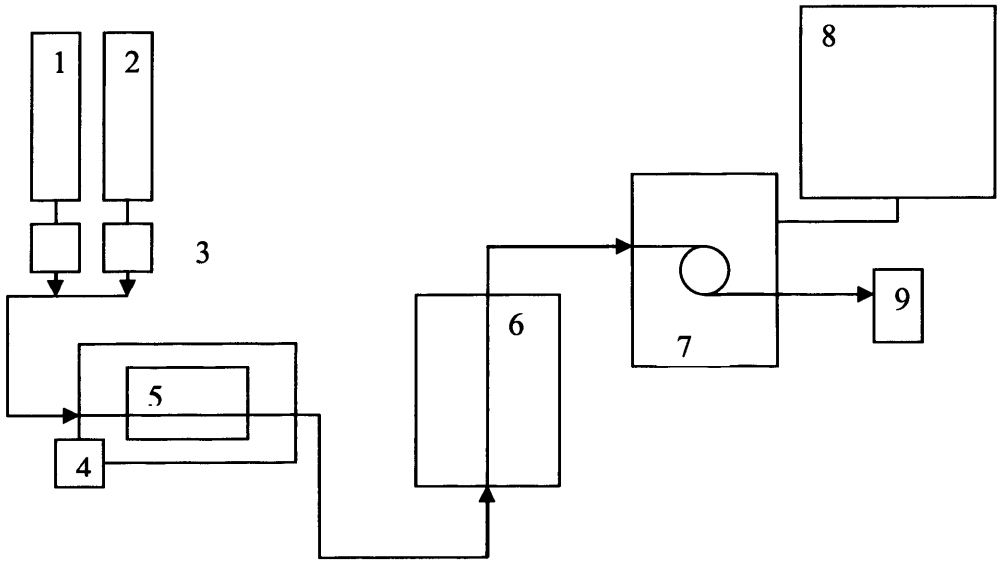

1= Helium cylinder, 2= Oxygen cylinder, 3= Mass flow controllers, 4= Water bath, 5= Liquid methanol, 6= Reactor (carbolite tube furnace and catalyst bed), 7= Gas chromatograph, 8= Computer, 9= Waste gases vented to fume hood.

Figure 2.6 The arrangement of the reactor for the selective oxidation of methanol.

2.3.4 Sample delivery

For all reactors, sample delivery and the GC oven temperature were programmed together to allow separation of the reactants and products. The oxidation of propane (complete and selective) had run times of 20 minutes and the oxidation of methanol had run times of 50 minutes. To separate the reactants and products two columns were present called the molsieve and Haysep/Porapak Q. The bypass configuration of the valve separated the CO_2 efficiently to prevent it irreversibly adsorbing onto the molsieve column which would have resulted in deactivation.

2.3.5 Data analysis

Calibration of all gases was carried out by injecting known amounts into the columns and graphs were plotted (see appendix). Response factor (RF) values were required to convert counts of each product found in the gas chromatograph into 'real' values. The RF values of each component were found from the gradient of the corresponding calibration chart. The calibration of the different systems was carried out regularly to ensure accurate analysis.

Once counts of each component were inserted into a spreadsheet conversions of propane or methanol were calculated. The method of calculating conversion was based on products, as low conversions were observed and this was the most accurate method.

$$\frac{\text{Initial counts of } H_c - \text{Final counts of } H_c}{\text{Initial counts of } H_c} \times 100 = \text{Conversion}$$

Selectivity was calculated by the following formula:

$$\frac{\text{Counts of A}}{\text{Sum of total product counts}} \times 100 = \text{Selectivity to A}$$

When calculating the proportion of different products it was necessary to account for different numbers of carbon present. For example, when calculating the selectivity of CO_2 or CO the counts were divided by 3 as they had only one carbon atom. For propene or other C_3 products no division was

required. At each temperature, an average of three runs was taken and an error value was calculated to be +/- 2% on average. Carbon balances were in the range of 95-105%.

2.4 References

[1] S. Brunauer, P. H. Emmett, E. Teller, *J. Am. Chem. Soc.*, **60** (1938) pp. 309.

[2] E. M. McCash, *Surface Chemistry*, Oxford University Press (2002).

[3] P. W. Atkins, *Physical Chemistry*, Oxford University Press, 6th Edition (2001).

[4] J. Goldstein, D. E. Newbury, D. C. Joy, P. Echlin, C. E. Lyman, E. Lifshin, L. Sawyer, *Scanning Electron Microscopy and X-ray Microanalysis*, 3rd Edition (2002).

Chapter 3

CHAPTER 3

Deep oxidation of propane using bimetallic catalysts on a titania support

3.1 Introduction

There has been increasing concern for the environment due to the emission of pollutants into the atmosphere. Volatile organic compounds (VOCs) are considered atmospheric pollutants [1] and are often present in low concentrations in many industrial gas exhaust systems. Legislative pressure is increasing on the permitted levels of VOCs that can be discharged to the atmosphere. For example, in Europe, the Gothenburg Protocol stated there must be a 40 % reduction in VOC emissions by 2010 [2]. VOCs are chemically diverse, but some of the most common and difficult to control are short chain alkanes.

The use of catalytic oxidation can allow careful control of VOC emissions and provide a cost effective route for VOC control. Thermal incineration of VOCs is an alternative route, but it is unfavourable due to the involvement of higher temperatures and the potential formation of noxious by-products, such as NO_x [3] and dioxins [4]. In contrast, the catalytic oxidative destruction of VOCs results in the formation of carbon dioxide and water more selectively [5]. Although carbon dioxide is a greenhouse gas it is preferable to the presence of VOCs in the atmosphere.

Pd-supported catalysts have been reported as some of the best catalysts for methane oxidation [6]. γ-Al_2O_3 has been extensively used as a support for such catalysts and industrial VOC oxidation catalysts, and this is mainly due to low manufacturing cost. Despite the extensive use of Pd supported γ-Al_2O_3 catalysts for the catalytic combustion of VOCs, various studies [2, 6, 7, 8, 9] have shown that other metal oxide supports, such as TiO_2, ZrO_2 and SnO_2, were more appropriate supports than γ-Al_2O_3 in the oxidation of hydrocarbons. In general, it has been proposed that the oxidation state of palladium is related to the activity of the supported catalyst, and that partially oxidized palladium is effective for propane combustion [10]. Hence the choice of support is crucial for the effectiveness of a VOC oxidation catalyst. Another important parameter which determines the activity of a VOC oxidation catalyst is the presence of a second active component that acts as a modifier.

Modifiers are generally added to promote activity and enhance resistance to deactivation. Thus, different promoters, such as vanadium [11], niobium [12], cobalt [13], cerium [14], lanthanum [15] and tungsten [16] are known to promote the activity of metal-supported catalysts for VOC oxidation. These studies have mainly been focussed on the modification of Pd-alumina catalysts, and have proposed different theories to account for the promotional effect on the oxidation of alkanes and mono-aromatics. In brief, the positive role of the different promoters in the case of short chain alkanes has generally been accounted for by different parameters, such as palladium particle size, catalyst reducibility and the Pd^0/Pd^{2+} surface ratio.

The catalytic activity of niobium-modified palladium-alumina catalysts has been previously reported in alkane combustion, showing a better performance than a Pd/Al_2O_3 catalyst [12]. These results were correlated with the presence of NbO_x species in intimate contact with palladium; and this led to partially oxidized palladium particles, which are a prerequisite for catalysts active for the combustion of propane [10].

The performance of a platinum catalyst was found to improve when it was dispersed onto a TiO_2 support doped with W^{6+} cations [16]. Doping and the metal particle size have an effect on catalytic activity. Platinum supported on titania with W^{6+} was more active than on gamma-alumina [17]. Due to the success with platinum, the investigation of the effect upon activity with palladium was carried out.

This chapter involved titania supported palladium catalysts modified by niobium and tungsten. A range of catalysts with varying loadings of Nb and W, from 1% to 6%, and Pd loadings, from 0.5% to 2%, on a titania support were prepared. Their activity for the deep oxidation of propane was studied and various characterisation techniques were employed to determine the active species present. This chapter has been published as a paper by Applied Catalysis A: General (see paper 1 in publications section).

3.2 Catalyst characterisation of niobium catalysts

3.2.1 BET surface area determination

The BET surface areas of the different titania catalysts were obtained using the procedure shown in the experimental chapter (2.2.1). Table 3.1 shows the surface areas for titania catalysts loaded with palladium and/or niobium.

Table 3.1 BET surface areas of Pd and Nb on a titania support.

Catalyst.	Surface area (m^2g^{-1}).
TiO_2	50
0.5%Pd/TiO_2	46
2%Pd/TiO_2	46
0.5%Pd/1.0%Nb/TiO_2	50
0.5%Pd/2.0%Nb/TiO_2	49
0.5%Pd/3.0%Nb/TiO_2	47
0.5%Pd/6.0%Nb/TiO_2	46
1.0%Pd/3.0%Nb/TiO_2	47
2.0%Pd/3.0%Nb/TiO_2	46
6.0%Nb/TiO_2	49

The surface area of the titania support was 50 m^2g^{-1} and this was slightly reduced by the addition of palladium and niobium as expected. This can be attributed to the filling of pores in the titania support as the metal species were added. The difference in porosity of these catalysts is the main factor determining their surface areas.

3.2.2 Powder X-ray Diffraction (XRD)

The powder XRD patterns of catalysts with different loadings of Pd and Nb on a titania support are shown in figures 3.1 and 3.2. The main crystalline phases of TiO_2 identified correspond to anatase and rutile, but mainly anatase. The relative amounts of these crystalline phases were not modified by the addition of palladium and niobium. Moreover, no peaks corresponding to Nb crystalline phases have been identified. This could be attributed to the presence of low concentrations of these species or the high dispersion of crystallites that are too small to be detected.

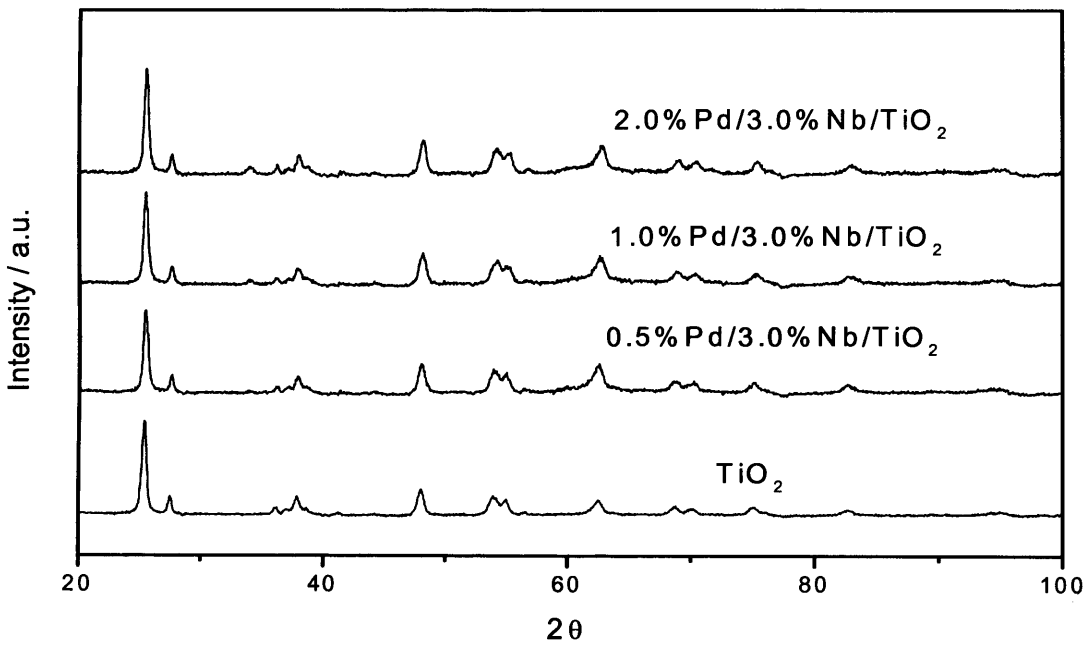

Figure 3.1 The XRD profiles of varying Pd loadings with constant Nb loading, on a titania support.

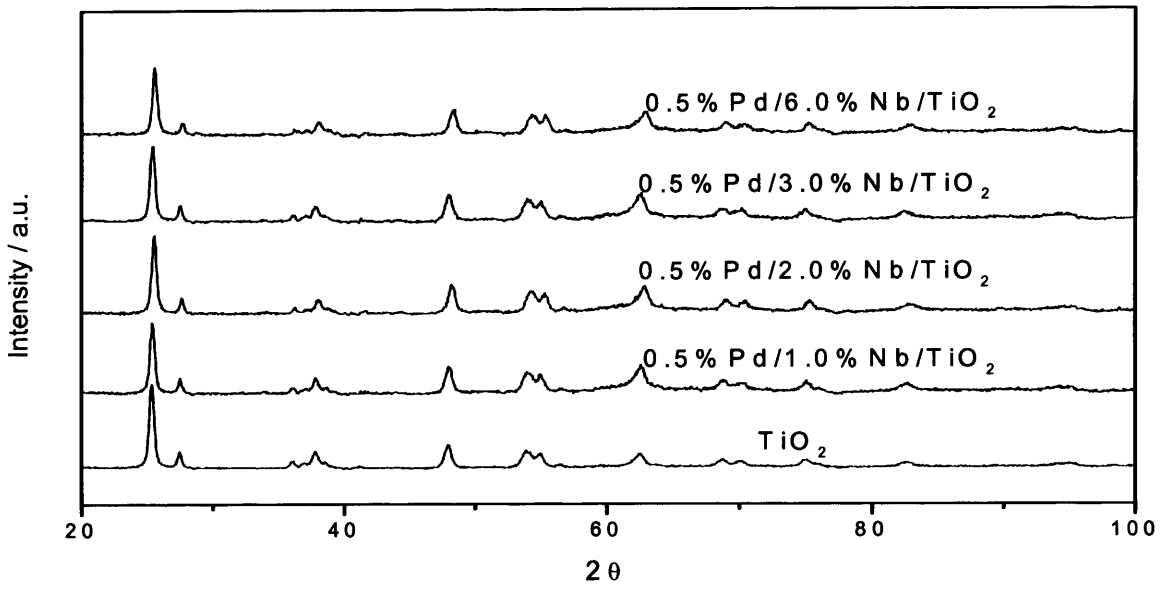

Figure 3.2 The XRD profiles of constant Pd loadings with varying Nb loading, on a titania support.

The Scherrer equation was used to calculate the average crystallite sizes of the catalysts. These values are reported in table 3.2. It is evident from the experimental data that the addition of niobium to the Pd/TiO_2 catalysts led to the formation of similar sized crystallites, independently of the Nb and/or the Pd loading. Thus, it can be suggested that the addition of niobium seems to stabilize an average crystallite size in the promoted catalysts. Diffraction peaks corresponding to metallic Pd were not detected in any catalyst.

Table 3.2 Average crystallite sizes for the different loadings of Pd and Nb on a titania support (n.d. = not detected)

Catalyst	Average crystallite size (nm)
0.5%Pd/TiO_2	n.d.
0.5%Pd/1.0%Nb/TiO_2	n.d.
0.5%Pd/2.0%Nb/TiO_2	13
0.5%Pd/3.0%Nb/TiO_2	14
0.5%Pd/6.0%Nb/TiO_2	13
1.0%Pd/3.0%Nb/TiO_2	13
2.0%Pd/3.0%Nb/TiO_2	14

3.2.3 Raman Spectroscopy

Figures 3.3 and 3.4 show the Raman spectra recorded from 0 to 3500 cm^{-1} for Pd and Nb on a titania support.

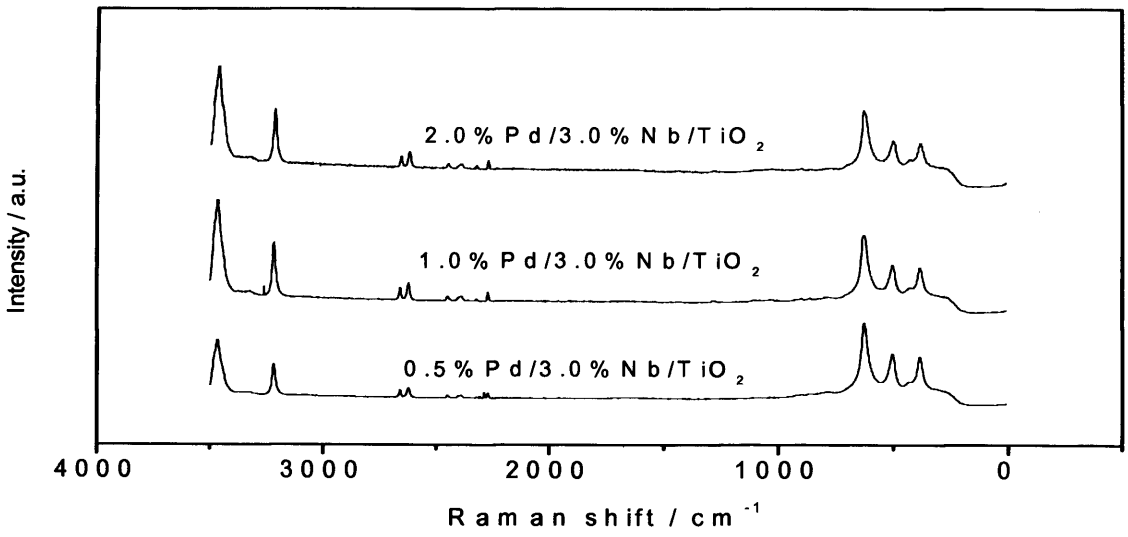

Figure 3.3 The Raman spectra of varying Pd loadings, with constant Nb loading, on a titania support.

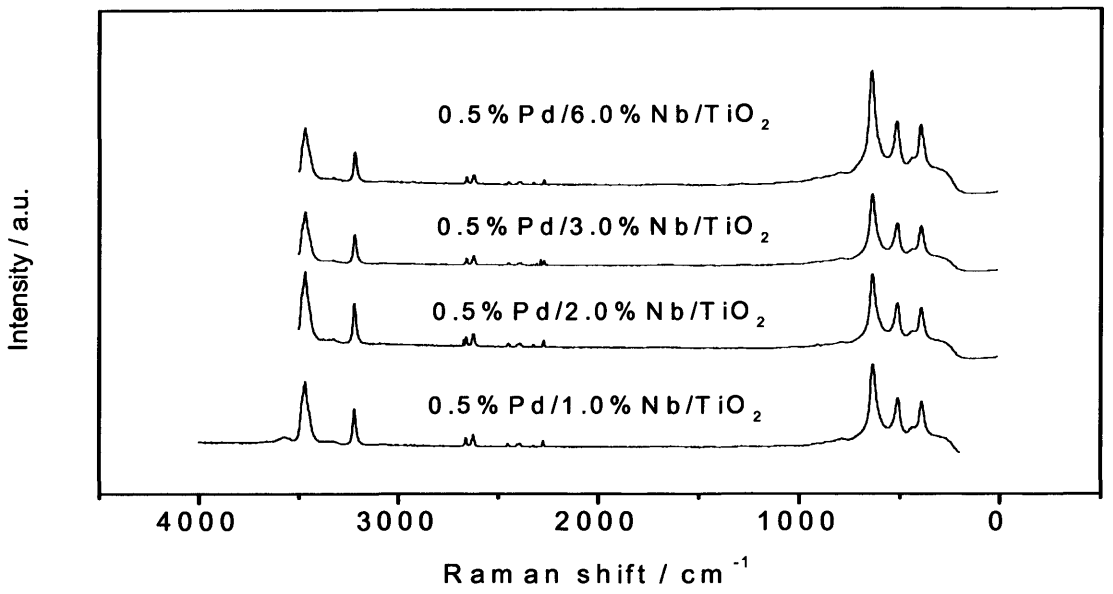

Figure 3.4 The Raman spectra of constant Pd loadings, with varying Nb loading, on a titania support.

Peaks at *ca* 650, 500, 400 cm^{-1} are characteristic of titania in its anatase phase, whilst peaks observed at 447 cm^{-1} and the shoulder at *ca* 605 cm^{-1} are ascribed to rutile [18]. The addition of the metal oxide on the titania support did not modify significantly the relative intensities of these bands, indicating that the structural composition of the support was not affected by the deposition of the supported phase. However, it is noteworthy that whilst the addition of either palladium or niobium alone does not lead to any displacement of the TiO_2 band when compared to the support alone, the co-addition of niobium and palladium to the titania shifts the anatase bands to lower frequencies by *ca* 10 cm^{-1}. This observation indicated that weaker Ti-O bonds were present in NbPd-catalysts. It has previously been noted by Kovalenko et al [19] that the addition of niobium to Pd/TiO_2 catalysts led to the generation of defects on the support surface. Thus, the shift of the Raman

bands was probably due to the shift of charge density from the support to either supported niobium or palladium species.

Raman spectra of $Pd/Nb/TiO_2$ catalysts showed no evidence for the presence of Nb_2O_5 crystallites, which would be indicated by a band at *ca* 675 cm^{-1} [20] for hexagonal Nb_2O_5, or a band at *ca* 260 cm^{-1} [18] for monoclinic Nb_2O_5 [21]. In addition, the detection of niobic acid ($Nb_2O_5 \cdot nH_2O$) with a wide band at *ca* 650 cm^{-1} [21] was hindered by masking due to the presence of a large band at 636 cm^{-1} due to the anatase phase.

3.2.4 Temperature Programmed Reduction (TPR)

TPR profiles for the $Pd/Nb/TiO_2$ catalysts are shown in figures 3.5 and 3.6.

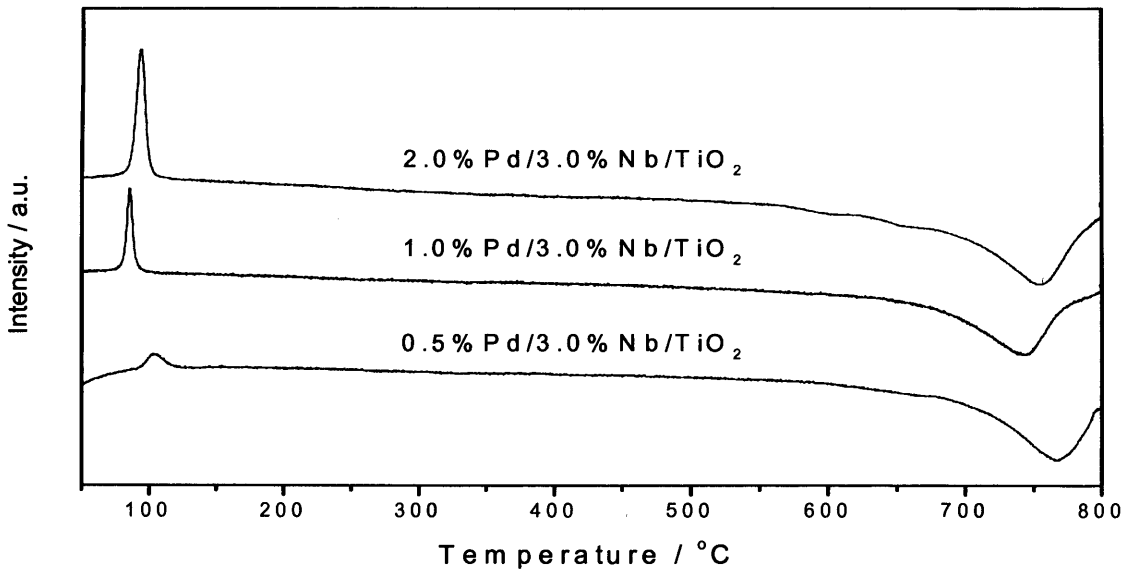

Figure 3.5 The TPR profiles of varying Pd loadings, with constant Nb loading, on a titania support.

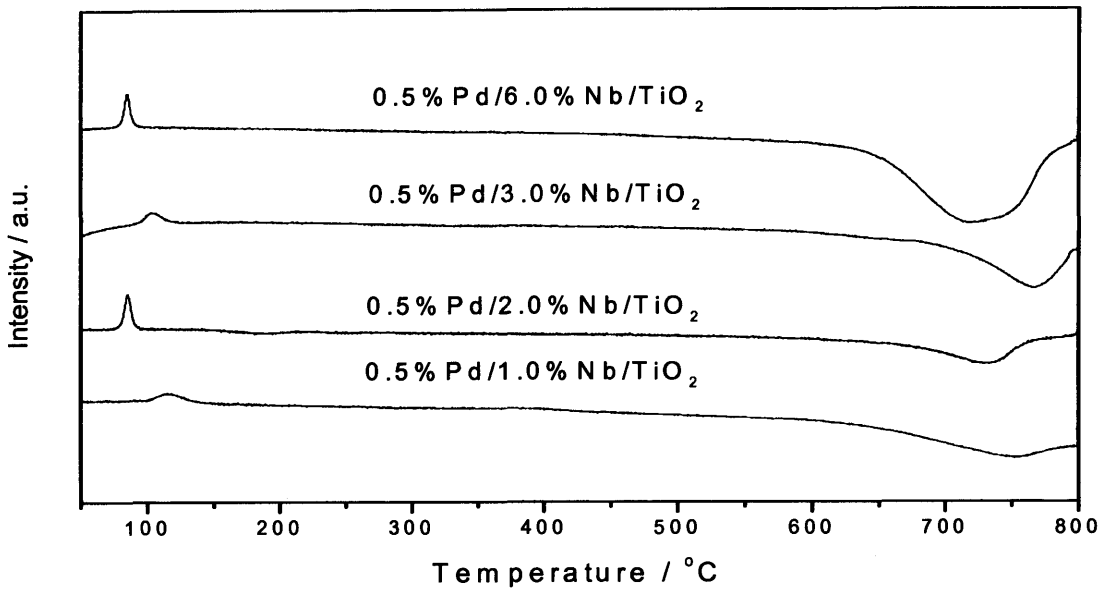

Figure 3.6 The TPR profiles of constant Pd loadings, with varying Nb loading, on a titania support.

All the catalysts containing palladium exhibited a negative peak, in the region of 50-80°C in the TPR profile, which has been related to the release of chemisorbed hydrogen (β-PdH phase). This negative peak increased in intensity with increasing palladium loading, but remained approximately constant for different niobium loadings. The TPR profiles show hydrogen consumption by the catalyst at different temperatures. Where hydrogen is consumed the peak goes down on the intensity scale, referred to as a positive peak. When the intensity of a peak increases up the scale it is referred to as a negative peak in this instance.

All niobium promoted Pd/TiO_2 catalysts showed a TPR peak at high temperatures (about 750°C), which increased in intensity with Nb loading; thus, this peak was attributed to the reduction of niobium surface species. It is

known [22] that niobium oxide is partially reducible when exposed to hydrogen at very high temperatures, and its reduction is facilitated by the presence of supported zero-valence metals on its surface. As a result, metals supported on niobium oxide are known to exhibit a strong metal-support interaction when reduced with hydrogen at high temperatures. In the absence of zero valence-metals, the reduction of Nb_2O_5 is partial and only occurs at temperatures greater than 1000°C. Hence, it can be concluded from TPR data that the incorporation of Pd decreases the reduction temperature of the niobium species considerably, but the reducibility of the niobium species were not significantly affected by altering either the Nb or the Pd concentrations.

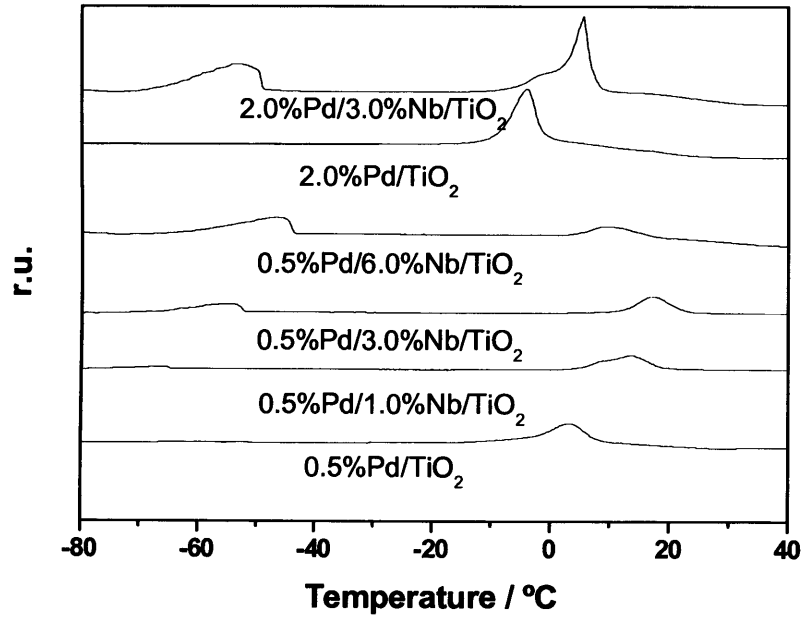

Figure 3.7 The sub ambient TPR profiles of varying Pd and Nb loadings on a titania support.

In addition, sub ambient TPR profiles were also determined (T. Davies) to probe the reducibility and nature of Pd sites in more detail. The various peaks observed can be assigned to the reduction of PdO_x to metallic Pd. It is evident, from figure 3.7, that Nb free Pd/TiO_2 catalysts only show a hydrogen reduction peak at ca. 0°C attributed to the reduction of palladium oxide particles. This peak was shifted to higher reduction temperatures after niobium addition, which was most likely related to a stronger interaction between the palladium oxide particles and the support [23].

Table 3.3. Hydrogen consumption during the sub-ambient temperature programme reduction experiments ($\mu molH_2/g$). Theoretical values in the case of $0.5\%Pd/TiO_2$ and $2.0\%Pd/TiO_2$ are 48 and 194 $\mu molH_2/g$, respectively (n.d.: not detected at temperatures lower than 450°C).

Catalyst.	First peak		Second peak	
	T_{max} (°C)	H_2 consumption ($\mu molH_2/g$)	T (°C)	H_2 consumption ($\mu molH_2/g$)
$0.5\%Pd/TiO_2$	n.d.	n.d.	3.1	40
$2\%Pd/TiO_2$	n.d.	n.d.	-4.2	143
$0.5\%Pd/1.0\%Nb/TiO_2$	-66	8.2	13	51
$0.5\%Pd/3.0\%Nb/TiO_2$	-55	40	17	51
$0.5\%Pd/6.0\%Nb/TiO_2$	-47	107	10	49
$2.0\%Pd/3.0\%Nb/TiO_2$	-53	86	5.6	180

According to the magnitude of hydrogen consumption (table 3.3) it is apparent that the corresponding hydrogen consumption was lower than the theoretical

value necessary to reduce all the palladium oxide in the case of the 0.5% Pd/TiO_2 catalyst. However, the hydrogen consumption for the catalysts with added niobium was close to the theoretical value predicted for reduction of palladium oxide. Therefore, the TPR indicated that the incorporation of niobium favoured the formation of totally oxidized palladium particles.

Surprisingly, figure 3.7 also showed that the incorporation of niobium brought about the presence of an additional hydrogen reduction peak at *ca.* -50 ºC. These peaks could not be assigned to the reduction of the palladium species, according to the hydrogen consumption values shown in table 3.3, since the hydrogen consumption peak at ca. 0ºC matched closely the theoretical values necessary to reduce all the palladium (II) oxide. In addition, the presence of significant quantities of palladium (IV) can be ruled out since these species were not identified in the X-ray photoelectron spectra (figure 3.8). Thus, the -50ºC hydrogen consumption peak can tentatively be assigned to the reduction of oxygen species with very high mobility.

3.2.5 Pulsed CO Chemisorption

CO chemisorption was employed (E. Ntainjua) in order to estimate the number of active Pd sites over the Nb promoted Pd/TiO_2 catalysts. An adsorption stoichiometry of Pd/CO = 1 was assumed. In table 3.4 it is also observed that the metal dispersion on 0.5%Pd/TiO_2 remarkably diminishes when Nb is added, meanwhile a similar number of Pd sites was observed when the Nb loading was increased. The number of Pd sites also increased with the Pd loading. For catalysts without Pd there was negligible uptake of

CO, demonstrating that CO adsorption was associated with the presence of Pd.

Table 3.4 Chemisorption results for $Pd/Nb/TiO_2$ catalysts.

Catalyst	Number of active Pd sites $(mol_{Pd}/g_{cat})^c$
$0.5\%Pd/TiO_2$	$1.64X10^{-4}$
$0.5\%Pd/1\%Nb/TiO_2$	$2.07X10^{-5}$
$0.5\%Pd/2\%Nb/TiO_2$	$1.90X10^{-5}$
$0.5\%Pd/3\%Nb/TiO_2$	$2.44X10^{-5}$
$0.5\%Pd/6\%Nb/TiO_2$	$2.26X10^{-5}$
$1.0\%Pd/3\%Nb/TiO_2$	$3.84X10^{-5}$
$2.0\%Pd/3\%Nb/TiO_2$	$6.02X10^{-5}$

3.2.6 X-ray Photoelectron Spectroscopy (XPS)

Several of the catalysts were analysed using XPS (A. Carley) and the results are shown in figures 3.8 and 3.9. The Pd(3d) spectra (figure 3.8) showed that for the pure $0.5\%Pd/TiO_2$ sample the Pd existed as both metallic species and PdO particles, the intensity ratio indicating a composition of 40% Pd^0 and 60% Pd^{2+}. The spectra from Nb promoted Pd/TiO_2 catalysts showed the complete absence of Pd^0, the palladium being present purely as PdO.

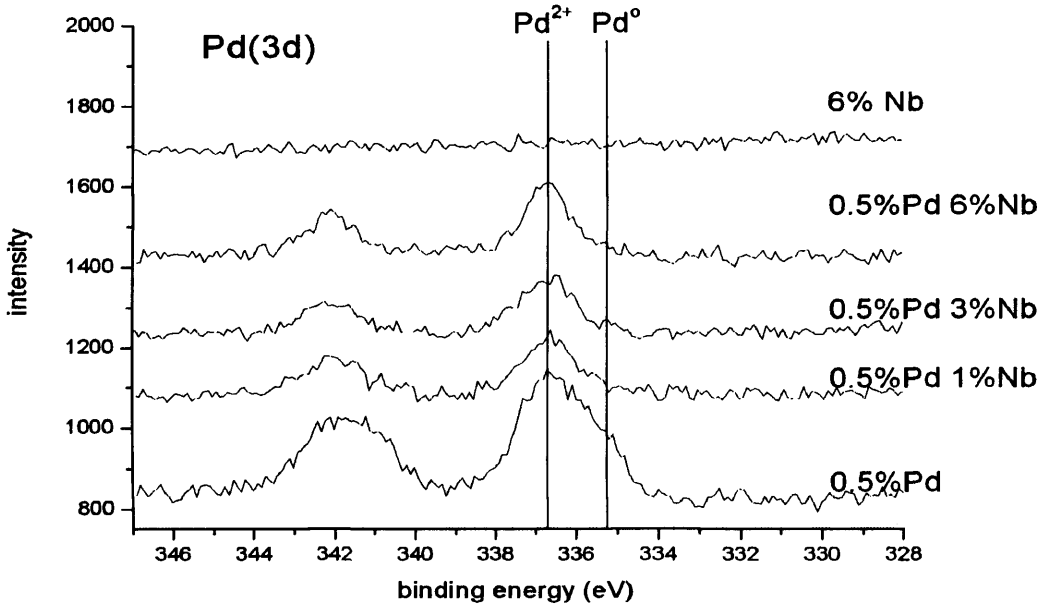

Figure 3.8 Pd(3d) X-ray photoelectron spectra for a series of Pd-Nb/TiO_2 catalysts, with loadings (wt.%) as shown.

In the Nb(3d) spectra (figure 3.9) the Nb($3d_{5/2}$) binding energy was constant for all samples, including the pure Nb/TiO_2 catalyst. The apparent large decrease in Nb(3d) intensity for the 6%Nb/TiO_2 sample compared with the 0.5%Pd/6%Nb/TiO_2 catalyst was confirmed in table 3.5, where surface elemental molar ratios derived from the XPS spectra are presented.

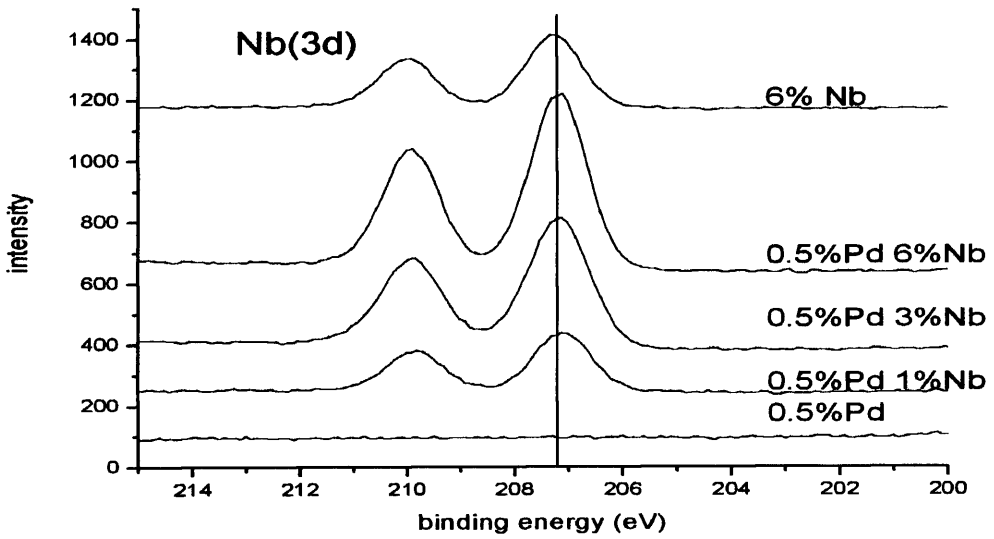

Figure 3.9 Nb(3d) X-ray photoelectron spectra for a series of Pd-Nb/TiO_2 catalysts, with loadings (wt.%) as shown.

Table 3.5 XPS-derived elemental molar ratios for a series of Pd-Nb/TiO_2 catalysts.

Catalyst	Molar ratios (XPS)			
	O/Ti	Pd/Ti	Nb/Ti	Nb/Pd
0.5%Pd/TiO_2	2.33	0.011	0.000	0.0
0.5%Pd/1.0%Nb/TiO_2	2.60	0.006	0.038	6.8
0.5%Pd/3.0%Nb/TiO_2	2.60	0.005	0.103	20.9
0.5%Pd/6.0%Nb/TiO_2	2.61	0.007	0.122	18.3
6.0%Nb/TiO_2	2.54	0.000	0.058	n/a

The Nb/Ti ratio for the pure Nb/TiO_2 catalyst was approximately 50% that for $0.5\%Pd/6\%Nb/TiO_2$, which was consistent with a significantly larger Nb_2O_5 crystallite size for pure Nb/TiO_2; in other words, the co-doped Pd induces a significantly increased dispersion in the niobium species. It can also be observed, in table 3.4, that the Pd/Ti ratio for the Pd/TiO_2 catalyst was higher than for the $Pd/Nb/TiO_2$ catalysts, and this was independent of the niobium loading. This result agrees with the XRD data and CO uptake values, indicating that the co-impregnation of Pd and Nb over the TiO_2 support resulted in lower dispersion of palladium particles. Moreover, the Pd/Ti ratio was approximately constant regardless of the niobium loading (table 3.4). Finally, there was no evidence for any chlorine species on the catalyst surface from the XPS studies.

3.3 Catalyst characterisation of tungsten catalysts

3.3.1 BET surface area determination

The surface areas for titania catalysts loaded with palladium and/or tungsten are shown in table 3.6. The addition of palladium or tungsten reduces the surface area of the titania support from 50 m^2g^{-1}. There does not appear to be a correlation between the different metal loadings and the surface area of the catalyst. The decrease in surface area may seem a small value but it may be a useful factor in determining why it has a low or high activity.

Table 3.6 BET surface areas of Pd and W on a titania support.

Catalyst.	Surface area (m^2g^{-1}).
3.0%W/TiO_2	48
6.0W/TiO_2	49
0.5%Pd/1.0%W/TiO_2	42
0.5%Pd/2.0%W/TiO_2	47
0.5%Pd/3.0%W/TiO_2	45
0.5%Pd/6.0%W/TiO_2	48
1.0%Pd/3.0%W/TiO_2	48
2.0%Pd/3.0%W/TiO_2	49

3.3.2 Powder X-ray Diffraction (XRD)

The powder XRD patterns of catalysts with different loadings of Pd and W on a titania support are shown in figures 3.10 and 3.11.

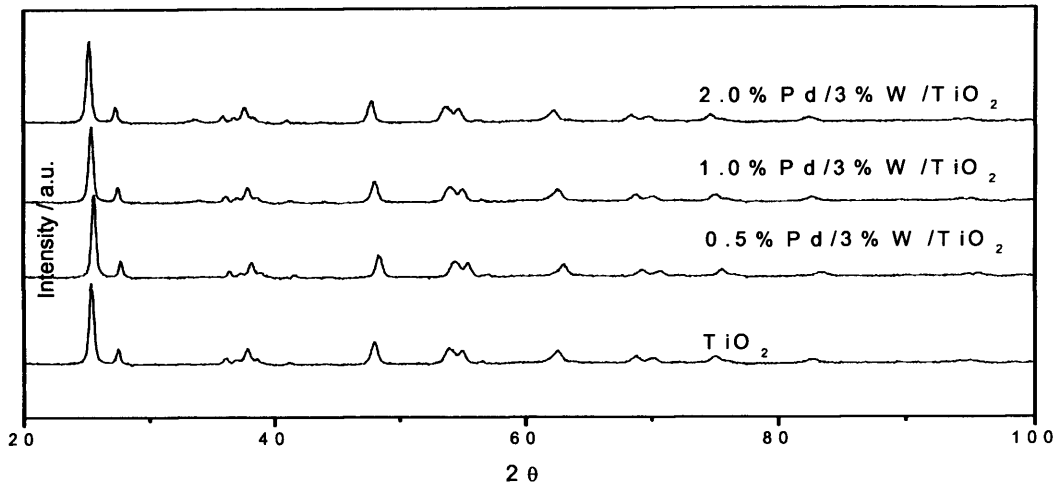

Figure 3.10 The XRD profiles of varying Pd loadings, with constant W loading, on a titania support.

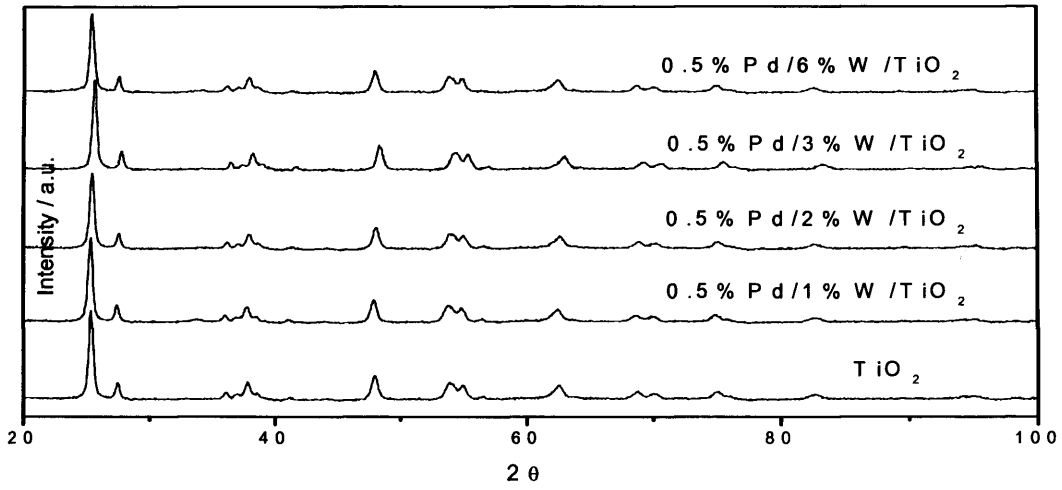

Figure 3.11 The XRD profiles of constant Pd loadings, with varying W loading, on a titania support.

From the figures 3.10 and 3.11 it is possible to see the main crystalline phase present was that of titania (rutile and anatase). The predominant phase of the titania was anatase from the d spacings and relative intensities.

The addition of palladium or tungsten did not modify the titania phase, even with high loadings. There was no phase found to be indicative of tungsten even at a 6% loading. Due to titania (anatase) being the only phase present, it indicated that the palladium and tungsten were highly dispersed [24]. This is also in keeping with the findings of Mendes et al [25].

3.3.3 Raman Spectroscopy

The Raman profiles of $Pd/W/TiO_2$ catalysts are shown in the figures 3.12, 3.13 and 3.14.

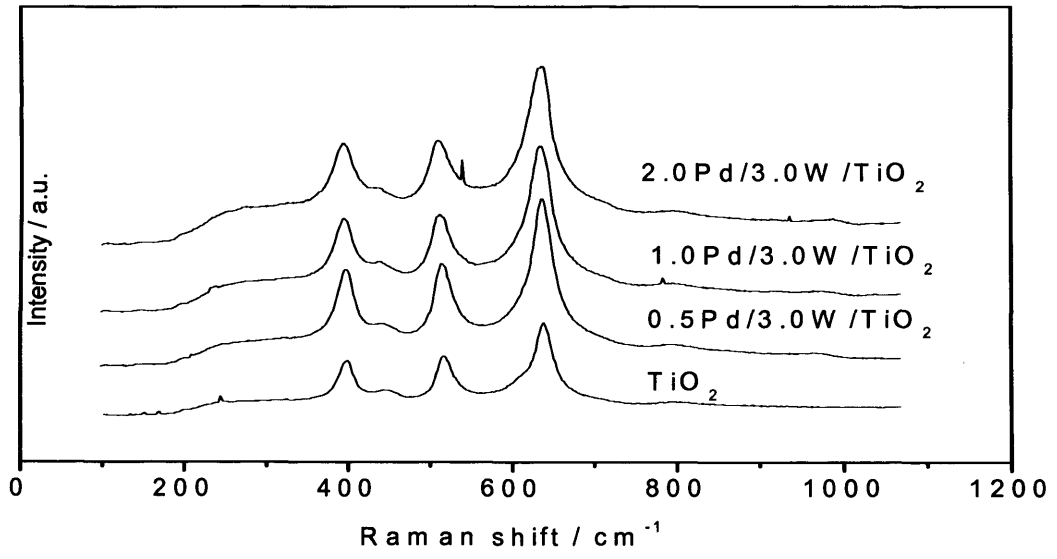

Figure 3.12 The Raman spectra of varying Pd loadings, with constant W loading, on a titania support.

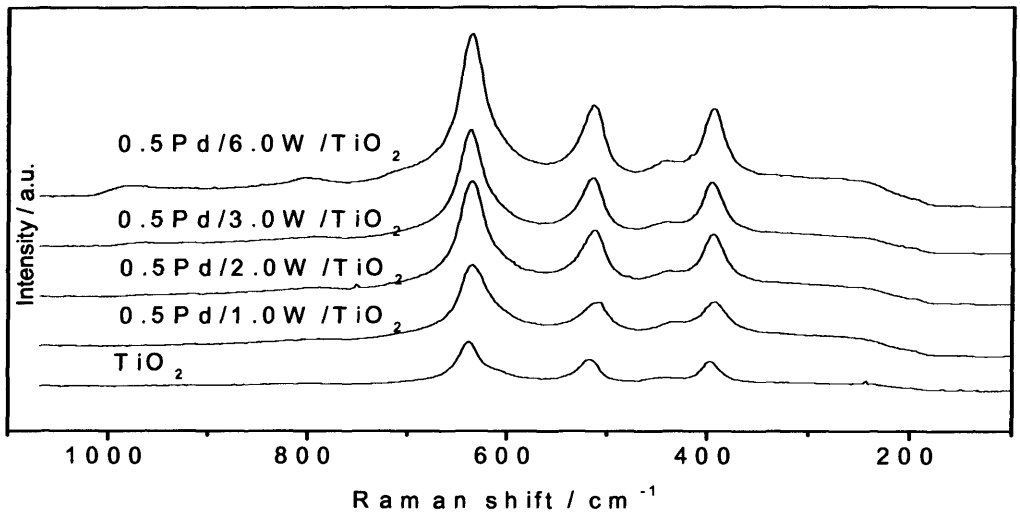

Figure 3.13 The Raman spectra of constant Pd loadings, with varying W loading, on a titania support.

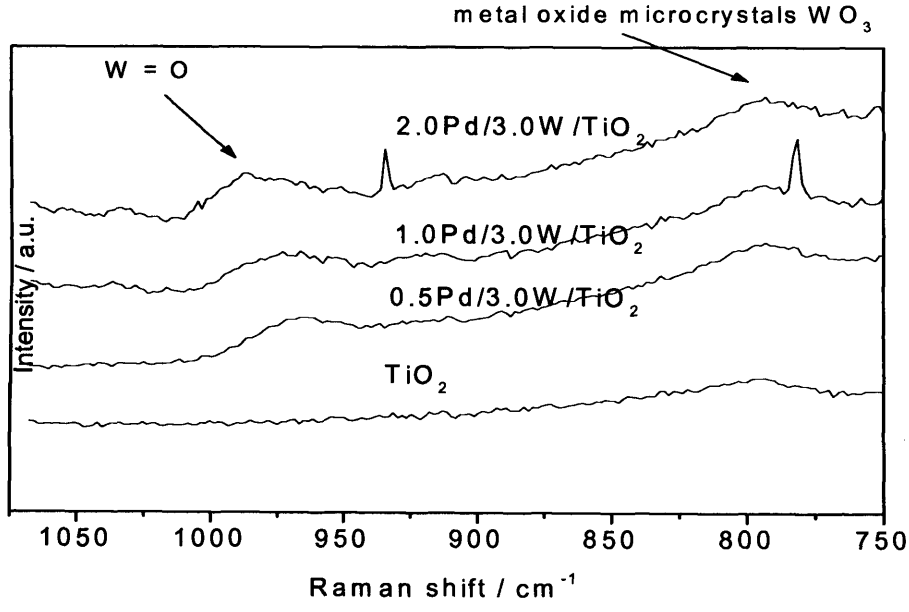

Figure 3.14 The Raman spectra of varying Pd loadings with constant W loading, on a titania support, in closer detail.

The Raman profiles, in figures 3.12 and 3.13, of the tungsten catalysts all show bands corresponding to the peaks of the titania support in the regions of 650, 510 and 400 cm^{-1}. This was indicative of the anatase phase of titania. Due to such strong Raman peaks of the support it limited the determination of any tungsten peaks below 700 cm^{-1}. On closer examination there were less intense peaks in the regions of 975 and 800cm^{-1} which are due to tungsten forming metal oxide microcrystals [26]. The peak at 975 cm^{-1} was due to a terminal W=O bond [27].

3.3.4 Temperature Programmed Reduction (TPR)

The TPR profiles of $Pd/W/TiO_2$ catalysts are shown in figures 3.15 and 3.16:

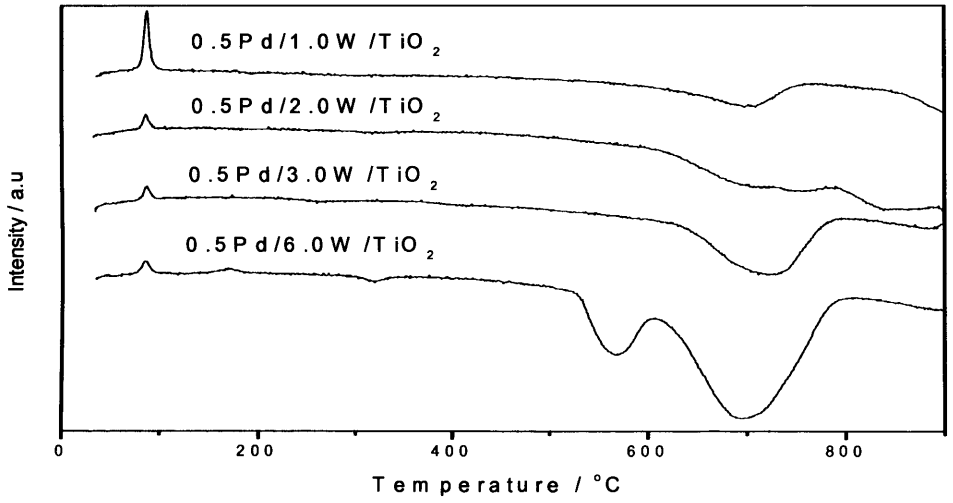

Figure 3.15 The TPR profiles of varying Pd loadings, with constant W loading, on a titania support.

The reduction features of the profiles of the tungsten catalysts show a general reduction peak in the region of 700°C. For the $0.5Pd/6.0W/TiO_2$ catalyst, two peaks were observed, in figure 3.16, one at 550 °C and the other at 700 °C.

This was similar to the TPR profiles found for bulk WO_3 [28]. The lower loadings of tungsten, showed a low intensity broad peak in the region of 700-800 °C. Features in this temperature region have been attributed to the reduction of WO_3 to WO_2 [29]. The further reduction to tungsten metal was not observed as this occurs at much higher temperatures of around 900°C. Lower loadings of tungsten (below monolayer coverage) have been found to be hard to reduce due to a strong interaction between WO_x and the support [30]. There are more intense reduction peaks with higher loadings of tungsten. Therefore with increased tungsten loadings, the WO_x-support interaction decreases and facilitates reduction of the catalyst.

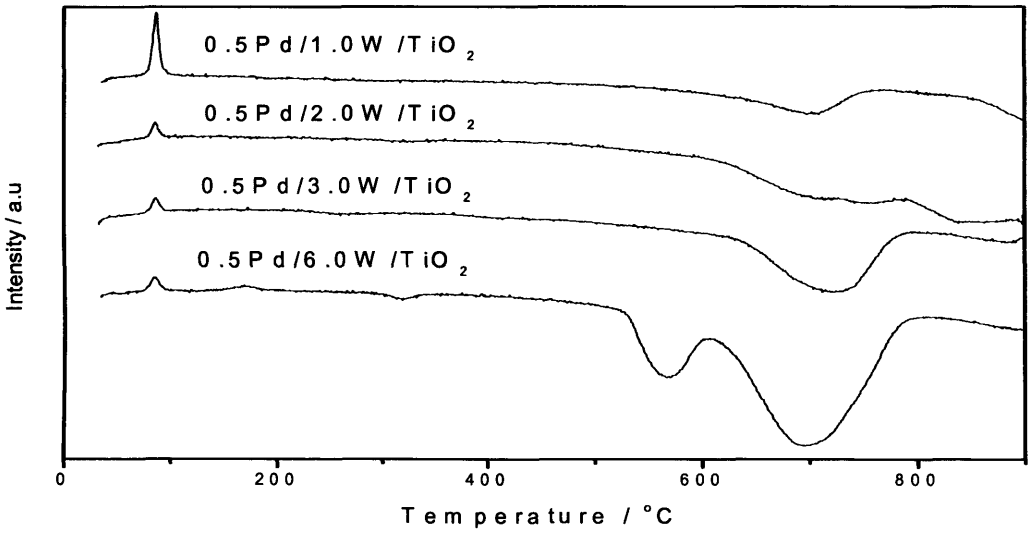

Figure 3.16 The TPR profiles of constant Pd loadings, with varying W loading, on a titania support.

There is a negative reduction peak at low temperature due to the release of chemisorbed hydrogen (β-PdH phase [31]) and also the decomposition of palladium hydride which is formed at room temperature. Peaks at higher temperatures are due to hydrogen consumption. It may be worth noting that

the negative peaks for all samples remain in the same region. The only difference seen is the intensity of the negative peak as for a high loading of palladium, such as 2.0% w.t., a more intense peak is observed in comparison to a loading of 0.5% w.t.

3.3.5 X-ray Photoelectron Spectroscopy (XPS)

The W(4f) spectra for the Pd-W/TiO_2 catalysts overlapped strongly with the Ti(3p) signal from the titania support, and thus the Ti(3p) spectrum from the tungsten-free catalyst was subtracted from the composite signal. The methodology is shown in figure 3.17: the Ti(3p) signal from titania (curve (a)) is scaled appropriately and subtracted from the composite spectrum from the Pd-W catalyst (curve (b)) to give the 'pure' W(4f) spectrum (curve (c)) which can then be quantified.

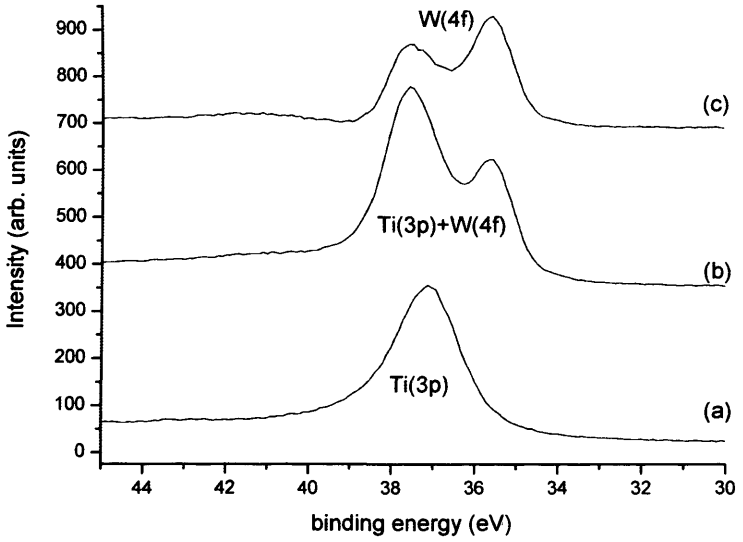

Figure 3.17 Ti(3p)+W(4f) spectra for (a) the 0.5 % W/TiO_2 catalyst, (b) the 0.5 % - 3% W/TiO_2 catalysts and (c) the results of subtracting the Ti(3p) contribution from spectrum (b).

A plot of the ratios of the integrated W(4f) intensity to the integrated Ti(2p) signal is shown in figure 3.18.

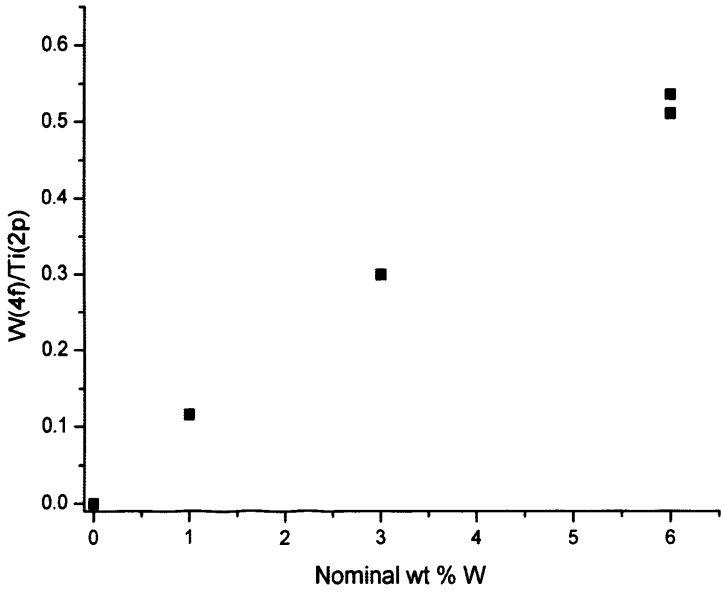

Figure 3.18 Plot of the ratio of the intensities of the W(4f) and Ti(2p) spectra against nominal W composition for the Pd-W catalysts.

There was an excellent linear correlation which was consistent with a high dispersion of tungsten over the catalyst surface. If there was significant agglomeration then a non-linear relationship would result.

From the Pd(3d) spectra, there was clear evidence for both Pd^{0} and Pd^{2+} sites in the 0.5 % Pd/TiO_2 sample, but only Pd^{2+} species were observed in the W-doped catalysts (Figure 3.19).

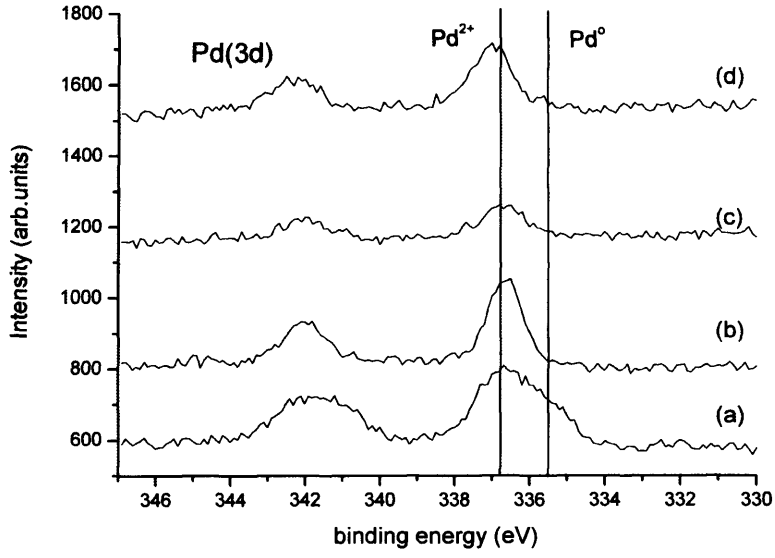

Figure 3.19 Pd(3d) spectra for the W-doped 0.5 % Pd/TiO_2 catalysts; W loadings are (a) 0 %, (b) 1 %, (c) 3 % and (d) 6 %.

Figure 3.20 shows that the surface Pd content decreased with increased W loading, indicating that the tungsten formed an over layer on the Pd/TiO_2 material.

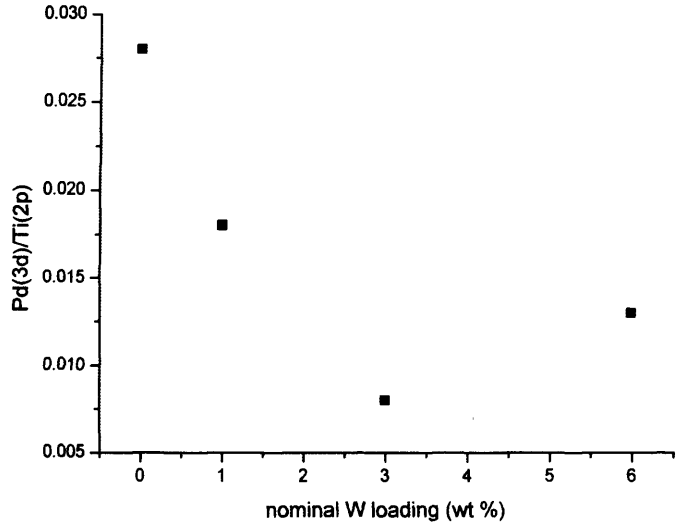

Figure 3.20 Pd(3d)/W(4f) intensity ratios for the W-doped Pd/TiO_2 catalysts, plotted against the nominal W loadings.

3.4 Results

3.4.1 VOC combustion over $Pd/Nb/TiO_2$

Figures 3.21 and 3.22 show the variation of the propane conversion with reaction temperature over Pd/TiO_2, Nb/TiO_2 and $Pd/Nb/TiO_2$ catalysts. The only reaction product observed in Pd-containing catalysts was CO_2.

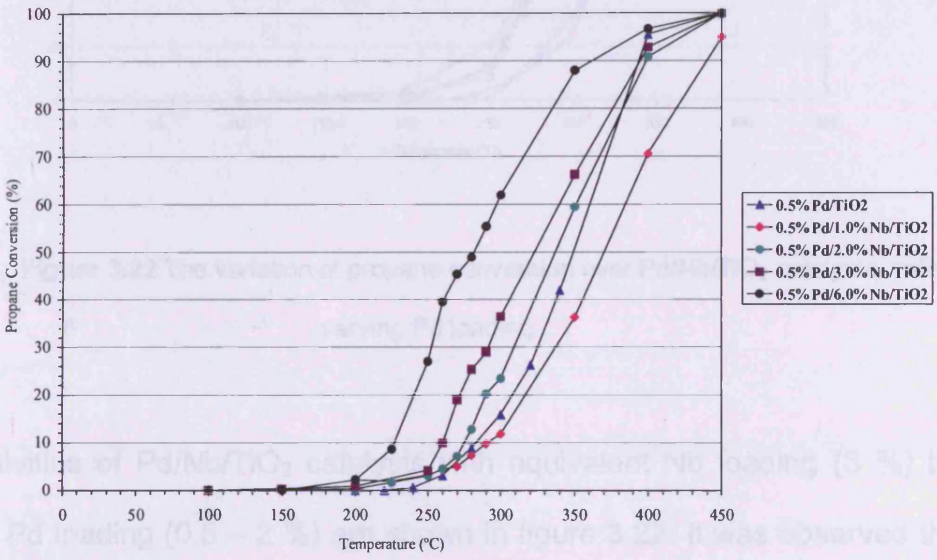

Figure 3.21 The variation of propane conversion over $Pd/Nb/TiO_2$ catalysts, with constant Pd loading.

Figure 3.21 shows the propane conversion with reaction temperature for catalysts with a fixed 0.5 wt.% Pd loading but varying Nb loadings. The addition of Nb to $0.5\%Pd/TiO_2$ promoted the activity of the catalyst for propane total oxidation, especially that with 6 wt. % Nb. This showed a considerably higher catalytic activity than the other Nb-containing catalysts, reaching 88% propane conversion at 350°C.

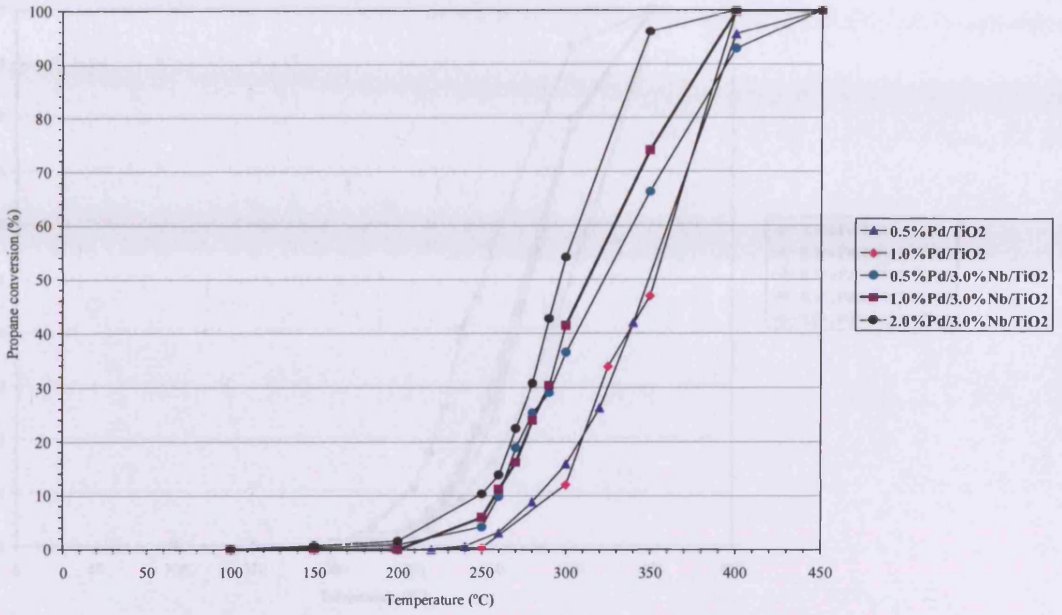

Figure 3.22 The variation of propane conversion over $Pd/Nb/TiO_2$ catalysts, with varying Pd loading.

The activities of $Pd/Nb/TiO_2$ catalysts with equivalent Nb loading (3 %) but varying Pd loading (0.5 – 2 %) are shown in figure 3.22. It was observed that the incorporation of increasing amounts of palladium to a given Nb content also led to an increase in catalytic activity. The highest conversion at 350°C was observed for the $2.0\%Pd/3.0\%Nb/TiO_2$ catalyst with 96%.

3.4.2 VOC combustion over $Pd/W/TiO_2$

The conversions of propane for different loadings of palladium and tungsten on a titania support are shown in figures 3.23 and 3.24. The only reaction product observed, throughout the temperature range explored, was CO_2.

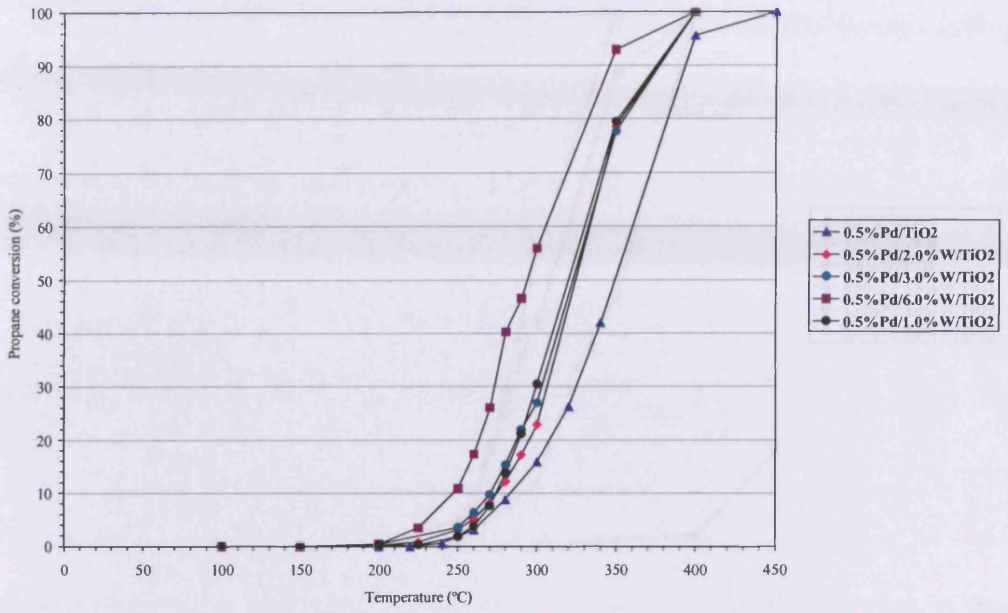

Figure 3.23 The variation of propane conversion over Pd/Nb/TiO_2 catalysts, with constant Pd loading.

Figure 3.23 shows the propane conversion, with increased reaction temperature, for catalysts with a fixed Pd loading of 0.5% wt. and varying W loadings. Initial activities were observed at 200°C for all catalysts containing tungsten, in figure 3.23. During this region of initial activity the temperature was increased at 10°C intervals until 300°C, after which the temperature was increased to 450°C at 50°C intervals. The propane conversion increased with temperature with 100% conversion at 450°C.

The lowest conversion observed in the temperature range 50-450°C was for the catalyst 0.5%Pd/TiO_2. With the addition of tungsten, the conversion for all loadings was promoted. The optimum loading was found for the 6% wt. of tungsten with a propane conversion of 92% at 350°C.

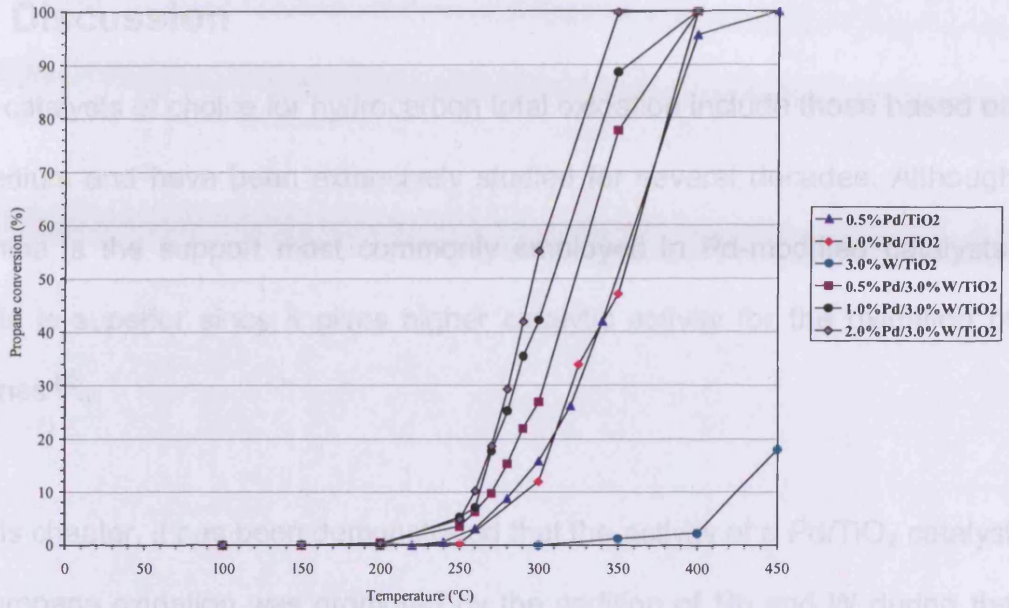

Figure 3.24 The variation of propane conversion over $Pd/W/TiO_2$ catalysts, with varying Pd loading.

The propane conversion, of catalysts with varying loadings of palladium, but a constant W loading of 3% wt., are shown in figure 3.24. The most active catalyst had a loading of 2.0% Pd and 3.0% W. All catalysts had 100% conversion at 450°C, except the catalyst with no Pd present. This indicated a synergistic effect between Pd and W in the conversion of propane. The maximum conversion observed for this low activity catalyst was 18% at 450°C.

3.5 Discussion

The catalysts of choice for hydrocarbon total oxidation include those based on palladium and have been extensively studied for several decades. Although alumina is the support most commonly employed in Pd-modified catalysts, titania is superior since it gives higher catalytic activity for the oxidation of alkanes [2].

In this chapter, it has been demonstrated that the activity of a Pd/TiO_2 catalyst for propane oxidation was promoted by the addition of Nb and W during the impregnation step of catalyst preparation, and there was a general increase of activity with increased modifier loading. A summary of the catalytic results, of those including niobium, are presented in table 3.7, where T_{10}, T_{50} and T_{90} (reaction temperatures for alkane conversions of 10, 50 and 90%, respectively) are shown.

The most active catalyst was the one with the highest Nb loading ($0.5\%Pd/6.0\%Nb/TiO_2$) with a remarkably higher activity than both the Nb-free $0.5\%Pd/TiO_2$ catalyst and especially the Pd-free Nb catalyst. These observations are important since the Nb-salts available commercially are *ca* 50 times cheaper than Pd-salts. Therefore, the addition of Nb to a Pd catalyst does not appreciably increase the cost of the catalyst but does increase the hydrocarbon total oxidation activity.

Table 3.7 Reaction temperatures for alkane conversions of 10, 50 and 90% and the corresponding surface area of $Pd/Nb/TiO_2$.

Catalyst.	T_{10} (°C)	T_{50} (°C)	T_{90} (°C)	BET surface area. m^2/g.
2.0%Pd/3.0%Nb/ TiO_2	250	290	340	46
1.0%Pd/3.0%Nb/ TiO_2	260	310	385	47
0.5%Pd/6.0%Nb/ TiO_2	225	280	370	46
0.5%Pd/3.0%Nb/ TiO_2	250	320	390	47
0.5%Pd/2.0%Nb/ TiO_2	265	325	395	49
0.5%Pd/1.0%Nb/ TiO_2	295	370	440	50
2.0%Pd/ TiO_2	285	350	390	46

The incorporation of niobium to Pd/TiO_2 catalysts increased the catalytic activity for propane catalytic combustion, requiring lower temperatures to achieve the same conversion. Thus, it would be interesting to clarify the role of niobium species in PdNb catalysts. Supported niobium species have been shown to exhibit significant Lewis and Brønsted acidity [32], and it has also been demonstrated that the niobium surface species on titania have some redox properties in addition to their acidic properties [33]. The presence of palladium in PdNb-catalysts has led to a lower aggregation of Nb species (XPS) and an increase in their reducibility (TPR). However, we consider that these facts are not directly responsible for the catalytic performance since i) Nb, regardless of the way it is structured, presents a very low reactivity for this reaction and ii) the most reducible Nb species in NbPd catalysts according to

the TPR experiments present the reduction bands at 650-700°C, which are temperatures much higher than those required for full conversion of propane.

Although niobium species do not seem to activate propane at low temperatures the addition of niobium clearly affects the nature of the Pd species, *i.e.* the palladium oxidation state, the redox properties and the palladium particle size. These parameters [10, 11] have been demonstrated to be very important in controlling the catalytic activity of palladium catalysts in VOC combustion reactions. XPS data clearly shows that the palladium oxidation state was affected by the presence of Nb. The nature of the Pd species seems to be indirectly affected by the niobium addition. It could be assumed that the presence of niobium species could change the electronic characteristics of the TiO_2 support, which is affecting the nature of the palladium species [20]. This assumption agrees with Raman data where it has been found that the simultaneous presence of Pd and Nb displaces the Raman frequencies of the TiO_2 support to lower frequencies. This effect has not been observed when only palladium is added to the support.

It is well known that metal dispersion is one of the factors controlling the catalytic activity of supported metal catalysts. Hicks *et al.* [34] showed that highly dispersed palladium oxide could be much less active than crystalline palladium oxide supported on alumina, due to the strong interaction with the support for small crystallites. In this chaper, it was observed that the average crystallite sizes were almost constant for the Nb promoted Pd/TiO_2 catalysts, independently of the niobium and palladium loading. It was also apparent that

although the number of active palladium sites was remarkably lower for Nb promoted 0.5%Pd/TiO_2 catalysts, the interaction of the palladium particles with the TiO_2 support was stronger, as the hydrogen consumption peak in the subambient TPR profile was shifted to higher temperatures. Thus, the variation of the catalytic activity after Nb promotion could not be interpreted by the variation in the dispersion. In addition, it can be observed that the activity per active site of 0.5%Pd/6.0%Nb/TiO_2 was much higher (about 10 times higher at 250ºC) than 0.5%Pd/3.0%Nb/TiO_2 even though they had a similar number of active Pd sites. Thus, other factors seem to be responsible for the synergistic effect observed in Nb promoted Pd/TiO_2 catalysts.

It is worth noting that the niobium synergistic effect on Nb promoted Pd/TiO_2 catalysts is more evident at higher niobium and palladium loadings. From subambient TPR data, it can be inferred that the positive niobium effect seems to be related to the magnitude of hydrogen consumption for the 50ºC reduction peak. Firstly, this peak has not been detected in the case of Nb free Pd/TiO_2 catalysts and, secondly, whilst the 0.5%Pd/1.0%Nb/TiO_2 catalyst only shows a marginal hydrogen consumption peak, 0.5%Pd/6.0%Nb/TiO_2 presents the greatest hydrogen consumption. These facts correlate well with their corresponding activities for propane total oxidation. Unfortunately, it has not been possible to unequivocally characterise the nature of these new and very easily reducible sites, although their formation seems to be related to the presence of palladium in close contact to niobium species on the TiO_2 support, favouring oxygen mobility. This fact could not only bring about the

formation of palladium particles in a totally oxidised state, but also the presence of very active oxygen species.

The effect of niobium on the catalytic performance of Pd/TiO_2 catalysts has been evaluated for the first time in this work. Surprisingly, even though niobium addition leads to completely oxidized palladium particles and with a stronger interaction with the support, the catalysts demonstrate improved performance. The positive effect has been accounted for by the presence of new and very reducible species detected in the subambient TPR profiles at *ca.* -50°C. This is the first time that the presence of these species has been reported.

A summary of the catalytic results, of those including tungsten, are presented in table 3.8, where T_{10}, T_{50} and T_{90} (reaction temperatures for alkane conversions of 10, 50 and 90%, respectively) are shown. The most active catalyst was the one with the highest loading of tungsten (0.5%Pd/6.0%W/ TiO_2) which was also the case for the niobium catalysts. This catalyst had a substantially lower temperature of activity compared to a W-free catalyst. The tungsten catalyst was not as promising as the most active niobium catalyst as T_{10} was 25°C higher at 250°C. The tungsten set of catalysts followed a similar pattern to those containing niobium. When tungsten was loaded onto a titania support, with palladium, an increased catalytic activity was observed for the complete combustion of propane. When tungsten and palladium were present together, regardless of loading, a lower temperature was required to obtain the same conversion as the catalysts with only Pd or W.

Table 3.8 Reaction temperatures for alkane conversions of 10, 50 and 90% and the corresponding surface area of $Pd/W/TiO_2$.

Catalyst	T_{10} (°C)	T_{50} (°C)	T_{90} (°C)	BET surface area. m^2/g.
2.0%Pd/3.0%W/ TiO_2	260	290	335	49
1.0%Pd/3.0%W/ TiO_2	260	305	345	48
0.5%Pd/6.0%W/ TiO_2	250	290	345	48
0.5%Pd/3.0%W/ TiO_2	270	320	370	45
0.5%Pd/2.0%W/ TiO_2	280	320	375	47
0.5%Pd/1.0%W/ TiO_2	270	320	375	42
1.0%Pd/ TiO_2	280	350	390	43

Work on mixed oxide catalysts in the past has shown the addition of a transition metal to significantly reduce the surface area and activities, with the exception of cobalt and nickel [35]. The enhancement of the rate must be due to electronic modifications rather than any physical redistributions of palladium. In the Raman studies, the presence of tungsten did not significantly modify electronic properties as the wavenumber of the different peaks was not shifted [36]. Through these Raman studies, tungsten microcrystals were detected.

A bulk WO_3 phase was not detected in the Raman spectra or in the XRD studies which suggests that the tungsten was present as surface species on the support [37]. XRD studies only detected the titania phase, which is in

keeping with other research [38]. The deposition of tungsten onto a titania support did not change the composition of the support and no diffraction peaks corresponding to tungsten were observed. Although tungsten was not detected in Raman or XRD, XPS studies on these catalysts have shown that tungsten was highly dispersed and formed an over layer on Pd/TiO_2.

From the temperature programmed reduction profiles, it was possible to see that with the most active catalysts, an intense, broad reduction peak was observed. In the case of 0.5%Pd/6.0%W/ TiO_2 there were two peaks present in the profile, indicative of bulk WO_3. This may have suggested a higher activity than niobium at this loading, due to niobium having a single peak, but this was not the case. The temperatures at which reduction occurred, for all the tungsten catalysts, was much higher than the reaction temperatures studied for the oxidation of propane. An increased reducibility with an increased loading of tungsten has been found in previous work [39] where studies were carried out with Pd and a zirconia support.

Yazawa et al. [10] suggested for propane combustion that the oxidation state of palladium affects the catalytic activity to a greater extent than the dispersion. Thus, they observed that partially oxidized palladium showed the highest catalytic activity for propane combustion. Similar behaviour was observed for the $Pd/Nb_2O_5/Al_2O_3$ catalytic system [12], where the addition of niobium to alumina supported Pd catalysts prevented the total oxidation of palladium, increasing the propane combustion activity. These authors proposed that the presence of NbO_x species in close contact with the palladium particles

modifies the oxidation state of Pd, favouring the ideal Pd^0/Pd^{2+} ratio. In this model, the co-existence of Pd and PdO on the Pd surface is a prerequisite since metallic Pd provides adsorption sites for the hydrocarbon molecule, and then, the adsorbed molecule diffuses to the PdO region and is oxidized to generate carbon dioxide and water. Accordingly, it could be expected that the synergistic effect between niobium/tungsten and palladium on TiO_2 supported catalysts is due to a similar effect. However, it can be clearly observed in the XPS spectra that although niobium and tungsten addition to Pd/TiO_2 catalysts has a significant effect on the palladium oxidation state, the surface of these particles is completely oxidized, and metallic palladium was not present irrespective of the niobium or tungsten content.

The incorporation of tungsten in Pd/TiO_2 catalysts has produced catalysts with higher activities for propane oxidation. The activity results agree with L'Argentiere *et al* where a maximum activity was found for a loading of 6% wt. of tungsten [40]. They suggested the presence of a Pd-WO_x interface allowed a higher activity for hydrogenation reactions and more resistance to sulphur poisoning. Although the application of this catalyst was for a hydrogenation reaction, the active species could be the same in the oxidation reactions. Also, Silva *et al* [41] found that the enrichment of $Pt-Al_2O_3$ with tungsten led to the formation of HWO_3 on a modified surface which increased the rate of propane oxidation.

Promising results involving tungsten in combination with palladium were found in the automotive industry where $Pd-WO_3/\gamma-Al_2O_3$ had a higher activity in the

oxidation of hydrocarbons than the Pt equivalent [42]. This catalyst has been used in the treatment of automotive exhaust gases since 1983. The synergetic relationship between palladium and tungsten was also observed in this chapter.

3.6 Conclusions

The activity of a palladium/titania catalyst for propane oxidation has been promoted by the addition of varying loadings of niobium and tungsten during the impregnation step of catalyst preparation. The catalytic activity was found to increase as the niobium, tungsten and/or palladium loading increased. The addition of Nb and W significantly changed the nature of the palladium from XPS studies. In addition, it has been observed that the addition of niobium increased the oxygen mobility. This promoted the presence of palladium species in a totally oxidised state and also produced easily reducible species. Niobium was found to exhibit higher activities than tungsten when present in a mixed oxide catalyst with palladium on a titanium oxide support. Niobium and tungsten exhibited the highest activities with a loading of 6% w.t. The best catalyst amongst the range of catalysts investigated was 0.5%Pd/6%Nb_2O_5/TiO_2 and CO_2 was the only product identified during the catalytic oxidation of propane.

3.7 References

[1] J. G. Watson, J. C. Chow, E. M. Fujita, *Atmospheric Environment* **35** (2001), pp. 1567-1584.

[2] T. Garcia, B. Solsona, S. H.Taylor., *Catalysis Letters* **97** (2004), pp 99-103.

[3] D. Giannopoulos, D.I. Kolaitis, A. Togkalidou, G. Skevis, M.A. Founti, *Fuel* **86** (2007), pp 1144-1152.

[4] T. Streibel, H. Nordsieck, K. Neuer-Etscheidt, J. Schnelle-Kreis, R. Zimmermann , *Chemosphere* **67** (2007), pp S155-S163.

[5] A. Janbey A, W. Clark, E. Noordally, S. Grimes, S. Tahir, *Chemosphere* **52** (2003), pp. 1041-1046.

[6] P. Gélin, M. Primet, *Applied Catalysis B: Environmental* **39** (2002), pp. 1-37.

[7] R. Spinicci, A. Tofanari, *Applied Catalysis* **227** (2002), pp. 159-169.

[8] D. Ciuparu, L. Pfefferle, *Catalysis Today* **77** (2002), pp. 167-179.

[9] K. Sekizawa, H. Widjaja, S. Maeda, Y. Ozawa, K. Eguchi, *Catalysis Today*, **59** (2000), pp. 69-74

[10] Y. Yazawa, H. Yoshida, N. Takagi, S. Komai, A. Satsuma, T. Hattori, *Journal of Catalysis* **187** (1999), pp.15-23.

[11] T. Garcia, B. Solsona, D. M. Murphy, K. L. Antcliff, S. H. Taylor, *Journal of Catalysis* **229** (2005), pp. 1-11.

[12] F. B. Noronha, D. A. G. Aranda, A. P. Ordine, M. Schmal, *Catalysis Today* **57** (2000), pp. 275-282.

[13] A. Törncrona, M. Skoglundh, P. Thormählen, E. Fridell and E. Jobson, *Applied Catalysis B: Environmental* **14** (1997), pp. 131-145.

[14] S. Colussi, A. Trovarelli, G. Groppi, J. Llorca, *Catalysis Communications* **8** (2007), pp. 1263-1266.

[15] G. Pecchi, P. Reyes, T. López and R. Gómez *Journal of Non-Crystalline Solids* **345-346** (2004), pp. 624-627.

[16] P. Papaefthimiou, T. Ioannides, X. E. Verykios, *Applied Catalysis B: Environmental* **15** (1998), pp. 75-92.

[17] P. Papaefthimiou, T. Ioannides, X. E. Verykios, *Applied Thermal Engineering* **18 (11)** (1998), pp. 1005-1012.

[18] A. Kubacka, M. Fernandez-Garcia, G. Colon, *Journal of Catalysis* **254** (2008), pp. 272-284.

[19] N.A. Kovalenko, T.S. Petkevich and Yu. G. Egiazarov, *Russian Journal of Applied Chemistry*, **72** (1999), pp.452-456.

[20] R. Brayner and F. Bozon-Verduraz, *Physical Chemistry Chemical Physics* **5** (2003), pp.1457-1466.

[21] T. Onfroy, O. V. Manoilova, S. B. Bukallah, D. M. Hercules, G. Clet, M. Houalla, *Applied Catalysis A: General* **316** (2007), pp. 184-190.

[22] J. G. Weissman, *Catalysis Today* **28** (1996), pp. 159-166.

[23] W.J. Shen, M. Okumura, Y. Matsumura and M. Haruta, *Applied Catalysis A* **213** (2001), pp. 225-232.

[24] L. S. Escandon, S. Ordonez, F. V. Diez, H. Sastre, *Catalysis* **78** (2003), pp. 191-196.

[25] F. M. T. Mendes, C. A. Perez, R. R. Soares, F. B. Noronha, M. Schmal, *Catalysis Today* **78 (1-4)** (2003), pp. 449-458.

[26] D. S. Kim, M. Ostromecki, I. E. Wachs, *Journal of Molecular Catalysis* **106(1-2)** (1996) pp. 93-102.

[27] M. Boulova, G. Lucazeau, *Journal of Solid State Chemistry* **167** (2002) pp. 242.

[28] D. C. Calabro, J. C. Vartuli, J. G. Santiesteban, *Topics in Catalysis* **18(3-4)** (2002) pp. 231-242.

[29] M. G. Fasco, S. A. Canavese, N. S. Figoli, *Catalysis Today* **107-108** (2005) pp. 778-784.

[30] R. Thomas, J. A. Moulijn, *Journal of Molecular Catalysis* **15** (1982) pp. 157.

[31] L. S. Escandon, S. Ordonez, F. V. Diez, H. Sastre, *Catalysis* **78** (2003), pp. 191-196.

[32] I. E. Wachs, Y. Chen, J.-M. Jehng, L. E. Briand and T. Tanaka *Catalysis Today*, **78** (2003), pp. 13-24.

[33] P. Viparelli, P. Ciambelli, L. Lisi, G. Ruoppolo, G. Russo, J. C. Volta, *Applied Catalysis A:General* **184** (1999), pp. 291-301.

[34] R.F. Hicks, H. Qi, M.L. Young and R.G. Lee. *Journal of Catalysis* **122** (1990), pp. 295- 306.

[35] H. Widjaja, K. Sekizawa, K. Eguchi, H. Arai, *Catalysis Today* **47** (1999), pp. 95-101.

[36] V. Lebarbier, G. Clet, M. Houalla, *Journal of Physical Chemistry B* **110** (2006) pp. 22608-22617.

[37] V. Lebarbier, G. Clet, M. Houalla, *Journal of Physical Chemistry B* **110** (2006) pp. 13905-13911.

[38] T. Onfroy, G. Clet, S. B. Bukallah, T. Visser, M. Houalla, *Applied Catalysis A: General* **298** (2006) pp. 80-87.

[39] M. Occhiuzzi, D. Cordischi, S. D. Rossi, G. Ferraris, D. Gazzoli, M. Valigi, *Applied Catalysis A: General* **351** (2008) pp. 29-35.

[40] P. C. L'Argentiere, N. S. Figoli, *Catalysis Letters* **53 (3-4)** (1998), pp. 149-153.

[41] M. A. P. Silva, R. M. Cardoso, M. Schmal, *Brazilian Journal of Chemical Engineering* **20 (1)** (2003), pp. 51-56.

[42] K. M. Adams, H. S. Gandhi, Industrial *Engineering of Chemical Production: Research and Development* **22** (1983) pp. 207-212.

Chapter 4

CHAPTER 4 The Oxidative Dehydrogenation of Propane Using Vanadium Oxides Supported on Nanocrystalline Cerium Oxide

4.1 Introduction

Traditional methods to produce alkenes include steam cracking and direct dehydrogenation of alkanes [1]. Oxidative dehydrogenation (ODH) is a promising emerging technology with the ability to convert light alkanes to more valuable olefin counterparts. The production of propene is required to manufacture acrolein, acrylic acid acrylonitrile and iso-propanol [2]. ODH has been extensively studied over supported vanadium oxide catalysts [3,4,5] but the current yields obtained are not satisfactory. Deep oxidation is favoured thermodynamically, over ODH, to form significant amounts of CO_x by-products; therefore a catalyst with high selectivity to the desired olefin at high conversion is the ultimate aim.

Alkanes are relatively cheap and abundant raw materials, and are therefore attractive chemical feedstocks. There has been consistent interest in this area of chemistry since the mid-1980s and there is still vast scope for improvement. The most promising catalysts have included supported molybdena and vanadium [6].

In the present work, the focus has been on different loadings of vanadium on a nanocrystalline ceria support [7]. To date, there has been very little work

focussing on the use of ceria as a support for propane ODH catalysts. This is somewhat surprising since ceria has many similarities with Titania, which has been widely and successfully employed. Ceria has been used in the control of automotive pollution since 1980 [8], mainly due to the ability to store and release oxygen. Hence, ceria has received much interest as a catalyst due to its redox behaviour. Recently, nanocrystalline ceria, produced by precipitation with urea, has been identified as a highly active hydrocarbon oxidation catalyst [9]. As a consequence of the high activity we have investigated the nanocrystalline ceria as a support for propane selective oxidation catalysts. Vanadium was selected as the supported component, as it has demonstrated selective alkane oxidation on a wide range of supports, such as alumina [10], zirconia [11] and magnesium oxide [12]. However, there is no previous data using a high surface area nanocrystalline ceria support. This chapter has been published as a paper by Topics in Catalysis (see paper 2 in publications section).

4.2 Characterisation

4.2.1 BET surface area determination

A range of ceria catalysts were prepared with different ratios of reactants and ageing times. BET was used to determine their surface area, as shown in table 4.1.

Table 4.1 BET surface areas of different ceria catalysts.

$(NH_4)_2Ce(NO_3)_6$(g)	Urea(g)	Ratio	Ageing time	Surface area m^2/g uncalcined	Surface area m^2/g calcined
30	30	1:1	24	108	91
20	40	1:2	24	55	94
16	48	1:3	3	56	113
8	24	1:3	6	63	104
20	60	1:3	24	34	136
12	48	1:4	3	73	79
10	40	1:4	6	32	91
10	40	1:4	24	98	132
40	20	2:1	24	72	76

The highest surface area, of 136 m^2g^{-1}, was observed for the ceria catalyst prepared in a ratio of 1:3 and aged for 24 hours. The ceria prepared by a ratio of 1:3 gave the highest surface areas ranging from 104 to 136 m^2g^{-1}. Due to this high surface area, further work based upon this ratio and ageing time was carried out.

The set of catalysts with vanadium supported on ceria followed a general pattern in their surface areas (shown in table 4.2). As the vanadium loading increased from 0.5% to 15% the surface area decreased from 58m^2g^{-1} to 12m^2g^{-1}. The ceria support with no vanadium loading had a surface area of 136 m^2g^{-1} and with just 0.5% loading of vanadium this was dramatically reduced. Exclusion to the pattern was exhibited by 2%VO_x/CeO_2 which had a

higher surface area of 94 m^2g^{-1}. To ensure this was a true result this anomaly was repeated and the same surface area was obtained. After the sudden increase in surface area for the 2% loading the value decreased again for the 5% loading of vanadium, 47 m^2g^{-1}, followed by the 10% loading, 33 m^2g^{-1}.

Table 4.2 BET surface areas of ceria supported catalysts.

Catalyst	Surface Area (m^2g^{-1})
$0.5\%VO_x/CeO_2$	58
$2\%VO_x/CeO_2$	94
$5\%VO_x/CeO_2$	47
$10\%VO_x/CeO_2$	33
$15\%VO_x/CeO_2$	12
TiO_2	50
$0.5\%VO_x/TiO_2$	46
$2\%VO_x/TiO_2$	29
$4\%VO_x/TiO_2$	16
$6\%VO_x/TiO_2$	21
$6.8\%VO_x/TiO_2$	46
$10\%VO_x/TiO_2$	34

The set of titania catalysts prepared for comparison gave a similar pattern in their surface areas. The support alone, titania (Degussa, P_{25}), had a surface area of 50 m^2g^{-1}. A loading of 0.5% vanadium only decreased the surface area to 46 m^2g^{-1} but with a 2% loading of vanadium it dropped to 29 m^2g^{-1}. The surface area continued to decrease until the monolayer coverage of 6.8% vanadium, where an increase was observed, with 46 m^2g^{-1}. At the higher loading of 10% vanadium the surface area started to decrease again with 34 m^2g^{-1}. The addition of vanadium to both supports resulted in a decrease in surface area. Reasons for this could be that the coverage of vanadium is approaching a monolayer or that a solid state reaction takes place forming a low surface area mixed oxide.

4.2.2 Powder X-ray Diffraction (XRD)

The powder X-ray diffraction patterns from CeO_2 and catalysts with vanadium loadings up to 5% showed a cerium (IV) oxide phase only (CeO_2, cerianite). Higher vanadium loadings showed a crystalline cerium vanadium oxide phase ($CeVO_4$, wakefieldite). From the XRD data it was also possible to determine the ceria crystallite size using line broadening in accordance with the Scherrer equation. Crystallite sizes remained similar for all catalysts, in the region of 32 to 33 nm. These data indicated that the size of crystallites were not altered by the addition of vanadium, and it is also interesting to note that the crystallite size for the 15% VO_X catalyst remained unaltered even though a bulk phase change was identified. The similar crystallite size indicates that the changes observed in surface area are related to differences in morphology and/or particle agglomeration.

Table 4.3 Phases present and crystallite sizes determined by X-ray diffraction.

Catalyst	XRD phase	Crystallite size (nm)
CeO_2	Cerium oxide (cerianite)	32.4
$0.5\%V_2O_5/CeO_2$	Cerium oxide (cerianite)	32.8
$2\%V_2O_5/CeO_2$	Cerium oxide (cerianite)	32.6
$5\%V_2O_5/CeO_2$	Cerium oxide (cerianite)	31.9
$10\%V_2O_5/CeO_2$	Cerium oxide (cerianite) Cerium vanadium oxide (wakefieldite) $CeVO_4$	32.1
$15\%V_2O_5/CeO_2$	Cerium oxide (cerianite) Cerium vanadium oxide (wakefieldite) $CeVO_4$	32.0

The XRD of the ceria catalysts showed only the phase of the support, until the higher loadings of 10.05%V_2O_5/CeO_2 and 15%V_2O_5/CeO_2. The absence of any other phases at lower loadings could be explained by the small particle size of the vanadium oxide being below the detection limit of the XRD or the presence of an amorphous vanadium containing phase. The XRD profiles of the catalysts used in the reactor showed the removal of the vanadium containing phase with only cerium oxide (cerianite) present, which showed decomposition occurred.

It was found that the titania support undergoes a phase transition from anatase to rutile, leading to a loss of surface area, at the high temperatures used in the reactor studies. This phase transition was found to occur at much lower temperatures when vanadium was present.

4.2.3 Raman Spectroscopy

The Raman spectra for the VO_x/CeO_2 catalysts are shown in figure 4.1 and for the ceria support alone in figure 4.2. The intensity of the dominant peak in the ceria spectrum made simultaneous presentation with the vanadium containing catalysts very difficult. Raman data, in figure 4.1, showed a main ceria peak for all catalysts at 456cm^{-1} [13] for vanadium loadings up to 5%. The Raman spectrum for the ceria support with no vanadium loaded is shown in figure 4.2 and has one very intense peak at 456cm^{-1}. At higher loadings of vanadium the intensity of the ceria peak decreased, in figure 4.1. With the addition of vanadium on the ceria support peaks associated with vanadium species were observed. Peaks at around 1030cm^{-1} were attributed to the

symmetric stretch of V=O in isolated VO_4 tetrahedra. Raman bands present at 909 and 1041cm^{-1} were associated with highly dispersed vanadium species, such as isolated VO_4 and polyvanadate species. The frequency at which bands occurred in the Raman spectrum shifted with increased vanadium loading. This suggested that as the loading increased the dispersed vanadium species interacted strongly with the nanocrystalline ceria support.

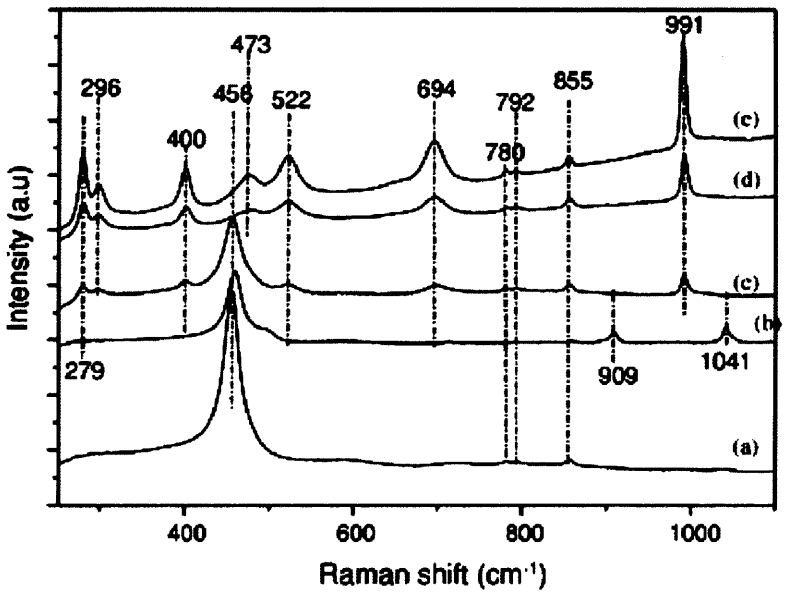

Figure 4.1 Raman spectra for a) 0.5%VO_x/CeO_2 b) 2%VO_x/CeO_2 c) 5%VO_x/CeO_2 d) 10%VO_x/CeO_2 e) 15%VO_x/CeO_2

Higher loadings, of 10 and 15 % vanadium, resulted in peaks being observed at ca. 280, 400, 522, 694 and 991cm^{-1}. The peaks observed were assigned to crystalline V_2O_5 although the majority of the peaks were of low intensity suggesting this phase was present as a minor component [14, 15]. Lower loadings of vanadium gave a clear peak indicative of the ceria support. For the higher loadings this peak was shifted to a slightly higher frequency and

was thought to be due to the formation of a mixed ceria vanadium oxide phase which was earlier identified by XRD studies.

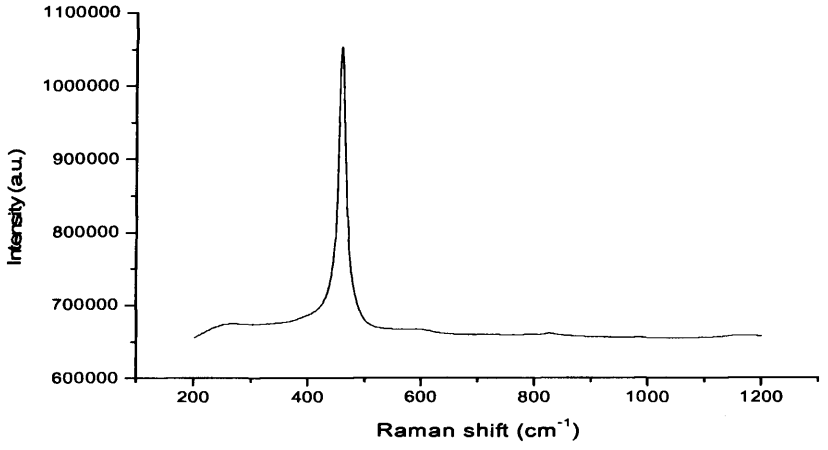

Figure 4.2 Raman spectrum for CeO_2

Table 4.4 Raman FWHM values for the VOx/CeO_2 catalysts.

Catalyst	Raman FWHM
CeO_2	21.4
$0.5\%V_2O_5/CeO_2$	23.2
$2\%V_2O_5/CeO_2$	25.7
$5\%V_2O_5/CeO_2$	29.8
$10\%V_2O_5/CeO_2$	28.5
$15\%V_2O_5/CeO_2$	38.0

The full width half maximum values of the main Raman peak of the ceria support are shown in table 4.4. With increased vanadium loading, the FWHM increased from 21.4 cm^{-1} for the ceria support alone to 38.0 cm^{-1} for the 15%

loading. This increase in FWHM has been associated with a decrease in crystallite size or increase in defect concentration. As the data obtained from X-ray diffraction showed the crystallite size did not change significantly it can be assumed that increasing the vanadium loading causes an increase in the catalyst defect concentration.

4.2.4 Scanning Electron Microscopy (SEM)

The catalysts were investigated by SEM and the effect of adding vanadium to the ceria support is shown in figures 4.3, 4.4. 4.5 and 4.6.

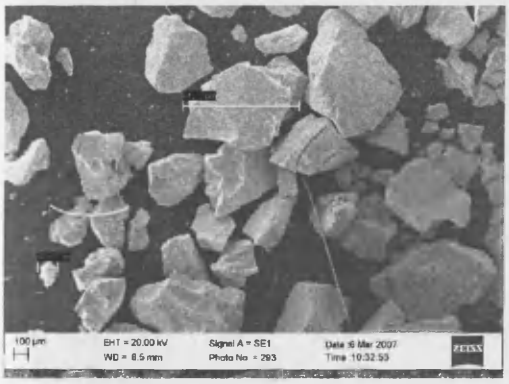

Figure 4.3 SEM image of CeO_2

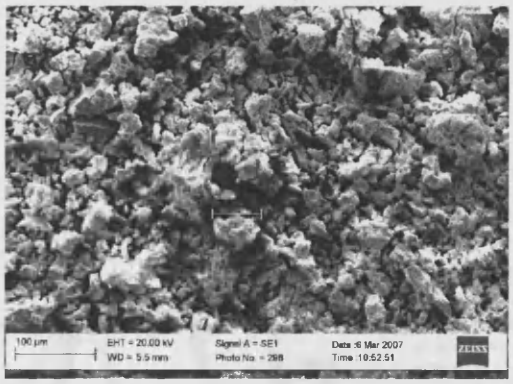

Figure 4.4 SEM image of $0.5\%VO_x/CeO_2$

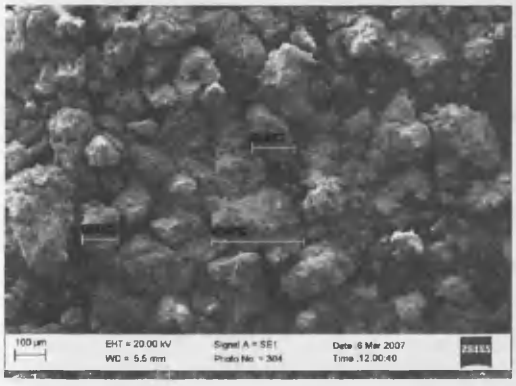

Figure 4.5 SEM image of $10\%VO_x/CeO_2$

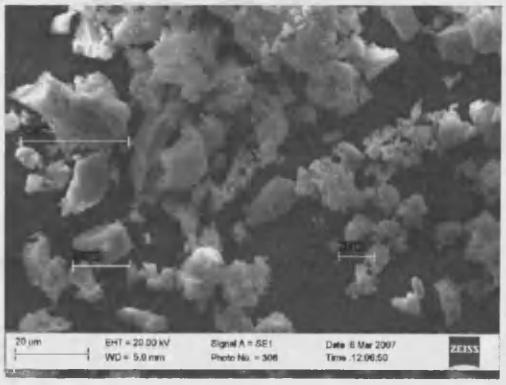

Figure 4.6 SEM image of $15\%VO_x/CeO_2$

The ceria support, figure 4.3, had large jagged particles (843μm) whereas with just 0.5% vanadium loaded on the support, figure 4.4, the morphology of

the powder changed to smaller 'fluffy' particles (59μm). Higher loadings of vanadium resulted in smaller particle sizes for 10% and 15%, figures 4.5 and 4.6 respectively. The greatest loading of vanadium, of 15%, resulted in the smallest of particles (16μm) with the same 'fluffy' appearance.

4.2.5 Temperature Programmed Reduction (TPR)

Temperature programmed reduction of the ceria and vanadia containing catalysts was carried out. Figure 4.7 shows the TPR profiles of these catalysts.

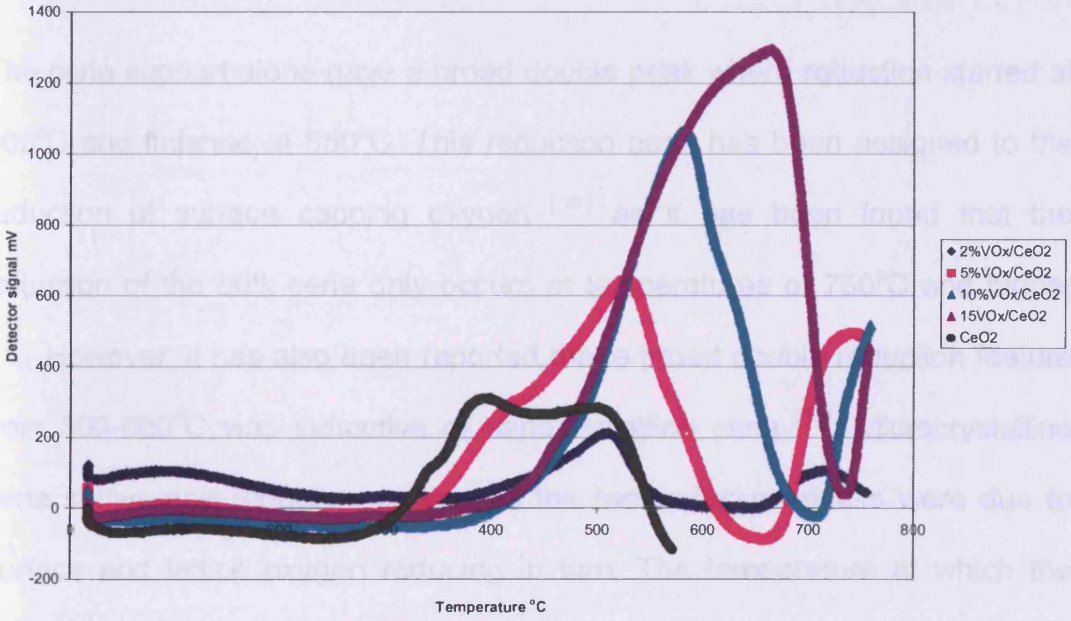

Figure 4.7 Temperature programmed reduction profiles for vanadia/ceria catalysts

Figure 4.7 shows that with higher vanadium loadings on the ceria support, the temperature at which reduction occurred increased. The figure also shows that with heightened temperatures increased hydrogen consumption was

observed. A summary of the redox behaviour of the catalysts is shown in table 4.5.

Table 4.5 Table showing the temperature of maximum reduction.

Catalyst	T_{max} (°C)
CeO_2	390 and 520
$2\%VO_x/CeO_2$	510
$5\%VO_x/CeO_2$	540
$10\%VO_x/CeO_2$	600
$15\%VO_x/CeO_2$	690

The ceria support alone gave a broad double peak where reduction started at 300°C and finished at 550°C. This reduction peak has been assigned to the reduction of surface capping oxygen [16] as it has been found that the reduction of the bulk ceria only occurs at temperatures of 750°C and higher [17]. However, it has also been reported that a broad double reduction feature from 300-600°C was indicative of nanocrystalline ceria [18]. Microcrystalline ceria shows one reduction peak, and the two reduction peaks were due to surface and lattice oxygen reducing in turn. The temperature at which the detector signal was most intense (T_{max}) was 390°C. This maximum corresponds to work carried out by *Trovarelli et al* [19] where they found Ce^{4+}/Ce^{3+} reduction of the surface was occurring.

As the vanadium content increased T_{max} was shifted to higher temperatures, as shown in table 4.5, and the peaks became broader with increased hydrogen consumption. With vanadium loaded on the ceria support there are

two possible redox couples which can occur. The first is the reduction of surface ceria, Ce^{4+}/Ce^{3+} and the second is the reduction of surface vanadium species, V^{4+}/V^{3+}. The higher loadings of vanadium, such as 15%, gave a TPR reduction peak in the region of 600°C, which has been found [20] to be due to the presence of a $CeVO_4$ phase on the surface. At lower loadings of vanadium the reduction peak is at lower temperatures due to the presence of VO_x surface species rather than $CeVO_4$. The ease of reduction of the different vanadium species determined their individual TPR profile. The higher loadings of vanadium form a cerium vanadate phase which is relatively hard to reduce compared to isolated vanadium species on the surface. The ceria support reduced easily, which reinforced its application as a redox material due to its ability to cycle between Ce^{4+} and Ce^{3+}.

4.2.6 X-ray Photoelectron Spectroscopy (XPS)

X-ray photoelectron spectroscopy studies were carried out on the catalysts and figure 4.8 shows the spectra of the Ce(3d) for the bare ceria support and the catalysts after loading with vanadium. The spectrum for CeO_2 was complex and comprised of three doublets, each spin-orbit split doublet corresponding to a different electron distribution in the final ion state after photoemission. The different final state electronic configurations are indicated on the spectrum. The highest loading of vanadium on the ceria support gave a vastly different profile to that of the support alone. Figure 4.8 f) showed the formation of Ce^{3+} species with the spectrum consisting of two doublets due to final state effects. Although the spectrum was dominated by Ce^{3+} features, there was an attenuated peak at 915 eV indicating the presence of Ce^{4+}.

From XPS data the formation of Ce^{3+} only occurred at loadings of 5% vanadium and higher.

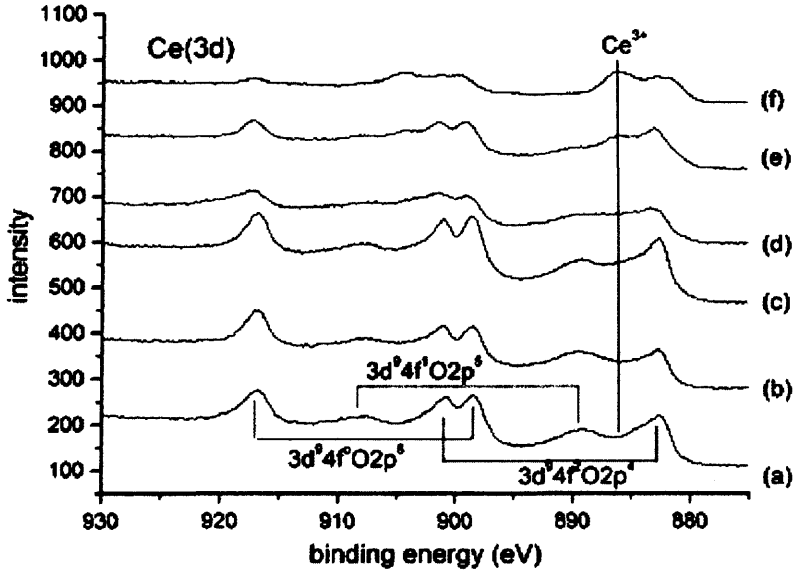

Figure 4.8 Ce(3d) X-ray photoemission spectra for a) the bare ceria support and with different V loadings: b) 0.5% c) 2% d) 5% e) 10% and f) 15%. Indicated on spectrum a) are the different final state electronic configurations giving rise to the three doublets.

In figure 4.9 the spectra of V(2p) shows monotonic increase in intensity with vanadium loading. The binding energies of the V(2p3/2) component indicated that the vanadium species were in the +5 oxidation state only and the symmetrical shape reflected the absence of the +4 contribution.

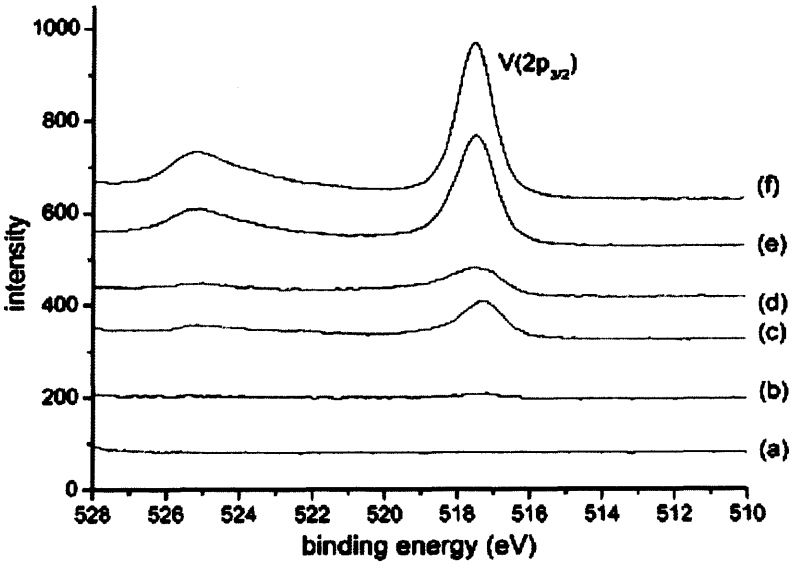

Figure 4.9 V(2p) X-ray photoemission spectra for a) the bare ceria support with different V loadings: b) 0.5% c) 2% d) 5% e) 10% and f) 15%.

4.3 Results

4.3.1 Propane oxidative dehydrogenation over ceria supported vanadium oxides

The conversions of propane for VO_X/CeO_2 catalysts with varying vanadium loadings are shown in figure 4.8.

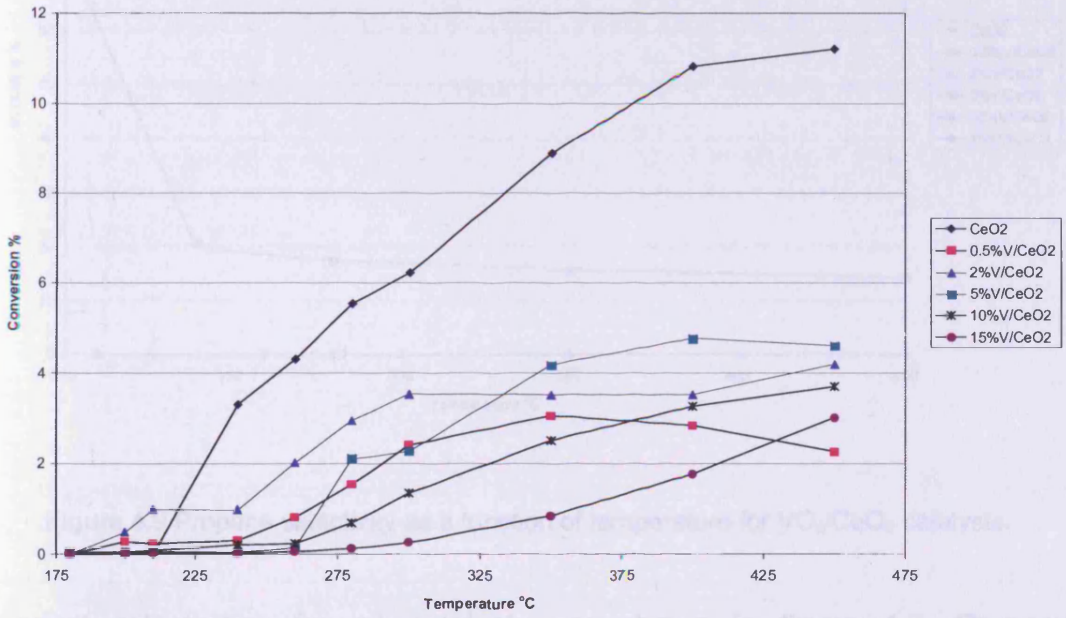

Figure 4.8 Propane conversion over VO_x/CeO_2 catalysts

Initial propane conversion was observed at 175°C. Propane conversion increased with temperature, reaching a maximum of 11% at 450°C for the ceria support with no vanadium loaded. For this catalyst the sole reaction product was CO_2.

Varying the vanadium loading on the ceria support influenced the propane conversion. Initial conversions, at 250°C, showed $2\%VO_x/CeO_2$ to have the highest conversion of 2% and $15\%VO_x/CeO_2$ to have the lowest conversion of 0.06%. However, at higher temperatures of 450°C, $5\%VO_x/CeO_2$ had a

conversion of 5% where 2%VO_x/CeO_2 only reached 4%. The catalyst with the lowest conversion overall was that of 15%VO_x/CeO_2, as the greatest conversion exhibited was only 2% at 450°C.

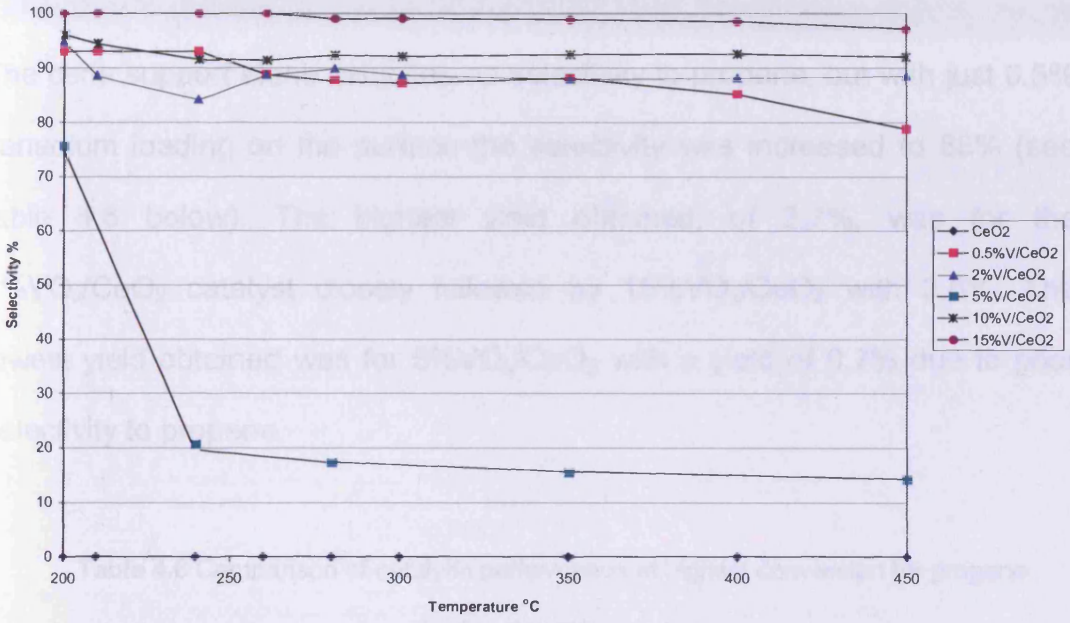

Figure 4.9 Propene selectivity as a function of temperature for VO_x/CeO_2 catalysts.

Product selectivities for all catalysts are shown in figure 4.9. Propene selectivity remained high for all catalysts, excluding the ceria support on its own, which exhibited no selectivity to propene. The catalyst exhibiting highest selectivity towards propene was 15%VO_x/CeO_2 which showed 99% at 200°C. The selectivity decreased slightly and remained high up to 450 °C (ca. 97%), but it must be noted that this was one of the least active catalysts.

The 5%VO_x/CeO_2 catalyst showed high conversion of propane but selectivity to propene was lower. Initial selectivity of 76% at 200°C was the lowest of all the vanadium catalysts studied and this steadily decreased to 14% at 450°C. Not surprisingly the highest selectivity observed for all catalysts was at low

conversion, in the temperature range 325-375°C. Overall, the most efficient catalyst, with good conversion and selectivity, was $2\%VO_x/CeO_2$ as the highest yield of propene was obtained.

The ceria support alone exhibited no selectivity to propene, but with just 0.5% vanadium loading on the surface the selectivity was increased to 88% (see table 4.6 below). The highest yield obtained, of 3.7%, was for the $2\%VO_x/CeO_2$ catalyst closely followed by $15\%VO_x/CeO_2$ with 3.6%. The lowest yield obtained was for $5\%VO_x/CeO_2$ with a yield of 0.7% due to poor selectivity to propene.

Table 4.6 Comparison of catalytic performance at highest conversion for propane oxidative dehydrogenation.

Catalyst	Temperature (°C)	Propane conversion (%)	Propene selectivity (%)	Per pass propene yield (%)
CeO_2	450	11.2	0	0
$0.5\%V_2O_5/CeO_2$	350	3.1	88.1	2.7
$2\%V_2O_5/CeO_2$	450	4.2	88.5	3.7
$5\%V_2O_5/CeO_2$	400	4.7	14.3	0.7
$10\%V_2O_5/CeO_2$	450	3.7	92.0	3.4
$15\%V_2O_5/CeO_2$	450	3.7	97.1	3.6

The propene per pass yields for each temperature were calculated and plotted in figure 4.10.

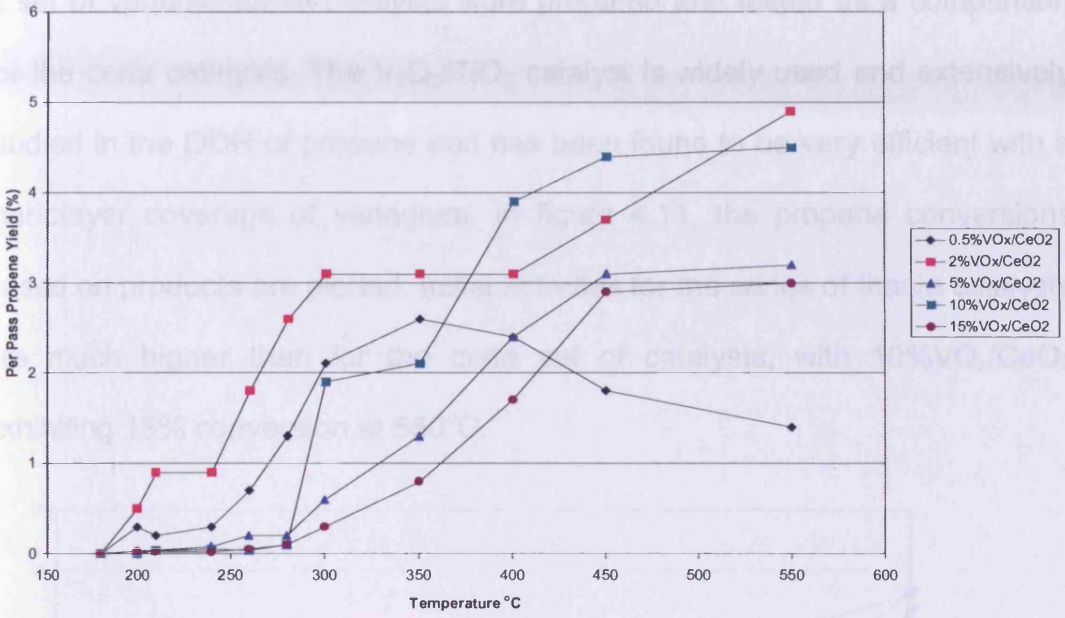

Figure 4.10 Per pass propene yields as a function of temperature.

The 2%VO_x/CeO_2 had the greatest overall yield which can be clearly seen in figure 4.10. Figure 4.10 is interesting as some catalysts have a continually increasing yield with temperature, whilst others go through a maximum.

4.3.2 Propane oxidative dehydrogenation over titania supported vanadium oxides

A set of vanadia/titania catalysts were prepared and tested as a comparison for the ceria catalysts. The V_2O_5/TiO_2 catalyst is widely used and extensively studied in the ODH of propane and has been found to be very efficient with a monolayer coverage of vanadium. In figure 4.11, the propane conversions based on products are plotted. Initial activities for the series of titania catalysts are much higher than for the ceria set of catalysts, with $10\%VO_x/CeO_2$ exhibiting 15% conversion at 550°C.

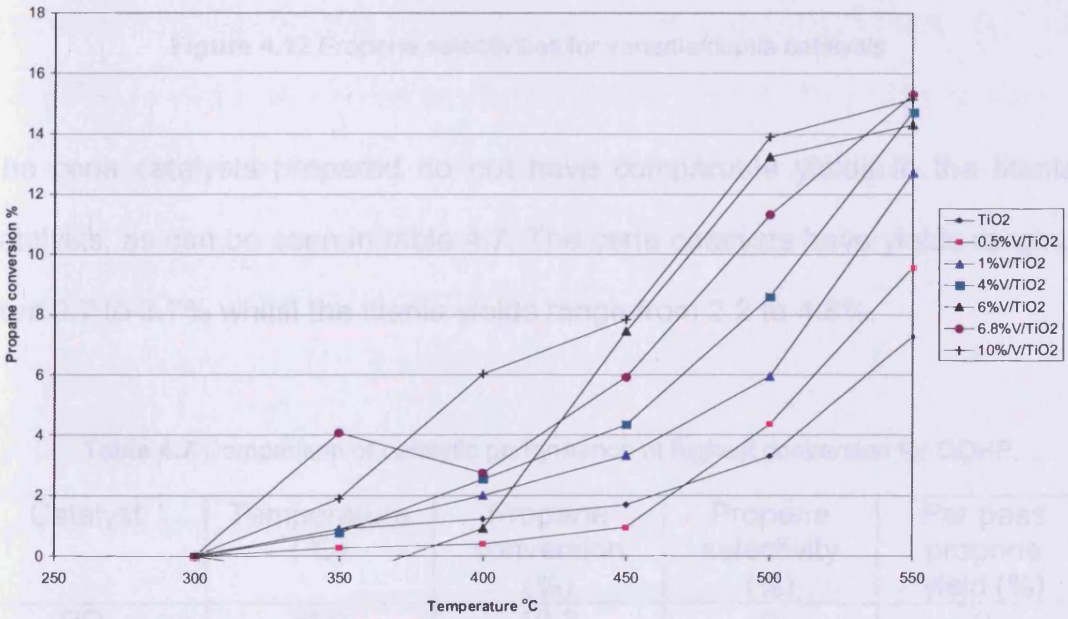

Figure 4.11 Conversion of propane for different vanadia/titania catalysts

The propene selectivities, figure 4.12, are much higher than the ceria set of catalysts with $4\%VOx/TiO_2$ reaching 93% at 300°C but decreasing to 40% at 550°C.

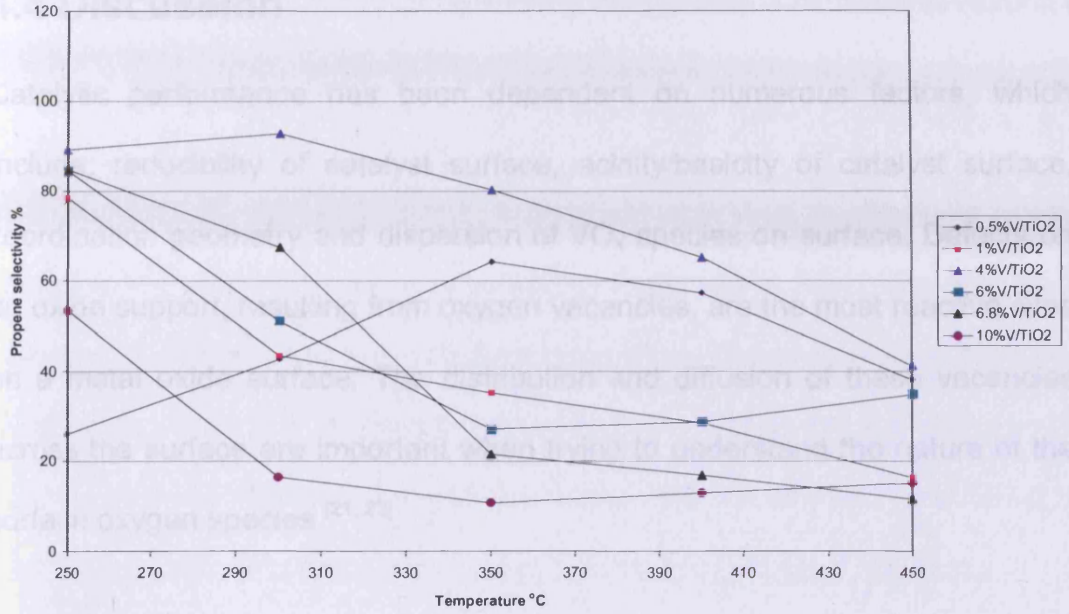

Figure 4.12 Propene selectivities for vanadia/titania catalysts

The ceria catalysts prepared do not have comparable yields to the titania catalysts, as can be seen in table 4.7. The ceria catalysts have yields ranging from 0.7 to 3.7% whilst the titania yields range from 2.2 to 4.8%.

Table 4.7 Comparison of catalytic performance at highest conversion for ODHP.

Catalyst	Temperature (°C)	Propane conversion (%)	Propene selectivity (%)	Per pass propene yield (%)
TiO_2	550	10.3	0	0
$0.5\%V_2O_5/TiO_2$	550	8.5	38.1	3.2
$2\%V_2O_5/TiO_2$	550	13.2	16.3	2.2
$4\%V_2O_5/TiO_2$	550	7.0	41.1	2.9
$6\%V_2O_5/TiO_2$	550	13.9	34.9	4.8
$6.8\%V_2O_5/TiO_2$	550	22.3	11.5	2.6
$10\%V_2O_5/TiO_2$	550	25.3	15.1	3.8

4.4 Discussion

Catalytic performance has been dependant on numerous factors, which include; reducibility of catalyst surface, acidity/basicity of catalyst surface, coordination geometry and dispersion of VO_x species on surface. Defects on an oxide support, resulting from oxygen vacancies, are the most reactive sites on a metal oxide surface. The distribution and diffusion of these vacancies across the surface are important when trying to understand the nature of the surface oxygen species [21, 22].

High selectivity was needed for the production of propene and most catalysts in this study exhibited selectivities in the region of 90%. This high selectivity can be ascribed to a surface with low acidity (high basicity) which allowed the alkene to desorb before undergoing further reactions to the carbon oxide by-products.

Ceria is of great interest, when considering the fact that the active sites of a catalyst are the surface defects. On the surface of ceria, oxygen vacancies are rapidly formed and eliminated giving the support a high oxygen storage capacity [23]. The main use of ceria has been for modern automotive exhaust treatment but has also been found to enhance transition metal performance in the water gas shift reaction, steam reforming and preferential oxidation of carbon monoxide. The surface oxygen vacancies on the ceria surface have been shown to be immobile at room temperature [24] but at higher temperatures linear clusters of vacancies form. The oxygen vacancies can bind the adsorbate more strongly and can also assist in their dissociation.

Adsorbed gases or catalytic reaction intermediates are able to interact simultaneously with several Ce^{3+} ions.

The mechanism by which ODH occurs on an oxide support has been discussed in detail [25] and is proposed to occur via a Mars Van Krevelen mechanism whereby "oxygen that is introduced into the alkene stems from the catalyst bulk". In this mechanism the catalyst is reduced, the bulk of the catalyst replenished with oxygen from the gas phase and the catalyst reoxidised. The rate determining step of ODH is the C-H bond activation.

Nanocrystalline materials exhibit high surface areas, high reactivity and high concentrations of oxygen vacancies and surface adsorbed species (in the case of ceria). The preparation method used with urea as a precipitating agent resulted in a much higher surface area than conventional methods of ceria preparation [26] with a higher activity being observed. It contained crystallites of a much smaller size and the formation of a much more active surface structure [27]. Due to the acid/basic and oxidation/reduction behaviour of ceria it makes it a suitable catalyst for many catalytic reactions.

When considering an additive for the ceria support it was proposed to test vanadium oxide, as this had been found to be highly suitable for a variety of reactions including the selective oxidation of hydrocarbons and the ODH of short chain alkanes. However, the activity and selectivity are dependant on the nature of the support and the dispersion of vanadium oxide on the surface.

The general observation of the catalysts in the study was that with increased vanadium loading the conversion of propane actually decreased. The lowest conversion of propane was observed for $15\%VO_x/CeO_2$ and this was the most selective catalyst for propene production. The ceria catalyst was a known combustion catalyst and it was expected to be 100% selective to carbon dioxide.

As conversion decreased from 11% for ceria to 4% for $15\%VO_x/CeO_2$, the vanadium present must have affected the reactive sites on the ceria support. The increased vanadium species on the ceria surface may decrease the reactive sites by blocking them as the Raman and XRD profiles showed spectra where vanadium species were present in large quantities. The highest selectivity observed was for a $CeVO_4$ phase rather than separate ceria and vanadium phases. In the higher loadings of vanadium on the ceria support, high FWHM values were obtained in the Raman spectra, suggesting the presence of more surface defects. An increased number of defects would promote the rate of oxidation if the defects were present on the catalyst surface. It is possible that the defects created interacted with the vanadium which was loaded on the surface. The interaction may have resulted in the defects being covered and therefore have no correlation to selectivity or activity of the catalysts. The nature of the active site needs to be determined to allow modification of catalysts, in the future, to obtain better yields.

The coverage of the vanadium is important on the ceria support. At low loadings, the ceria support will remain uncovered and more side reactions to

form CO_x can occur. At higher loadings there is the disadvantage of decreased conversion due to the blocking of propane activation sites. The coordination of the vanadium on the surface will determine the selectivity of the reaction taking place due to different oxygen supplies from the crystal lattice structure [28]. The TPR profiles allow a correlation between the reducibility of the different catalysts prepared and their activity in the ODH propane. Upon increased vanadium loading the reducibility of the catalysts is decreased, which may be explained by a stronger interaction of the vanadium with the support ($CeVO_4$ phase). A stronger bond would hinder the surface oxygen from participating in the propane activation process therefore reducing the conversion but allowing a selective process to occur as consecutive oxidation to CO_x would be limited. Ceria alone has a low selectivity, and relatively low temperature of reducibility, due to adsorbed oxygen species being highly active and unselective in their reactions.

A small loading of vanadium, 0.5%, had a dramatic effect on the product distribution of propane ODH. Vanadium has been shown [23] to limit ceria in its ease of changing oxidation state from Ce^{4+}/Ce^{3+} and favours the Ce^{3+} state to form the $CeVO_4$ phase. At the higher loadings this phase is more pronounced, with low conversions of propane but high selectivities to propene. The correlation between reducibility of the catalysts and activity/selectivity was not clear. All the vanadia-ceria catalysts gave conversion and selectivity to propene before the temperatures at which reduction occurred. It was found that the hydrogen consumption and T_{max} of the TPR studies increased with increased vanadium loading on the support. The highest selectivity observed

was for the highest loading of vanadium, 15%, therefore it could be assumed that a highly reducible catalyst was responsible for such high selectivity.

Alkanes have a lower reactivity compared to the corresponding olefin so selectivity is paramount in designing a new catalyst, which needs to be intrinsically multifunctional. The bonding of the vanadium to the oxide support is important as it has a strong influence over the activity and selectivity [29]. The vanadium can be present in different forms, depending on the amount loaded on the support. Below a monolayer coverage, dispersed vanadium is observed but above a monolayer coverage there is also the formation of V_2O_5 crystallites [30]. Vanadia has a higher surface density than most other metal oxides and this allows greater selectivity of the catalyst [31]. Often the side products and undesirable products of a catalytic reaction are due to the oxide support being exposed.

4.5 Conclusions

Ceria on its own was very active for the total oxidation of propane under the conditions used for oxidative dehydrogenation but it exhibited no selectivity towards propene with its sole product being carbon dioxide. The addition of vanadium resulted in switching the activity of ceria to give appreciable selectivity to propene. The lower loadings of vanadium gave highly dispersed vanadia species, which were selective to propene. The higher loadings of vanadium resulted in the formation of a mixed cerium vanadium phase, which was also active in the ODH of propane. The formation of a mixed phase was

of the most interest for future work where conditions could be optimised to give improved yields.

4.6 References

[1] B. Frank, A. Dinse, O. Ovsitser, E. V. Kondratenko, R. Schomacker, *Applied Catalysis A.* **323** (2007) pp. 66.

[2] T. Davies, S. H. Taylor, *Journal of Molecular Catalysis A.* **220** (2004) pp. 77.

[3] E. Heracleous, M. Machli, A. A. Lemonidou, I. A. Vasalos, *Journal of Molecular Catalysis A.* **232** (2005) pp. 29.

[4] P. Viparelli, P. Ciambelli, L. Lisi, G. Ruoppolo, G. Russo, J. C. Volta, *Applied Catalysis A.* **184 (2)** (1999) pp. 291.

[5] B. Mitra, I. E. Wachs, G. Deo, *Journal of Catalysis* **240 (2)** (2006) pp. 151.

[6] F. C. Meunier, A. Yasmeen, J. R. H. Ross, *Catalysis Today* **37** (1997) pp. 33.

[7] T. Garcia, B. E. Solsona, S. H. T. Taylor, *Applied Catalysis B.* **66 (1-2)** (2006) pp. 92.

[8] M. Salazer, D. A. Berry, T. H. Gardner, D. Shekhawat, D. Floyd, D., *Applied Catalysis A.* **310** (2006) pp. 54.

[9] S. Zhao, R. J. Gorte, *Applied Catalysis A* **277** (2004) pp. 129.

[10] T. Blasco, J. M. Galli, L. Nieto, F. Trifiro, *Journal of Catalysis* **169** (1997) pp. 203.

[11] K. Chen, E. Iglesia, A. T. Bell, *Journal of Catalysis* **192** (2000) pp. 197.

[12] C. Tellez, M. Abon, J. A. Dalmon, C. Mirodatos, J. Santamaria, *Journal of Catalysis* **195** (2000) pp. 113.

[13] W. H. Weber, K. C. Hass, J. R. McBride, *Physical Chemistry Review B* **48** (1993) pp. 178.

[14] A. Khodakov, B. Olthof, A. T. Bell, E. Iglesia, *Journal of Catalysis* **181** (1999) pp. 205.

[15] K. J. Chao, C. N. Wu, H. Chang, L. J. Lee, S. F. Hu, *Journal of Physical Chemistry B* **101** (1997) pp. 6341.

[16] H.C. Yao, Y. F. Yu Yao, *Journal of Catalysis* **86** (1984) pp. 254.

[17] D. Andreeva, R. Nedyalkova, L. Ilieva, M. V. Abrashev, *Applied Catalysis B* **52** (2004) pp. 157.

[18] H. J. Choi, J. Moon, H. B. Shim, K. S. Han, E. G. Lee, K. D. Jung, *Journal of Americam Ceramic Society* **89 (1)** (2000) pp. 343.

[19] A. Trovarelli, G. Dolcetti, C. De Leitenburg, J. Kaspar, P. Finetti, A. Santoni, *Journal of Chemistry Society: Faraday Transmissions* **88** (1992) pp. 1311.

[20] C. T. Au, W. D. Zhang, H. L. Wan, *Catalysis Letters* **37** (1996) pp. 241.

[21] E. Ntainjua, T. Garcia, B. Solsona, S. H. Taylor, *Catalysis Today* **137** (2008) pp. 373.

[22] E. Ntainjua, T. Garcia, B. Solsona, S. H. Taylor, *Applied Catalysis B* **76** (2007) pp. 248.

[23] Campbell, C. T., Peden, C. H. F., *Science* **309 (5735)** (2005) pp. 713.

[24] M.V. Martinez-Huerta, G. Deo, J. L. G. Fierro, M. A. Banares, *Journal of Physical Chemistry* **111** (2007) pp. 18708.

[25] Stelzer, J. B., Caro, J., Fait, M., *Catalysis Communications* **6 (1)** (2005) pp. 1.

[26] Ying, J. Y., Tschope, A., *Journal of Chemical Engineering* **64** (1996) pp. 225.

[27] Garcia, T., Solsona, B., Taylor, S. H., *Catalysis Letters* **105 (3-4)** (2005) pp. 183.

[28] M. Machli, A. A. Lemonidou, *Catalysis Letters* **99 (3-4)** (2005) pp. 221.

[29] C. L. Pieck, M. A. Banares, J. L. G. Fierro, *Journal of Catalysis* **224 (1)** (2004) pp. 1.

[30] G. Deo, I. E. Wachs, J. Haber, *Critical Review Surface Chemistry* **4** (1994) pp. 141.

[31] I.E. Wachs, G. Deo, J.-M. Jehng, D.S. Kim, *Heterogeneous Hydrocarbon Oxidation* **638** (1996) pp. 292.

Chapter 5

CHAPTER 5 The Oxidative Dehydrogenation of Propane using Nanocrystalline Metal Oxides

5.1 Introduction

In 1959, Feynman [1] first suggested the importance of nanomaterials which created great interest in the field. The properties of the nanocrystalline material differed greatly to the bulk with often high surface areas but limited stability. A range of metal oxides, including cobalt, iron and manganese, were prepared using a solid state reaction which is known to produce a nanocrystalline cobalt oxide [2]. Preparation variables were investigated by changing the ratios of the corresponding nitrate and ammonium bicarbonate.

It is proposed [3] that highly ionic metal oxides, such as Co_3O_4, Fe_2O_3 and MnO_2, are generally total oxidation catalysts although selective behaviour in ODH is possible. Transition metal based catalysts provide a cheap and selective option for the oxidation of organic materials. Cobalt oxide is one of the most active binary oxides for catalytic combustion [4] and has been used in the oxidation of CO since the 1920s [5]. It is an active component in the catalytic purification of exhaust gases and has a high activity in hydrocarbon combustion.

Iron oxide has several applications including ammonia and Fischer-Tropsch synthesis, carbon monoxide hydration and oxidation, water gas shift reaction,

NO_x and soot removal, decomposition of alcohols and hydrogen peroxide to name only a few [6]. The catalytic application of iron oxide is important but it should also be noted that it has a critical role in magnetic recording media, magnetic fluids for storage, MRI enhancement and sensors.

As an oxide, manganese is active in the complete oxidation of light paraffins but when used as a support for molybdenum it is active for the oxidative dehydrogenation of propane [7]. Manganese oxide, as an octahedral molecular sieve, has been used for the ODH of 1-butene but with little selectivity (15-20%) to the desired product, 1,3-butadiene [8]. Other applications of manganese oxide in catalysis include the selective catalytic reduction of NO, removal of hydrogen sulphide [9] and the oxidation of CO, methane and hydrocarbons [10].

Many materials and chemical intermediates derived from propene are used in consumer products. Propene is used to produce acrolein, acrylic acid acrylonitrile, and iso-propanol [11, 12]. The demand for these products is driven by the high growth rate of the plastics industry. The aim of propane ODH is to obtain the corresponding olefin, propene. Steam cracking, catalytic cracking and direct dehydrogenation have all been used to obtain the desired product but are energy intensive and inefficient processes. Oxidative dehydrogenation provides an alternative to the traditional methods as it can overcome thermodynamic constraints due to the presence of oxygen. There are several advantages of the ODH method which include the reaction being exothermic, the raw material being an alkane (cheap and abundant) and the process is

carried out at lower temperatures than previous techniques. However the disadvantages of ODH include deep oxidation being favoured to form CO_x products, alkane activation is difficult and high selectivity of the catalyst is required.

5.2 Characterisation

5.2.1 BET surface area determination

5.2.1.1. Cobalt oxides

The BET surface areas for the cobalt catalysts, shown in table 5.1, have no correlation to the different ratios of reactants to which they were prepared.

Table 5.1 BET surface areas of Co_3O_4 with different preparation ratios.

Ratio (of cobalt nitrate to ammonium bicarbonate)	Surface area (m^2g^{-1})
5:0	38
5:1	54
5:2	102
5:3	74

The cobalt oxide ratio of 5:1 had the lowest surface area of 54 m^2g^{-1} which increased to 102 m^2g^{-1} for the 5:2 ratio but then decreased to 74 m^2g^{-1} for the 5:3 ratio. Past work on nanocrystalline cobalt oxide [2] reported a maximum surface area of 159m^2g^{-1} by the solid state reaction.

Higher surface areas were observed where more ammonium bicarbonate was present. The increased amount of ammonium bicarbonate may have caused differences in the grinding process. The lowest surface area was observed for the 5:1 ratio. This could be explained by not enough ammonium bicarbonate being present to react with the entire cobalt nitrate. The highest surface area was that of Co_3O_4 5:2. Therefore it is suggested this was an ideal ratio of the nitrate and carbonate. In the case of cobalt oxide 5:3, there was an excess of ammonium bicarbonate. A decrease in surface area could be explained by the carbonate clumping together along the cobalt oxide surface. The evolution of ammonia formed during the reaction disperses through the mixture giving a high surface area. The reaction taking place during the preparation is:

$$2Co(NO_3)_2.6H_2O + 5NH_4HCO_3 \rightarrow Co_2(OH)_2CO_3 + 4NH_4NO_3 + NH_3 + 4CO_2 + 14H_2O$$

5.2.1.2 Iron oxides

The surface areas for the iron oxides prepared are shown in table 5.2.

Table 5.2 BET surface areas of Fe_2O_3 with different preparation ratios.

Ratio (of iron nitrate to ammonium bicarbonate)	Surface area (m^2g^{-1})
5:0	56
5:1	29
5:2	52
5:3	62

The highest surface area was observed for the ratio of 5:3 with 62 m^2g^{-1}. As the ratio lowered the surface area decreased to 52 m^2g^{-1} for the 5:2 ratio and 29 m^2g^{-1} for the 5:1 ratio. It is proposed that a larger amount of ammonium bicarbonate has beneficial effects in terms of increasing the iron oxide surface area.

5.2.1.3 Manganese oxides

The surface areas for the manganese oxides prepared are shown in table 5.3.

Table 5.3 BET surface areas of MnO_2 with different preparation ratios.

Ratio (of manganese nitrate to ammonium bicarbonate)	Surface area (m^2g^{-1})
5:0	22
5:1	62
5:2	78
5:3	76

The manganese oxides followed a similar pattern to that found for the cobalt oxides. There was no direct correlation between the ratio of the reactants and the surface area of the oxide formed. The highest surface area was found for the ratio 5:2 with 78 m^2g^{-1}, followed by the ratio 5:3 with 76 m^2g^{-1} and finally the 5:1 ratio with 62 m^2g^{-1}. The manganese oxide prepared from the manganese nitrate alone had the lowest surface area of all the oxides with 22

m^2g^{-1}. This highlighted the importance of the solid state preparation method to give high surface area materials.

5.2.2 Powder X-ray Diffraction (XRD)

5.2.2.1 Cobalt oxides

The cobalt oxide catalysts prepared all gave the Co_3O_4 cubic phase from X-ray diffraction studies. The cobalt oxide which was prepared with no ammonium bicarbonate had a crystallite size of 80nm (table 5.4) which increased to 87nm with the 5:1 ratio. Due to experimental error this difference in crystallite size was negligible. When the amount ammonium bicarbonate was increased for the ratio of 5:2, the crystallite size decreased significantly to 29nm. However, for the ratio of 5:3 the crystallite size increased again to 88 nm.

Table 5.4 XRD phases and crystallite sizes for the different cobalt oxides prepared.

Cobalt oxide	XRD phase identified	Crystallite size (nm)
5:0	Co_3O_4 cubic	80
5:1	Co_3O_4 cubic	87
5:2	Co_3O_4 cubic	29
5:3	Co_3O_4 cubic	88

5.2.2.2 Iron oxides

The iron oxide catalysts prepared all gave α-Fe_2O_3 rhombohedral phase from x-ray diffraction studies. The crystallite sizes were much larger than those found for the cobalt oxides with the largest being 285 nm for the 5:3 ratio. It was observed that as more ammonium bicarbonate was incorporated in the preparation the crystallite size increased. The iron nitrate with no ammonium bicarbonate (5:0) had a crystallite size of 88 nm (table 5.5) which increased to 143 nm for the 5:1 ratio and 171 nm for the 5:2 ratio.

Table 5.5 XRD phases and crystallite sizes for the iron oxides.

Iron oxide	XRD phase identified	Crystallite size (nm)
5:0	α-Fe_2O_3 rhombohedral syn-hematite	88
5:1	α-Fe_2O_3 rhombohedral syn-hematite	143
5:2	α-Fe_2O_3 rhombohedral syn-hematite	171
5:3	α-Fe_2O_3 rhombohedral syn-hematite	285

5.2.2.3 Manganese oxides

The manganese oxide catalysts prepared all gave the MnO_2 hexagonal phase in x-ray diffraction studies except the 5:3 ratio which showed the presence of a MnO_2 tetragonal phase. The crystallite sizes calculated were even smaller

than those found for the cobalt oxides with the smallest crystallite size being 15 nm for the 5:3 ratio.

Table 5.6 XRD phases and crystallite sizes for the manganese oxides.

Manganese oxide	XRD phase identified	Crystallite size (nm)
5:0	MnO_2 hexagonal Syn-akhtenskite	171
5:1	MnO_2 hexagonal Syn-akhtenskite	54
5:2	MnO_2 hexagonal Syn-akhtenskite	44
5:3	MnO_2 tetragonal Syn-akhtenskite	15

5.2.3 Raman Spectroscopy

5.2.3.1 Cobalt oxides

The Raman profiles for the different cobalt oxides prepared are shown in figure 5.1. The different preparation methods for the different cobalt oxides did not have an effect on the band positioning but did affect the intensity of the peaks observed.

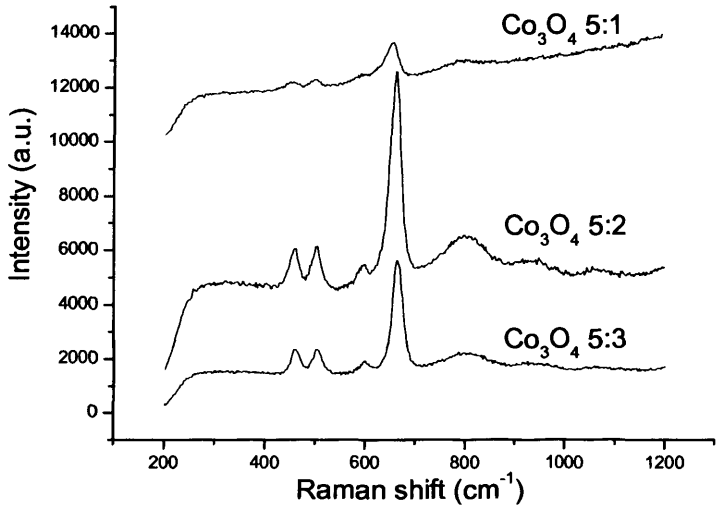

Figure 5.1 Raman spectra of the different cobalt oxides prepared.

All of the cobalt oxides gave Raman spectra indicative of Co_3O_4 [13]. The FWHM (full width half maximum) values of the main peak in the cobalt profiles are shown in table 5.7. From the FWHM values, it is possible to see that as the ratio of nitrate to carbonate increases, the peak becomes narrower.

Table 5.7 Table of FWHM values for the cobalt oxides.

Catalyst	FWHM of main peak ($\sim 650cm^{-1}$)
Co_3O_4 5:1	32.46
Co_3O_4 5:2	27.76
Co_3O_4 5:3	25.05

5.2.3.2 Iron oxides

The Raman profiles for the different iron oxides prepared are shown in figure 5.2. Obtaining the Raman spectra for iron oxides is scarce in research and in

comparison with the other catalysts studied the peaks are of a very low intensity.

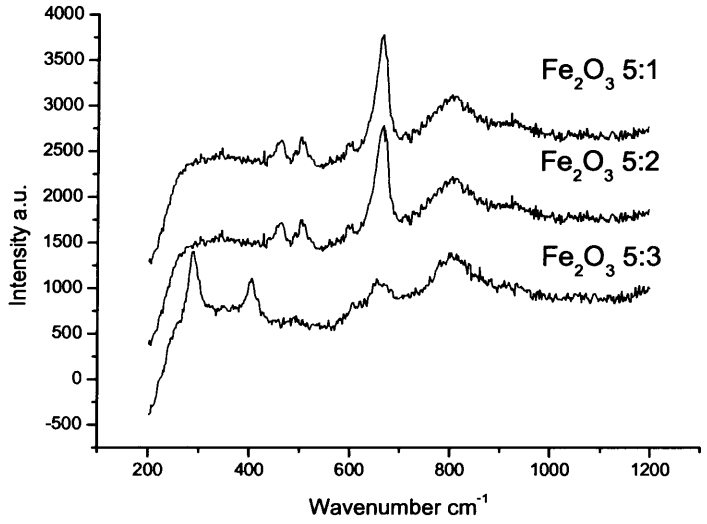

Figure 5.2 Raman spectra of the different iron oxides prepared.

The Raman profiles for all the iron oxides were of the hematite Fe_2O_3 phase [14,15]. The FWHM values, shown in table 5.8, were unable to help draw any conclusions. Problems arose due to Fe_2O_3 5:3 having such a low intensity main peak so no FWHM value could be obtained.

Table 5.8 Table of FWHM values for the iron oxides.

Catalyst	FWHM of main peak (~680cm^{-1})
Fe_2O_3 5:1	45.95
Fe_2O_3 5:2	46.06
Fe_2O_3 5:3	n/a

5.2.3.3 Manganese oxides

The Raman profiles for the different manganese oxides prepared are shown in figure 5.3. Manganese dioxide is known to be highly unstable under laser radiation due to being light sensitive [16]. It is also difficult to measure without it transforming into a different structure such as Mn_3O_4 or Mn_2O_3 due to a thermal reaction taking place [17].

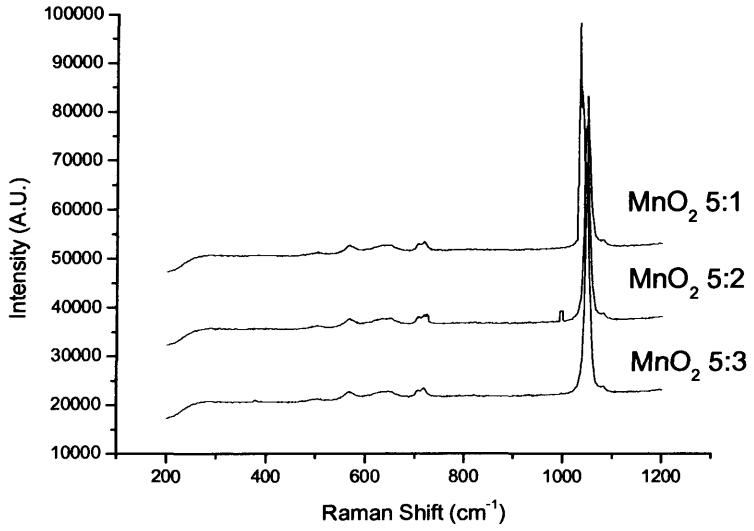

Figure 5.3 Raman profiles for the different manganese oxides prepared.

Small bands were observed in the region of 500-700cm^{-1} and these were attributed to bending modes of Mn_3O_4. A small band at 1000cm^{-1} was also assigned to a terminal stretch of Mn=O. The intense band at 1050cm^{-1} could not be assigned to a different form of manganese oxide but was thought to be due to a NCN symmetrical stretching mode [18].

The FWHM values for the main peak observed are shown in table 5.9. Although the Raman profiles are not of the MnO_2 expected, the FWHM do

decrease with increased ratio, similar to the cobalt oxides. This pattern could be related to the particle size and the preparation of the oxide.

Table 5.9 Table of FWHM values for the manganese oxides.

Catalyst	FWHM of main peak (~1500cm^{-1})
MnO_2 5:1	20.14
MnO_2 5:2	19.01
MnO_2 5:3	17.23

5.2.4 Temperature Programmed Reduction (TPR)

5.2.4.1 Cobalt oxides

The TPR profiles for the cobalt oxide catalysts are shown in figure 5.4. All the profiles give similar peaks with a small peak in the region of 150-180°C and a more pronounced peak at 200-250°C.

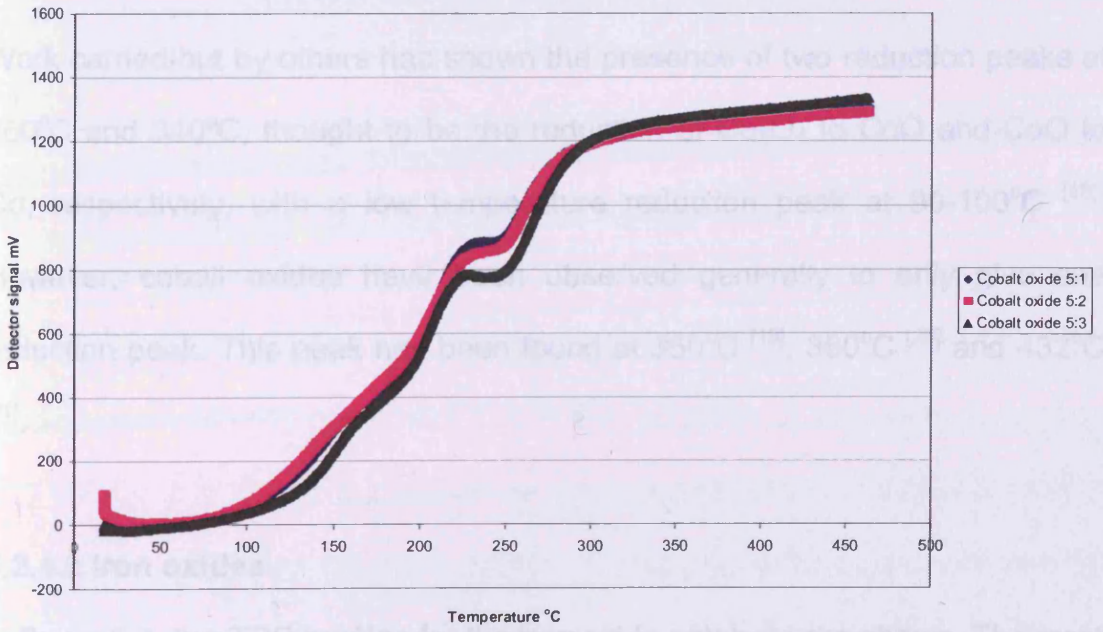

Figure 5.4 TPR profiles for the cobalt oxides prepared.

The curve kept increasing as the catalyst continues to reduce above this temperature, even with small amounts of catalyst being tested. The reduction process was continually repeated until a good profile was obtained at a much lower temperature ramp rate of $1°C/min^{-1}$, and this is shown in figure 5.5.

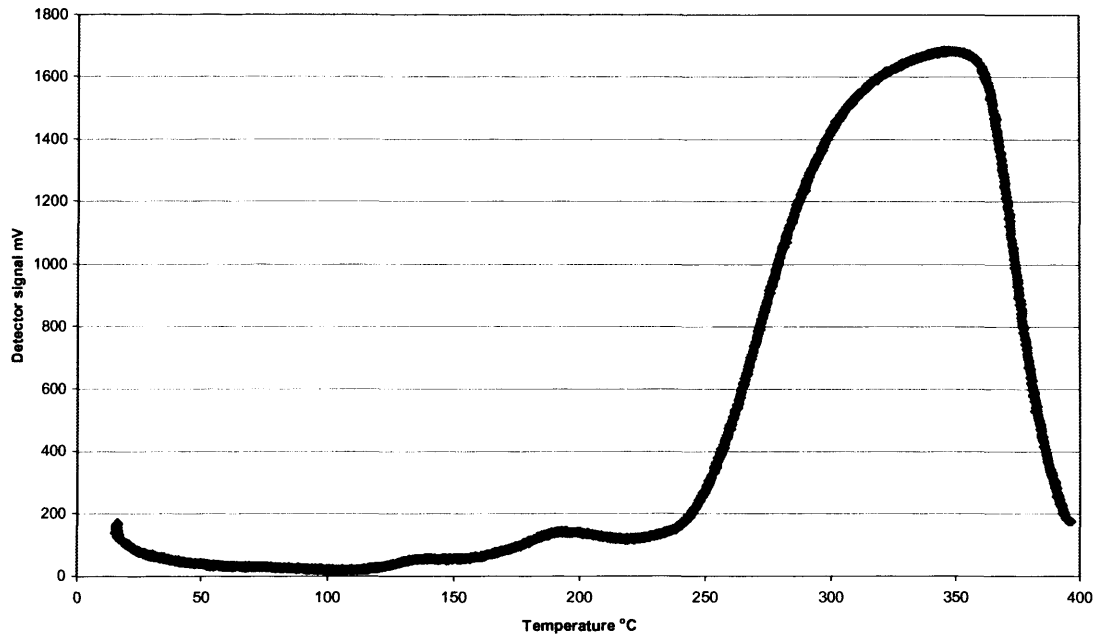

Figure 5.5 TPR profile for Co_3O_4 5:1.

Work carried out by others has shown the presence of two reduction peaks at 260°C and 340°C, thought to be the reduction of Co_3O_4 to CoO and CoO to Co, respectively, with a low temperature reduction peak at 90-100°C [15]. However, cobalt oxides have been observed generally to only give one reduction peak. This peak has been found at 350°C [19], 360°C [20] and 432°C [21].

5.2.4.2 Iron oxides

In figure 5.6, the TPR profiles for the iron oxide catalysts are shown. The most intense reduction peak was observed for the ratio 5:3, followed by 5:2 and 5:1.

The reduction profile consists of a small shoulder peak starting at 240°C for all ratios and then a second more intense peak, approximately three times the intensity of the shoulder peak. The reduction stopped at 400°C for the 5:2 ratio but continued till 420°C for the 5:1 and 5:3 ratios.

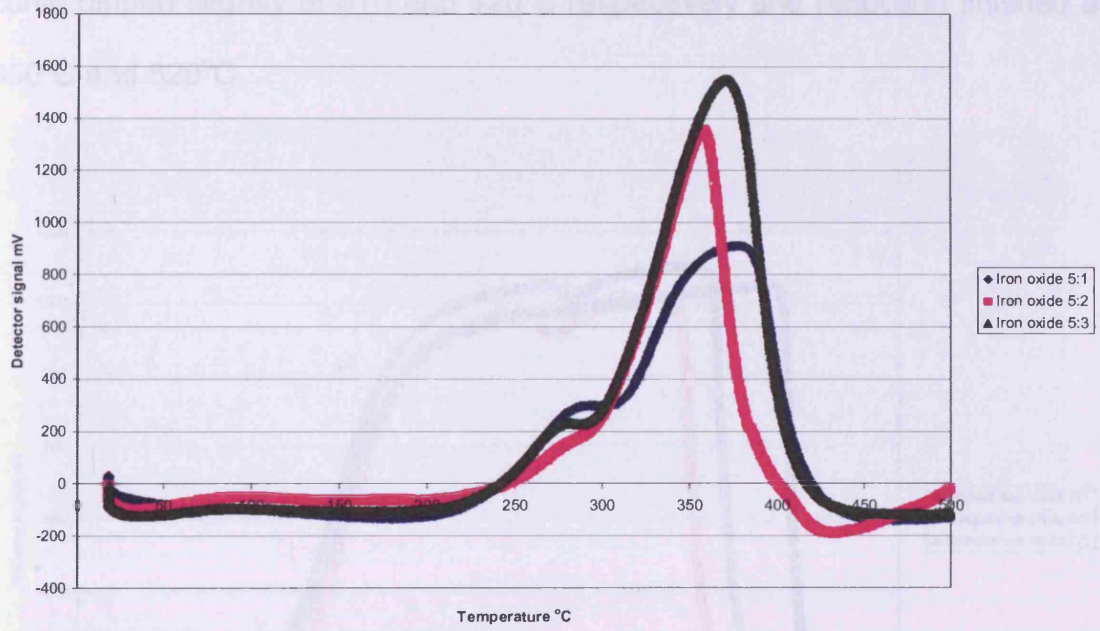

Figure 5.6 TPR profiles for the iron oxides prepared.

Work in this area has found the same pattern in reduction profiles [5] with two separate reduction peaks. The smaller low temperature peak was 13% of the total surface area under the reduction curve and the species responsible for this was the reduction of hematite to magnetite (α – Fe_2O_3 to Fe_3O_4). The second, more intense peak, was due to the reduction of magnetite to metallic iron (Fe_3O_4 to α Fe). It is possible for the two peaks to completely overlap if the heating rates are too high; with lower heating rates it was possible to separate the two peaks fully. Unfortunately in the work carried out, a lower heating rate than the one used was not possible.

5.2.4.3 Manganese oxides

In figure 5.7, the TPR profiles for the manganese oxides are shown. The highest area under the reduction curve was observed for the 5:3 ratio with reduction starting at 400°C and finishing at 700°C. The 5:1 and 5:2 ratios had a reduction curve which consisted of two peaks overlapping. The reduction curve dipped slightly at 410 and 420°C respectively and reduction finished at 650°C and 620°C.

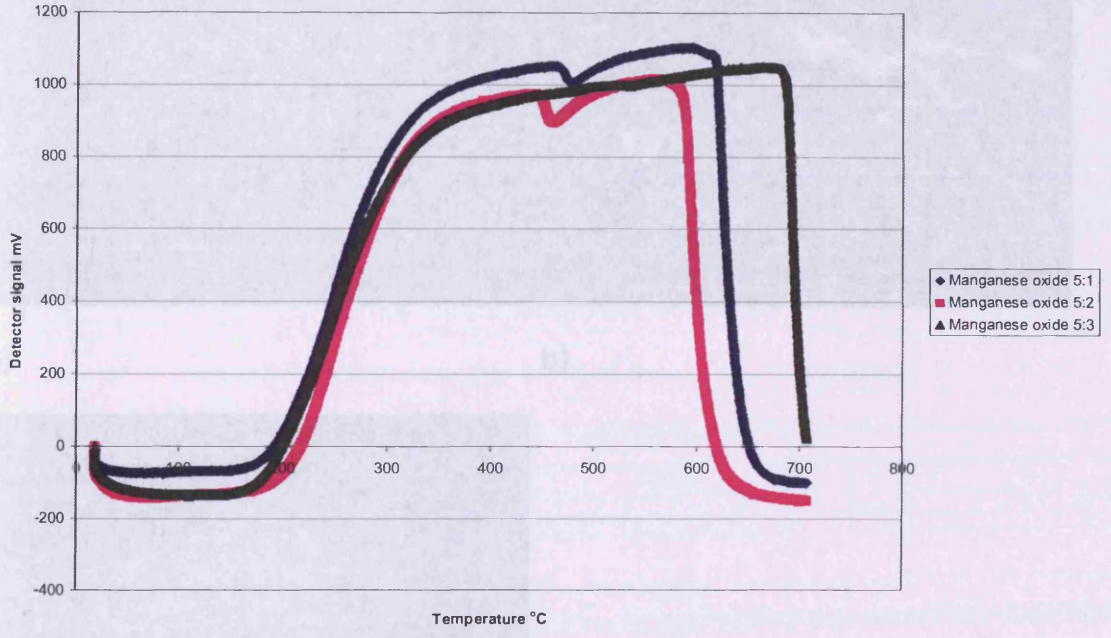

Figure 5.7 TPR profiles for the manganese oxides prepared.

It has been found that the preparation method has an effect upon the reducibility of MnO_2 [22]. Contrasting findings on the TPR of MnO_2 have ranged from one peak [23] to three peaks [24]. In figure 5.9, a double peak is observed for MnO_2 ratios 5:1 and 5:2 but for ratio 5:3 the double peak was less prominent. The temperatures at which reduction occurred was indicative of MnO_2 reducing to Mn_2O_3 and further reducing to Mn_3O_4. The final reduction

step at 469°C was found to be Mn_3O_4 reducing to MnO where thermodynamic restrictions meant no further reduction could occur [25].

5.2.5 Scanning Electron Microscopy (SEM)

The different oxides or cobalt, iron and manganese were investigated using SEM, as described in chapter 2.

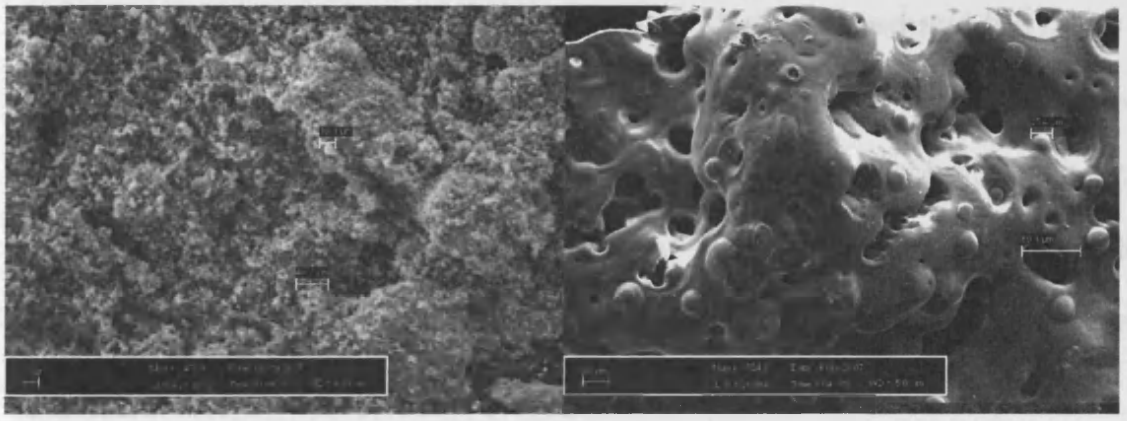

a) b)

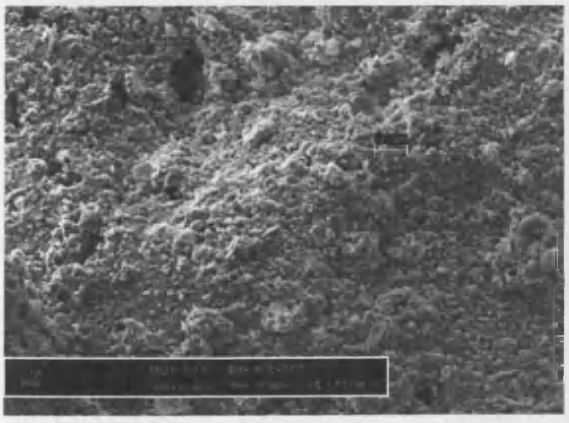

c)

Figure 5.8 a) Image of Co_3O_4 5:1 b) Image of Fe_2O_3 5:1 c) Image of MnO_2 5:1

In figure 5.8a and 5.8c, the 5:1 ratios of Co_3O_4 and MnO_2 respectively can be observed. The morphology of these two oxides were very similar with fine particles ranging from 19.4μm to 40.2μm. The SEM image of the iron oxide

ratio 5:1, figure 5.8b, showed a very different morphology with a smooth surface and no individual particles being observed. Holes within the oxide measured 25.4μm to 69.1μm.

5.2.6 X-ray Photoelectron Spectroscopy (XPS)

5.2.6.1 Cobalt oxides

XPS studies were carried out on the cobalt oxides prepared and the ratios of oxygen to cobalt are shown in table 5.9. The O/Co ratio for all the cobalt oxides prepared was much lower than the commercial cobalt oxide from Aldrich. This higher value has been attributed to the presence of sodium in the form of Na_2O. From the oxides prepared the ratios of oxygen to cobalt were very similar and of negligible difference.

Table 5.9 Ratios of oxygen to cobalt found from XPS studies

Cobalt oxide sample	O/Co atom ratio
5:1	-
5:2	1.01
5:3	1.05
Nitrate 5:0	1.00
Aldrich	1.38

5.2.6.2 Iron oxides

XPS studies were carried out on the iron oxides prepared and the ratios of oxygen to iron are shown in table 5.10. The O/Fe ratio for the oxides prepared were very similar and of negligible difference. The iron nitrate (preparation ratio of 5:0) had a lower ratio of oxygen to iron.

Table 5.9 Ratios of oxygen to iron found from XPS studies

Iron oxide sample	O/Fe atom ratio
5:1	1.54
5:2	1.55
5:3	1.51
Nitrate 5:0	1.38

5.2.6.3 Manganese oxides

XPS studies were carried out on the manganese oxides prepared and the ratios of oxygen to manganese are shown in table 5.11. The O/Mn ratio for all the manganese oxides were very similar and of negligible difference excluding the 5:1 MnO_2. The 5:1 ratio of MnO_2 had a substantially higher ratio of oxygen to manganese, of 3.03. This value was almost double the figure found for the other preparation ratios of the manganese oxides.

Table 5.9 Ratios of oxygen to manganese found from XPS studies

Manganese oxide sample	O/Mn atom ratio
5:1	3.03
5:2	1.62
5:3	1.66
Nitrate 5:0	1.84

5.3 Results

5.3.1 ODH propane over cobalt oxide

The conversions of propane for the different cobalt oxide catalysts prepared are shown in figure 5.9.

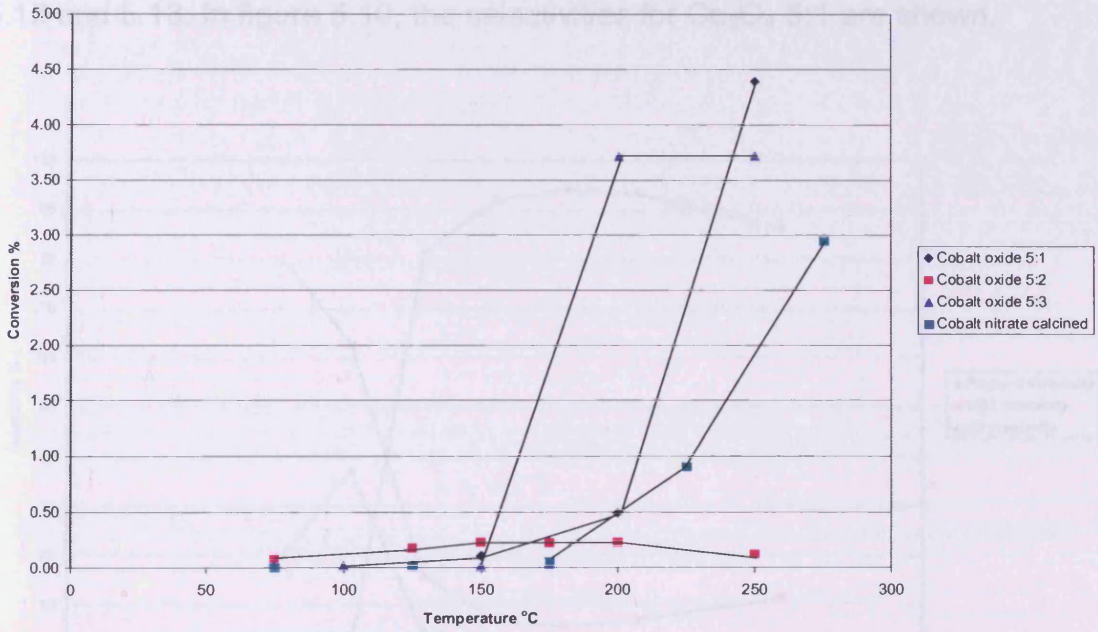

Figure 5.9 Conversions of propane over different cobalt oxide catalysts.

An initial propane conversion was observed at 75°C. The lowest conversion of propane was observed for the cobalt oxide, prepared with a ratio of 5:2, which only reached 0.3% at 200°C. The cobalt oxide prepared with a ratio of 5:1 exhibited the highest conversion of 4.5% at 250°C, which was closely followed by the 5:3 ratio with 3.7%.

Cobalt nitrate was calcined in static air to form a cobalt oxide for comparison. It was found that for this cobalt oxide the initial conversion observed was at much higher temperatures (175°C) than the cobalt oxides prepared by the solid state technique. However, even though a higher temperature for initial

conversion was required, a maximum conversion of 2.9% at 275°C was observed which was much greater than the 5:2 ratio.

The cobalt oxides prepared formed propene, CO_2 and C_3 products (such as acrolein). The selectivity to these products are shown in figures 5.10, 5.11, 5.12 and 5.13. In figure 5.10, the selectivities for Co_3O_4 5:1 are shown.

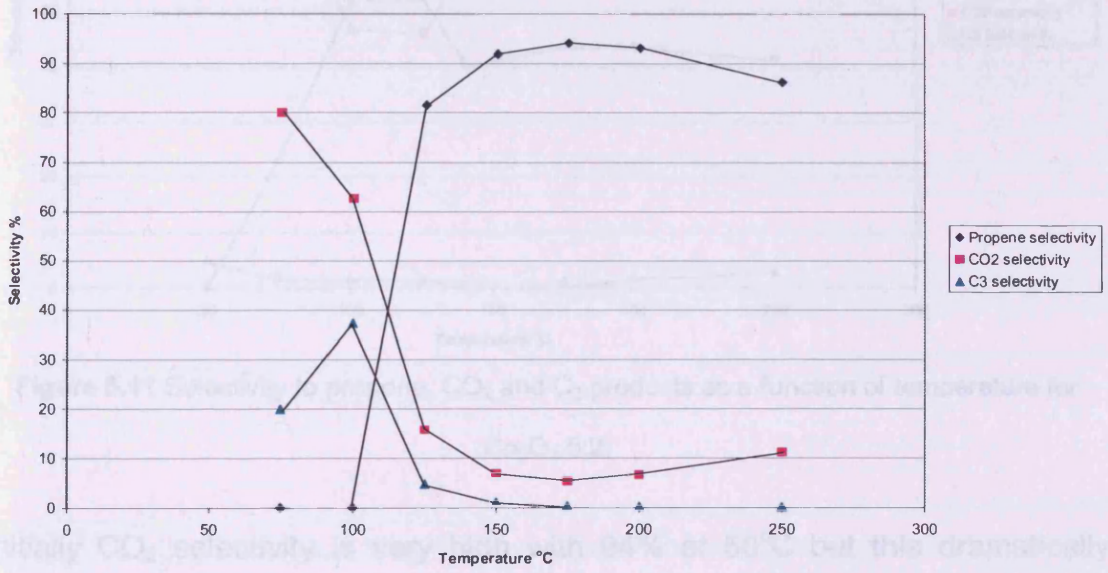

Figure 5.10 Selectivity to propene, CO_2 and C_3 products as a function of temperature for Co_3O_4 5:1.

Selectivity to propene, the desired product, was over 90% at 150°C and remained high up to 250°C. As the selectivity to propene was high, selectivity to CO_2 was very low with only 11% at 250°C. At low temperatures of 75-125°C relatively large amounts of C_3 products were observed with a selectivity maximum of 37%, although due to a very low conversion the yield was negligible.

Figure 5.11 shows the selectivities of Co_3O_4 5:2, which was vastly different to Co_3O_4 5:1.

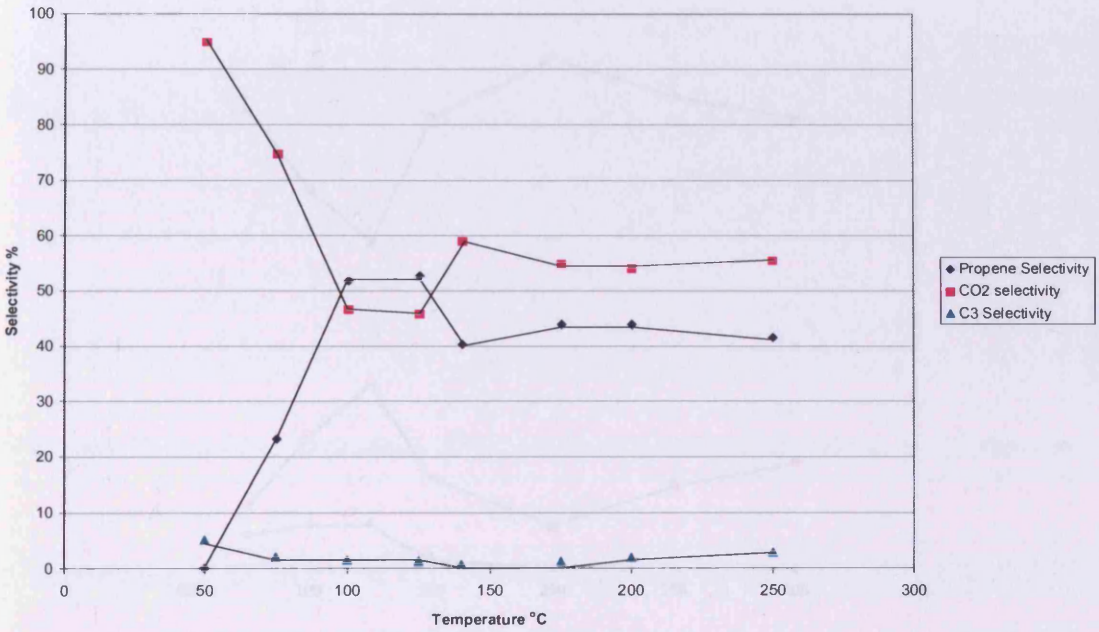

Figure 5.11 Selectivity to propene, CO_2 and C_3 products as a function of temperature for Co_3O_4 5:2.

Initially CO_2 selectivity is very high with 94% at 50°C but this dramatically drops to 47% at 100°C. At 150°C the selectivity to CO_2 increases to 59% and then remains constant at ~54% till 250°C. The selectivity to propene reaches a maximum of 53% at 100°C which then decreases to 40% at 150°C and continues in this region till 250°C. The C_3 products for this catalyst were negligible.

The selectivities for the Co_3O_4 5:3 catalyst are shown in figure 5.12. The selectivity to propene was high with 83% at only 50°C. This increased to 92% at 200°C and then began to decrease to 80% at 300°C. The selectivity to CO_2

was the lowest of all the cobalt catalysts prepared and did not go beyond 34% for the whole temperature range explored.

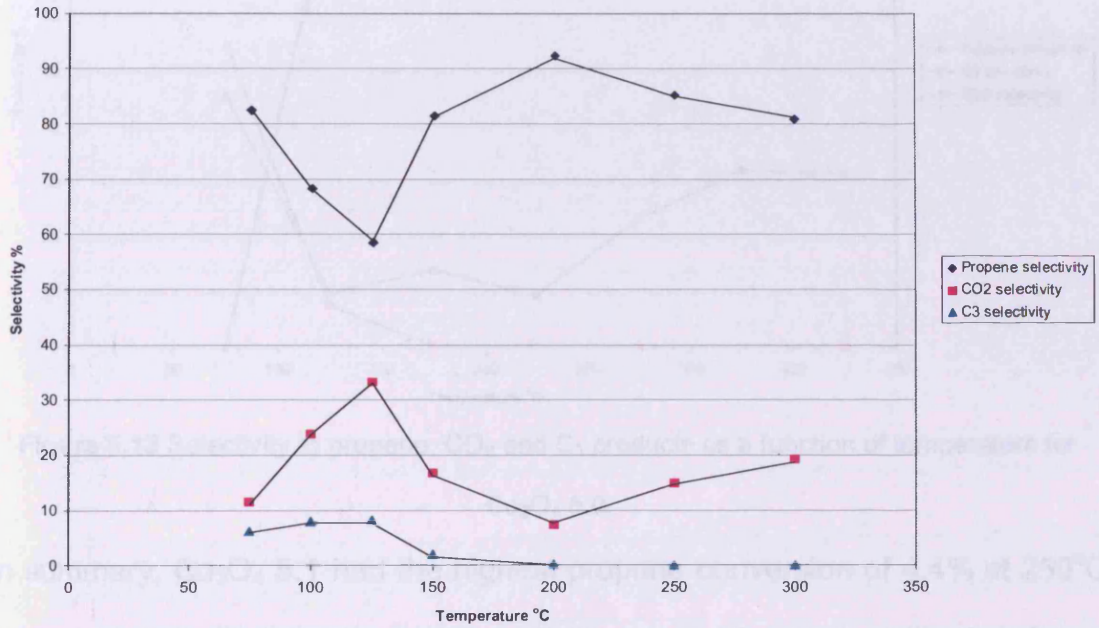

Figure 5.12 Selectivity to propene, CO_2 and C_3 products as a function of temperature for Co_3O_4 5:3.

In figure 5.13, the selectivities for the cobalt nitrate catalyst showed a similar pattern to the Co_3O_4 5:1 catalyst. Selectivity to propene was 83% at 100°C which only decreased to 68% at 350°C. The selectivity to C_3 products was negligible apart from at low temperatures of 100°C.

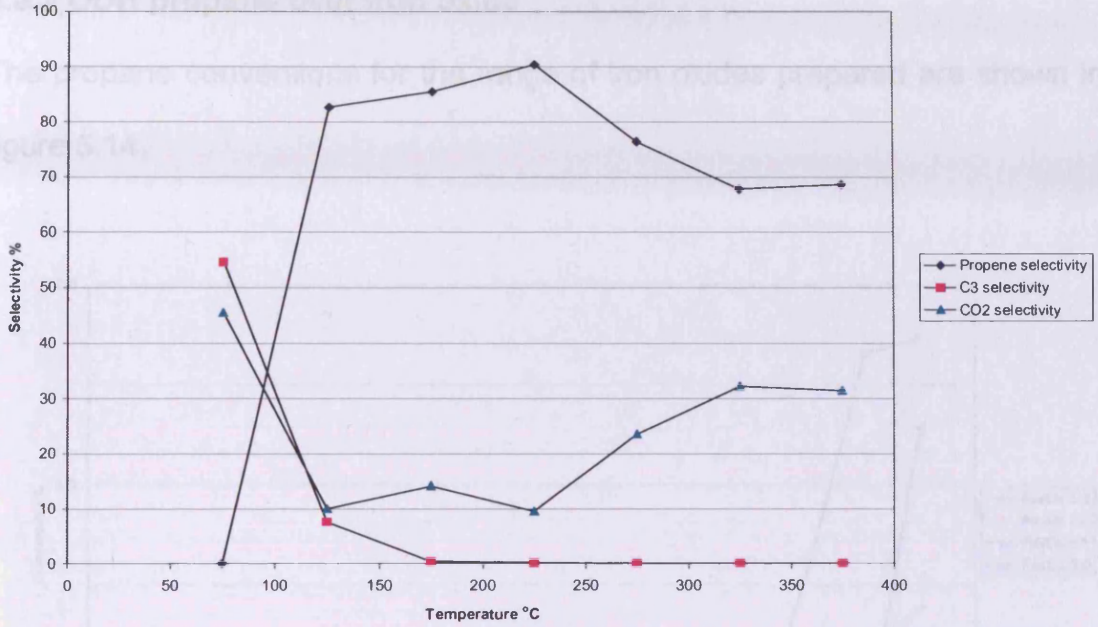

Figure 5.13 Selectivity to propene, CO_2 and C_3 products as a function of temperature for Co_3O_4 5:0.

In summary, Co_3O_4 5:1 had the highest propane conversion of 4.4% at 250°C followed by Co_3O_4 5:3 with 3.7% at 200°C and finally Co_3O_4 5:2 with 0.3% at 200°C. The cobalt nitrate calcined actually gave a higher activity than the Co_3O_4 5:2 catalyst, with 3% propane conversion at 250°C. However, it should be noted that this required a higher temperature for initial activity of 175°C while the cobalt oxides prepared by the solid state method were active at only 75°C.

The 5:1 and 5:3 Co_3O_4 catalysts gave the highest selectivities to propene with 94 and 92% respectively. The cobalt nitrate only gave 90% propene selectivity but this dropped to 68% at 375°C where the solid state catalysts remained above 80%. This highlights the fact that the preparation method of these cobalt oxides is important in the oxidative dehydrogenation of propane.

5.3.2 ODH propane over iron oxide

The propane conversions for the range of iron oxides prepared are shown in figure 5.14.

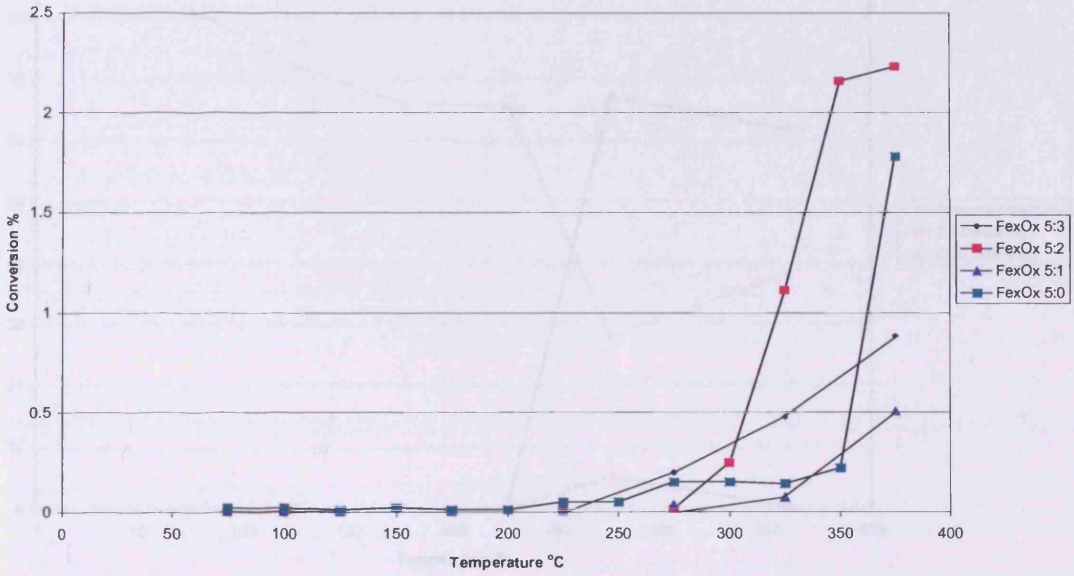

Figure 5.14 Conversions of propane over different iron oxide catalysts.

The highest conversion was exhibited by iron 5:2 with 2.3% at 375°C. The 5:1, 5:3 and iron nitrate catalysts all exhibited very low conversions, compared to the 5:2 ratio, with less than 2% conversion of propane up to 300°C. The iron nitrate catalyst was the most active of the low conversion group, with 1.9% conversion at 350°C, followed by 5:1 with 0.8% and 5:3 with 0.5% conversion at the same temperature.

The selectivities for the different iron oxides are shown in figures 5.15, 5.16, 5.17 and 5.18. In figure 5.15, the iron oxide 5:1 catalyst showed no selectivity to propene until 275°C, with the primary product of reaction being carbon

dioxide. At 275°C, selectivity to propene reached 67% but at 350°C had already started to decrease to 62%.

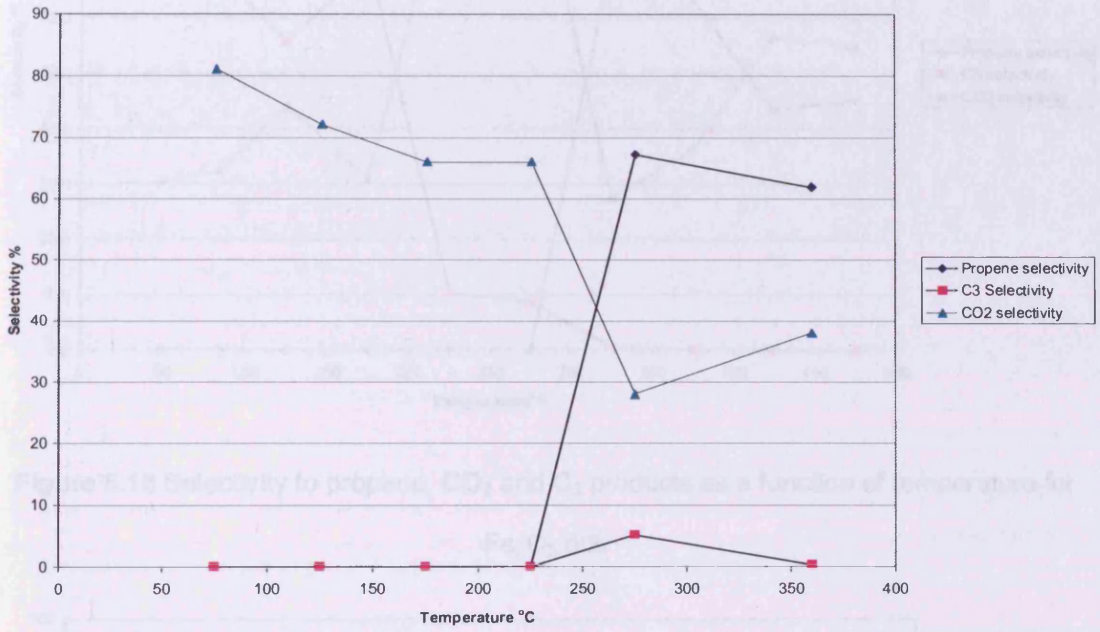

Figure 5.15 Selectivity to propene, CO_2 and C_3 products as a function of temperature for Fe_2O_3 5:1.

The selectivities are shown in figure 5.16 for iron oxide 5:2. At 100-175°C C_3 products, such as acrolein, were the primary products of the reaction with up to 70% selectivity (but negligible yields). At 175°C the selectivity to carbon dioxide dramatically increased from ~30% to more than 90%. Only at 300°C was any propene actually observed with 73% selectivity and CO_2 selectivity dropped to 27%. The selectivity to propene steadily decreased to 45% at 475°C with CO_2 selectivity increasing to 55%.

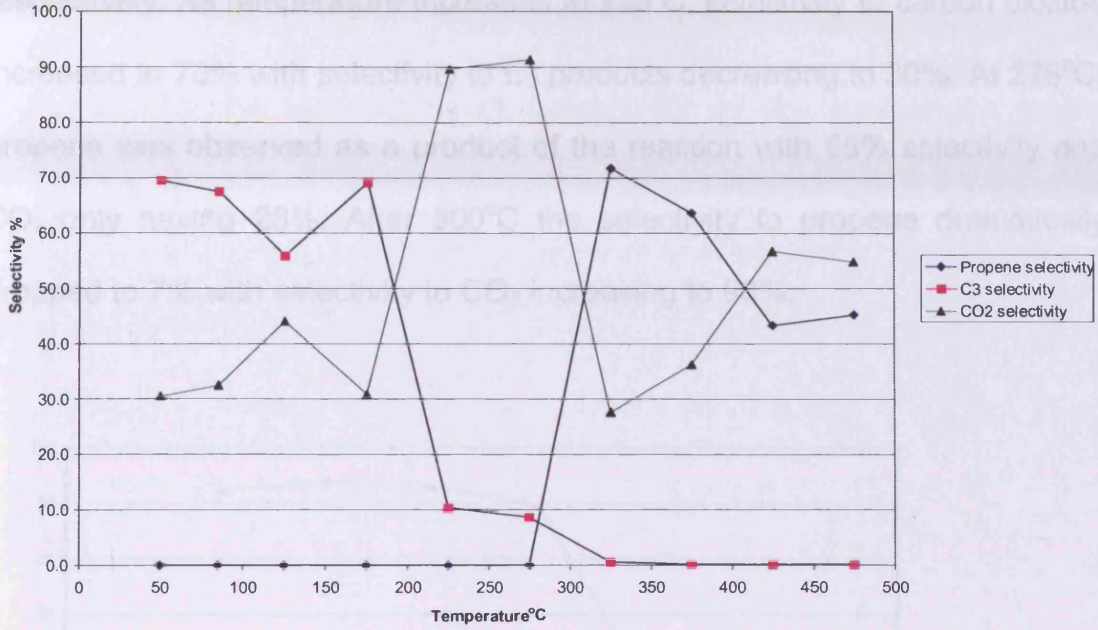

Figure 5.16 Selectivity to propene, CO_2 and C_3 products as a function of temperature for Fe_2O_3 5:2.

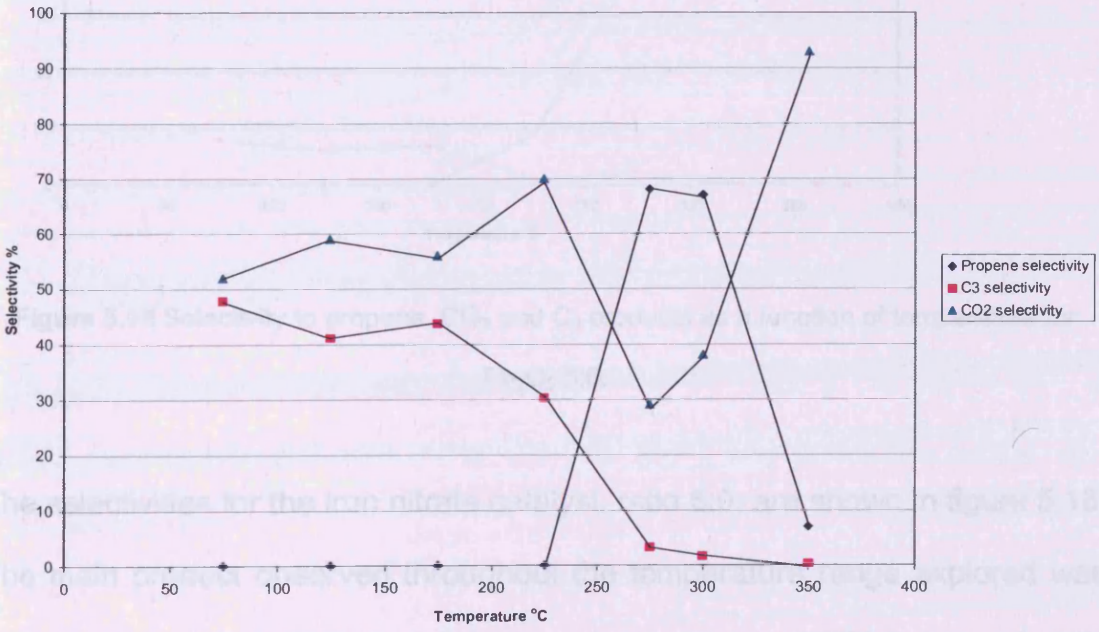

Figure 5.17 Selectivity to propene, CO_2 and C_3 products as a function of temperature for Fe_2O_3 5:3.

The selectivities for iron oxide 5:3 are shown in figure 5.17. At 75°C, the only products of conversion were CO_2 and C_3 compounds, with 52 and 48%

respectively. As temperature increased to 225°C, selectivity to carbon dioxide increased to 70% with selectivity to C_3 products decreasing to 30%. At 275°C, propene was observed as a product of the reaction with 68% selectivity and CO_2 only having 28%. After 300°C the selectivity to propene dramatically dropped to 7% with selectivity to CO_2 increasing to 93%.

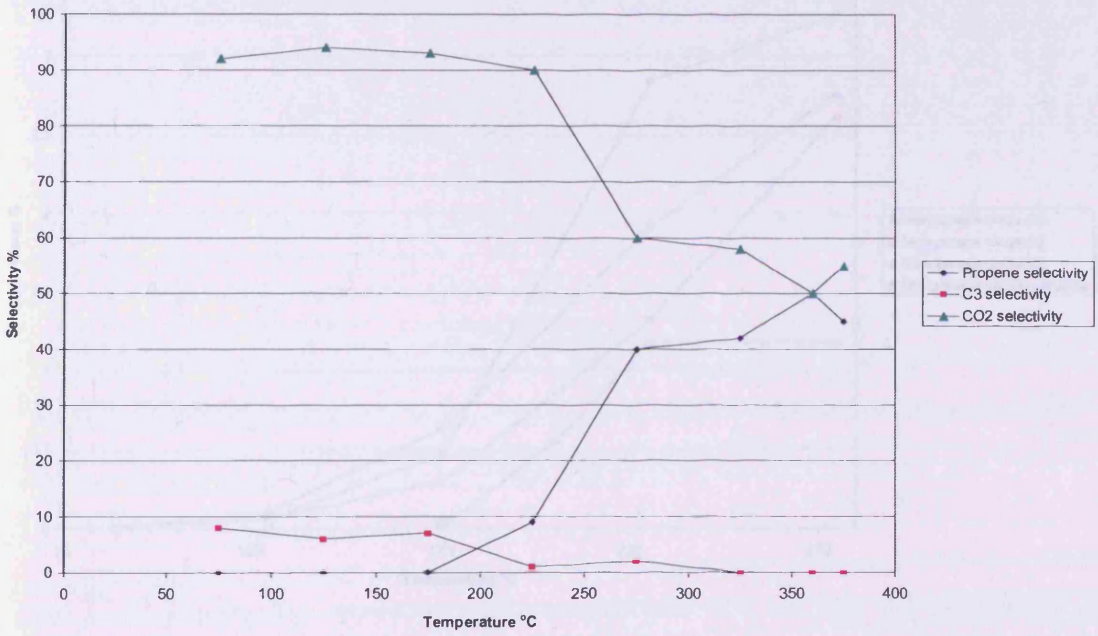

Figure 5.18 Selectivity to propene, CO_2 and C_3 products as a function of temperature for Fe_2O_3 5:0.

The selectivities for the iron nitrate catalyst, ratio 5:0, are shown in figure 5.18. The main product observed throughout the temperature range explored was carbon dioxide. Selectivity to propene was detected at 225°C but at only 9%. The maximum propene selectivity was 50% at 350°C.

5.3.3 ODH propane over manganese oxide

In figure 5.19, the conversions of propane for all the manganese oxides prepared are shown. All of the manganese oxides prepared by the solid state method showed similar conversions with the manganese nitrate exhibiting a lower conversion.

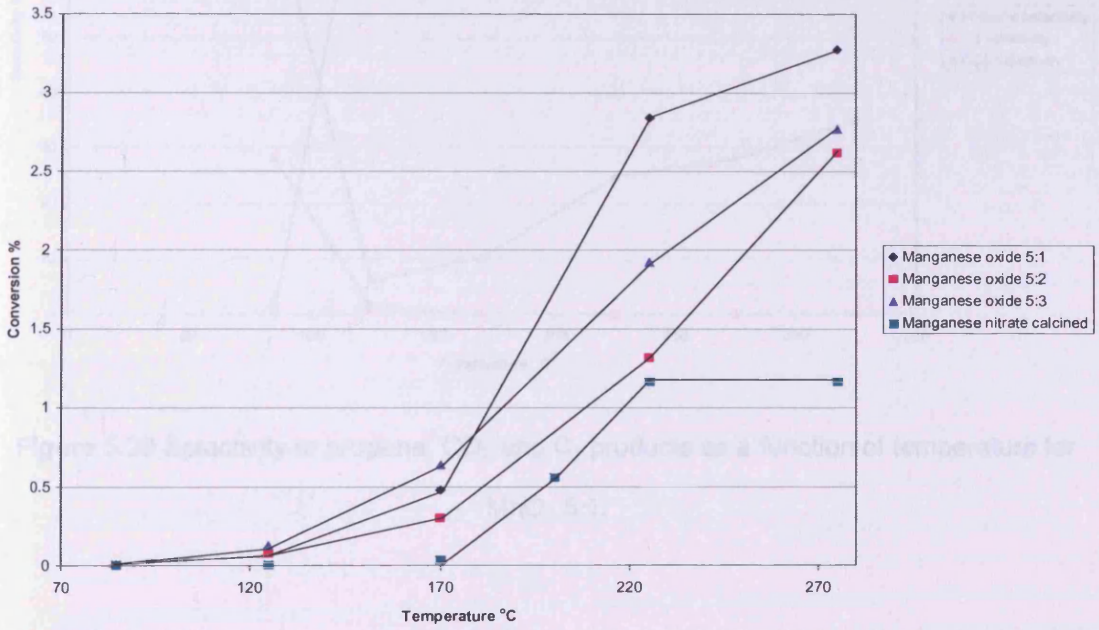

Figure 5.19 Conversions of propane over different manganese oxide catalysts.

The most active catalyst was the manganese 5:1 with 3.4% conversion at 270°C, followed by 5:3 with 2.7%, 5:2 with 2.6% and finally the nitrate with 1.2% conversion.

The selectivity graphs for the different manganese oxides are shown in figures 5.20, 5.21, 5.22 and 5.23.

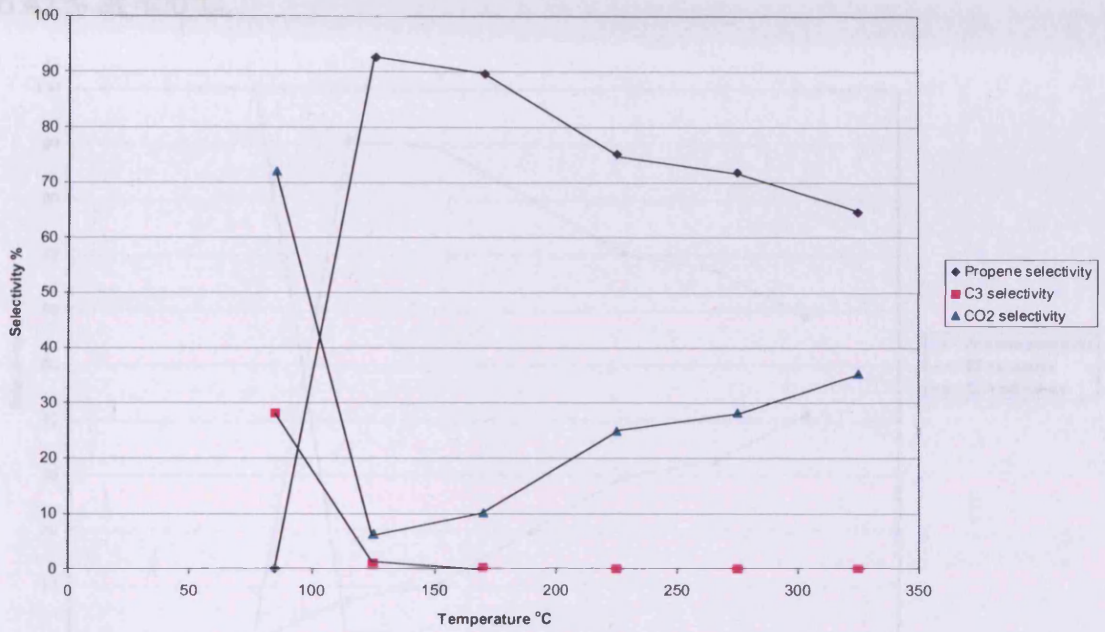

Figure 5.20 Selectivity to propene, CO_2 and C_3 products as a function of temperature for MnO_2 5:1.

Figure 5.20 shows the selectivity of manganese 5:1. At low temperatures of 75°C the catalyst was only selective to CO_2 and C_3 products with selectivities of 72 and 28% respectively. As temperature increased to 125°C the selectivity switched to propene being the primary product with 92%. The selectivity to propene remained high over the temperature range explored and was 65% selective at 325°C. As the selectivity to propene gradually decreased with temperature, the selectivity to CO_2 increased and C_3 products were negligible.

The selectivities for manganese 5:2 are shown in figure 5.21. At 100°C, selectivity to C_3 products was 100% which dramatically fell to 2% at 150°C. Propene was observed as the primary reaction product at 150°C with 91%

selectivity and this steadily decreased to 59% at 400°C. As the propene selectivity decreased with increased temperature, selectivity to CO_2 increased to 41% at 400°C.

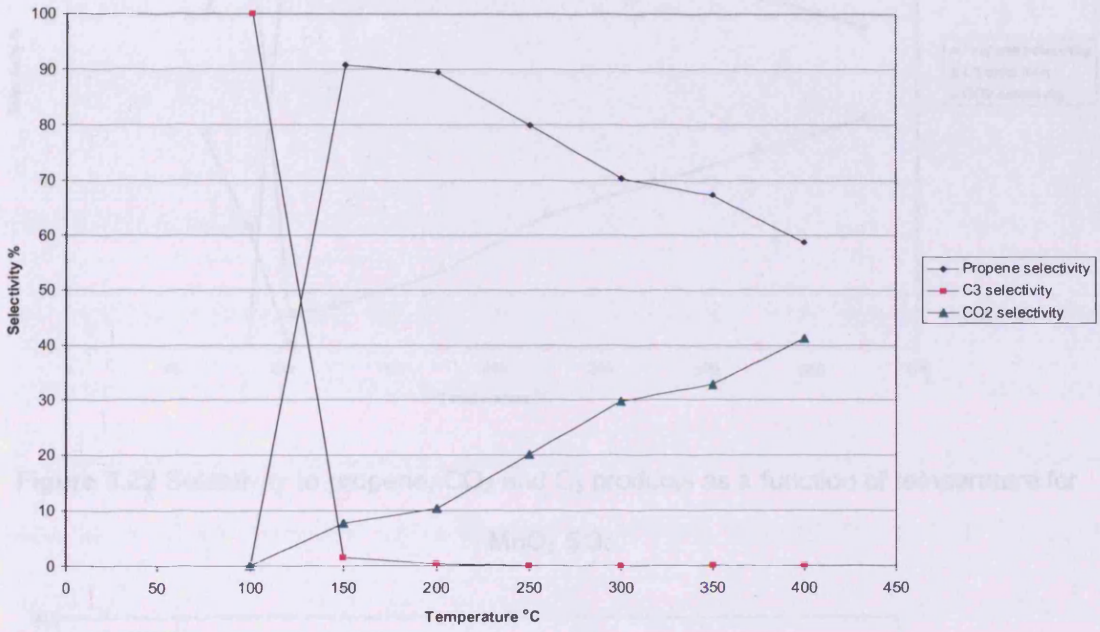

Figure 5.21 Selectivity to propene, CO_2 and C_3 products as a function of temperature for MnO_2 5:2.

The selectivities for manganese 5:3 are shown in figure 5.22. At low temperatures of 60°C only CO_2 and C_3 products were observed with selectivities of 60 and 40% respectively. Propene was first observed at 100°C with 94% selectivity as selectivity to CO_2 dropped to 6%. As temperature increased selectivity to propene steadily decreased to 58% at 375°C and selectivity to CO_2 increased to 42%.

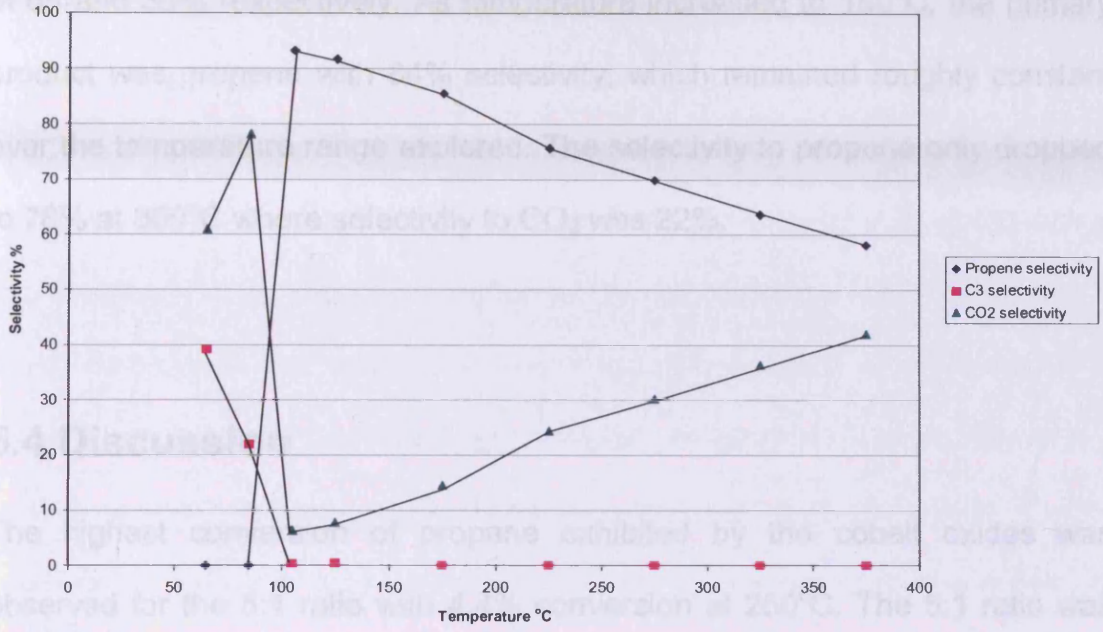

Figure 5.22 Selectivity to propene, CO_2 and C_3 products as a function of temperature for MnO_2 5:3.

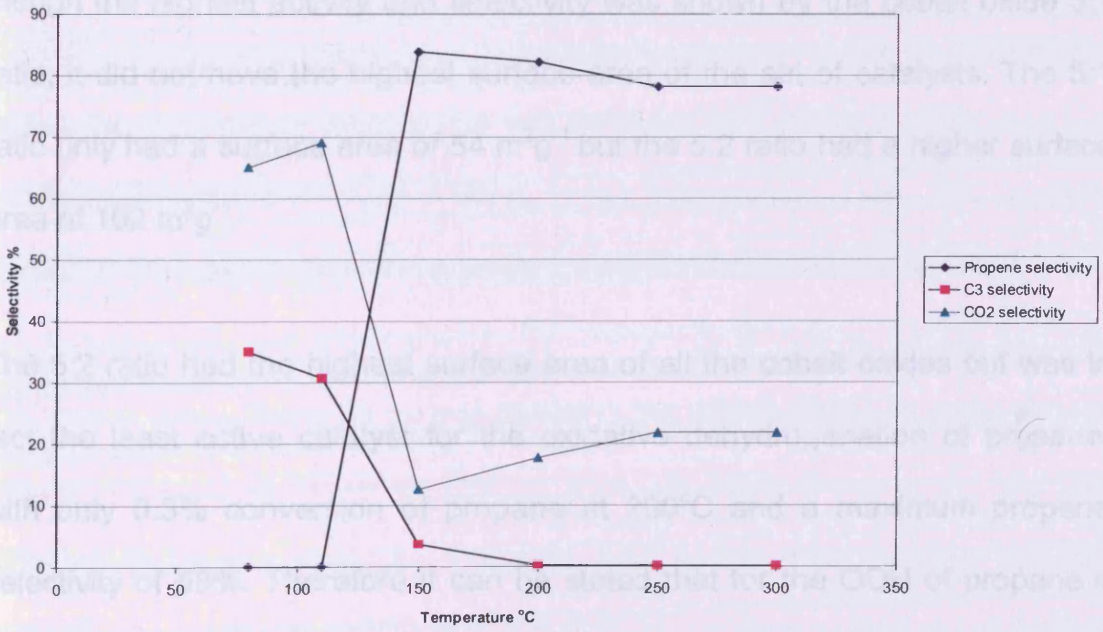

Figure 5.23 Selectivity to propene, CO_2 and C_3 products as a function of temperature for MnO_2 5:0.

Selectivities for manganese nitrate are shown in figure 5.23. At 80°C, the primary products of the reaction were CO_2 and C_3 products with selectivities

of 65 and 35% respectively. As temperature increased to 150°C, the primary product was propene with 84% selectivity, which remained roughly constant over the temperature range explored. The selectivity to propene only dropped to 78% at 300°C where selectivity to CO_2 was 22%.

5.4 Discussion

The highest conversion of propane exhibited by the cobalt oxides was observed for the 5:1 ratio with 4.4% conversion at 250°C. The 5:1 ratio was the most active in converting propane and the selectivity to the desired propene product was the highest with over 90% selectivity at 150°C. Even though the highest activity and selectivity was shown by the cobalt oxide 5:1 ratio, it did not have the highest surface area of the set of catalysts. The 5:1 ratio only had a surface area of 54 m^2g^{-1} but the 5:2 ratio had a higher surface area of 102 m^2g^{-1}.

The 5:2 ratio had the highest surface area of all the cobalt oxides but was in fact the least active catalyst for the oxidative dehydrogenation of propane, with only 0.3% conversion of propane at 200°C and a maximum propene selectivity of 53%. Therefore it can be stated that for the ODH of propane it was not essential to have a high surface area. The cobalt oxides prepared in this study were of a much higher surface area than other work in this field, where surface areas of 20m^2g^{-1} were obtained [14]. The differences in surface area are due to the development of the Co_3O_4 spinel structure at the expense of the amorphous structure of the basic carbonate [26].

The 5:3 ratio of cobalt oxide also exhibited high activity. The preparation involved large quantities of ammonium bicarbonate, therefore it could be suggested that it was increased amounts of nitrogen or carbon that resulted in improved activity and selectivity. Perhaps nitrogen formed part of the active site responsible for the ODH propane. The incorporation of nitrogen into a metal oxide has been shown to decrease the number of acid sites [27] therefore this may explain the high selectivity to propene. Acid catalysts are unable to produce alkenes, such as propene, with high selectivity [3]. The relationship between the ratios of ammonium bicarbonate and the activity of the cobalt oxides are not directly correlated as the ratio 5:2 had such a low conversion. A suggestion for this could be that there was not enough of the nitrogen/carbonate species to act in the same way as the 5:3 ratio, but not enough vacant sites either for it to be just the activity of Co_3O_4 from nitrate alone. The 5:1 ratio of cobalt oxide was more active than the 5:2 ratio and had less ammonium bicarbonate present in the preparation. From XPS studies, carbon and nitrogen were not found to be present on the oxide surface.

The cobalt oxide prepared by just calcining the cobalt nitrate in static air was not as active or selective as the cobalt oxide ratios 5:1 and 5:3 but was significantly greater than the 5:2 ratio. The cobalt nitrate had a propane conversion of 2.9% at 275°C and a maximum propene selectivity of 83% at 100°C. A small amount of the ammonium bicarbonate (in the case of ratio 5:1) may have been enough to permeate through the surface to form the active sites found to be responsible for the ODH reaction.

The lattice oxygen in the Co_3O_4 spinel structure was found to participate in the Mars Van Krevelen mechanism therefore the redox properties of the cobalt oxides were important [28]. The cobalt oxide 5:1 had the lowest temperature of reduction and high hydrogen consumption. In a spinel structure, the CoO bond has a lower energy therefore it can easily undergo the reduction process [29]. The mechanism of propane oxidation involves the formation of propoxide species on the catalyst surface. The deposition of the propoxide is termed the selectivity determining step [31]. Complete oxidation occurs when chemisorbed oxygen reacts with the hydrocarbon. For the ODH of propane, selective products are observed when easily accessible lattice oxide ions are near the catalyst surface [30].

The highest conversion observed for the iron oxides prepared was that of the 5:2 ratio with 2.3% propane conversion at 375°C. The 5:2 ratio also had the highest selectivity to propene with a maximum selectivity of 73%. The iron oxides with ratios 5:1 and 5:3 gave very low conversions of propane which even at 300°C did not exceed 0.3% conversion. Even though the 5:2 ratio was the most active iron oxide in terms of high conversion and selectivity, it required a very high temperature to observe any propene at all. The desired reaction product was not detected until 325°C for the 5:2 but for the other ratios it was present at 50°C lower. The differences in selectivity were not that significant with a difference of only 5 and 6% in the case of the 5:1 and 5:3 ratios respectively. A difference of 50°C is significant however when considering a catalyst for industrial applications. The highest yield observed

was 1.6%, as stated in table 5.10, and this was the same value reported in literature [31].

Table 5.10 Maximum yields of propene obtained from different oxides studied.

Catalyst	Temperature °C	Conversion %	Selectivity to propene %	Yield of propene %
Co_3O_4 5:1	250	4.4	86	**3.8**
Co_3O_4 5:2	200	0.3	44	0.1
Co_3O_4 5:3	200	3.7	92	3.4
Co_3O_4 nitrate	275	3.0	68	2.0
Fe_2O_3 5:1	360	0.5	62	0.3
Fe_2O_3 5:2	325	2.2	72	**1.6**
Fe_2O_3 5:3	325	0.5	68	0.3
Fe_2O_3 nitrate	360	1.8	45	0.8
MnO_2 5:1	270	3.4	72	**2.4**
MnO_2 5:2	270	2.6	74	1.9
MnO_2 5:3	270	2.7	70	1.9
MnO_2 nitrate	270	1.2	78	0.9

The surface area of the iron oxides was directly correlated to the ratios of reactants from which they were prepared. A higher amount of ammonium bicarbonate gave a higher surface area, therefore the highest surface area was observed for the 5:3 ratio with $62m^2g^{-1}$. The most active iron oxide did not have the highest surface area as the 5:2 ratio had a surface area of $52m^2g^{-1}$. The lowest surface area was observed for the 5:1 ratio and this was the least active of the iron oxides in terms of propane conversion. Although the iron oxides prepared were not of high surface areas, oxides of lower values were prepared with $38m^2g^{-1}$ [33] and even $6.6m^2g^{-1}$ [32].

The XRD phases for all the iron oxides gave a phase of Fe_2O_3 with the largest crystallite sizes of all the cobalt and manganese oxides. The most active iron oxide ratio of 5:2 had a crystallite size of 171 nm. However, the smallest

crystallite size was actually observed for the iron nitrate alone, with 88nm, which gave a lower conversion of 1.9% at 350°C. The order of activity does not appear to be related to the crystallite size of the iron oxides. The 5:2 ratio of iron oxide gave a similar conversion to the cobalt oxides but had a much larger crystallite size, although the selectivity of the cobalt oxides was much higher at lower temperatures. Therefore from comparing differences in propene selectivity, the crystallite size is very important.

The reducibility of the iron oxides appears related to the conversion of propane. The iron oxides began to reduce at around 250°C and this was the temperature at which significant conversions of propane were observed. Furthermore, the reaction was only selective to propene at this point. It can thus be concluded that the redox properties of the iron oxides determined the ODH reaction of propane.

The SEM images of the iron oxides displayed a rather strange morphology. The surface was not made up of small regular shaped particles, like cobalt and manganese. Instead a smooth surface was observed with round holes and circular elevations, which was in keeping with other research findings where much lower surface areas were obtained [35].

The highest conversion exhibited by the manganese oxides was from the 5:1 ratio with 3.4% conversion at 270°C with a yield of 2.4%. The 5:2 and 5:3 ratios closely followed both with a 1.9% yield. The 5:3 ratio actually gave the highest selectivity to propene with a maximum of 94% at 100°C but

dramatically dropped to 58% at 375°C. Although the 5:1 ratio had a maximum selectivity to propene of 92%, a higher selectivity over a wider temperature range was obtained for the 5:3 ratio. The 5:1 ratio had a surface area of $62m^2g^{-1}$ and a yield of 2.4% compared to the 5:0 ratio with a surface area of 22 m^2g^{-1} and a yield of 0.9%. The 5:2 and 5:3 ratios actually gave the same maximum yield of 1.9% but with higher surface areas of 78 and $76m^2g^{-1}$ respectively. Therefore it can be stated that for the manganese oxides, the activity of propane ODH (in terms of conversion and yield) is related to the surface area of the catalyst. A small surface area is not active for the desired reaction but other factors may be responsible for this.

The crystalline phase present for all the manganese oxides was a hexagonal MnO_2 phase. The only difference was observed for the 5:3 ratio which had a tetragonal phase with the smallest crystallite size of 15nm. The 5:0 ratio (manganese nitrate) had the largest crystallite size of 171nm. The combination of a low surface area and a large crystallite size explains the low activity and selectivity observed for this catalyst in propane ODH. The pattern emerging from the crystallite sizes is that an increased amount of ammonium bicarbonate gives a smaller crystallite size.

The area under the TPR curve of the 5:3 ratio was the largest, followed by the 5:1 ratio, 5:2 ratio and then the nitrate. All manganese oxides start to reduce at similar temperatures of around 200°C. The 5:3 ratio however has the highest maximum temperature of reduction of 700°C. The reducibility of the manganese oxides was not directly related to the propane conversion or the

propene selectivity. However the temperatures at which the oxides were undergoing reduction were the same as those where high yields were obtained. This relationship again highlights the importance of redox properties in catalysis.

The highest yields of propene obtained were for cobalt oxide 5:1 with 3.8%, iron oxide 5:2 with 1.6% and manganese oxide 5:1 with 2.4%. From XPS studies, these catalysts had the highest ratios of oxygen to the metal, with the manganese oxide having the highest ratio of 3.03. The FWHM values, found from Raman spectroscopy, were also higher for the most active catalysts. These values were in keeping with XRD studies and the crystallite size calculated.

5.5 Conclusions

Co_3O_4, Fe_2O_3 and MnO_2 were prepared by using different preparation ratios of the corresponding nitrate with ammonium bicarbonate and tested for the ODH of propane. The highest yield observed was for the Co_3O_4 5:1 ratio with 3.8%, which was much higher than the iron and manganese oxides. The activity observed was attributed to the spinel structure which the cobalt oxide formed alongside a small crystallite size, high reducibility and high ratio of O/Co.

5.6 References

[1] R. P. Feynman, *Miniaturization*, Reinhold, New York, 1961.

[2] T. E. Davies, T. Garcia, B. Solsona, S. H. Taylor, *Chemical Communications* (2006) pp. 3417-3419.

[3] G. Busca, E. Finocchio, G. Ramis, G. Ricchiardi, *Catalysis Today* **32** (1996) pp. 133-143.

[4] E. Finocchio, R. J. Willey, G. Busca, V. Lorenzelli, *Journal of Chemistry Society: Faraday Transmissions,* **93 (1)** (1997) pp. 175.

[5] M. J. Pollard, B. A. Weinstock, T. E. Bitterwolf, P. R. Griffiths, A. P. Newbery, J. B. Paine, *Journal of Catalysis* **254 (2)** (2008) pp. 218.

[6] R. H. Spitzer, F. S. Manning, W. O. Philbrook, *Transactions of the Metallurgical Society of AIME* **236** (1966) pp. 726.

[7] L. E. Cadus, O. Ferretti, *Applied Catalysis A: General* **233 (1-2)** (2002) pp. 239-253.

[8] V. V. Krishnan, S. L. Suib, *Journal of Catalysis* **184 (2)** (1999) pp. 305-315.

[9] M. A. Baltanas, A. B. Stiles, J. R. Katzer, *Applied Catalysis* **28** (1986) pp.13.

[10] Y. Han, F. Chen, Z. Zhong, K. Ramesh, E. Widjaja, L. Chen, *Catalysis Communications* **7 (10)** (2006) pp. 739-744.

[11] R. K. Grasselli, J. D. Burrington, *Advances in Catalysis* **30** (1981) pp. 133.

[12] E. Serwicka, J. B. Black, J. Goodenough, *Journal of Catalysis* **106** (1987) pp. 23.

[13] V. G. Hadjiev, M. N. Iliev, I. V. Vergilov, *Journal of Physical Chemistry: Solid State Physics* **21** (1998) pp. 199-201.

[14] D. L. A. Faria, S. V. Silva, M. T. Oliveira, *Journal of Raman Spectroscopy* **28** (1999) pp. 873-878.

[15] D. Bersani, P. P. Lottici, M. Montenero, *Journal of Raman Spectroscopy* **30** (1999) pp. 355-360.

[16] E. Widjaja, J. T. Sampanthar, *Analytica Chimica Acta* **585** (2007) pp. 241-245.

[17] I. T. Yardley, *Laser Chemistry Processing at the Micron Level*, Laser Hand-book, North Holland, Amsterdam, (1985).

[18] R. L. Frost, J. Kristol, L. Rintoul, J. T. Kloprogge *Molecular and Bimolecular Spectroscopy* **56 (9)** (2000) pp. 1681-1691.

[19] G. Fierro, M. L. Jacono, M. Inversi, R. Dragone, P. Porta, *Topics in Catalysis* **10** (2000) pp. 39.

[20] P. Y. Lin, M. Skoglundh, L. Löwendahl, J. E. Otterstedt, L. Dahl, K. J annson, M. Nygren, *Applied Catalysis B: Environmental* **6** (1995) pp. 237-254.

[21] J. Jansson, *Journal of Catalysis* **194** (2000) pp. 55.

[22] P. R. Ettireddy, N. Ettireddy, S. Mamedov, P. Boolchand, P. G. Smirniotis, *Applied Catalysis B: Environmental* **76** (2007) pp. 123-134.

[23] F. Roozeboom, M. G. Mittlemeijer-Hardeger, J. A. Mouljin, J. Medma, U. H. J. de Beer, P. J. Gellings, *Journal of Physical Chemistry* **84** (1980) pp. 2783.

[24] H. Bosch, B. J. Kip, J. G. van Ommen, P. J. Gellings, *Journal of Chemistry Society: Faraday Transmissions* I **80** (1984) pp. 2479.

[25] I. R. Leith, M. G. Howden, *Applied Catalysis* **37** (1988) pp. 75.

[26] J. Jansson, A. E. C. Palmqvist, E. Fridell, M. Skoglundh, L. Österlund, P. Thormählen, V. Langer, *Journal of Catalysis* **211** (2002) pp. 387-397.

[27] N. Fripiat, R. Conanec, A. Auroux, Y. Laurent, P. Grange, *Journal of Catalysis* **167** (1997) pp. 543-549.

[28] E. Finocchio, G. Busca, V. Lorenzelli, V. S. Escribano, *Journal of Chemistry Society: Faraday Transmissions* **92 (9)** (1996) pp. 1587-1593.

[29] B. Solsona, T. E. Davies, T. Garcia, I. Vàzquez, A. Dejoz, S. H. Taylor, *Applied Catalysis B: Environmental* **66 (1-2)** (2006) pp. 92-99.

[30] S. E. Golunski, A. P. Walker, *Journal of Catalysis* **204** (2001) pp. 209-218.

[31] P. Michorczyk, P. Kuśtrowski, L. Chmielarz, J. Ogonowski, *React. Kinet. Catal. Lett.* **82 (1)** (2004) pp. 121-130.

[32] B. L. Yang, S. B. Lee, D. D. Cheng, W. S. Chang, *Journal of Catalysis* **141** (1993) pp. 161-170.

Chapter 6

CHAPTER 6

Methanol oxidation using nanocrystalline metal oxides

6.1 Introduction

From studies on the ODH propane, shown in chapter 5, a range of cobalt, iron and manganese catalysts were found to be active at low temperatures. The investigation of these catalysts for the oxidation of methanol was carried out with the aim of a low operating temperature. The chemical reactions of methanol have important applications in different areas including catalysis, fuel cells and biological processes. Methanol is a cheap and abundant raw material, as it is produced naturally from the anaerobic metabolism of bacteria. When methanol undergoes different chemical reactions it has the advantage of forming beneficial, value-added products such as formaldehyde.

Formaldehyde is produced industrially by the catalytic oxidation of methanol. The main catalysts used for this reaction include catalysts based on silver metal [1], a mixture of iron/molybdenum [2] and vanadium oxides [3]. The formation of formaldehyde is possible by the action of sunlight and oxygen with methane in the atmosphere. Generally the oxidation of methane is not feasible industrially as the formaldehyde formed is more reactive than the methane.

Formaldehyde is very important for industry as it is a building block for the synthesis of compounds with significant applications. Formaldehyde is most commonly known in history for its use as a tissue fixative in the embalming process. The current applications of this compound include the formation of products such as urea formaldehyde resin, melamine resin, phenol formaldehyde resin, polyoxymethylene plastics, 1,4-butanediol and methylene diphenyl diisocyanate [4]. In terms of applications these compounds are used in permanent adhesives, paints, explosives, sanitary products, disinfectants and biocides [5]. The production of formaldehyde has increased to (2.5-2.7) x 10^7 tonnes per year [6] therefore it is one of the world's most important chemicals for industry.

The formation of formaldehyde from methanol is based on an oxidative dehydrogenation reaction. Partial oxidation is not the preferred route in this case as ODH provides a single step reaction and with the catalyst employed; high activities and selectivities are observed with mild conditions. The disadvantage of using this method is the formation of carbon by-products such as carbon dioxide, which are thermodynamically favourable.

The current catalyst mainly used by industry, with a yield of over 80%, is based on the silver catalysed route to formaldehyde [6] due to relatively low costs and high yields. However, the operating temperature of the catalyst is around 650°C therefore it would be preferable to lower this temperature but to still obtain high yields of the desired product.

6.2 Results

6.2.1 Selective oxidation of methanol over cobalt oxide

The conversions of methanol for the different cobalt oxides prepared are shown in figure 6.1.

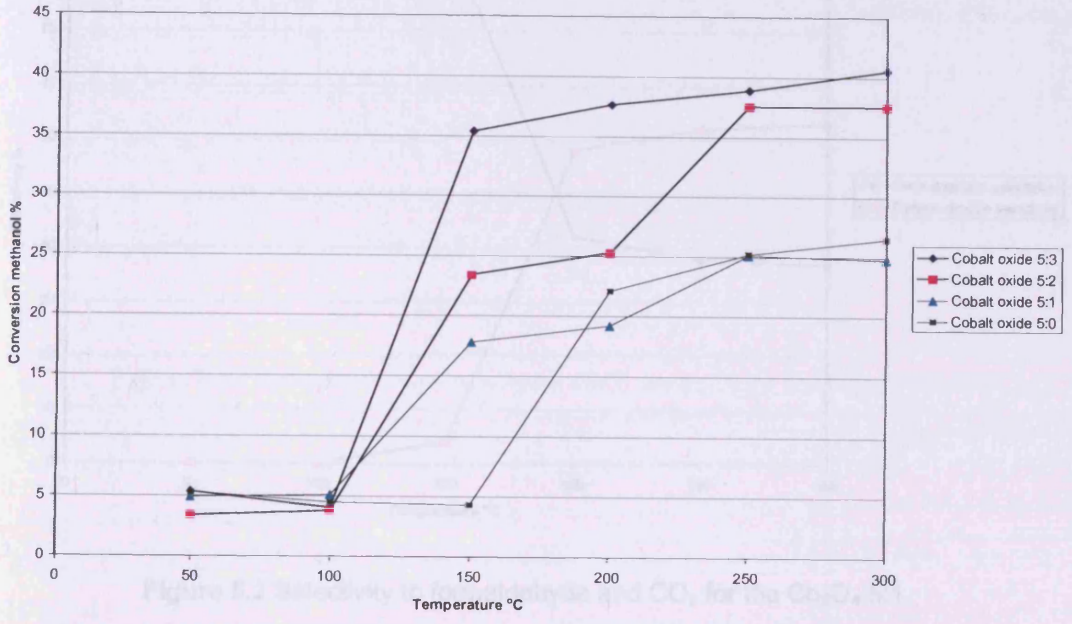

Figure 6.1 Conversions of methanol over different cobalt oxide catalysts.

All the cobalt oxides prepared had an initial activity at 50°C with a 5% conversion for the 5:3 ratio. At only 100°C this conversion increased to 35% and finally to 40.6% at 300°C. The highest conversions observed were for the 5:3 ratio which was closely followed by the 5:2 ratio at 300°C with 37.6%, the 5:0 ratio with 26.5% and finally the 5:1 ratio with 24.8%. The cobalt nitrate calcined (5:0) exhibited the lowest conversion, below 5%, until 200°C where a conversion slightly higher than the 5:1 ratio was observed.

The selectivities for the cobalt oxide with ratio 5:1 are shown in figure 6.2. The maximum selectivity to formaldehyde was 100% at only 50°C. Carbon dioxide

formation occurred between 150-300°C increasing from 62 to 64% selectivity as selectivity to formaldehyde decreased.

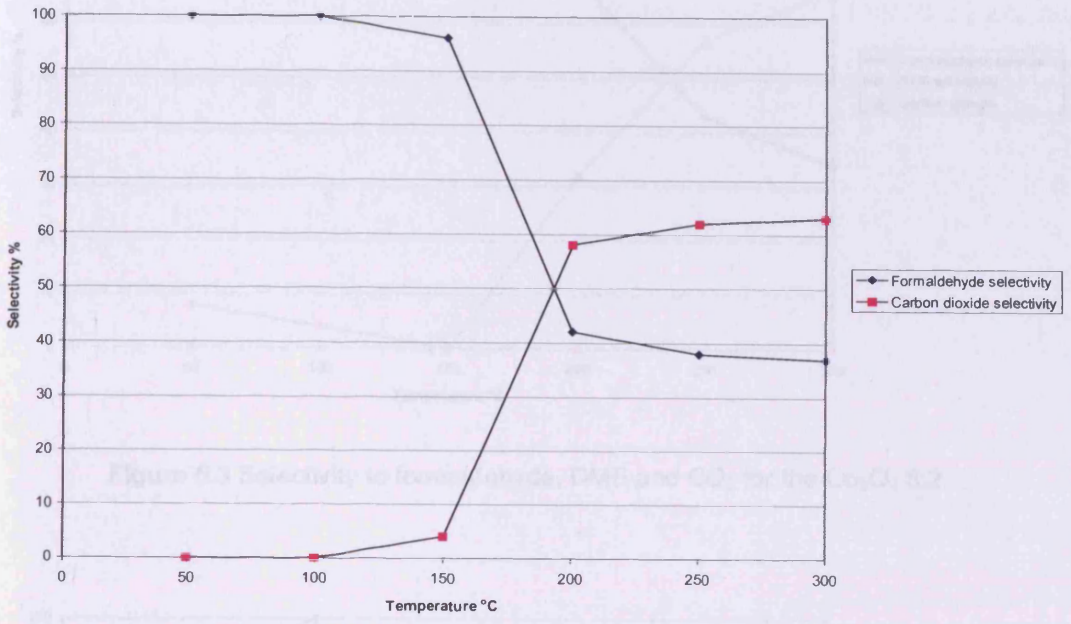

Figure 6.2 Selectivity to formaldehyde and CO_2 for the Co_3O_4 5:1.

The selectivities for cobalt oxide 5:2 are shown in figure 6.3. At 50°C, the main product observed was formaldehyde with 92% selectivity. The minor product observed at 50°C was DME with only 8% selectivity which was not detected above 100°C. As the amount of DME diminished, the selectivity to formaldehyde was able to increase to 100% at 150°C. Carbon dioxide was formed at 200°C with a selectivity of 32%, causing the selectivity to formaldehyde to decrease to 68%. The selectivity to carbon dioxide continued to increase to 66% at 300°C with formaldehyde selectivity continuing to decrease to 34%.

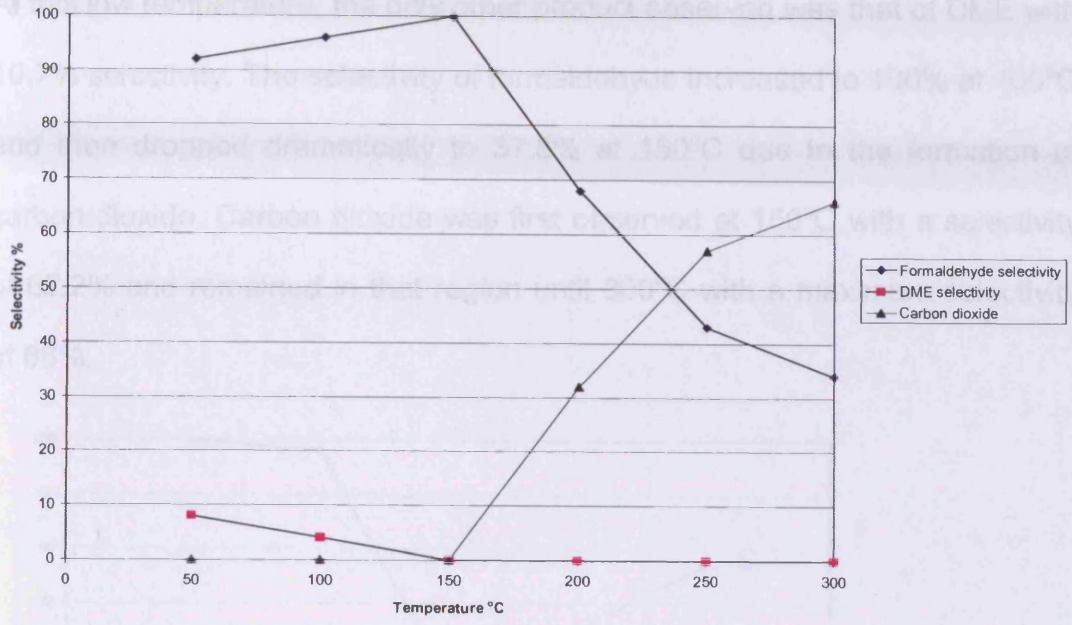

Figure 6.3 Selectivity to formaldehyde, DME and CO_2 for the Co_3O_4 5:2.

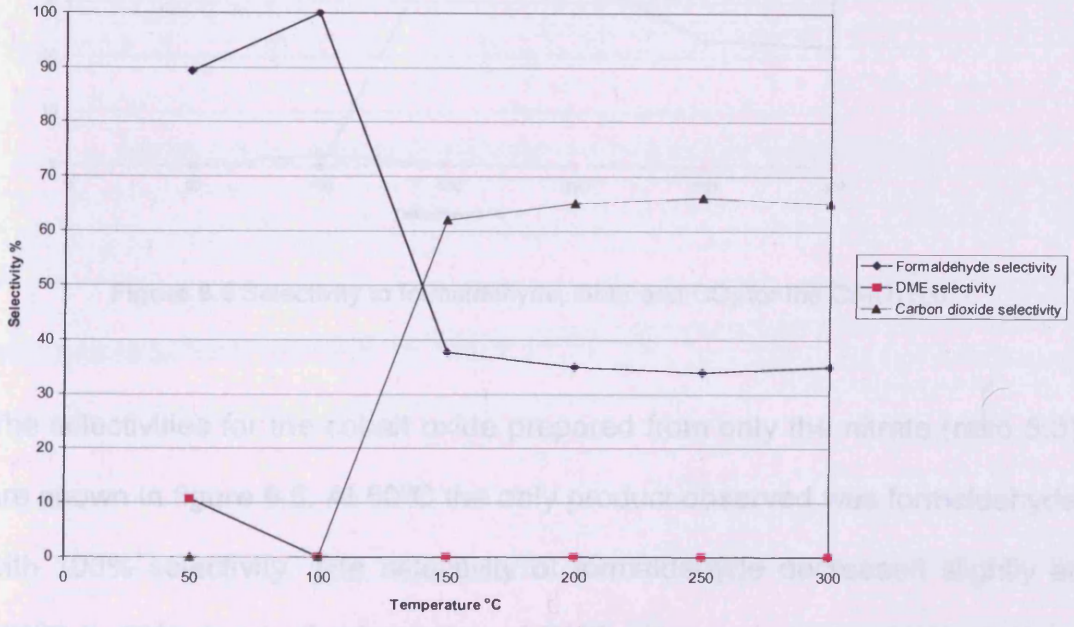

Figure 6.4 Selectivity to formaldehyde, DME and CO_2 for the Co_3O_4 5:3.

The selectivities for cobalt oxide, ratio 5:3, are shown in figure 6.4. At 50°C, the catalyst exhibited 89.3% selectivity to the desired product formaldehyde.

At this low temperature, the only other product observed was that of DME with 10.7% selectivity. The selectivity of formaldehyde increased to 100% at 100°C and then dropped dramatically to 37.8% at 150°C due to the formation of carbon dioxide. Carbon dioxide was first observed at 150°C with a selectivity of 62.2% and remained in that region until 300°C with a maximum selectivity of 66%.

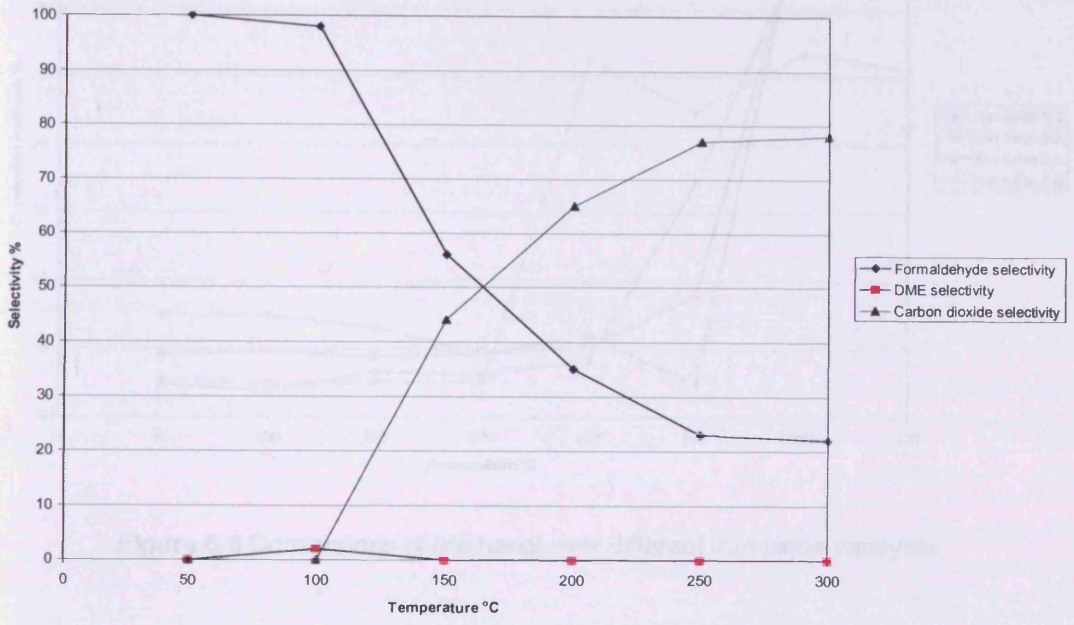

Figure 6.5 Selectivity to formaldehyde, DME and CO_2 for the Co_3O_4 5:0.

The selectivities for the cobalt oxide prepared from only the nitrate (ratio 5:0) are shown in figure 6.5. At 50°C the only product observed was formaldehyde with 100% selectivity. The selectivity of formaldehyde decreased slightly at 100°C to 98% due to the formation of DME with a selectivity of 2%. Carbon dioxide was detected at 150°C with a selectivity of 44% causing the selectivity to formaldehyde to drop even further to 56%. The selectivity to carbon dioxide increased to a maximum of 78% at 300°C.

6.2.2 Selective oxidation of methanol over iron oxide

The conversions of methanol for the different iron oxide catalysts prepared are shown in figure 6.6.

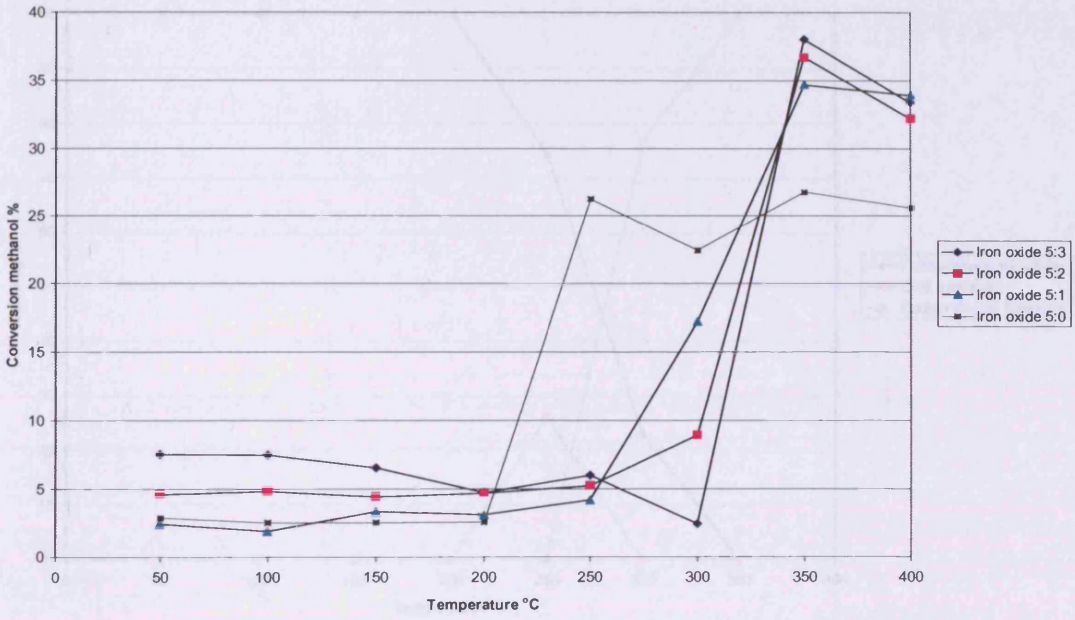

Figure 6.6 Conversions of methanol over different iron oxide catalysts.

The highest conversion was exhibited by the 5:3 ratio with 38% at 350°C, followed closely by 5:2 with 36.7%, 5:1 with 35% and the iron nitrate calcined with 27% conversion.

The 5:3 ratio also had the highest initial activity with 8% conversion at 50°C. The iron nitrate had an initial activity of only 4% which suddenly increased at 250°C to 26% but then it reached a plateau. The iron oxides with ratios 5:2 and 5:3 remained at the lowest conversions for the longest temperature range and only increased to the highest conversions at 300°C. The 5:1 ratio had an initial activity of 3.5% and increased to its maximum conversion at 250°C. At

300°C the order of activity was in fact inverse to the maximum conversion order observed at 350°C. The iron oxide 5:0 had the highest conversion at 300°C with 22.4% conversion, followed by iron oxide 5:1 with 17.2%, iron oxide 5:2 with 8.9% and finally iron oxide 5:3 with 2.4%.

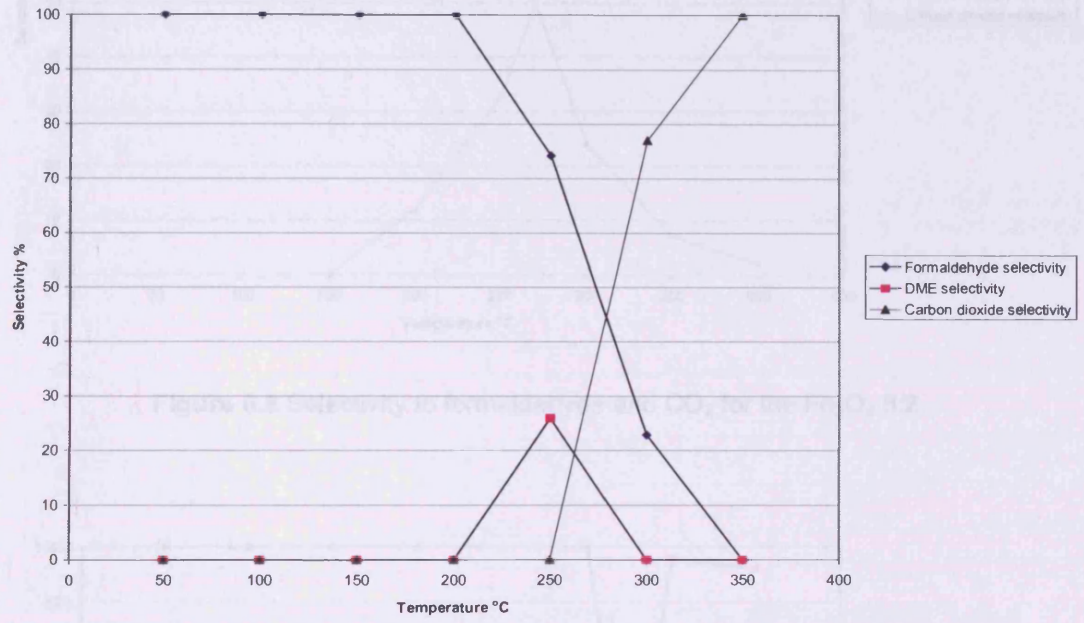

Figure 6.7 Selectivity to formaldehyde, DME and CO_2 for the Fe_2O_3 5:1.

The selectivities for the iron oxide 5:1 are shown in figure 6.7. The selectivity to formaldehyde was 100% until 200°C and only dropped to 0% selectivity at 350°C. DME was present only at 250°C with 25% selectivity. The formation of carbon dioxide occurred at 300°C with 100% selectivity at 350°C.

The selectivities for the iron oxide 5:2 are shown in figure 6.8. The catalyst gave 100% selectivity to formaldehyde from 50°C to 150°C. Above 150°C the selectivity to formaldehyde decreased dramatically to 2% at 400°C, while the selectivity to carbon dioxide increased to near 100%. The only products observed were formaldehyde and carbon dioxide.

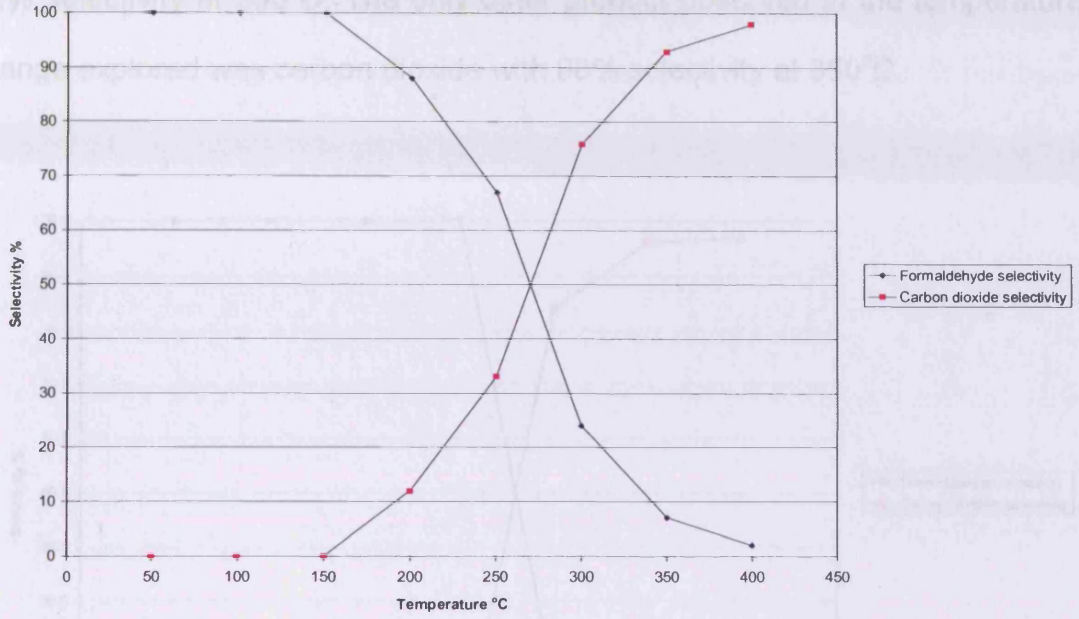

Figure 6.8 Selectivity to formaldehyde and CO_2 for the Fe_2O_3 5:2.

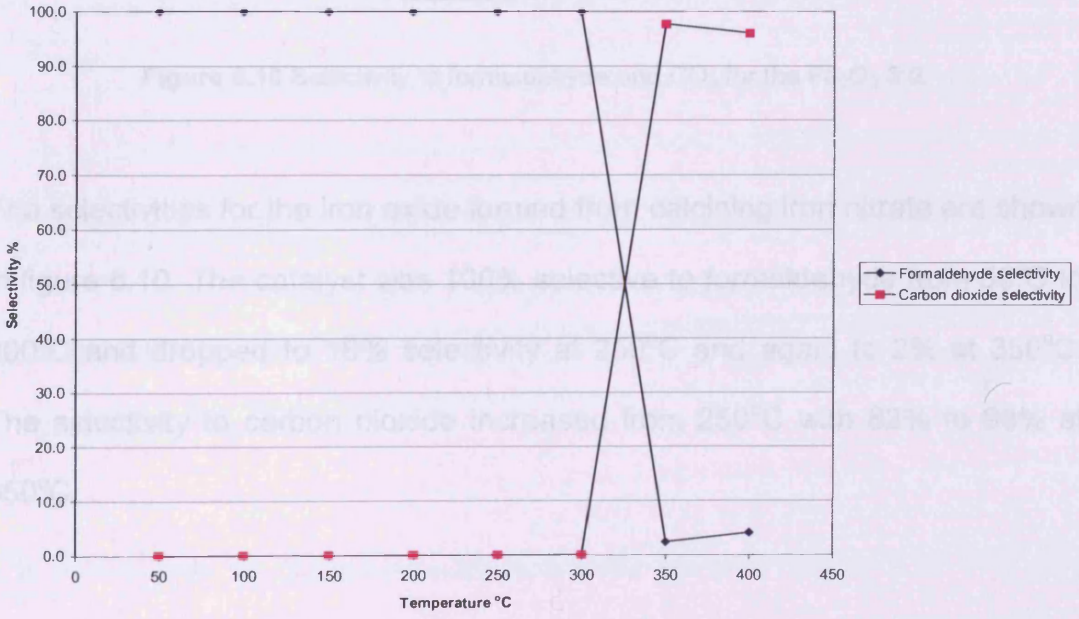

Figure 6.9 Selectivity to formaldehyde and CO_2 for the Fe_2O_3 5:3.

The selectivities for the iron oxide 5:3 are shown in figure 6.9. The catalyst was 100% selective to formaldehyde from 50°C until 300°C and dropped to

2% selectivity at 350°C. The only other product observed in the temperature range explored was carbon dioxide with 98% selectivity at 350°C.

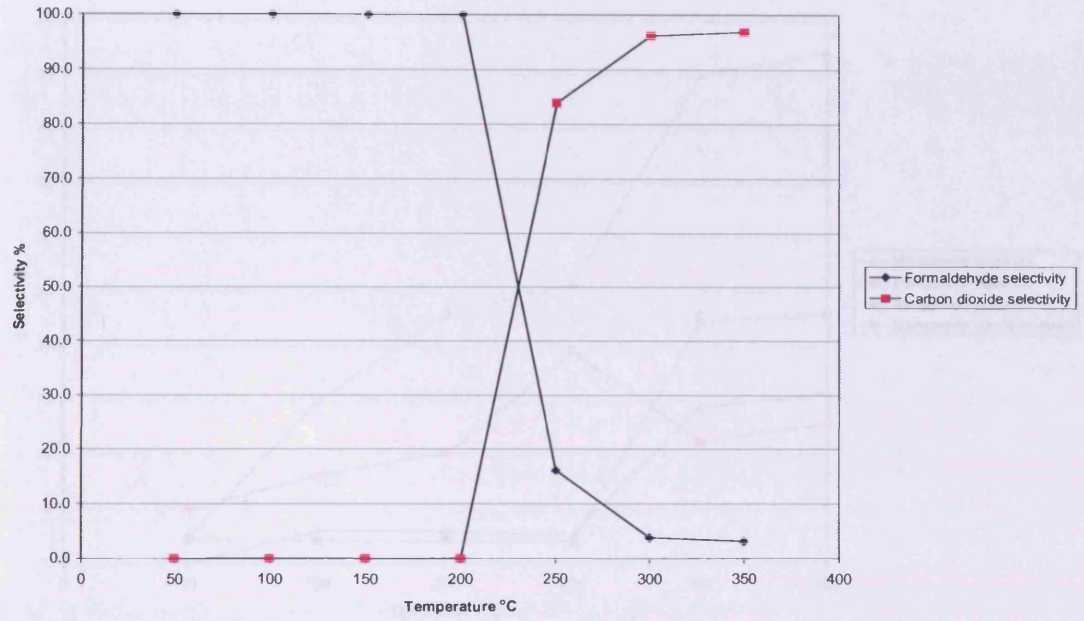

Figure 6.10 Selectivity to formaldehyde and CO_2 for the Fe_2O_3 5:0.

The selectivities for the iron oxide formed from calcining iron nitrate are shown in figure 6.10. The catalyst was 100% selective to formaldehyde from 50°C to 200°C and dropped to 18% selectivity at 250°C and again to 2% at 350°C. The selectivity to carbon dioxide increased from 250°C with 82% to 98% at 350°C.

6.2.3 Selective oxidation of methanol over manganese oxide

The conversions of methanol for the different manganese oxide catalysts prepared are shown in figure 6.11.

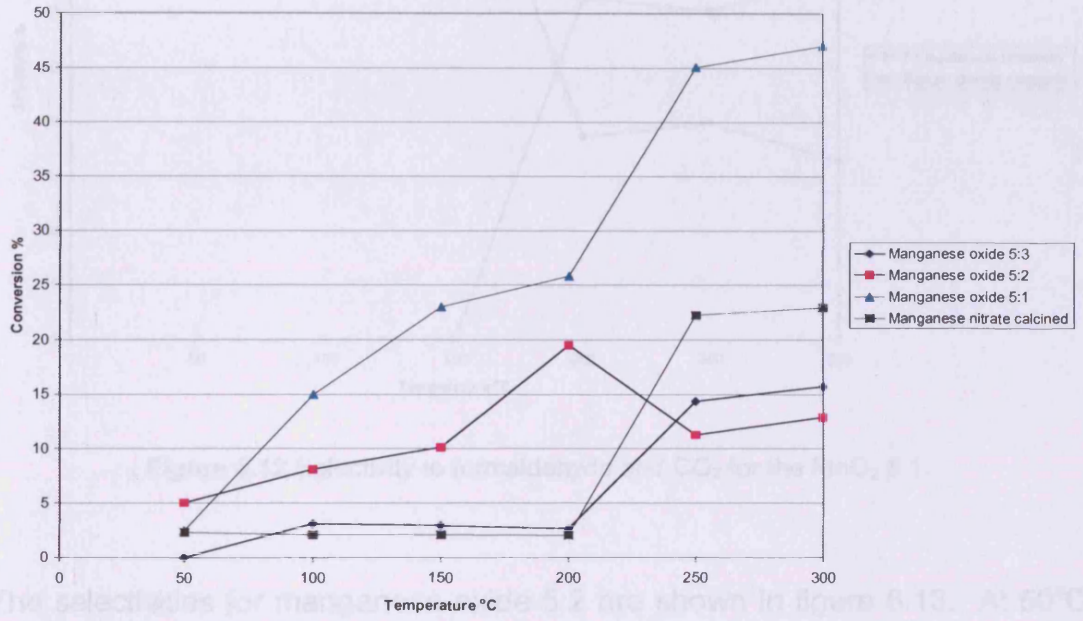

Figure 6.11 Conversions of methanol over different manganese oxide catalysts.

An initial activity was observed at 50°C for all catalyst excluding the 5:3 ratio with an initial activity at 100°C. The highest conversion was observed for the 5:1 ratio with 47% at 300°C, followed by 5:0 with 23%, 5:2 with 19% and the 5:3 ratio with 16% conversion.

The selectivities for manganese oxide 5:1 are shown in figure 6.12. The only products observed throughout the temperature range explored were formaldehyde and carbon dioxide. The catalyst was 100% selective to formaldehyde from 50°C to 150°C. At 200°C the presence of carbon dioxide was observed with a selectivity of around 60% and therefore the selectivity to formaldehyde dropped to 40%.

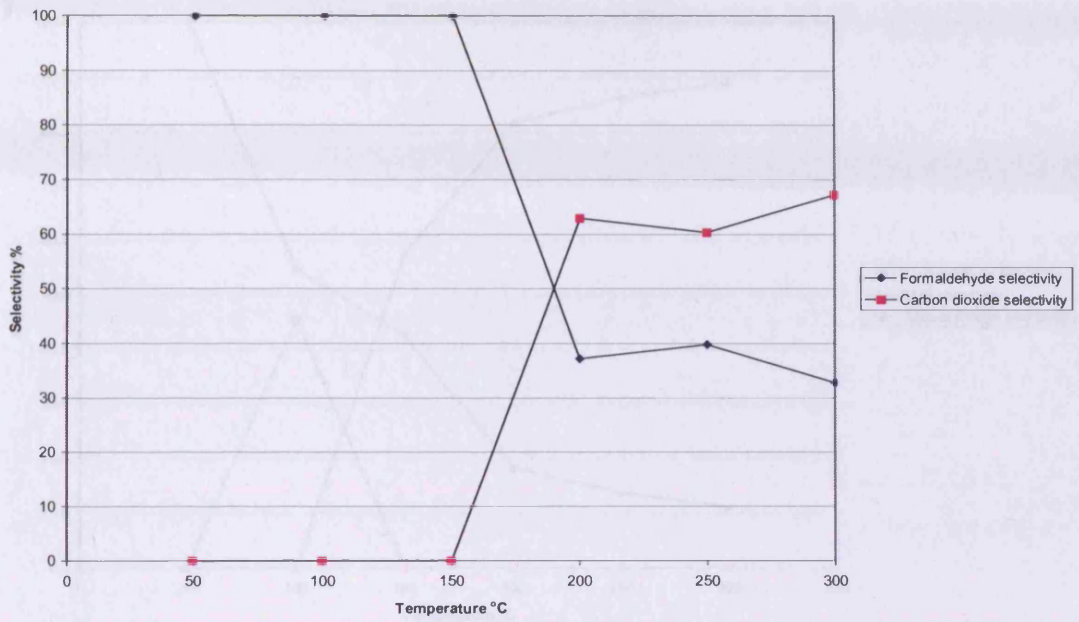

Figure 6.12 Selectivity to formaldehyde and CO_2 for the MnO_2 5:1.

The selectivities for manganese oxide 5:2 are shown in figure 6.13. At 50°C the catalyst was 100% selective to formaldehyde but dropped dramatically to 14% selectivity by 250°C and 11% at 300°C. DME was only present around 100°C with 45% selectivity but this fell to 0% by 150°C as carbon dioxide was observed. The selectivity to carbon dioxide increased as the selectivity to formaldehyde decreased with a maximum selectivity of 89% at 300°C.

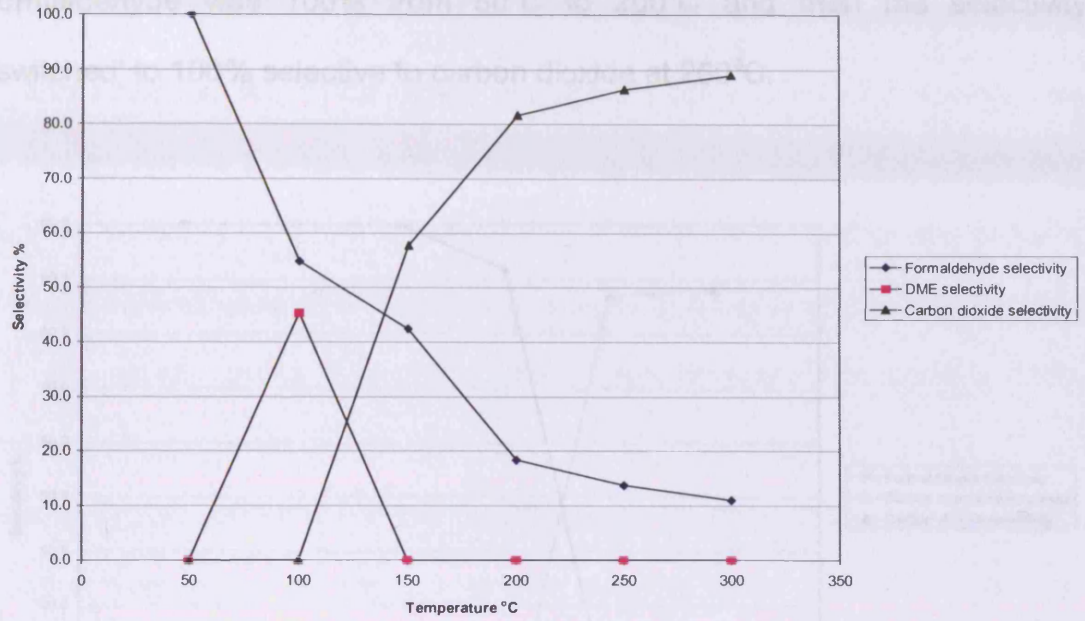

Figure 6.13 Selectivity to formaldehyde, DME and CO_2 for the MnO_2 5:2.

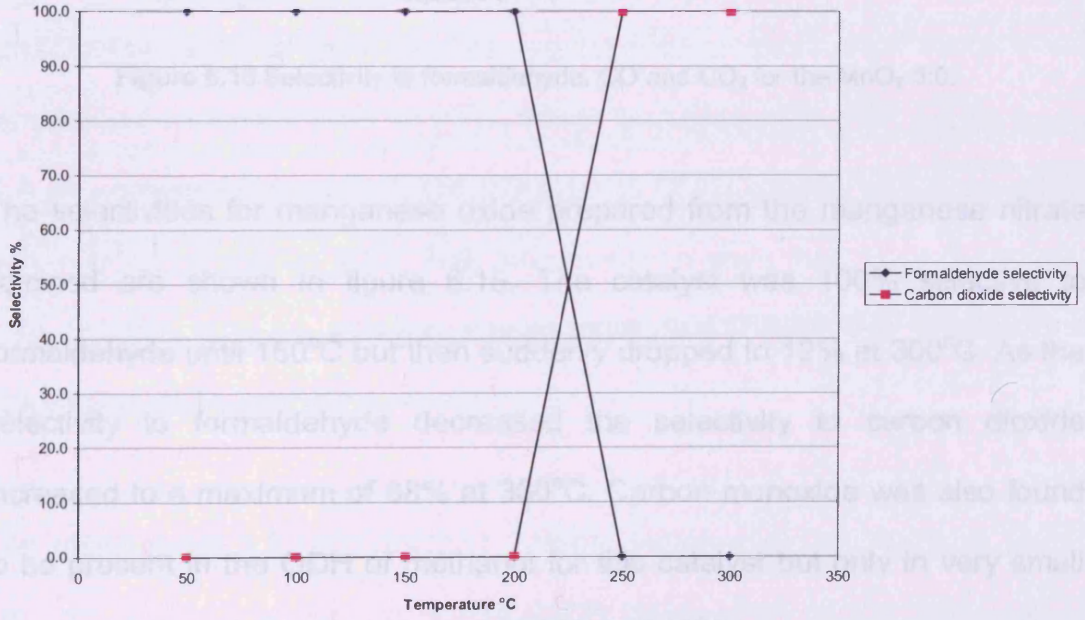

Figure 6.14 Selectivity to formaldehyde and CO_2 for the MnO_2 5:3.

The selectivities for manganese oxide 5:3 are shown in figure 6.14. The only products observed were formaldehyde and carbon dioxide. The selectivity to

formaldehyde was 100% from 50°C to 200°C and then the selectivity 'switched' to 100% selective to carbon dioxide at 250°C.

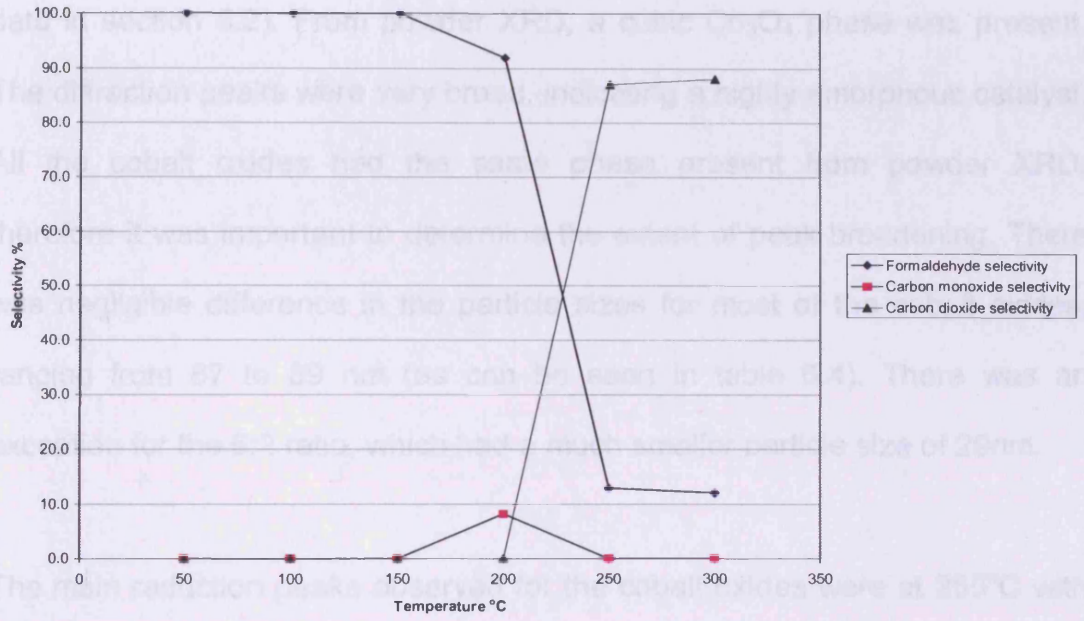

Figure 6.15 Selectivity to formaldehyde, CO and CO_2 for the MnO_2 5:0.

The selectivities for manganese oxide prepared from the manganese nitrate calcined are shown in figure 6.15. The catalyst was 100% selective to formaldehyde until 150°C but then suddenly dropped to 12% at 300°C. As the selectivity to formaldehyde decreased the selectivity to carbon dioxide increased to a maximum of 88% at 300°C. Carbon monoxide was also found to be present in the ODH of methanol for this catalyst but only in very small quantities with a maximum selectivity of 9% at 200°C.

6.3 Discussion

In the cobalt series of catalysts, the highest conversion of methanol was observed for the 5:3 ratio with a surface area of 74 m^2g^{-1} (characterisation data in section 5.2). From powder XRD, a cubic Co_3O_4 phase was present. The diffraction peaks were very broad, indicating a highly amorphous catalyst. All the cobalt oxides had the same phase present from powder XRD, therefore it was important to determine the extent of peak broadening. There was negligible difference in the particle sizes for most of the cobalt oxides, ranging from 87 to 89 nm (as can be seen in table 5.4). There was an exception for the 5:2 ratio, which had a much smaller particle size of 29nm.

The main reduction peaks observed for the cobalt oxides were at 250°C with small low temperature peaks at 125 and 190°C. Previous work [7] found a low temperature reduction peak at 90°C, which was present in TPR profile figure 5.7. The cobalt oxides were found to be in the Co_3O_4 phase. Therefore cobalt was in a high oxidation state. This high oxidation state may have resulted in very reactive oxygen species, which gave rise to the low temperature reduction peaks observed.

The cobalt oxide 5:2 ratio reached a formaldehyde yield of 23.4% at 150°C (see figure 6.16), which was considerably higher than all the other cobalt oxides in the study. The catalyst was very selective for formaldehyde with moderate conversions of methanol. The 5:2 ratio had the highest surface area of all the cobalt oxides, with 102 m^2g^{-1}. The high surface area may be related to the high selectivity observed. From table 5.4, the average crystallite size of

Co_3O_4 5:2 was 29nm. Therefore it can be concluded that a highly crystalline cubic Co_3O_4, with a high surface area, was responsible for the yields obtained.

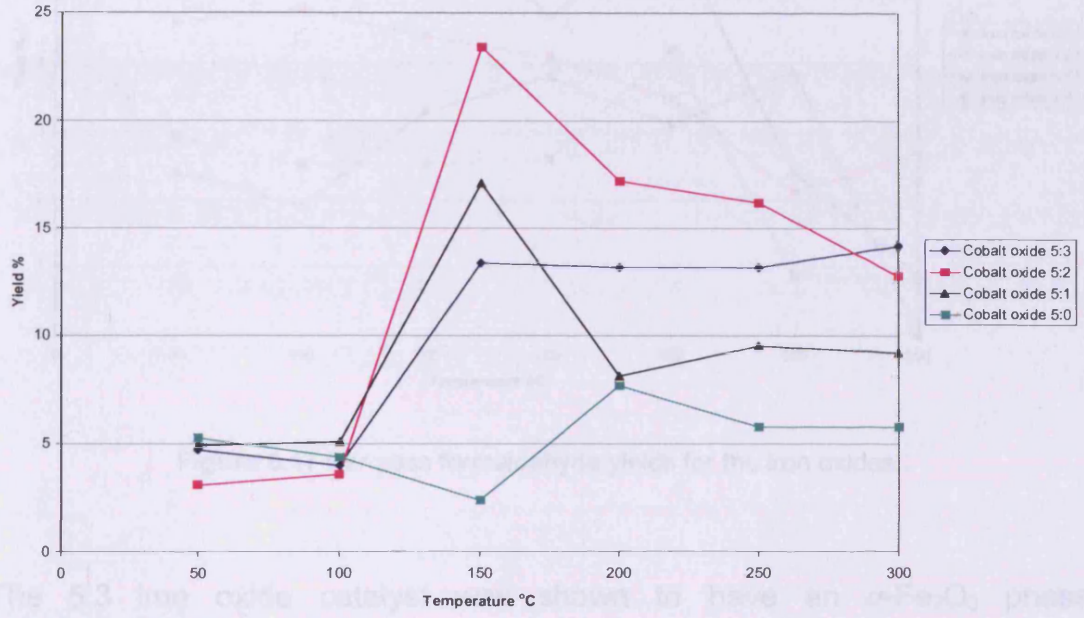

Figure 6.16 Per pass formaldehyde yields for the cobalt oxides.

In the iron series of catalysts the most active ratio, in terms of formaldehyde yield, was the 5:3 ratio. A maximum yield of 7.5%, in figure 6.17, was obtained in the temperature range 50-100°C but this then dropped as the temperature increased to 400°C. The cobalt oxides gave much higher yields, even though the iron oxide selectivities were greater for the desired product. Most of the iron oxides were 100% selective to formaldehyde, even at 300°C for the 5:3 ratio. However, it should be noted that generally 200°C was the maximum temperature for this high selectivity.

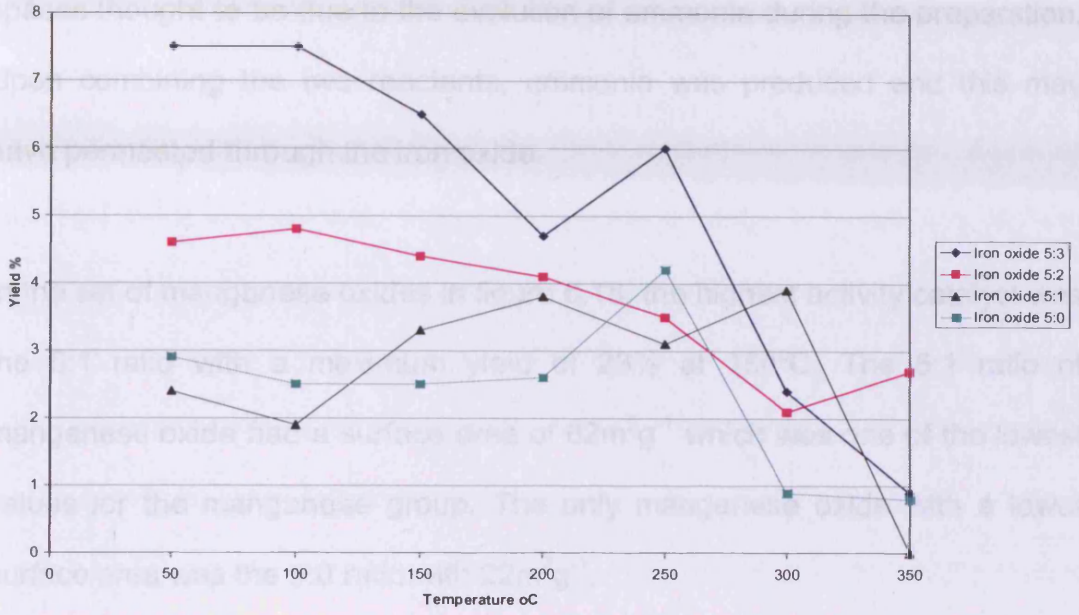

Figure 6.17 Per pass formaldehyde yields for the iron oxides.

The 5:3 iron oxide catalyst was shown to have an α-Fe_2O_3 phase (rhombohedral syn-hematite) from powder XRD (in section 5.2). This phase was present in all the iron oxides. The particle size was 285nm for the 5:3 ratio indicating, for the iron oxides, that a small crystallite size was not required for high selectivity at ambient temperatures. The 5:3 ratio had the highest surface area for this set of catalysts with $62m^2g^{-1}$ and largest crystallite size. It is thought that a higher surface area gives higher selectivity and conversion due to more sites of reaction being exposed. This was the case for the cobalt oxides studied, where the 5:2 ratio of cobalt had the highest surface area of $102m^2g^{-1}$ and highest yield of 17.2%.

SEM studies showed an intriguing surface morphology (in section 5.2). The cobalt oxides all had fine, regular shaped particles. Iron oxide however, did not have fine particles. The surface appeared smooth with 'holes' and vacant

spaces thought to be due to the evolution of ammonia during the preparation. Upon combining the two reactants, ammonia was produced and this may have permeated through the iron oxide.

In the set of manganese oxides in figure 6.18, the highest activity catalyst was the 5:1 ratio with a maximum yield of 23% at 150°C. The 5:1 ratio of manganese oxide had a surface area of $62m^2g^{-1}$ which was one of the lowest values for the manganese group. The only manganese oxide with a lower surface area was the 5:0 ratio with $22m^2g^{-1}$.

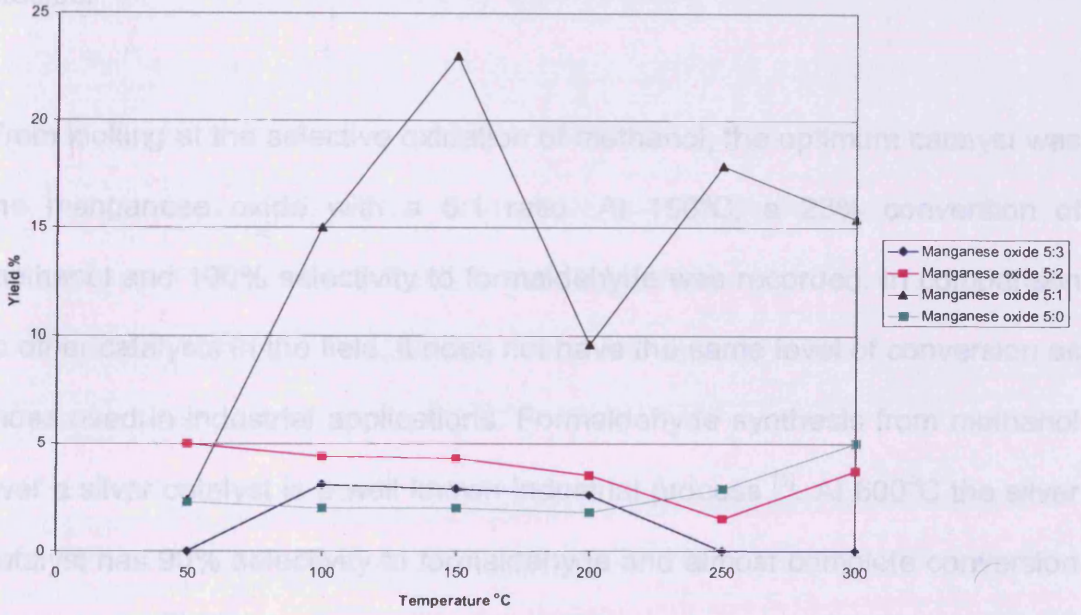

Figure 6.18 Per pass formaldehyde yields for the manganese oxides.

From powder XRD, the phase present for all the manganese oxides was MnO_2 (hexagonal, syn-akhtenskite). Broad diffraction peaks were observed due to a highly amorphous surface. The 5:3 ratio of MnO_2 had the smallest particle size of 15nm but the 5:1 ratio had a much larger size of 54nm. The particles of the 5:3 ratio may have been too small to allow selective oxidation

of methanol as exposed oxygen sites at such a high density would have lead to complete oxidation. In TPR studies, the 5:1 ratio of manganese oxide had the most intense reduction at the lowest temperature which can be related to the high activity observed. From XPS studies, MnO_2 5:1 had the highest oxygen to metal ratio of all the catalysts in this study, including those of cobalt and iron. The MnO_2 5:1 catalyst had an O/Mn ratio of 3.03 which was almost 50% higher than the other manganese oxides. The average values for cobalt and iron oxides were 1.0 and 1.5 respectively. The high ratio of O/Mn found for MnO_2 5:1 helps to explain why it was more active than the other oxides studied.

From looking at the selective oxidation of methanol, the optimum catalyst was the manganese oxide with a 5:1 ratio. At 150°C, a 23% conversion of methanol and 100% selectivity to formaldehyde was recorded. In comparison to other catalysts in the field, it does not have the same level of conversion as those used in industrial applications. Formaldehyde synthesis from methanol over a silver catalyst is a well known industrial process [1]. At 600°C the silver catalyst has 90% selectivity to formaldehyde and almost complete conversion of methanol [8]. The manganese catalyst may not give complete conversion but lower temperatures were explored. Low temperature activity is very important to reduce costs and unwanted emissions. Therefore 100% selectivity at 150°C is promising for future work.

A low temperature catalyst, based on Sn and Mo oxide, gave a conversion of 64% at 210°C and selectivity of 21%. The Sn/Mo oxide catalyst [9] was less

active than the MnO_2 5:1 but a higher yield of 95% was found for V-Mg-O catalysts. It was found that a higher surface area gave higher methanol conversions and selectivity to formaldehyde [5].

When trying to evaluate the reasons for activity and selectivity it is necessary to understand the mechanism of the reaction taking place. Formaldehyde is formed from a methoxide intermediate adsorbing on the surface and this can occur by two different processes [10]. One is dehydrogenation where hydrogen is transferred from the methyl group on the methanol molecule to the hydroxyl group forming H_2 directly. The other route involves oxidative dehydrogenation where the hydrogen transfers from the methyl group to surface oxygen on the catalyst, forming hydroxyl groups. These hydroxyl groups then leave two electrons on the catalyst which are capable of reducing the surface. ODH was the preferred route as it had a smaller energy barrier. Formaldehyde is formed from ODH involving the transfer from methyl to surface oxygen and subsequent reduction of metal site [11].

An excess of oxygen favours complete oxidation products such as carbon monoxide and carbon dioxide (and water). It has also been proposed [12] that oxygen which is molecularly adsorbed on the catalyst surface acts as a precursor to give atomic oxygen. It is useful to calcine the catalyst sample before using in the reactor for this reason. The presence of strongly bound oxygen in the uppermost layer of the catalyst can only catalyse methanol dehydrogenation, in the case of the silver catalyst. The adsorption of

methanol does not occur on an oxygen free surface [2]. Therefore, in the case of cobalt, iron and manganese oxides they seem suitable for the reaction.

When SiO_2 was studied [13], the main product observed was CO, even though with further analysis it was discovered formaldehyde was actually formed first but was subsequently oxidised/reduced to form the CO product. This occurred at temperatures over 500°C which would explain why at higher temperatures the selectivity to formaldehyde was not very high. The formation of CO_2 is through a different route as it is the oxidation intermediate produced from the dehydrogenation of formaldehyde.

The selective oxidation of methanol involves the activation of the methanol O-H bond to form surface methoxide species and hydrogen atoms [14]. When O_2 is absent, methanol decomposition is the main reaction above 250°C. In the work carried out there was a point around 250°C where selectivities changed from formaldehyde being the main product. This may have been due to oxygen being consumed in oxidation below 250°C.

Formaldehyde is normally unstable at high temperatures as it easily decomposes to H_2 and CO (or with oxygen forms H_2O and CO_2) and can be further oxidised to HCOOH from the presence of weakly bound surface atomic oxygen. Therefore high selectivities to formaldehyde cannot be expected when this reaction occurs. Low temperature activity catalysts are required to avoid temperatures where formaldehyde reacts further. Manganese is

promising with such high selectivity at low temperatures although the conversion of methanol may need to be improved.

6.4 Conclusions

The ODH of methanol was studied over a range of cobalt, iron and manganese oxides. Previous characterisation studies indicated the presence of Co_3O_4, Fe_2O_3 and MnO_2 phases respectively. The highest yield obtained was 23% for the MnO_2 with ratio 5:1. The activity was attributed to an optimal particle size of 54nm where a greater number of low coordination defect lattice oxygen site would have been present and a high O/Mn ratio of 3.03.

6.5 References

[1] E. Cao, A. Gavriilidis, *Catalysis Today* **110** (2005) pp. 154-163.

[2] M. Qian, M. A. Liauw, G. Emig, *Applied Catalysis A: General* **238** (2003) pp. 211-222.

[3] L. J. Burcham, G. T. Gao, X. T. Gao, I. E. Wachs, *Topics in Catalysis* **11** (2000) pp. 85.

[4] M. Cozzolino, R. Tesser, M. D. Serio, P. D'Onofrio, E. Santacesaria, *Catalysis Today* **128** (2007) pp. 191-200.

[5] G. V. Isaguliants, I. P. Belomestnykh, *Catalysis Today* **100** (2005) pp. 441-445.

[6] M. Qian, M. A. Liauw, G. Emig, *Applied Catalysis A: General* **238** (2003) pp. 211-222.

[7] T. E. Davies, T. Garcia, B. Solsona, S. H. Taylor, *Chemical Communications* (2006) pp. 3417-3419.

[8] L. Leferts, J. G. Ommen, J. R. H. Ross, *Applied Catalysis* **23** (1986) pp. 385- 402.

[9] N. G. Valente, L. A. Luis, E. Cadus, *Applied Catalysis* **205** (2001) pp. 201-214.

[10] G. Busca, *Journal of Molecular Catalysis* **50** (1989) pp. 241.

[11] C. J. Machiels, W. H. Cheng, U. Chowdry, W. E. Farneth, F. Hong, E. M. McCarron, A. W. Sleight, *Applied Catalysis* **25** (1986) pp. 249.

[12] J. F. Deng, X. H. Xu, J. H. Wang, Y. Y. Liao, B. F. Hong, *Catalysis Letters* **32** (1995) pp. 159.

[13] S. Yao, F. O. Yang, S. Shimumora, H. Sakurai, K. Tabata, E. Suzuki, *Applied Catalysis A: General* **198** (2000) pp. 43-50.

[14] T. Ohtake, T. Mori, Y. Morikawa, *Journal of Natural Gas Chemistry* **16** (2007) pp. 1-5.

Chapter 7

CHAPTER 7

Final discussion and future work

7.1 Niobium and tungsten catalysts

Varying amounts of niobium and tungsten were loaded on Pd/TiO_2 by a wet impregnation preparation and tested for their activity as oxidation catalysts. It was found that the incorporation of niobium or tungsten increased the activity for the complete oxidation of propane. The temperatures of conversion were much lower than for those catalysts without niobium or tungsten present. Increased loadings of niobium or tungsten on Pd/TiO_2 promoted activity for the complete oxidation of propane. The optimum loading for Nb and W was 6% with the most active catalyst in this study being $0.5\%Pd/6\%Nb_2O_5/TiO_2$.

The activity of the Nb and W containing catalysts has been attributed to their ability to alter the nature of palladium. From XPS studies it was found that when Nb or W were present no metallic palladium was present. This increased the oxygen mobility and produced easily reducible species.

7.2 Ceria and vanadium catalysts

Nanocrystalline ceria was prepared by a precipitation method and varying amounts of vanadium were loaded onto the support. Ceria alone was found to be a complete oxidation catalyst of propane where the only product observed was CO_2. With only 0.5% vanadium loaded on the ceria support, selective

oxidation to propene was found. Increased loadings of vanadium resulted in the formation of a mixed cerium vanadium phase which gave propene yields of 3.7%. Currently, the best catalyst for the ODH of propane is based on V/MgO with yields of 52% at 500°C [1]. Although the yields obtained on ceria based catalysts are incomparable to those obtained industrially, the low temperature activity found can promote future work in this area. The formation of a mixed cerium vanadate phase was of the most interest for future work where conditions could be optimised to give improved yields.

7.3 Cobalt, iron and manganese oxide catalysts

7.3.1 ODH propane

Cobalt, iron and manganese oxides were prepared by grinding the corresponding nitrate with different ratios of ammonium bicarbonate. These oxide catalysts were tested for their activity in the oxidative dehydrogenation of propane. The highest propene yield observed was for the Co_3O_4 5:1 ratio with 3.8%, which was similar to the results found for vanadia/ceria based catalysts. This yield was nowhere near the 52% obtained by V/MgO. The cobalt oxide had 80% selectivity to propene at temperatures as low as 150°C. The activity observed was attributed to the spinel structure which the cobalt oxide formed alongside a small crystallite size, high reducibility and high ratio of O/Co. Although the yields of propene were not satisfactory the low temperature activity gives scope for future work to understand the mechanism of the reaction taking place.

7.3.2 ODH methanol

Cobalt, iron and manganese oxides were prepared by grinding the corresponding nitrate with different ratios of ammonium bicarbonate. These oxide catalysts were tested for their activity in the oxidation of methanol. The highest yield of formaldehyde obtained was 23% for the MnO_2 with ratio 5:1. The activity was attributed to an optimal particle size of 54nm where a greater number of low coordination defect lattice oxygen site would have been present and a high O/Mn ratio of 3.03. A 23% yield of formaldehyde is much higher than those found for the ODH of propane in previous chapters. However, in the oxidation of methanol, formaldehyde yields of up to 95% have been obtained [2].

7.4 Future work

The characterisation methods used were useful in trying to explain the activities of the different catalysts. Further studies are necessary to help understand the nature of the catalytic activity. UV-visible spectrometry may have been useful as any electron transfers taking place can be observed by the absorption edge in the electronic spectra of the dispersed metal oxide. The acid-base properties of the catalyst surface should be probed by IR spectral studies to identify their density, location and distribution. Temporal analysis of products would allow the surface reaction mechanism on the catalyst to be identified by determining the kinetics and chemical conversions taking place.

7.5 References

[1] T. Punniyamurthy, S. Velusamy, J. Iqbal, *Chemistry Review* **105** (2005) pp. 2329-2363.

[2] L. Leferts, J. G. Ommen, J. R. H. Ross, *Applied Catalysis* **23** (1986) pp. 385- 402.

Appendix

Appendix

8.1 Mass Flow Controller (MFC) calibration

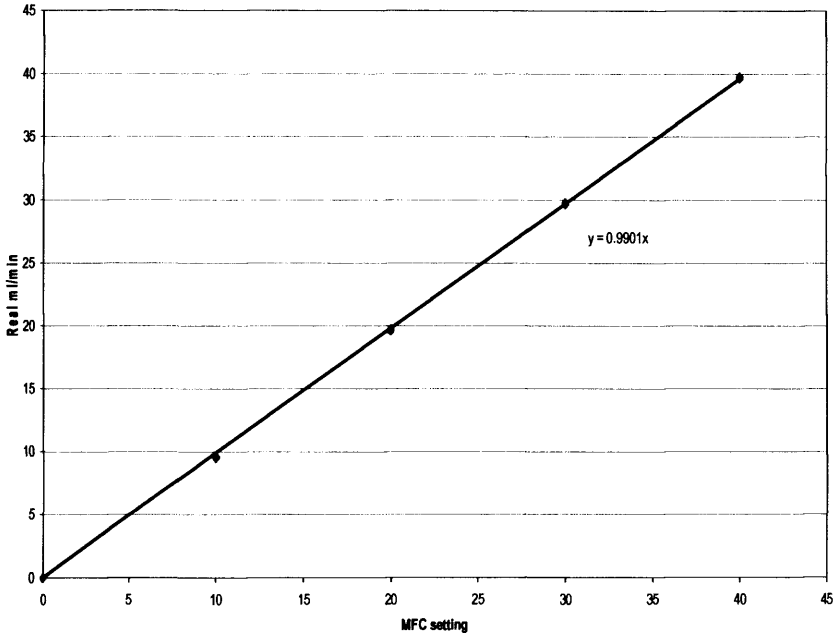

Figure 8.1.1 Helium MFC calibration

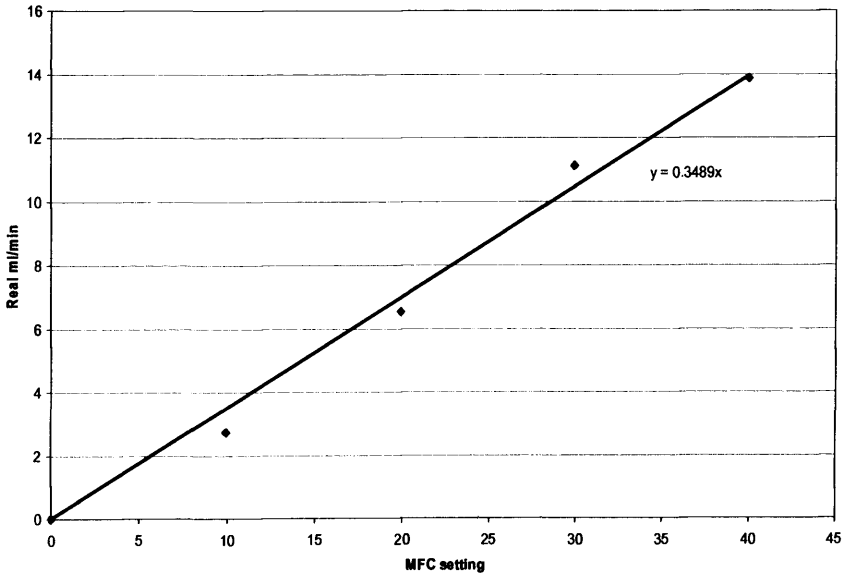

Figure 8.1.2 Propane MFC calibration

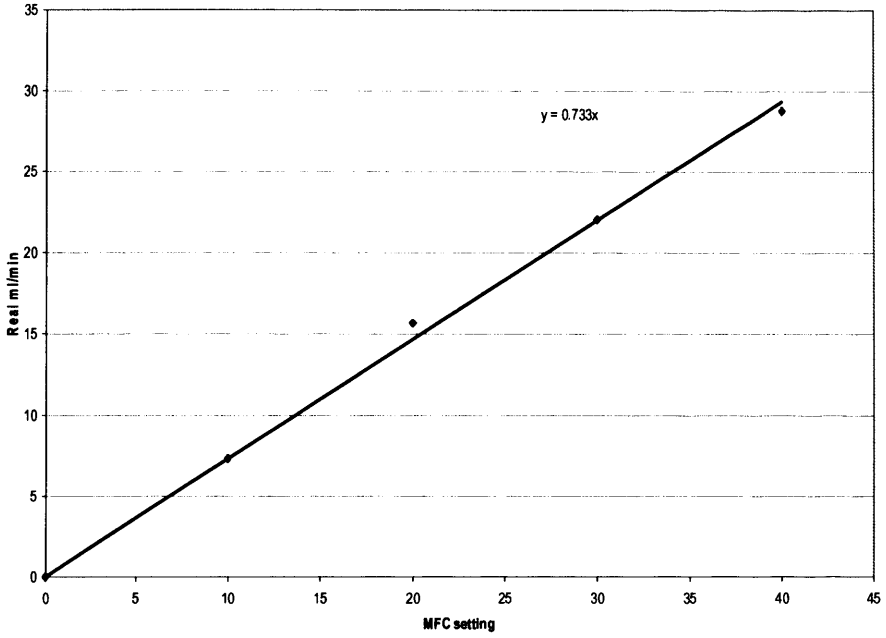

Figure 8.1.3 Oxygen MFC calibration

8.2 Standard Deviation values

Table 8.1 Standard deviation values of propane conversion for cobalt oxides in chapter 5

Temperature °C	Co_3O_4 5:1	Co_3O_4 5:2	Co_3O_4 5:3
100	0.0789	0.0329	0.0140
125	0.00135	0.0000602	0.0233
150	0.000483	0.000412	0.000345
175	0.000796	0.0258	0.0254
200	0.140	0.000916	0.116
250	0.0308	0.0104	0.0322

Publications

Publication 1

Applied Catalysis A: General 350 (2008) 63–70

Contents lists available at ScienceDirect

Applied Catalysis A: General

journal homepage: www.elsevier.com/locate/apcata

Deep oxidation of propane using palladium–titania catalysts modified by niobium

Marie Taylor [a], Edwin Ntainjua Ndifor [a], Tomas Garcia [b], Benjamin Solsona [c], Albert F. Carley [a], Stuart H. Taylor [a,*]

[a] Cardiff Catalysis Institute, School of Chemistry, Cardiff University, Main Building, Park Place, Cardiff CF10 3AT, UK
[b] Instituto de Carboquímica (CSIC), C/Miguel Luesma, 50018 Zaragoza, Spain
[c] Departament d'Enginyeria Química, Universitat de València, C/ Dr. Moliner 50, 46100 Burjassot, Valencia, Spain

ARTICLE INFO

Article history:
Received 10 April 2008
Received in revised form 30 July 2008
Accepted 30 July 2008
Available online 13 August 2008

Keywords:
VOCs
Catalytic oxidation
Propane
Niobium
Palladium
Titania

ABSTRACT

Pd/TiO_2 catalysts modified by niobium have been prepared and tested for the complete oxidation of propane. The catalysts have been characterised by BET, XRD, laser Raman spectroscopy, XPS, DRS and TPR. The incorporation of niobium into Pd/TiO_2 catalysts resulted in a marked increase in the catalytic activity compared to the Nb-free Pd/TiO_2 catalysts, and the activity increased as the niobium and/or palladium loading increased. The addition of Nb significantly modified the nature of the palladium and niobium species. There was a marked increase in the oxygen mobility after niobium addition. This could not only promote the presence of palladium species in a totally oxidized state but also resulted in the formation of new and very easily reducible species identified by subambient TPR. It was concluded that the niobium synergistic effect is due to the presence of these active oxygen species.

1. Introduction

In recent years, there has been increasing concern for the environment due to the emission of pollutants to the atmosphere. Volatile organic compounds (VOCs) are considered atmospheric pollutants [1] and are often present in low concentrations in many industrial gas exhaust systems. Legislative pressure is increasing on the permitted levels of VOCs that can be discharged to the atmosphere. For example, the Gothenburg Protocol stated there must be a 40% reduction in VOC emissions by 2010 [2]. VOCs are chemically diverse, but some of the most common and difficult to control are short-chain alkanes. There are several potential abatement techniques, and the use of catalytic oxidation allows for careful control of emissions and provides a cost effective route for VOC control. Thermal incineration of VOCs is an alternative route, but it is unfavourable due to the involvement of higher temperatures and the potential formation of noxious by-products, such as NO_x [3] and dioxins [4]. In contrast, the catalytic oxidative destruction of VOCs results in the formation of carbon dioxide and water more selectively [5]. Although carbon dioxide is a greenhouse gas it is preferable to the presence of VOCs in the atmosphere.

Pd-supported catalysts have been reported as some of the best catalysts for methane oxidation [6]. γ-Al_2O_3 has been extensively used as a support for such catalysts and industrial VOC oxidation catalysts, and this is mainly due to low manufacturing cost. Despite the extensive use of Pd-supported γ-Al_2O_3 catalysts for the catalytic combustion of VOCs, various studies [2,6–11] have shown that other metal oxide supports, such as TiO_2, ZrO_2 and SnO_2, can be more appropriate supports than γ-Al_2O_3 in the oxidation of hydrocarbons. In particular, we have shown that TiO_2 can result in more active catalysts than those supported on alumina [2,11].

In general, it has been proposed that the oxidation state of palladium is related to the activity of the supported catalyst, and that partially oxidized palladium is effective for propane combustion [10]. Hence the choice of support is crucial for the effectiveness of a VOC oxidation catalyst. Another important parameter which determines the activity of a VOC oxidation catalyst is the presence of a second active component that acts as a modifier. Modifiers are generally added to promote activity and enhance resistance to deactivation. Thus, different promoters, such as vanadium [11], niobium [12], cobalt [13], cerium [14] and lanthanum [15], are known to promote the activity of metal-supported catalysts for VOC oxidation. These studies have mainly been focused on the modification of Pd–alumina catalysts, and

* Corresponding author. Tel.: +44 29 2087 4062.
E-mail address: taylorsh@cardiff.ac.uk (S.H. Taylor).

0926-860X/$ – see front matter © 2008 Elsevier B.V. All rights reserved.
doi:10.1016/j.apcata.2008.07.045

have proposed different theories to account for the promotional effect on the oxidation of alkanes and mono-aromatics. In brief, the positive role of the different promoters in the case of short-chain alkanes has generally been accounted for by different parameters, such as palladium particle size, catalyst reducibility and the Pd^0/Pd^{2+} surface ratio.

The catalytic activity of niobium-modified palladium–alumina catalysts has been previously reported in alkane combustion, showing a better performance than a Pd/Al_2O_3 catalyst [12]. These results were correlated with the presence of NbO_x species in intimate contact with palladium; and this led to partially oxidized palladium particles, which are a prerequisite for catalysts active for the combustion of propane [10].

In this work we have extended previous studies investigating high-activity titania-supported palladium catalysts modified by vanadium, by probing the effect of modifying the supported palladium catalyst with niobium. It is interesting to explore if metal oxides with low redox properties, such as Nb_2O_5, also exert a positive effect on the performance of TiO_2-supported palladium catalysts. These are the first data available on these catalysts and we have concentrated on probing the activity for the complete oxidation of propane, an excellent model for short-chain alkanes, which are amongst some of the most difficult VOCs to oxidize.

2. Experimental

2.1. Catalyst preparation

$Pd/Nb/TiO_2$ catalysts were prepared by a wet impregnation technique. A known amount of palladium(II) chloride (Aldrich, 99%) was dissolved in a minimum amount of hot de-ionised water ($\sim$10 ml g^{-1}). The solution was then heated to 80 °C, with continuous stirring, followed by the addition of an appropriate amount of ammonium niobium(V) oxalate. Titanium dioxide ($\sim$5 g, Degussa P_{25}. SA_{BET} = 50 $m^2 g^{-1}$) was added to the heated solution and stirred continuously at 80 °C to form a paste which was dried in an oven at 110 °C for 24 h. The resulting solid was ground in a pestle and mortar and calcined in static air at 550 °C for 6 h.

2.2. Catalyst characterisation

Catalyst surface areas were determined by multi-point N_2 adsorption at 77 K, the data being analysed in accordance with the BET method. Powder X-ray diffraction was used to identify the crystalline phases present in the catalysts. An Enraf Nonius FR590 sealed tube diffractometer, with a monochromatic Cu $K\alpha_1$ source operated at 40 kV and 30 mA was used. XRD patterns were calibrated against a silicon standard and phases were identified by matching experimental patterns to the JCPDS powder diffraction file.

A Renishaw system-1000 dispersive laser Raman microscope was used for recording of Raman spectra. The excitation source used was an Ar ion laser (514.5 nm) operated at a power of 20 mW. The laser was focused on powdered samples placed on a microscope slide to produce a spot size of *ca.* 3 μm in diameter. A backscattering geometry with an angle of 180° between illuminating and collected radiation was used for data collection.

Temperature-programmed reduction and pulsed CO chemisorption were performed using a micrometrics Autochem 2910 apparatus with a thermal conductivity detector. The reducing gas used was 10% H_2 in argon with a total flow rate of 50 ml min^{-1}. The temperature range explored was from −100 to 900 °C with a heating rate of 10 °C min^{-1}. Palladium dispersion for the Pd/TiO_2 catalysts was determined by pulsed CO chemisorption at 35 °C using an Ar flow of 20 ml min^{-1} and pulses of 0.36 ml of 10% CO in Ar. Prior to CO uptake determination, all samples were treated under flowing hydrogen (50 ml min^{-1}) at 500 °C and then flushed by Ar (20 ml min^{-1}) for 60 min. In order to calculate the metal dispersion, an adsorption stoichiometry of Pd/CO = 1 was assumed.

X-ray photoelectron spectra were recorded on a Kratos Axis Ultra DLD spectrometer employing a monochromatic Al Kα X-ray source (75–150 W) and analyser pass energies of 160 eV (for survey scans) or 40 eV (for detailed scans). Samples were mounted using double-sided adhesive tape and binding energies referenced to the C(1s) binding energy of adventitious carbon contamination which was taken to be 284.7 eV.

Diffuse reflectance spectroscopy (DRS) analyses were performed on a Perkin Elmer Lambda 25 spectrophotometer equipped with an integrating sphere. Spectra were taken on the catalysts in the range of 800–200 nm with the certified reflectance standard as reference.

2.3. Catalyst activity

Catalytic activity was measured using a fixed bed laboratory micro-reactor. For each experiment, 50 mg of powdered catalyst was placed in a 1/4 in. o.d. stainless steel reactor tube. The reactor feed contained 5000 vppm propane in air with a total flow rate of 50 ml min^{-1}. Catalysts were packed to a constant volume to give a gas hourly space velocity of 45,000 h^{-1}. The reactants and products were analysed by an online gas chromatograph with a thermal conductivity and flame ionisation detector. The reaction temperature was varied in the range 100–400 °C, the temperature being measured by a thermocouple placed in the catalyst bed. The differences between the inlet and outlet concentrations were used to calculate conversion data, and all carbon balances were found to be 100 ± 10%. Analyses were made at each temperature until steady-state activity was attained, and three consistent analyses were taken and data averaged. Blank experiments were conducted in an empty reactor, which showed negligible activity over the temperature range used in this study.

3. Results

3.1. Catalyst characterisation

A summary of the catalysts prepared is shown in Table 1. The surface area of the titania support was 50 $m^2 g^{-1}$ and this was slightly reduced by the addition of palladium and niobium as expected. This can be attributed to the filling of pores in the titania support as the metal species were added. The difference in porosity of these catalysts is the main factor determining their surface areas. It can also be observed in Table 1 that the niobium surface coverages range from 25 to 80% of the theoretical monolayer [16] as the total monolayer surface coverage correspond to 5–6 Nb atoms/nm^2. CO chemisorption was employed in order to estimate the number of active Pd sites over the Nb-promoted Pd/TiO_2 catalysts. An adsorption stoichiometry of Pd/CO = 1 was assumed. In this table is also observed that the metal dispersion on 0.5%Pd/TiO_2 remarkably diminishes when Nb is added; meanwhile a similar number of Pd sites was observed when the Nb loading was increased. The number of Pd sites also increased with the Pd loading. For catalysts without Pd there was negligible uptake of CO, demonstrating that CO adsorption was associated with the presence of Pd.

The powder XRD patterns of selected catalysts are shown in Fig. 1. The main crystalline phases of TiO_2 identified correspond to anatase and rutile, mainly anatase. The relative amounts of these crystalline phases were not modified by the addition of palladium

Table 1
Characteristics of the range of catalysts

Catalyst	Pd (wt.%)[a]	Nb_2O_5 (wt.%)[a]	Nb surface coverage (%)[b]	Surface area ($m^2\,g^{-1}$)	Number active Pd sites (mol_{Pd}/g_{cat})[c]	Average PdO particle size (nm)[d]
TiO_2	–	–	–	50	–	–
0.5%Pd/TiO_2	0.5	–	–	46	1.64×10^{-4}	n.d.
6.0%Nb/TiO_2	–	6.0	85	47	–	–
0.5%Pd/1.0%Nb/TiO_2	0.5	1.0	10	50	2.07×10^{-5}	n.d.
0.5%Pd/2.0%Nb/TiO_2	0.5	2.0	25	49	1.90×10^{-5}	13
0.5%Pd/3.0%Nb/TiO_2	0.5	3.0	40	47	2.44×10^{-5}	14
0.5%Pd/6.0%Nb/TiO_2	0.5	6.0	85	46	2.26×10^{-5}	13
1.0%Pd/3.0%Nb/TiO_2	1.0	3.0	40	47	3.84×10^{-5}	13
2.0%Pd/3.0%Nb/TiO_2	2.0	3.0	40	46	6.02×10^{-5}	14

n.d.: not detected.
[a] Nominal value.
[b] Total monolayer coverage: 5.8 Nb atoms/nm^2 [16].
[c] By CO chemisorption, Pd/CO = 1.
[d] By XRD.

and niobium. Moreover, no peaks corresponding to Nb crystalline phases have been identified. This could be attributed to the presence of low concentrations of these species or the high dispersion of crystallites that are too small to be detected. However, diffraction peaks corresponding to PdO (JCPDS 85-0624), with the most characteristic peak at 33.9°, have been observed in all the Pd-containing catalysts. The intensity of this peak was higher in NbPd-catalysts than in Nb-free Pd catalysts. In addition the intensity of this peak increases as the Pd or Nb loading increases.

The Scherrer equation was used to calculate the average crystallite sizes of the Pd–O nanocrystals in the Nb-promoted Pd/TiO_2 catalysts. These data are reported in Table 1. It is evident from the experimental data that the addition of niobium to the Pd/TiO_2 catalysts led to the formation of similar-sized palladium crystallites, independently of the Nb and/or the Pd loading. Thus, it can be suggested that the addition of niobium seems to stabilize an average palladium crystallite size in the promoted catalysts. Diffraction peaks corresponding to metallic Pd were not detected in any catalyst.

Figs. 2 and 3 show the Raman spectra recorded from 400 to 1050 cm^{-1} for the set of niobium/palladium catalysts. Peaks at *ca.* 650, 500 and 400 cm^{-1} are characteristic of titania in its anatase phase, whilst peaks observed at 447 cm^{-1} and the shoulder at *ca.*

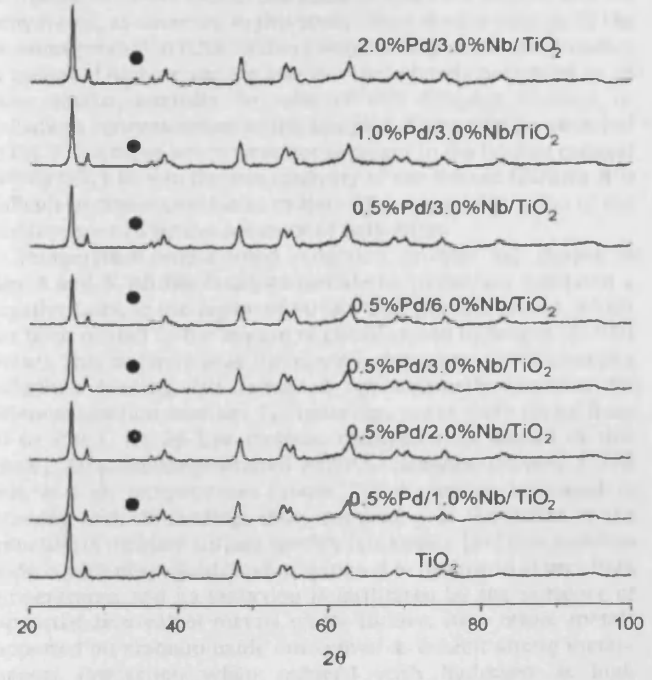

Fig. 1. XRD patterns for Pd/Nb_2O_5/TiO_2 catalysts. (●) PdO.

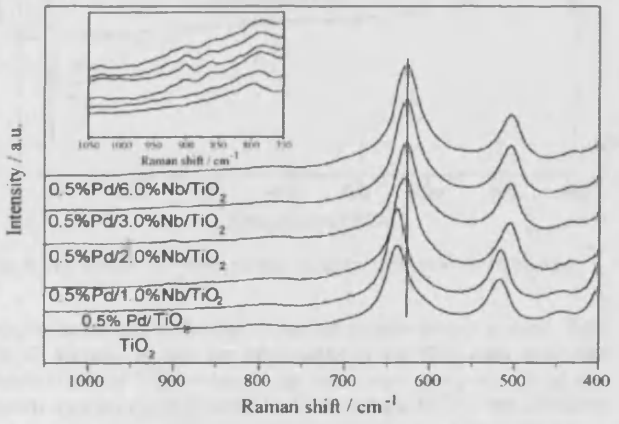

Fig. 2. Raman spectra for Pd/Nb_2O_5/TiO_2 catalysts with different Nb loadings.

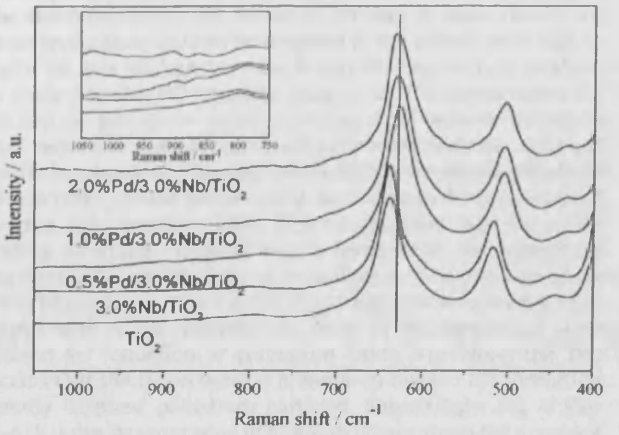

Fig. 3. Raman spectra for Pd/Nb_2O_5/TiO_2 catalysts with different Pd loadings.

605 cm^{-1} are ascribed to rutile [17]. In agreement with the XRD results, the addition of metal oxide on the titania support did not modify significantly the relative intensities of these bands, indicating that the structural composition of the support was not affected by the deposition of the supported phase. However, it is noteworthy that whilst the addition of either palladium or niobium alone does not lead to any displacement of the TiO_2 band when compared to the support alone, the co-addition of niobium and palladium to the titania shifts the anatase bands to lower frequencies by *ca.* 10 cm^{-1}. This observation indicates that weaker Ti–O bonds are present in NbPd-catalysts. It has previously been noted by Kovalenko et al. [18] that the addition of niobium to Pd/TiO_2 catalysts led to the generation of defects on the support surface. Thus, the shift of the Raman bands is probably due to the shift of charge density from the support to either supported niobium or palladium species.

Also in agreement with XRD results, Raman spectra of Pd/Nb/TiO_2 catalysts (Fig. 2) show no evidence for the presence of Nb_2O_5 crystallites, which would be indicated by a band at *ca.* 675 cm^{-1} [19] for hexagonal Nb_2O_5, or a band at *ca.* 260 cm^{-1} for monoclinic Nb_2O_5 [16,19]. In addition, the detection of niobic acid ($Nb_2O_5 \cdot nH_2O$) with a wide band at *ca.* 650 cm^{-1} [19,20] is hindered by masking due to the presence of a large band at 636 cm^{-1} due to the anatase phase.

Although no bulk niobium containing phases were identified from the Raman study some low intensity features were present that could indicate the presence of highly dispersed niobium-containing species. The positive identification of these species was difficult due to the exceptionally low intensity of the features. Analysis of the Raman spectra of Nb-containing catalysts in the 750–1050 cm^{-1} region showed the presence of peaks at *ca.* 865, 900 and 920 cm^{-1}. It has been reported [20] that the Raman bands between 980 and 1030 cm^{-1} are associated with the terminal Nb=O vibration of the isolated surface metal oxide species, whilst Raman bands characteristic of the bridging Nb–O–Nb bonds associated with polymerized surface species appear in the range 860–940 cm^{-1}. It has also been reported [20] that the band attributed to Nb=O species disappeared when the sample was not dehydrated, as observed in this study. Thus, Raman spectra of the niobium-promoted 0.5%Pd/TiO_2 catalysts only show the presence of hydrated niobate surface species. These bands presented in all cases similar intensity, in spite of the different niobium or palladium concentrations of the samples. It can also be observed in Fig. 3 that these bands were not apparent in the Pd-free catalyst (3%Nb/TiO_2). Due to the low intensity of the Raman features it is difficult to obtain conclusive evidence for any modification of the niobium species by the presence of palladium.

Temperature-programmed reduction profiles are shown in Figs. 4 and 5. All the catalysts containing palladium exhibited a negative peak, in the region of 50–80 °C in the TPR profile, which has been related to the release of chemisorbed hydrogen (β-PdH phase). This negative peak increased in intensity with increasing palladium loading, but remained approximately constant for different niobium loadings. No reduction peaks were found from 50 to 950 °C for Pd-free niobium catalysts (not shown in this figure). All niobium-promoted Pd/TiO_2 catalysts showed a TPR peak at high temperatures (about 750 °C), which increased in intensity with Nb loading; thus, this peak was attributed to the reduction of niobium surface species. It is known [21] that niobium oxide is partially reducible when exposed to hydrogen at very high temperatures, and its reduction is facilitated by the presence of supported zero-valent metals on its surface. As a result, metals supported on niobium oxide are known to exhibit strong metal–support interaction when reduced with hydrogen at high temperatures. In the absence of zero-valent metals, the reduction

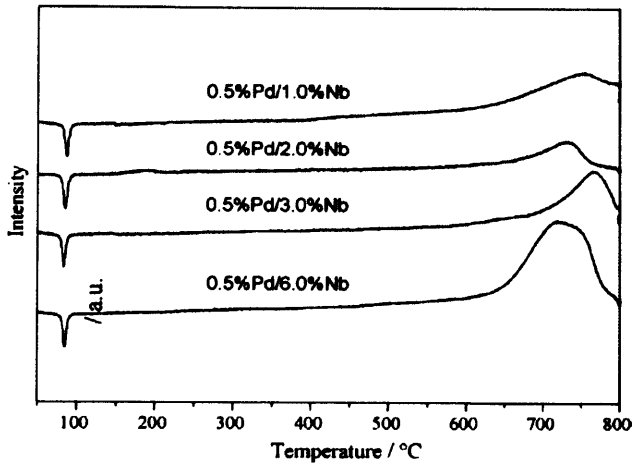

Fig. 4. TPR profiles for Pd/Nb_2O_5/TiO_2 catalysts with different Nb loadings.

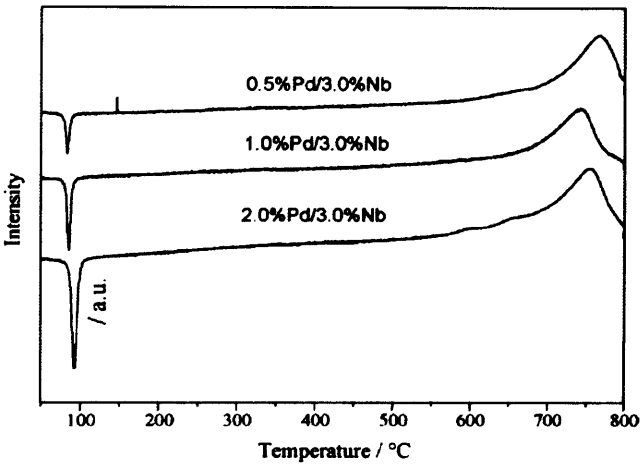

Fig. 5. TPR profiles for Pd/Nb_2O_5/TiO_2 catalysts with different Pd loadings.

of Nb_2O_5 is partial and only occurs at temperatures greater than 1000 °C. Hence, it can be concluded from TPR data that the incorporation of Pd decreases the reduction temperature of the niobium species considerably, but the reducibility of the niobium species was not significantly affected by altering either the Nb or the Pd concentrations.

In addition, subambient TPR profiles were also determined to probe the reducibility and nature of Pd sites in more detail. The various peaks observed can be assigned to the reduction of PdO_x to metallic Pd. It is evident from Fig. 6 that Nb-free Pd/TiO_2 catalysts only show a hydrogen reduction peak at *ca.* 0 °C attributed to the reduction of palladium oxide particles. This peak is shifted to higher reduction temperatures after niobium addition, which is most likely related to a stronger interaction between the palladium oxide particles and the support [22]. According to the magnitude of hydrogen consumption (Table 2) it is apparent that the corresponding hydrogen consumption is lower than the theoretical value necessary to reduce all the palladium oxide in the case of the 0.5%Pd/TiO_2 catalyst. However, the hydrogen consumption for the catalysts with added niobium was close to the theoretical value predicted for reduction of palladium oxide. Therefore, the TPR indicates that the incorporation of niobium favours the formation of totally oxidized palladium particles. Surprisingly, Fig. 6 also shows that the incorporation of niobium brings about the presence of an additional hydrogen reduction peak at *ca.* −50 °C. These

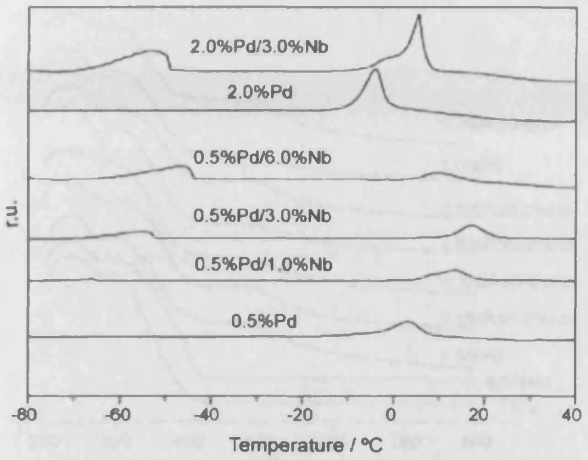

Fig. 6. Subambient TPR profiles for different $Pd/Nb_2O_5/TiO_2$ catalysts.

Table 2
Hydrogen consumption during the subambient temperature-programmed reduction experiments ($\mu molH_2/g$)

Catalyst	First peak		Second peak	
	T_{max} (°C)	H_2 consumption ($\mu molH_2/g$)	T (°C)	H_2 consumption ($\mu molH_2/g$)
$0.5\%Pd/TiO_2$	n.d.	n.d.	3.1	40
$2\%Pd/TiO_2$	n.d.	n.d.	−4.2	143
$0.5\%Pd/1.0\%Nb/TiO_2$	−66	8.2	13	51
$0.5\%Pd/3.0\%Nb/TiO_2$	−55	40	17	51
$0.5\%Pd/6.0\%Nb/TiO_2$	−47	107	10	49
$2.0\%Pd/3.0\%Nb/TiO_2$	−53	86	5.6	180

Note: Theoretical values in the case of complete reduction of Pd^{2+} to Pd^0 for catalysts containing 0.5 and 2.0 wt.% Pd are 48 and 194 $\mu molH_2/g$, respectively.

peaks cannot be assigned to the reduction of the palladium species, according to the hydrogen consumption values shown in Table 2. The hydrogen consumption peak at *ca.* 0 °C matches closely the theoretical values necessary to reduce all the palladium(II) oxide. In addition, the presence of significant quantities of palladium(IV) can be ruled out since these species have not been identified in the X-ray photoelectron spectra (Fig. 7). Thus, the −50 °C hydrogen consumption peak can tentatively be assigned to the reduction of oxygen species with very high mobility.

Several of the catalysts were analysed using XPS and the results are shown in Figs. 7 and 8. The Pd(3d) spectra (Fig. 7) show that for

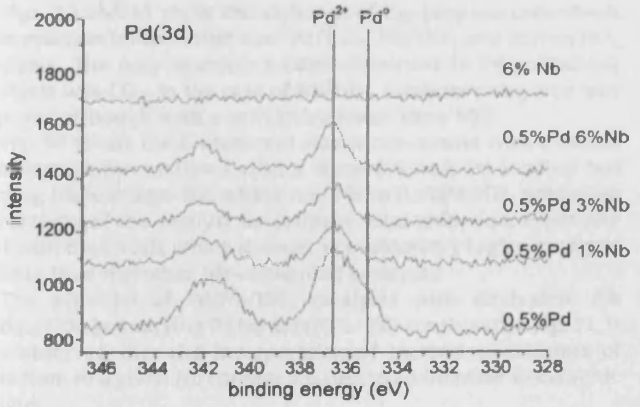

Fig. 7. Pd(3d) X-ray photoelectron spectra for a series of $Pd-Nb/TiO_2$ catalysts, with loadings (wt.%) as shown.

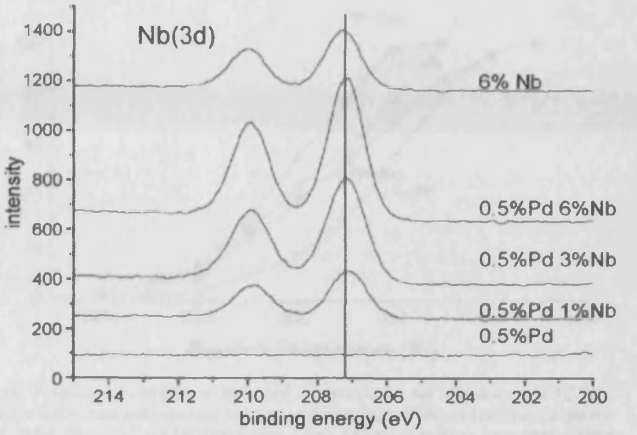

Fig. 8. Nb(3d) X-ray photoelectron spectra for a series of $Pd-Nb/TiO_2$ catalysts, with loadings (wt.%) as shown.

the pure $0.5\%Pd/TiO_2$ sample the Pd exists as both metallic species and PdO particles, the intensity ratio indicating a composition of 40% Pd^0 and 60% Pd^{2+}. The spectra from Nb-promoted Pd/TiO_2 catalysts show the complete absence of Pd^0, the palladium being present purely as PdO. In the Nb(3d) spectra (Fig. 8) the Nb($3d_{5/2}$) binding energy is constant for all samples, including the pure Nb/TiO_2 catalyst. The apparent large decrease in Nb(3d) intensity for the $6\%Nb/TiO_2$ sample compared with the $0.5\%Pd/6\%Nb/TiO_2$ catalyst is confirmed in Table 3, where surface elemental molar ratios derived from the XP spectra are presented. The Nb/Ti ratio for the pure Nb/TiO_2 catalyst is approximately 50% that for $0.5\%Pd/6\%Nb/TiO_2$, which is consistent with a significantly larger Nb_2O_5 crystallite size for pure Nb/TiO_2; in other words, the co-doped Pd induces a significantly increased dispersion in the niobium species. It can also be observed in Table 3 that the Pd/Ti ratio for the Pd/TiO_2 catalyst was higher than for the $Pd/Nb/TiO_2$ catalysts, and this was independent of the niobium loading. This result agrees with the XRD data and CO uptake values, indicating that the co-impregnation of Pd and Nb over the TiO_2 support resulted in lower dispersion of palladium particles. Moreover, the Pd/Ti ratio was approximately constant regardless of the niobium loading (Table 3). Finally, there was no evidence for any chlorine species on the catalyst surface from the XPS studies.

Fig. 9 displays the diffuse reflectance spectra obtained for the Nb-promoted and unpromoted Pd/TiO_2 catalysts at different Nb and Pd loadings. DRS spectra of the $3\%Nb/TiO_2$ catalyst and TiO_2 support are also shown for comparative purposes. These spectra are dominated by the strong adsorption edge characteristic of semiconductors like TiO_2. The presence of these absorption bands did not allow clear identification of possible palladium or niobium bands located in this region. However, Fig. 9 also shows the presence of a broad band at *ca.* 470 nm, which is attributed to the d–d transition band of palladium. These bands can be assigned to PdO according to Noronha et al. [12]. Unfortunately, we could not

Table 3
XPS-derived elemental molar ratios for a series of $Pd-Nb/TiO_2$ catalysts

Sample	Molar ratios (XPS)			
	O/Ti	Pd/Ti	Nb/Ti	Nb/Pd
$0.5\%Pd/TiO_2$	2.33	0.011	0.000	0.0
$0.5\%Pd/1.0\%Nb/TiO_2$	2.60	0.006	0.038	6.8
$0.5\%Pd/3.0\%Nb/TiO_2$	2.60	0.005	0.103	20.9
$0.5\%Pd/6.0\%Nb/TiO_2$	2.61	0.007	0.122	18.3
$6.0\%Nb/TiO_2$	2.54	0.000	0.058	n/a

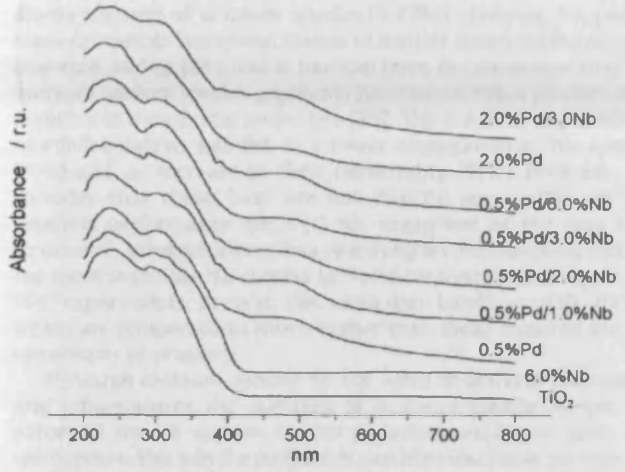

Fig. 9. DRS-UV spectra for $Pd/Nb/TiO_2$ catalysts.

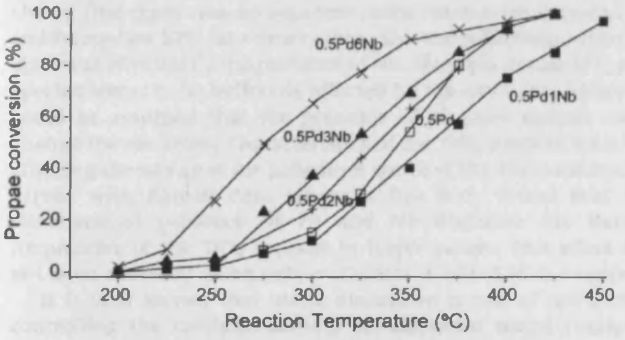

Fig. 10. Propane conversion at different temperatures for Nb-promoted Pd/TiO_2 catalysts with constant palladium loading and varying niobium loading. Catalysts: (□) 0.5%Pd/TiO_2; (■) 0.5%Pd/1%Nb/TiO_2; (+) 0.5%Pd/2%Nb/TiO_2; (▲) 0.5%Pd/3%Nb/TiO_2; (×) 0.5%Pd/6%Nb/TiO_2.

detect any major change in the wavenumber of this band after niobium addition. Finally, the d–d transition bands (500 and 530 nm) cited in the literature were not observed, suggesting that no electronic interaction between Nb and Pd species was taking place [23].

3.2. Catalyst activity

Figs. 10 and 11 show the variation of the propane conversion with reaction temperature over Pd/TiO_2, Nb/TiO_2 and $Pd/Nb/TiO_2$ catalysts. The only reaction product observed in Pd-containing catalysts was CO_2. In the case of Nb/TiO_2 catalysts propylene was detected although with a selectivity lower than 10%.

Fig. 10 shows the evolution of alkane conversion with reaction temperature for catalysts with a fixed 0.5 wt.% Pd loading but varying Nb loadings. The addition of Nb to 0.5%Pd/TiO_2 promoted the activity of the catalyst for propane total oxidation, especially that with 6 wt.% Nb, which showed a considerably higher catalytic activity than the other Nb-containing catalysts.

The activities of $Pd/Nb/TiO_2$ catalysts with equivalent Nb loading (3%) but varying Pd loading (0.5–2%) are shown in Fig. 11. It was observed that the incorporation of increasing amounts of palladium to a given Nb content also led to an increase in catalytic activity.

Stability tests over the most representative catalyst, 0.5%Pd/6.0%Nb/TiO_2, were carried out. This catalyst has been tested in the oxidation of propane for 2 days at 325 °C maintaining the same conversion during this period. After this, a new cycle, as that shown in Fig. 10, was carried out and no significant differences could be identified, as measurement of the second light-off curve after time-on-line was superimposeable on the curve obtained for the fresh catalyst.

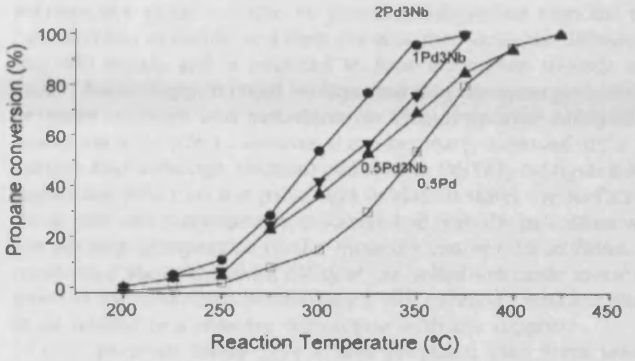

Fig. 11. Propane conversion at different temperatures for Nb-promoted Pd/TiO_2 catalysts with constant niobium loading and varying palladium loading. Catalysts: (□) 0.5%Pd/TiO_2; (▲) 0.5%Pd/3%Nb/TiO_2; (▼) 1%Pd/3%Nb/TiO_2; (●) 2%Pd/3%Nb/TiO_2.

4. Discussion

Palladium-based catalysts are the catalysts of choice for hydrocarbon total oxidation and have been extensively studied for several decades. Although alumina is the support most commonly employed in Pd-modified catalysts, titania is superior since it gives higher catalytic activity for the oxidation of alkanes [2]. In the present study it has been demonstrated that the activity of a Pd/TiO_2 catalyst for propane oxidation was promoted by the addition of Nb during the impregnation step of catalyst preparation, and there was a general increase of activity with increase in modifier loading. A summary of all the catalytic results obtained in the present study is presented in Table 4, where T_{10}, T_{50} and T_{90} (reaction temperatures for alkane conversions of 10, 50 and 90%, respectively) are shown. The most active catalyst was the one with the highest Nb loading (0.5%Pd/6.0%Nb/TiO_2) with a remarkably higher activity than both the Nb-free 0.5%Pd/TiO_2 catalyst and especially the Pd-free Nb catalyst. These observations are important since the Nb-salts available commercially are *ca.* 50 times cheaper than Pd-salts. Therefore, the addition of Nb to a Pd catalyst does not appreciably increase the cost of the catalyst but does increase the hydrocarbon total oxidation activity.

In this work, we have observed that the incorporation of niobium to Pd/TiO_2 catalysts increases the catalytic activity for propane catalytic combustion, requiring lower temperatures to achieve the same conversion. Thus, it would be interesting to

Table 4
Summary of catalyst activity comparing activities at different temperatures and the rate of propane conversion per active Pd site at 250 °C ($mol_{C3}/(mol_{Pd}\ h)$)

Catalyst	T_{10} (°C)	T_{50} (°C)	T_{90} (°C)	r_{C3} ($mol_{C3}/(mol_{Pd}\ h)$)
0.5%Pd/TiO_2	280	345	390	1.7×10^3
0.5%Pd/1.0%Nb/TiO_2	280	365	430	1.4×10^4
0.5%Pd/3.0%Nb/TiO_2	250	320	390	2.0×10^4
0.5%Pd/6.0%Nb/TiO_2	225	280	370	1.5×10^5
1.0%Pd/3.0%Nb/TiO_2	260	310	385	1.9×10^4
2.0%Pd/3.0%Nb/TiO_2	250	290	340	2.0×10^4
6.0%Nb/TiO_2	>500			–

clarify the role of niobium species in PdNb-catalysts. Supported niobium species have been shown to exhibit significant Lewis and Brønsted acidity [24], and it has also been demonstrated that the niobium surface species on titania have some redox properties in addition to their acidic properties [25]. The presence of palladium in PdNb-catalysts has led to a lower aggregation of Nb species (XPS) and an increase in their reducibility (TPR). However, we consider that these facts are not directly responsible for the catalytic performance since (i) Nb, regardless of the way it is structured, presents a very low reactivity for this reaction and (ii) the most reducible Nb species in NbPd-catalysts according to the TPR experiments present the reduction bands at 650–700 °C, which are temperatures much higher than those required for full conversion of propane.

Although niobium species do not seem to activate propane at low temperatures the addition of niobium clearly affects the nature of the Pd species, *i.e.* the palladium oxidation state, the redox properties and the palladium particle size. These parameters [10,11] have been demonstrated to be very important in controlling the catalytic activity of palladium catalysts in VOC combustion reactions. In this way, although DRS spectra have shown that there was no apparent redox interaction between Nb and Pd species, XPS data clearly show that the palladium oxidation state was affected by the presence of Nb. Thus, the nature of the Pd species seems to be indirectly affected by the niobium addition. It could be assumed that the presence of niobium species could change the electronic characteristics of the TiO_2 support, which is affecting the nature of the palladium species [18]. This assumption agrees with Raman data where it has been found that the simultaneous presence of Pd and Nb displaces the Raman frequencies of the TiO_2 support to lower values. This effect has not been observed when only palladium is added to the support.

It is well known that metal dispersion is one of the factors controlling the catalytic activity of supported metal catalysts. Hicks et al. [26] showed that highly dispersed palladium oxide could be much less active than crystalline palladium oxide supported on alumina, due to the strong interaction with the support for small crystallites. In the present study, it is observed that the number of active Pd sites and also the average Pd crystallite sizes are almost constant for the Nb-promoted Pd/TiO_2 catalysts, independently of the niobium and palladium loading. It is also apparent that although the number of active palladium sites is remarkably lower for Nb-promoted 0.5%Pd/TiO_2 catalysts, the interaction of the palladium particles with the TiO_2 support is stronger, as the hydrogen consumption peak in the subambient TPR profile is shifted to higher temperatures. Thus, the variation of the catalytic activity after Nb promotion could not be interpreted by the variation in the dispersion. In addition, it can be observed that the activity per active site of 0.5%Pd/6.0%Nb/TiO_2 was much higher, about 10 times higher at 250 °C, than 0.5%Pd/3.0%Nb/TiO_2, although they had a similar number of active Pd sites. Thus, other factors seem to be responsible for the synergetic effect observed in Nb-promoted Pd/TiO_2 catalysts.

Yazawa et al. [10] suggested for propane combustion that the oxidation state of palladium affects the catalytic activity to a greater extent than the dispersion. Thus, they observed that partially oxidized palladium showed the highest catalytic activity for propane combustion. Similar behaviour was observed for the $Pd/Nb_2O_5/Al_2O_3$ catalytic system [12], where the addition of niobium to alumina-supported Pd catalysts prevented the total oxidation of palladium, increasing the propane combustion activity. These authors proposed that the presence of NbO_x species in close contact with the palladium particles modifies the oxidation state of Pd, favouring the ideal Pd^0/Pd^{2+} ratio. In this model, the co-existence of Pd and PdO on the Pd surface is a prerequisite since metallic Pd provides adsorption sites for the hydrocarbon molecule, and then, the adsorbed molecule diffuses to the PdO region and is oxidized to generate carbon dioxide and water. Accordingly, it could be expected that the synergistic effect between niobium and palladium on TiO_2-supported catalysts is due to a similar effect. However, it can be clearly observed in the XP spectra that although niobium addition to Pd/TiO_2 catalysts has a significant effect on the palladium oxidation state, the surface of these particles is completely oxidized, and metallic palladium was not present irrespective of the niobium content. In addition, as mentioned above the reducibility of the palladium oxide species is lower in the case of Nb-promoted Pd/TiO_2 catalysts, which is likely to be related to a stronger interaction with the support.

In a previous study [27] it was proposed that there was a relationship between the acidity of metal-supported catalysts and the activity for propane combustion. To check for such a relationship in this work TPD-NH_3 experiments over representative catalysts (0.5Pd, 0.5Pd1Nb and 0.5Pd6Nb) were carried out. According to these results the NH_3 consumption was similar for the three catalysts; meanwhile the temperature of the maximum for the TPD-NH_3 signal (243, 242 and 252 °C for 0.5Pd, 0.5Pd1Nb and 0.5Pd6Nb catalysts, respectively) increased only slightly with the addition of Nb, indicating a marginally higher strength of the acid sites in the sample with the highest Nb loading. Although the effect of acidity of the support on the catalytic performance cannot be ruled out we do not think this small change in the acidity is the main factor responsible for the different catalytic behaviour observed.

It is worth noting that the niobium synergistic effect on Nb-promoted Pd/TiO_2 catalysts is more evident at higher niobium and palladium loadings. From subambient TPR data, it can be inferred that the positive niobium effect seems to be related to the magnitude of hydrogen consumption for the *ca.* −50 °C reduction peak. Firstly, this peak has not been detected in the case of Nb-free Pd/TiO_2 catalysts and, secondly, whilst the 0.5%Pd/1.0%Nb/TiO_2 catalyst only shows a marginal hydrogen consumption peak, 0.5%Pd/6.0%Nb/TiO_2 presents the greatest hydrogen consumption. These facts correlate well with their corresponding activities for propane total oxidation. Unfortunately, it has not been possible to unequivocally characterise the nature of these new and very easily reducible sites, although their formation seems to be related to the presence of palladium in close contact to niobium species on the TiO_2 support, favouring oxygen mobility. This fact could not only bring about the formation of palladium particles in a totally oxidized state, but also the presence of very active oxygen species.

The effect of niobium on the catalytic performance of Pd/TiO_2 catalysts has been evaluated for the first time in this paper. Surprisingly, even though niobium addition leads to completely oxidized palladium particles and with a stronger interaction with the support, the catalysts demonstrate improved performance. The positive effect has been accounted for by the presence of new and very reducible species detected in the subambient TPR profiles at *ca.* −50 °C. To the best of our knowledge, this is the first time that the presence of these species has been reported. Further studies are in progress on the nature of these very active species on niobium-promoted Pd/TiO_2 catalysts.

5. Conclusions

The activity of a palladium/titania catalyst for propane oxidation has been promoted by the addition of varying loadings of niobium during the impregnation step of catalyst preparation. The catalytic activity was found to increase as the niobium and/or palladium loading increased, and the addition of Nb significantly changed the nature of the palladium. In addition, it has been

observed that the niobium promotion increased the oxygen mobility. This fact could not only promote the presence of palladium species in a totally oxidized state, but also produced new and very easily reducible species. 0.5%Pd/6%Nb_2O_5/TiO_2 was the best catalyst amongst the range of catalysts investigated and CO_2 was the only product identified during the catalytic oxidation of propane.

Acknowledgements

Benjamin Solsona thanks DGICYT through Project CTQ2006-09358/BQU for financial support. Marie Taylor and Edwin Ntainjua would like to thank the School of Chemistry, Cardiff University for funding.

References

[1] J.G. Watson, J.C. Chow, E.M. Fujita, Atmos. Environ. 35 (2001) 1567–1584.
[2] T. Garcia, B. Solsona, S.H. Taylor, Catal. Lett. 97 (2004) 99–103.
[3] D. Giannopoulos, D.I. Kolaitis, A. Togkalidou, G. Skevis, M.A. Founti, Fuel 86 (2007) 1144–1152.
[4] T. Streibel, H. Nordsieck, K. Neuer-Etscheidt, J. Schnelle-Kreis, R. Zimmermann, Chemosphere 67 (2007) S155–S163.
[5] A. Janbey, W. Clark, E. Noordally, S. Grimes, S. Tahir, Chemosphere 52 (2003) 1041–1046.
[6] P. Gélin, M. Primet, Appl. Catal. B: Environ. 39 (2002) 1–37.
[7] R. Spinicci, A. Tofanari, Appl. Catal. A 227 (2002) 159–169.
[8] D. Ciuparu, L. Pfefferle, Catal. Today 77 (2002) 167–179.
[9] K. Sekizawa, H. Widjaja, S. Maeda, Y. Ozawa, K. Eguchi, Catal. Today 59 (2000) 69–74.
[10] Y. Yazawa, H. Yoshida, N. Takagi, S. Komai, A. Satsuma, T. Hattori, J. Catal. 187 (1999) 15–23.
[11] T. Garcia, B. Solsona, D.M. Murphy, K.L. Antcliff, S.H. Taylor, J. Catal. 229 (2005) 1–11.
[12] F.B. Noronha, D.A.G. Aranda, A.P. Ordine, M. Schmal, Catal. Today 57 (2000) 275–282.
[13] A. Törncrona, M. Skoglundh, P. Thormählen, E. Fridell, E. Jobson, Appl. Catal. B: Environ. 14 (1997) 131–145.
[14] S. Colussi, A. Trovarelli, G. Groppi, J. Llorca, Catal. Commun. 8 (2007) 1263–1266.
[15] G. Pecchi, P. Reyes, T. López, R. Gómez, J. Non-Cryst. Solids 345–346 (2004) 624–627.
[16] J.-M. Jehng, I.E. Wachs, Chem. Mater. 3 (1991) 100–107.
[17] A. Kubacka, M. Fernandez-Garcia, G. Colon, J. Catal. 254 (2008) 272–284.
[18] N.A. Kovalenko, T.S. Petkevich, Yu.G. Egiazarov, Russ. J. Appl. Chem. 72 (1999) 452–456.
[19] R. Brayner, F. Bozon-Verduraz, Phys. Chem. Chem. Phys. 5 (2003) 1457–1466.
[20] T. Onfroy, O.V. Manoilova, S.B. Bukallah, D.M. Hercules, G. Clet, M. Houalla, Appl. Catal. A: Gen. 316 (2007) 184–190.
[21] J.G. Weissman, Catal. Today 28 (1996) 159–166.
[22] W.J. Shen, M. Okumura, Y. Matsumura, M. Haruta, Appl. Catal. A 213 (2001) 225–232.
[23] A.L. Guimarães, L.C. Dieguez, M. Schmal, Ann. Brazil. Acad. Sci. 76 (2004) 825–832.
[24] I.E. Wachs, Y. Chen, J.-M. Jehng, L.E. Briand, T. Tanaka, Catal. Today 78 (2003) 13–24.
[25] P. Viparelli, P. Ciambelli, L. Lisi, G. Ruoppolo, G. Russo, J.C. Volta, Appl. Catal. A: Gen. 184 (1999) 291–301.
[26] R.F. Hicks, H. Qi, M.L. Young, R.G. Lee, J. Catal. 122 (1990) 295–306.
[27] Y. Yazawa, N. Kagi, S.I. Komai, A. Satsuma, Y. Murakami, T. Hattori, Catal. Lett. 72 (2001) 157–160.

Publication 2

Top Catal (2009) 52:1660–1668
DOI 10.1007/s11244-009-9307-0

ORIGINAL PAPER

The Oxidative Dehydrogenation of Propane Using Vanadium Oxide Supported on Nanocrystalline Ceria

Marie N. Taylor · Albert F. Carley · Thomas E. Davies · Stuart H. Taylor

Published online: 27 May 2009

Abstract Nanocrystalline ceria was prepared as a support for vanadium oxide catalysts and tested for the oxidative dehydrogenation of propane. Nanocrystalline ceria is very active for the total oxidation of propane under conditions used for oxidative dehydrogenation. The addition of vanadium results in a switch of activity to produce propene with appreciable selectivity. The catalyst performance depends on the vanadium loading. Lower vanadium loadings resulted in catalysts with highly dispersed vanadia species, which were selective towards propene production. Higher vanadium loadings resulted in the formation of a mixed cerium–vanadium phase, which was also active for propane selective oxidation. A catalyst with an intermediate loading was far less selective. Catalysts were characterised by a range of techniques (including XRD, laser Raman, TPR, SEM/EDX and XPS), and the activity of the catalysts can be related to their structure and chemistry.

Keywords Ceria vanadium oxide · Propane · Propene · Selective oxidation · Oxidative dehydrogenation

1 Introduction

At present the demand for olefins is increasing, and it is expected to continue increasing for some time. In particular, the requirements for ethane and propene are growing. For example, propene is increasingly required to manufacture acrolein, acrylic acid acrylonitrile and iso-propanol, as well as for use as a monomer for polymer production. Presently, the traditional methods to produce alkenes include steam cracking, fluidised catalytic cracking (FCC) and direct alkane dehydrogenation [1]. For steam cracking ethane is the preferred product over propene, whilst the demand for propene is growing faster than the demand for ethane. Similarly, FCC produces ethane preferentially, and so the product distributions from both processes may not be ideal to meet the demand. Direct catalytic dehydrogenation also suffers from the fact that thermodynamically yields of olefins are severly limited. Furthermore, the catalysts suffer from extensive deposition of carbonaceous material and therefore undergo extensive deactivation. Against this background there has been considerable interest to investigate other possible routes for olefin production.

The oxidative dehydrogenation (ODH) of alkanes is a promising emerging technology, which has the potential to produce a range of light olefins. Alkanes are attractive chemical feedstocks as they are relatively cheap and abundant. The use of an oxidative process results in an exothermic reaction, and therefore does not impose thermodynamic limits on the product yields, which are inherent in endothermic dehydrogenation reactions. However, using an oxidative reaction, deep oxidation is favoured thermodynamically, over selective oxidation, to form significant amounts of CO_x by-products. Therefore, identification of catalysts with high selectivity to the desired olefin at high conversion is the ultimate aim. If efficient catalysts can be developed alkane ODH could provide a more cost effective route for olefin production over the existing technology. However, considerably better catalysts are required to persuade operators to replace existing processes, which are operating with much depreciated capital costs under optimised conditions.

Propane ODH has been widely studied for many years and many different catalysts demonstrate activity and

M. N. Taylor · A. F. Carley · T. E. Davies · S. H. Taylor (✉)
Cardiff Catalysis Institute, School of Chemistry, Cardiff University, Main Building, Park Place, Cardiff CF10 3AT, UK
e-mail: taylorsh@Cardiff.ac.uk

selectivity [2]. Catalysts include supported chromium oxide [3], molybdenum containing catalysts [4–7] and more recently, complex multi-component metal oxide catalysts containing both molybdenum and vanadium. These multi-component catalysts, such as V–Mo–Te–Nb mixed oxides [8], are complex, and the formation of the active phase is critical to maximise performance. The most extensively studied catalysts are those based on supported vanadium oxide [2], and. the acidic/basic properties of the supported catalysts are found to be a strong determining factor in the catalytic performance. Additionally the vanadia loading and its interaction with the support are also important controlling factors. A range of different supports have been investigated, and these have used supports with basic, acidic and amphoteric properties. Supports employed commonly include Al_2O_3 [9–11] TiO_2 [12], SiO_2 [13, 14], ZrO_2 [15, 16] and MgO [10, 11]. In particular vanadia supported on MgO has demonstrated promising activity and selectivity to propene although there still seems to be general disagreements in the literature about the active site and the V–Mg–O phase responsible for the higher selectivity. [17–19]. V_2O_5/TiO_2 catalysts have also proved to be successful, demonstrating relatively high activity and a low temperature of activation, which has led to further studies focusing on the addition of various promoters [20, 21].

To date, there has been very little work focussing on the use of ceria as a support for propane ODH catalysts. This is somewhat surprising since ceria has many similarities with Titania, which has been widely and successfully employed. Ceria has been used in the control of automotive pollution for many years [22], mainly due to the ability to store and release oxygen. Recently, nanocrystalline ceria, produced by precipitation with urea, has been identified as a highly active hydrocarbon oxidation catalyst [23–25]. As a consequence of the high activity we have investigated the nanocrystalline ceria as a support for propane selective oxidation catalysts. Vanadium was selected as the supported component, as it has demonstrated selective propane oxidation activity [2]. Vanadia catalysts supported on ceria have previously been used for the ODH of ethane [26] and propane [27] and demonstrate selective production of alkenes, however, there are no previous data using a high surface area nanocrystalline ceria support.

2 Experimental

2.1 Catalyst Preparation

Ceric ammonium nitrate (Aldrich, 99.99%) was dissolved in de-ionised water and mixed with urea (Aldrich, 98%) in a 1:3 molar ratio. The solution was stirred whilst heating to 100 °C until a white gel formed. The gel was aged for 24 h at 100 °C and the final precipitate collected by filtration. The solid was dried at 120 °C for 12 h and calcined in static air at 400 °C for 10 h. This material was denoted as the ceria support.

Appropriate amounts of ammonium metavanadate (Aldrich, 99.99%) were dissolved in the minimum amount of hot water with oxalic acid (Aldrich, 98%, 1.58 g). When completely dissolved the appropriate amount of the ceria support was added to the solution and continuously stirred for 1 h. The resulting mixture was dried at 80 °C for 24 h and calcined in static air at 550 °C for 6 h. A range of catalysts containing nominal vanadium loadings from 0.5 to 30% were prepared.

2.2 Catalyst Characterisation

Catalyst surface areas were determined by multi-point N_2 adsorption at 77 K, the data being analysed in accordance with the BET method. Powder X-ray diffraction was used to identify the crystalline phases present in the catalysts. An Enraf Nonius FR590 sealed tube diffractometer, with a monochromatic $CuK_{\alpha 1}$ source operated at 40 kV and 30 mA was used. XRD patterns were calibrated against a silicon standard and phases were identified by matching experimental patterns to the JCPDS powder diffraction file.

Raman spectra were recorded using a Renishaw system 1000 dispersive laser Raman microscope. The excitation source used was an Ar ion laser (514.5 nm) operated at a power of 20 mW. The laser was focused on powdered samples placed on a microscope slide to produce a spot size of ca. 3 μm in diameter. A backscattering geometry with an angle of 180° between illuminating and collected radiation was used for data collection.

Temperature programmed reduction was performed using a Thermo 1100 TPD/R/O apparatus with a thermal conductivity detector. The reducing gas used was 10% H_2 in argon with a total flow rate of 50 mL min^{-1}. The temperature range explored was from 30 to 800 °C with a heating rate of 10 °C min^{-1}.

Scanning electron microscopy (SEM) and energy dispersive X-ray (EDX) analyses were performed on a carl zeiss EVO-40 fitted with backscatter detector and Oxford instrument SiLi detector. Samples were mounted on aluminium stubs using adhesive carbon discs and they were analysed uncoated. Vanadium content of the catalysts was determined using EDX, and selected data were confirmed using atomic absorption spectroscopy (AAS).

XPS measurements were made on a Kratos Axis Ultra DLD spectrometer using monochromatised AlKα radiation, and analyser pass energies of 160 eV (survey scans) or 40 eV (detailed scans). Binding energies are referenced to the C(1 s) peak from adventitious carbonaceous contamination, assumed to have a binding energy of 284.7 eV.

2.3 Catalyst Activity

Catalytic performance was measured using a fixed bed laboratory micro-reactor at atmospheric pressure. For each experiment, 0.25 g of powdered catalyst was placed in a $^1/_4$ inch o.d. quartz reactor tube. The propane/oxygen/helium ratio was 2/1/8.5, with a total flow rate of 40 mL min^{-1}. Catalysts were packed to a constant volume to give a constant gas hourly space velocity of 9600 h^{-1}. The reactants and products were analysed by a Varian 3800 online gas chromatograph using Porapak Q and molsieve columns, with thermal conductivity and flame ionisation detectors. The temperature range 100–450 °C was explored and the reaction temperature was measured by a thermocouple placed in the catalyst bed. The differences between the inlet and outlet concentrations were used to calculate conversion data, and all carbon balances were in the range 100 ± 10%.

3 Results and Discussion

Figure 1 shows the conversion of propane for VO_X/CeO_2 catalysts with varying vanadium loadings. Initial propane conversion was observed at 175 °C. Propane conversion increased with temperature, reaching a maximum of 11% at 450 °C for the ceria support with no vanadium loaded. For this catalyst the sole reaction product was CO_2.

Varying the vanadium loading on the ceria support influenced the propane conversion. Initial conversions, at 250 °C, showed that 2.5% V/CeO_2 had the highest conversion of 2%, and 30% V/CeO_2 had the lowest conversion of 0.06%. However, at higher temperatures of 450 °C, 10% V/CeO_2 had a conversion of 5%, whereas 2.5% V/CeO_2 only reached 4%. The catalyst with the lowest conversion overall was that of 30% V/CeO_2, as the greatest conversion exhibited was only 2% at 450 °C.

Propene selectivities for all catalysts are shown in Fig. 2. Propene selectivity remained high for all catalysts, excluding the ceria support alone, which exhibited no selectivity to propene. For the vanadia supported catalysts the only other reaction product, additional to propene, was CO_2. The catalyst exhibiting highest selectivity towards propene was 30% V/CeO_2, which showed 99% at 200 °C. The selectivity decreased slightly as the temperature was increased, but remained high up to 450 °C (ca. 97%). However, it must be noted that this was one of the least active catalysts. The 10% V/CeO_2 catalyst showed high conversion of propane but selectivity to propene was lower. Initial selectivity of 76% at 200 °C was the lowest of all the vanadium catalysts studied and this steadily decreased to 14% at 450 °C. Not surprisingly the highest selectivity observed for all catalysts was at low conversion, in the temperature range 325–375 °C.

The ceria support alone exhibited no selectivity to propene, but with just 0.5% vanadium loading on the surface the selectivity was increased to 88%, see Table 1. The highest yield obtained, of 3.7%, was for the 2.5% V/CeO_2 catalyst closely followed by 30% V/CeO_2 with 3.6%. The lowest yield obtained was for 10% V/CeO_2 with a yield of 0.7% due to poor selectivity to propene. A very similar trend was also observed if the per pass propene yields were compared at constant conversion (Table 1).

All of the catalysts were characterised using laser Raman spectroscopy, powder X-ray diffraction, and scanning electron microscopy and X-ray photoelectron spectroscopy. A number of the catalysts characteristics are summarised in Table 2). The surface area of the ceria without any vanadium added was 78 m^2 g^{-1}, and generally the surface area decreased as the loading of vanadium was increased. Vanadium loadings were measured using EDX, and selected data were corroborated using AAS. In general, the vanadium loadings were in good agreement with the expected loading. The exception was the 10% V/CeO_2

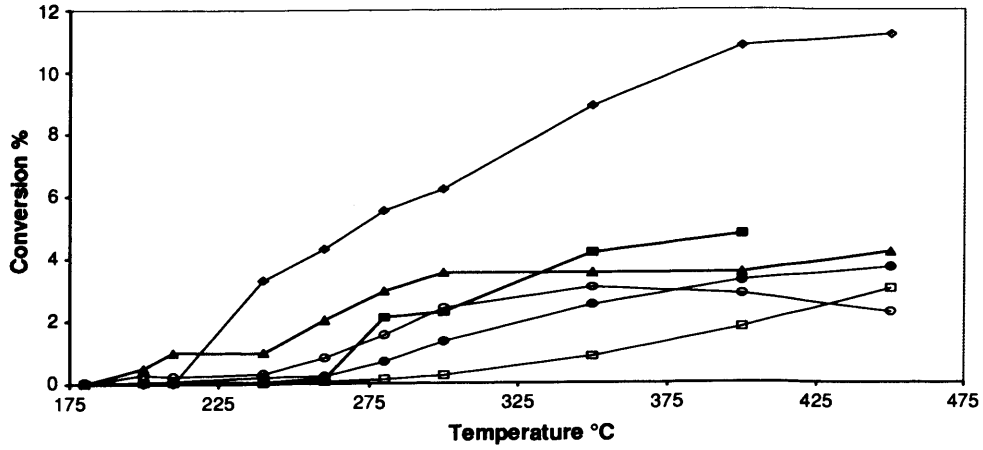

Fig. 1 Comparison of conversion of propane over the range of catalysts as a function of temperature: Symbols *open diamond* CeO_2, *open circle* 0.5% V/CeO_2, *filled triangle* 2.5% V/CeO_2, *filled square* 10% V/CeO_2, *filled circle* 20% V/CeO_2 *open square* 30% V/CeO_2

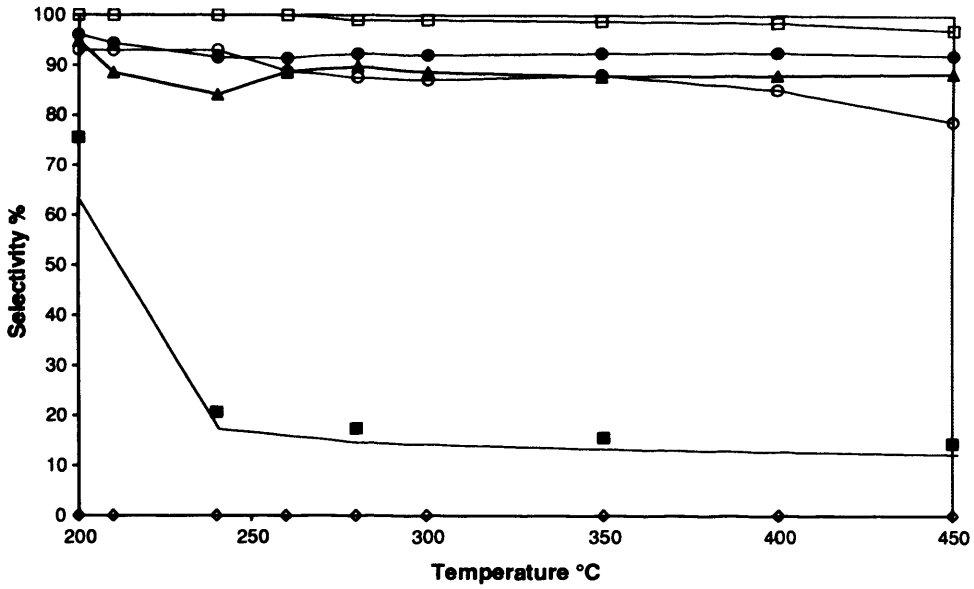

Fig. 2 Comparison of propene selectivity from propane oxidation over the range of catalysts as a function of temperature: Symbols *open diamond* CeO_2, *open circle* 0.5% V/CeO_2, *filled triangle* 2.5% V/CeO_2, *filled square* 10% V/CeO_2, *filled circle* 20% V/CeO_2 *open square* 30% V/CeO_2

Table 1 Summary of performance of ceria supported vanadium oxide catalysts for propane oxidation

Catalyst	Maximum propene yield				Performance at constant conversion			
	Temp. (°C)	Conv. (%)	Sel. (%)[a]	Yield (%)[b]	Temp. (°C)	Conv. (%)	Sel. (%)[a]	Yield (%)[b]
CeO_2	–	–	0	0	–	–	0	0
0.5% V/CeO_2	350	3.1	88	2.7	230	2	88	1.8
2.5% V/CeO_2	450	4.2	89	3.7	290	2	89	1.8
10% V/CeO_2	400	4.7	14	0.7	260	2	16	0.3
20% V/CeO_2	450	3.7	92	3.4	280	2	93	1.8
30% V/CeO_2	450	3.7	97	3.6	330	2	98	2.0

[a] Selectivity to propene

[b] Perpass yield of propene

Table 2 Summary of catalyst characterisation data

Catalyst	V conc./wt%[a]	$SA_{BET}/m^2\ g^{-1}$	Crystalline phases[b]	Crystallite size/nm[c]	Raman FWHM[d]/cm^{-1}	TPR peak maximum/°C
CeO_2	–	78	CeO_2	32.4	21.4	350 and 550
0.5% V/CeO_2	0.43	58	CeO_2	32.8	23.2	500
2.5% V/CeO_2	2.59	49	CeO_2	32.6	25.7	500
10% V/CeO_2	13.80	47	CeO_2	31.9	29.8	465
20% V/CeO_2	19.44	33	CeO_2	32.1	–	550
			$CeVO_4$			
30% V/CeO_2	30.56	12	CeO_2	32.0	–	565
			$CeVO_4$			

[a] Determined by EDX and confirmed by AAS

[b] Determined from XRD

[c] Determined by X-ray line broadening

[d] FWHM for ceria peak at 456 cm^{-1}

catalyst, which had a marginally higher vanadium loading than expected.

Characterisation of crystalline phases using powder XRD identified two different, and distinct phases, depending on the vanadium loading employed. The diffraction patterns from CeO_2 and catalysts with vanadium loadings up to 10% showed a cerium (IV) oxide phase only (cerianite). The catalysts with loadings below 10% vanadium did not show any evidence for any crystalline vanadium-containing phase. Higher vanadium loadings showed the presence of a crystalline cerium vanadium oxide phase ($CeVO_4$, called wakefieldite), and this was simultaneously present with CeO_2. From the XRD data it is also possible to determine the ceria crystallite size using line broadening in accordance with the Scherrer equation (Table 2). Crystallite sizes remained similar for all catalysts, in the region of 32–33 nm. These data indicate that the size of the primary crystallites were not altered by the addition of vanadium, and it is also interesting to note that the crystallite size for the 20 and 30% V/CeO_2 catalysts remained unaltered, even though a bulk phase change was identified. The consistent crystallite size indicates that the variation of surface area observed is more likely to be related to differences of morphology and/or particle agglomeration.

Laser Raman spectroscopy data are shown in Fig. 3 for the range of catalysts. Data for the ceria support alone are not included as the intensity of the dominant peak in the spectrum makes simultaneous presentation with the spectra of the vanadium containing catalysts difficult. The spectra for the CeO_2 only showed a Raman band centered at a frequency of 456 cm^{-1}, which is characteristic of CeO_2 vibrations (the triply degenerate TO mode). Other much less intense Raman bands typical of CeO_2 were not observed at ca. 272 and 595 cm^{-1} (doubly degenerate TO mode and non-degenerate LO mode, respectively [28]). The main Raman feature at 456 cm^{-1} for CeO2 was observed for all the catalysts as the V loading was increased up to 10%. With the addition of V onto the ceria Raman bands associated with vanadium species were observed. Raman bands at ca. 1030 cm^{-1} are typically attributed to the V=O symmetric stretch in isolated VO_4 tetrahedra. Whilst a very broad band over the region 900–950 cm^{-1}, and usually centred around 920 cm^{-1}, is often assigned to the V=O terminal vibration of polyvanadate species [29–32]. Raman bands were present at 909 and 1041 cm^{-1} in the 0.5, 2.5 and 10% V catalysts. These could be associated with highly dispersed vanadium species, such as isolated VO_4 and polyvanadate species. The frequency shifts observed suggests that the dispersed vanadium species interacted strongly with the nanocrystalline support. As the vanadium loading was increased to 2.5 and 10% the intensity of the ceria peak at 456 cm^{-1} decreased.

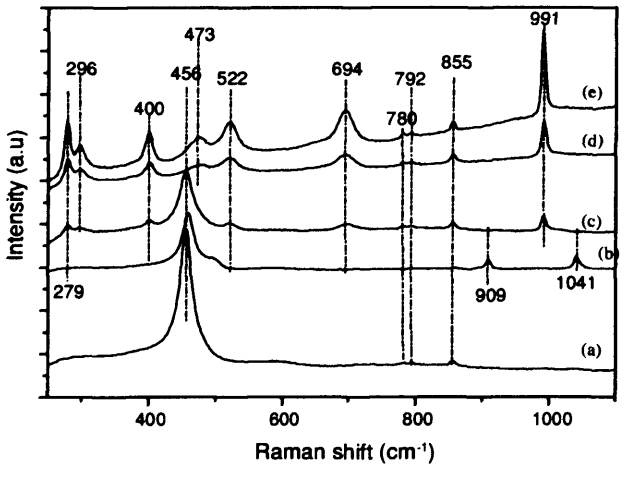

Fig. 3 Laser Raman characterisation of the vanadium loaded ceria catalysts: (a) 0.5% V/CeO_2 (b) 2.5% V/CeO_2 (c) 10% V/CeO_2 (d) 20% V/CeO_2 (e) 30% V/CeO_2

As the vanadium loading increased up to 10%, the full width half maximum of the main Raman peak of the ceria also increased systematically from 21.4 cm^{-1} for CeO_2 to 29.8 cm^{-1} for 10% V/CeO_2 (Table 2). The increase of the ceria Raman peak FWHM has been associated with a decrease of crystallite size and/or an increase of defect concentration [24, 25]. The XRD data showed that the crystallite size did not significantly change as the V loading increased and it is therefore evident that increasing the V loading resulted in a possible increase of the catalyst defect concentration.

For the catalysts with 20 and 30% vanadium loading a series of well defined peaks were observed atca. 270, 400, 522, 694 and 991 cm^{-1}. These set of peaks have been assigned to crystalline V_2O_5 [33, 34] and indicate the presence of the crystalline oxide on the surface of the catalysts. The majority of peaks indicative of crystalline V_2O_5 were present with low intensity in the 10% V/CeO_2 catalyst. Implying that it was present to a minor extent. As mentioned earlier the intense peak at 456 cm^{-1} for ceria was not observed in the spectra of the 20 and 30% vanadium catalysts. However, both catalysts showed a Raman band at 473 cm^{-1}, which cannot be unequivocally assigned, but may be associated with the mixed cerium vanadium oxide phase identified by XRD.

Although some differences were observed between the catalysts from XRD and laser Raman characterisation, in general the catalysts can be divided into two similar groups. Those with lower loadings of vanadium showed the crystalline CeO_2 phase with some evidence for dispersed vanadium oxide species, whilst catalysts with higher loadings showed an additional mixed vanadium cerium oxide crystalline phase. In order to determine any morphological differences between catalysts scanning electron

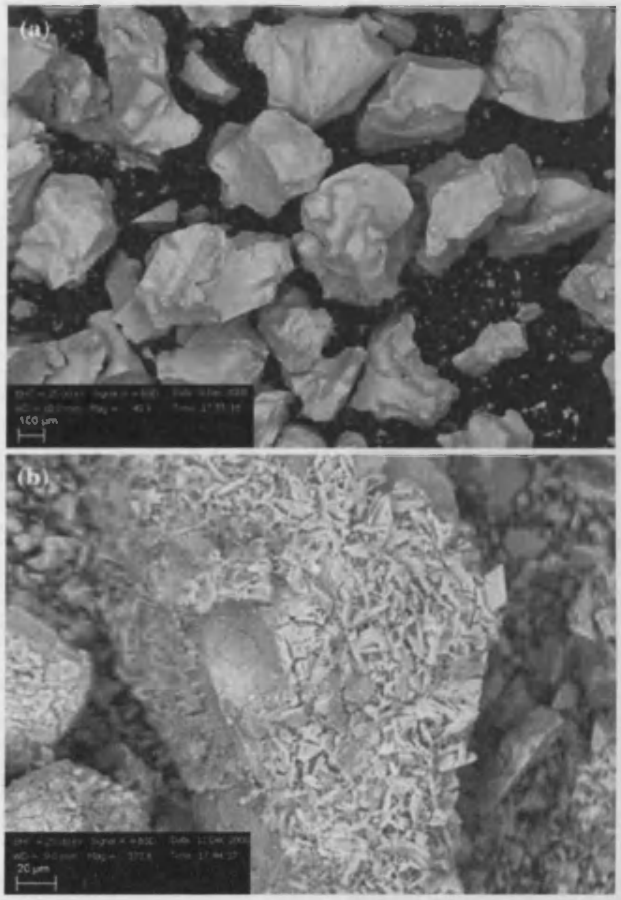

Fig. 4 Back scattered scanning electron microscopy Images of ceria support: **a** fresh support after calcination, **b** ceria support after treatment with oxalic acid without vanadium

microscopy studies were also undertaken. The nanocrystalline ceria support used in the present study has been extensively characterised previously [23, 24]. However, in the present study the ceria support was subject to treatment with oxalic acid in addition to ammonium metavanadate during the procedure to impregnate with vanadium. To seperate the effect of oxalic acid treatment on the ceria, from vanadium addition, the support was treated with oxalic acid solution of the same concentration as that used for vanadium addition. There was no discernable differences distinguishable from XRD and laser Raman for the oxalic acid treated and untreated ceria. However, a significant change of the ceria morphology was apparent (Fig. 4). Exposure of the ceria support to oxalic acid solution resulted in the formation of a more fibrous needle like surface morphology that was not present on the untreated ceria.

The effect of adding vanadium onto the ceria in the presence of oxalic acid solution is shown in Fig. 5. The addition of more vanadium up to 10% resulted in the needle-like morphology becoming increasingly more prominent and also the morphology became more well-defined. Increasing the vanadium loading above 10–20% and 30% resulted in a total change of morphology. The needle-like morphology was not present in the higher loading catalysts. The back scattered electron image of the catalysts showed differences in contrast, suggesting some in homogeneity of composition. EDX analysis of different points of the 20% catalyst (Fig. 6) clearly identified that there were differences in composition on a microscopic scale. Cracks were also evident on the surface of the catalysts and this indicates that the particles may have undergone some degree of disintegration to form some smaller particles. The 30% vanadium catalyst was more porous than the other catalysts and large pores were clearly visible on the surface (Fig. 7). The particle size of the 30% catalyst was also larger than the other catalysts, although it must be noted that although particle sizes altered crystallite sizes did not change significantly for the range of catalysts.

The redox behaviour of the catalysts was examined using temperature programmed reduction experiments, and a summary of the data are given in Table 2. Studies on the ceria support showed a very broad double reduction feature ranging from 300 to 600 °C. This was indicative of nanocrystalline ceria [35], as microcrystalline ceria only usually shows one reduction peak. The two peaks were due to the reduction of surface and lattice oxygen respectively. Once vanadium was added onto the ceria support there was modification of the redox properties of the catalyst. The high temperature feature became far more pronounced and the feature with a maximum around 350 °C was no longer measureable. For the catalysts with 0.5, 2.5 and 10% vanadium loading reduction was more facile than the ceria support as the magnitude of hydrogen consumption increased and the temperature of reduction was reduced to 500 °C for the 0.5 and 2.5% V catalysts and to 460 °C for the 10% V catalyst. The 20 and 30% V catalysts did not show evidence for enhanced ease of reducibility when compared with the ceria support, in fact the 30% catalyst was more difficult to reduce.

The characterisation techniques discussed so far focus more on bulk characterisation, but it is also important to probe the surface of the catalysts. To address this, X-ray photoelectron spectroscopy studies were also performed. The XPS results provide a powerful corroboration of the XRD data. Figure 8 shows the Ce(3d) spectra obtained for the bare ceria support and the catalysts after loading with vanadium. The spectrum for CeO_2 (Fig. 8a) is complex and comprises three doublets, each spin-orbit split doublet corresponding to a different electron distribution in the final ion state after photoemission. The different final state electronic configurations are indicated on the spectrum. The spectral profile for the 30% V-doped material (Fig. 8f)

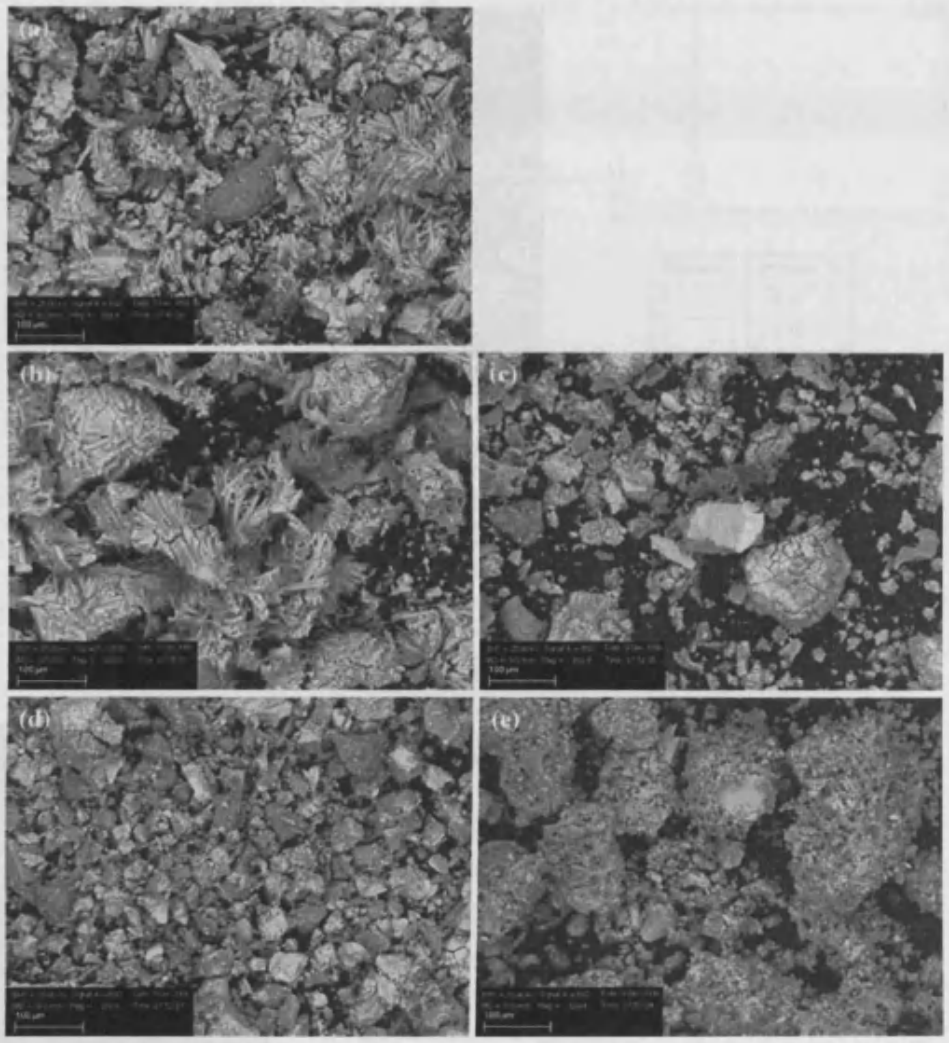

Fig. 5 Back scattered scanning electron microscopy Images of ceria supported vanadium catalysts: **a** 0.5% V/CeO_2, **b** 2.5% V/CeO_2, **c** 10% V/CeO_2, **d** 20% V/CeO_2, **e** 30% V/CeO_2

is dramatically different from that of the ceria support, reflecting the formation of Ce^{3+} species, the spectrum of which consists of two doublets due again to final state effects as indicated. Although this spectrum is dominated by Ce^{3+} features, the attenuated peak at ca. 915 eV indicates that some Ce^{4+} species are also present. This is consistent with the XRD results (Table 2). Evidence in the XPS data for Ce^{3+} formation begins to appear at a V loading of only 10%, and develops with increasing V content. The V(2p) spectra (Fig. 9) show a monotonic increase in intensity with V loading; the binding energy of the $V(2p_{3/2})$ component indicates that the V species are in the 5^+ oxidation state only and the symmetrical shape reflects the absence of any 4^+ contribution.

The trends in propane oxidation activity and selectivity can be explained by considering the structure and chemistry of the different catalysts. The ceria alone without the addition of vanadium was very active for propane oxidation and the only product was carbon oxides. This is consistent with the exceptionally high activity of nanocrystalline ceria, which has been attributed to the small crystallite size, high surface area, high defect concentration and ease of surface reduction leading to highly reactive oxygen species facile for deep oxidation [24, 25]. The addition of vanadia to the surface of the ceria resulted in a significant reduction of propane conversion and also resulted in the formation of the selective propene product. This switch of reactivity was in part due to the blocking of the ceria surface with selective vanadium species, which were most probably isolated vanadyl species and polyvanadate species for the catalysts with lower vanadium loadings. The 10% vanadium catalyst was the most active of the vanadium catalysts and it also showed much lower propene selectivity compared with the others. The 10% catalyst showed the highest ceria defect concentration and was the easiest to reduce, and these factors in combination with the presence of highly dispersed

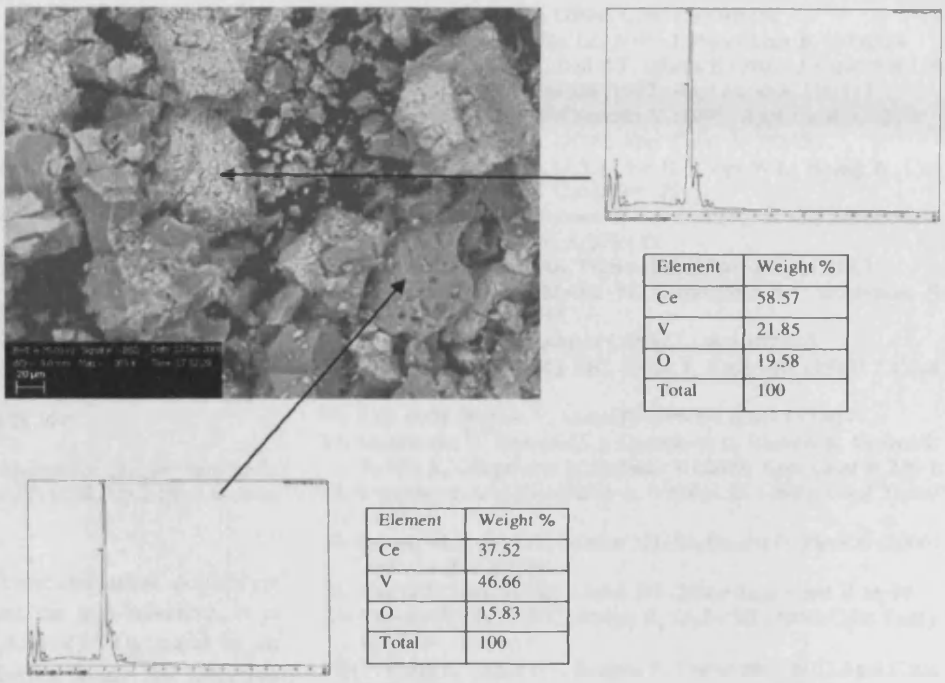

Element	Weight %
Ce	58.57
V	21.85
O	19.58
Total	100

Element	Weight %
Ce	37.52
V	46.66
O	15.83
Total	100

Fig. 6 Backscattered electron image and micro EDX analysis of the 20% V/CeO_2 catalyst

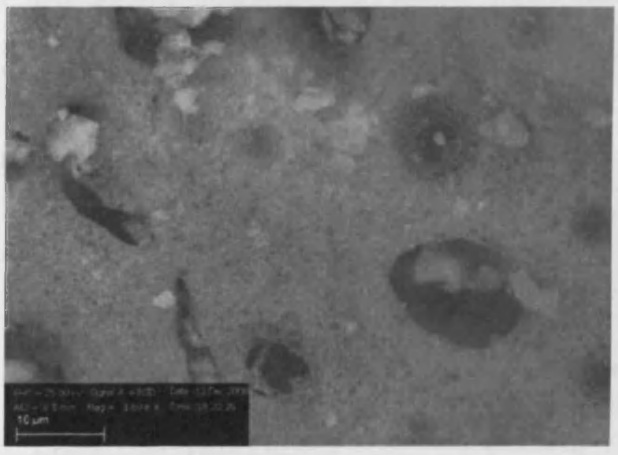

Fig. 7 Backscattered scanning electron microscopy image of the 30% V/CeO_2 catalyst

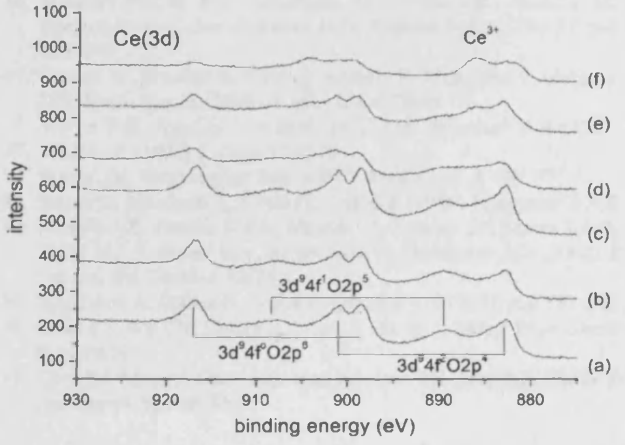

Fig. 8 Ce(3d) X-ray photoemission spectra for (a) the bare ceria support and with different V loadings: (b) 0.5%, (c) 2.5%, (d) 10%, (e) 20% and (f)30%. Indicated on spectrum (a) are the different final state electronic configuration giving rise to the three doublets

V_2O_5 and the absence of mixed oxide formation for the CeO_2 phase provide a possible explanation for the preferred total oxidation behaviour. Increasing the vanadium loading above10% resulted in a switch back to propane selective oxidation, and this coincided with the formation of the mixed oxide phase $CeVO_4$, with subsequent reduction of the quantity of the nanocrystalline CeO_2 phase. Indeed for the highest loading catalyst there was a much higher concentration of surface Ce^{3+}, which could explain the low selectivity towards CO_X as facile oxygen species associated with Ce^{4+} were reduced, and hence high propene selectivity was achieved.

4 Conclusions

Nanocrystalline ceria is very active for the total oxidation of propane under conditions used for oxidative dehydrogenation. However, the addition of vanadium results in a switch of activity to produce propene with appreciable selectivity. The catalyst performance depends on the vanadium loading. Lower vanadium loadings resulted in catalysts with highly dispersed vanadia species, which were selective towards propene production. Higher vanadium loadings resulted in the formation of a mixed cerium–vanadium phase, which

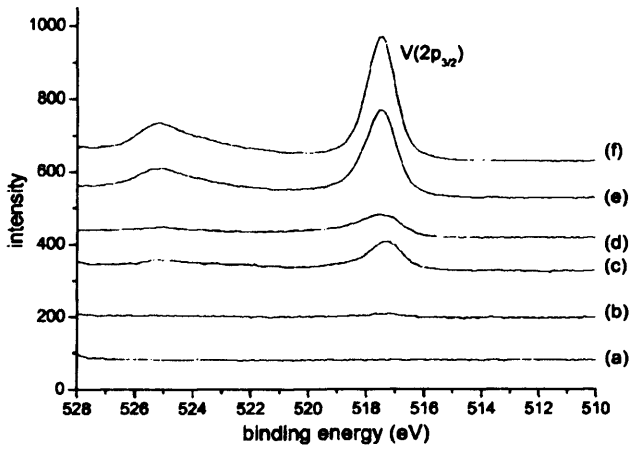

Fig. 9 V(2p) X-ray photoemission spectra for (a) the bare ceria support and with different V loadings: (b) 0.5%, (c) 2.5%, (d) 10%, (e) 20% and (f) 30%

was also active for propane selective oxidation. A catalyst with an intermediate loading was far less selective. It is apparent that the mixed oxide phase $CeVO_4$ could be an interesting system worthy of further study for selective propane ODH.

Acknowledgments We would like to thank Cardiff University, School of Chemistry and EPSRC for funding.

References

1. Frank B, Dinse A, Ovsitser O, Kondratenko EV, Schomacker R (2007) Appl Catal A 323:66
2. Cavani F, Ballarini N, Cericola A (2007) Catal Today 127:113
3. Al-Zahrani SM, Jibril BY, Abasaeed AE (2003) Catal Today 81:507
4. Meunier FC, Yasmeen A, Ross JRH (1997) Catal Today 37:33
5. Yoon Y-S, Fujikawa N, Ueda W, Moro-oka Y, Lee K-W (1995) Catal Today 24:327
6. Chen K, Xie S, Bell AT, Iglesia E (2001) J Catal 198:232
7. Davies T, Taylor SH (2004) Catal Lett 93:151
8. Zhau Z, Gao X, Wachs IE (2003) J Phys Chem B 107:6333
9. Argyle MD, Chen K, Bell AT, Iglesia E (2002) J Catal 208:139
10. Blasco T, López Nieto JM (1997) Appl Catal A 157:117
11. Mamedov EA, Cortés Corberán V (1995) Appl Catal A 127:1
12. Ueda W, Oshihara K (2000) Appl Catal A 200:135
13. Liu Y-M, Feng W-L, Li T-C, He H-Y, Dai W-L, Huang W, Cao Y, Fan K-N (2006) J Catal 239:125
14. Pena ML, Dejoz A, Fornes V, Rey F, Vazquez MI, Lopez Nieto JM (2001) Appl Catal A 209:155
15. Pieck CL, Banares MA, Fierro JLG (2004) J Catal 224:1
16. Christodoulakis A, Machli M, Lemonidou AA, Boghosian S (2004) J Catal 222:293
17. Chaar M, Patel D, Kung H (1998) J Catal 109:463
18. Michalakos PM, Kung MC, Jahan I, Kung HH (1993) J Catal 140:226
19. Sam DSH, Soenen V, Volta JC (1990) J Catal 123:417
20. Grzybowsk B, Słoczyński J, Grabowski R, Samson K, Gressel I, Wcisło K, Gengembre L, Barbaux Y (2002) Appl Catal A 230:1
21. Lemonidou AA, Nalbandian L, Vasalos IA (2000) Catal Today 61:333
22. Salazer M, Berry DA, Gardner TH, Shekhawat D, Floyd D (2006) Appl Catal A 310:54
23. Garcia T, Solsona BE, Taylor SH (2006) Appl Catal B 66:92
24. Ntainjua E, Garcia NT, Solsona B, Taylor SH (2008) Catal Today 137:373
25. Ntainjua E, Garcia NT, Solsona B, Taylor SH (2007) Appl Catal B 76:248
26. Martınez-Huerta MV, Coronado JM, Ferna'ndez-Garcı'a M, Iglesias-Juez A, Deo G, Fierro JLG, Banares MA (2004) J Catal 225:240
27. Daniell W, Ponchel A, Kuba S, Anderle F, Weingand T, Gregory DH, Knozinger H (2002) Topics Catal 20:65
28. Weber WH, Hass KC, McBride JR (1993) Phys Rev B 48:178
29. Wachs IE (1990) J Catal 124:570
30. Wachs IE, Weckhuysen BM (1997) Appl Catal A 157:67
31. Busca G, Marchetti L, Centi G, Trifiro F (1986) Langmuir 2:568
32. Rodella CB, Franco RWA, Magon CJ, Donoso JP, Nunes LAO, Saeki MJ, Aegerter MA, Sargentelli V, Florentino AO (2002) J Sol Gel Sci Technol 83:25
33. Khodakov A, Olthof B, Bell AT, Iglesia E (1999) J Catal 181:205
34. Chao KJ, Wu CN, Chang H, Lee LJ, Hu SF (1997) J Phys Chem B 101:6341
35. Choi HJ, Moon J, Shim HB, Han KS, Lee EG, Jung KD (2006) J Am Ceram Soc 89:343